PHOTOPHYSICS AND PHOTOCHEMISTRY OF MULTIPLY BONDED METAL-METAL DIMERS

by

I-Jy Chang

A DISSERTATION

Submitted to
Michigan State University
in partial fulfillment of the requirements
for the degree of

DOCTOR OF PHILOSOPHY

Department of Chemistry

1988

ABSTRACT

PHOTOPHYSICS AND PHOTOCHEMISTRY OF MULTIPLY BONDED METAL-METAL DIMERS

by

I-Jy Chang

The excited state dynamics and excited state chemistry of multiply bonded metal-metal complexes ($M\overset{n}{-}M$) have been investigated. The lowest energy excited state, $^1(\delta\delta^*)$, of dimolybdenum tetrahalo(tetrakis)phosphine ($Mo_2X_4P_4$) has been studied by using emission and time-resolved picosecond laser spectroscopy. Emission quantum yields and lifetimes are significantly affected by the electronic configuration of the individual molecule and are only slightly affected by the eclipsed-to-staggered conformational changes. Molecules with D_{2d} symmetry possess high emission quantum yields and long lifetimes, complexes with D_{2h} symmetry possess lower emission quantum yields and shorter lifetimes. Transient absorption spectra of $Mo_2X_4P_4$ complexes display decays corresponding to prompt relaxation of the $^1(\delta\delta^*)$ excited state to ground state. In addition, complexes possessing phosphines with sterically bulky constituents (e.g. monodentate or bidentate phenyl phosphines) exhibit a long-lived nonemissive excited state. It is believed that this nonemissive excited state is due to the dissociation of the phosphine ligands within a solvent cage.

A new class of multiply bonded dimolybdenum phosphate dimers, $Mo_2(HPO_4)_4^{4-}$ and $Mo_2(HPO_4)_4^{3-}$, has been prepared and spectroscopically and electrochemically characterized. The electronic absorption spectrum of $Mo_2(HPO_4)_4^{4-}$ in acidic solution is typical $M\overset{4}{-}M$ species with the $\delta^2 \rightarrow \delta\delta^*$ transition occurring at 516 nm. Cyclic voltammograms of phosphoric acid solutions of $Mo_2(HPO_4)_4^{4-}$ are characterized by two reversible waves at -0.67 and -0.25 V vs. SCE that have been assigned to the $Mo_2(HPO_4)_4^{3-/4-}$ and $Mo_2(HPO_4)_4^{2-/3-}$ couples, respectively. Oxidation of $Mo_2(HPO_4)_4^{4-}$ produces the mixed-valence dimer $Mo_2(HPO_4)_4^{3-}$, which exhibits an intense near-infrared absorption band which is assigned to the $\delta \rightarrow \delta^*$ transition. Irradiation ($\lambda > 355$ nm) of phosphoric acid solutions of the $M\overset{4}{-}M$ dimer leads to facile production of $Mo_2(HPO_4)_4^{2-}$ and hydrogen. The photochemical reaction mechanism is consistent with sequential one-electron oxidation of the Mo_2 core [i.e., Mo_2(II,II) → Mo_2(II,III) → Mo_2(III,III)]. Electronic absorption spectra of the $Mo_2(HPO_4)_4^{n-}$ (n = 2, 3, 4) dimers in the ultraviolet spectral region, wavelength-dependent quantum yield measurements, and photochemical studies of phosphate dimers under N_2O atmospheres confirm the assignment of a $\pi\pi^*$ photoactive state of Mo_2 phosphato complexes.

Chemistry from the $^1(\delta\delta^*)$ excited state of the $Mo_2(HPO_4)_4^{4-}$ complex is circumvented by proton quenching. To this end, a novel photoreceptor, $Mo_2(O_2P(OC_6H_5)_2)_4$, was prepared to promote the low energy multielectron reactions. This diphenyl phosphate dimolybdenum species exhibits $\delta^2 \rightarrow \delta\delta^*$ absorption at 515 nm in CH_2Cl_2 solution. Cyclic voltammograms show two reversible waves

at +0.06 and +1.00 V vs. SCE which correspond to $Mo_2(O_2P(OC_6H_5)_2)_4^{+/0}$ and $Mo_2(O_2P(OC_6H_5)_2)_4^{2+/+}$ couples, respectively. One electron oxidation of $Mo_2(O_2P(OC_6H_5)_2)_4$ yields mixed-valence $Mo_2(O_2P(OC_6H_5)_2)_4^{+}$ species which is a direct analogue to the $Mo_2(HPO_4)_4^{3-}$. In spite of the similarity of $Mo_2(O_2P(OC_6H_5)_2)_4$ to $Mo_2(HPO_4)_4^{4-}$, $Mo_2(O_2P(OC_6H_5)_2)_4$ emits directly from $^1(\delta\delta^*)$ excited state in nonaqueous solutions. The preserved $^1(\delta\delta^*)$ lifetime is long enough to permit direct reactions of the excited state in nonaqueous solution. Visible irradiation ($\lambda >$ 530 nm) of solutions containing $Mo_2(O_2P(OC_6H_5)_2)_4$ and $ClCH_2CH_2Cl$ results in the facile oxidation of the metal core and the production of ethylene.

To My Parents,

Shiow-Ing and Jong-Way

ACKNOWLEDGMENTS

I would like to thank Dr. Daniel G. Nocera for his encouragement, guidance and friendship during the course of this study. His scientific insight has opened my eye and directed me into a new field.

I also like to express my gratitude to the present members of the group for their friendship, encouragement and many helpful discussions. More importantly, they have created a great working atmosphere to make my graduate life enjoyable.

I must express my thanks to Dr. Jay R. Winkler at Brookhaven National Laboratory. I was fortunate to have the opportunity to work with him. From his guidance I learned how to use the picosecond laser instrument. Moreover, I learned how to review results in different way from him.

Finally, I like to thank my parents and family, without their support and love I could not finish this study.

TABLE OF CONTENTS

LIST OF TABLES

LIST OF FIGURES

CHAPTER I

INTRODUCTION

A central theme of inorganic chemistry is the activation of small molecules by transition metal complexes. The main difficulty of small molecule activation chemistry lies in the large kinetic and/ or thermodynamic barriers which typically confront these activation reactions. To this end, inorganic photochemistry can play an important role in the activation of small molecules, because the energy of the electronically excited transition metal complex can be utilized to surmount these reaction barriers. Owing to the fact that small molecule activation reactions involve oxidation-reduction chemistry, the development of the photoredox reaction pathways of transition metal complexes is crucial to the ultimate design of photochemical activation schemes.

Since Adamson's[1] initial studies in which the electron transfer reactivity of the LMCT excited state of $Co(NH_3)_5I$ was demonstrated, the energetics and mechanisms of photoinduced electron transfer of a large number of transition metal complexes have been delineated.[2-5] A feature of paramount importance is that the metal complex in its excited state is a considerably stronger oxidant and

reductant than in its ground state. The reduction potentials of an excited state can be estimated from its spectroscopic energy (0-0 transition defined as $E_{0\text{-}0}$ (M/M^*)) and the oxidation and reduction potentials of the ground state species as follows,

$$E^*_{red}\ (M^*/M^-) = E^o_{red}\ (M/M^-) + E_{0\text{-}0}\ (M/M^*) \qquad (1)$$

$$E^*_{ox}\ (M^+/M^*) = E^o_{ox}\ (M^+/M) - E_{0\text{-}0}\ (M/M^*) \qquad (2)$$

The Latimer diagram shown in Figure 1 illustrates the simple thermodynamic relations described by equations (1) and (2). This enhanced redox reactivity of electronically excited complexes has been exploited in the experimental testing of electron transfer theories,[6-11] the elucidation of photoinduced electron transfer in biological systems,[12-15] and the activation of small molecules for the design of solar energy conversion schemes.[16-21] In the case of the latter, because most small molecule activation processes involve two or more electrons, present photocatalytic schemes have relied on coupling the one-electron chemistry of electronically excited complexes to drive the overall multielectron process. This photochemistry is exemplified in the water-splitting reactions of mononuclear polypyridyl complexes. The tris(bipyridyl)ruthenium (II) ion, $Ru(bpy)_3^{2+}$, provides the cornerstone example of this photochemistry. Electronically excited $Ru(bpy)_3^{2+}$ ion, $[Ru(bpy)_3^{2+}]^*$, produced by visible irradiation can readily transfer one electron to acceptors, such as methylviologen (i.e. MV^{2+}).[22,23] The reduced viologen reacts with protons in the presence of colloidal platinum to

Figure 1. Latimer diagram for a transition metal complex M. The relationship among the 0, 0 transition energy ($E_{0\text{-}0}$) and the ground and excited state redox potentials is described by equations (1) and (2).

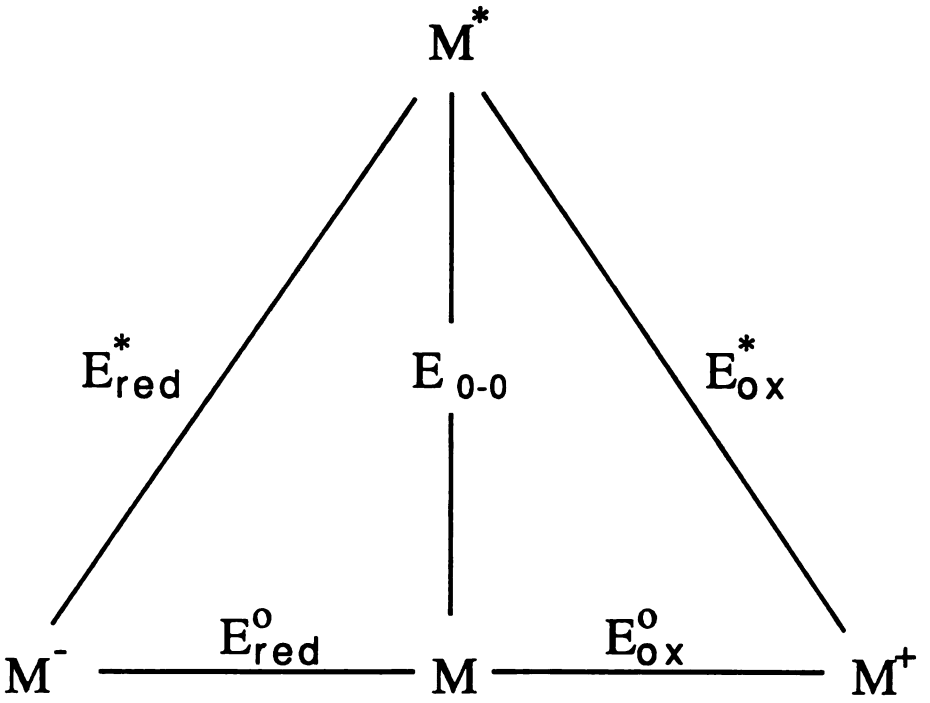

Figure 1

produce hydrogen.[24] This chemistry is described in the following scheme,

$$Ru(bpy)_3^{2+} \xrightarrow{h\nu} Ru(bpy)_3^{2+*} \quad (3)$$

$$Ru(bpy)_3^{2+*} + MV^{2+} \longrightarrow Ru(bpy)_3^{2} + MV^{+} \quad (4)$$

$$MV^{+} + H^{+} \xrightarrow{Pt} MV^{2+} + 1/2\ H_2 \quad (5)$$

Scheme I

The platinum catalyst couples the one electron chemistry of MV^+ to the two-electron hydrogen production chemistry by effectively storing the reducing equivalents of the viologen. The photogenerated oxidant $Ru(bpy)_3^{3+}$ produced in Scheme I is a strong oxidant. It has been shown that $Ru(bpy)_3^{3+}$ can react with water or hydroxide in the presence of a RuO_2 catalyst under suitable conditions to produce oxygen.[25] In principle, the hydrogen and oxygen photochemistry of the $Ru(bpy)_3^{2+}$ system can be combined to construct the photocatalytic water-splitting cycle schematically represented in Figure 2.[26-28] This photocatalytic chemistry has been realized to a limited extent with bifunctional photosystems employing colloidal semiconductors.[29-33] A schematic illustration of one such bifunctional photosystem is displayed in Figure 3.[30] An electronically excited sensitizer donates an electron to the conduction band of the colloidal TiO_2 particle. Protons are reduced to hydrogen at platinum dispersed on the surface of the semiconductor particle. The oxidized sensitizer takes an electron from the valence band of the TiO_2/RuO_2 particle and ensuing oxidation of water is mediated

Figure 2. Schematic illustration of a water-splitting cycle involving photosensitizer, electron relay, and redox catalysts.

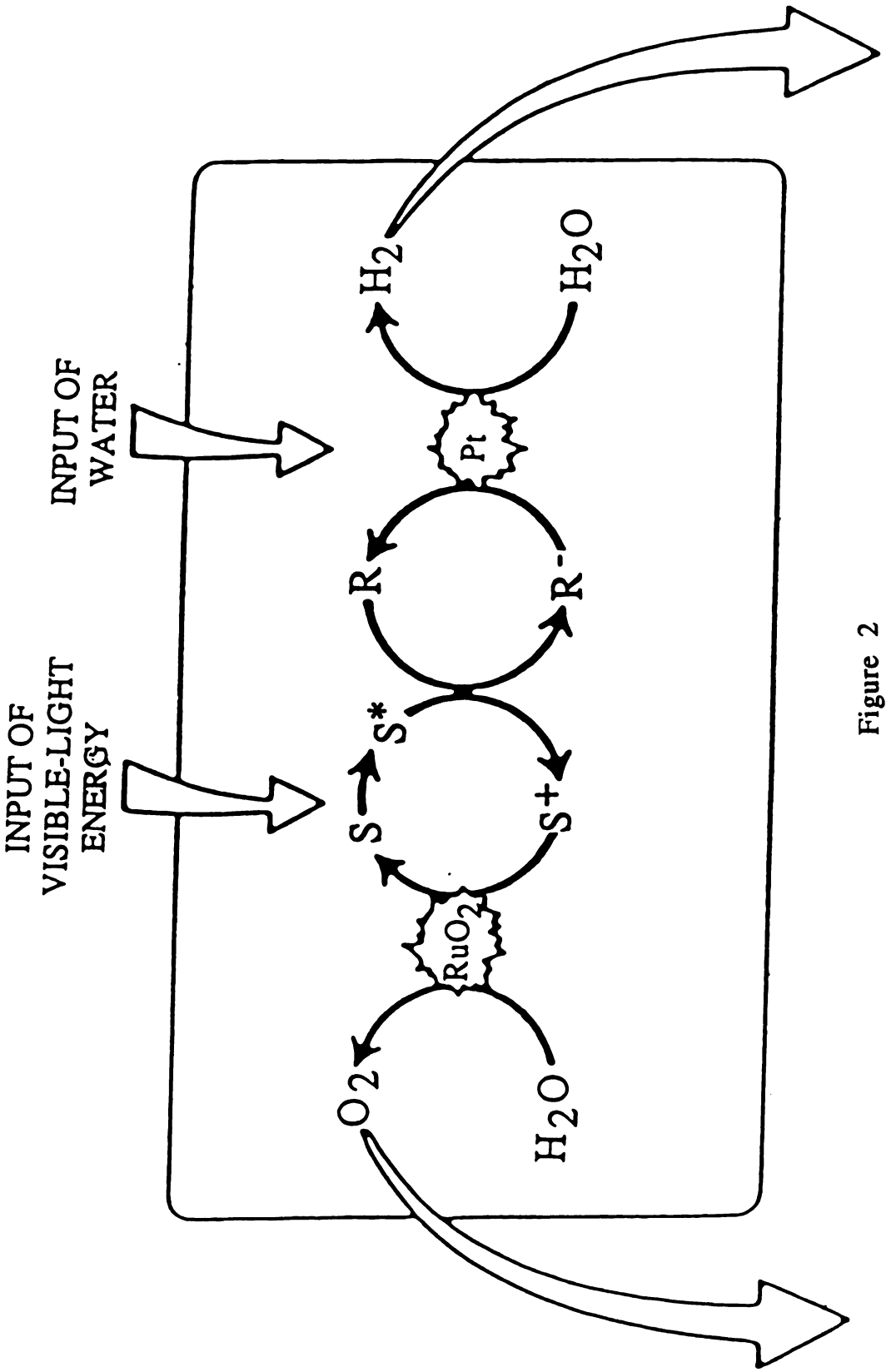
INPUT OF VISIBLE-LIGHT ENERGY
INPUT OF WATER
O_2
H_2O
RuO_2
S
S*
S+
R
R-
Pt
H_2
H_2O

Figure 2

Figure 3. Water-splitting photochemistry of a bifunctional catalyst involving modified semiconductor particles. CB, conduction band; EF, energy of Fermi level; R, electron relay (e.g. MV^{2+}); and S, sensitizer (e.g. $Ru(bpy)_3^{2+}$) (ref 30).

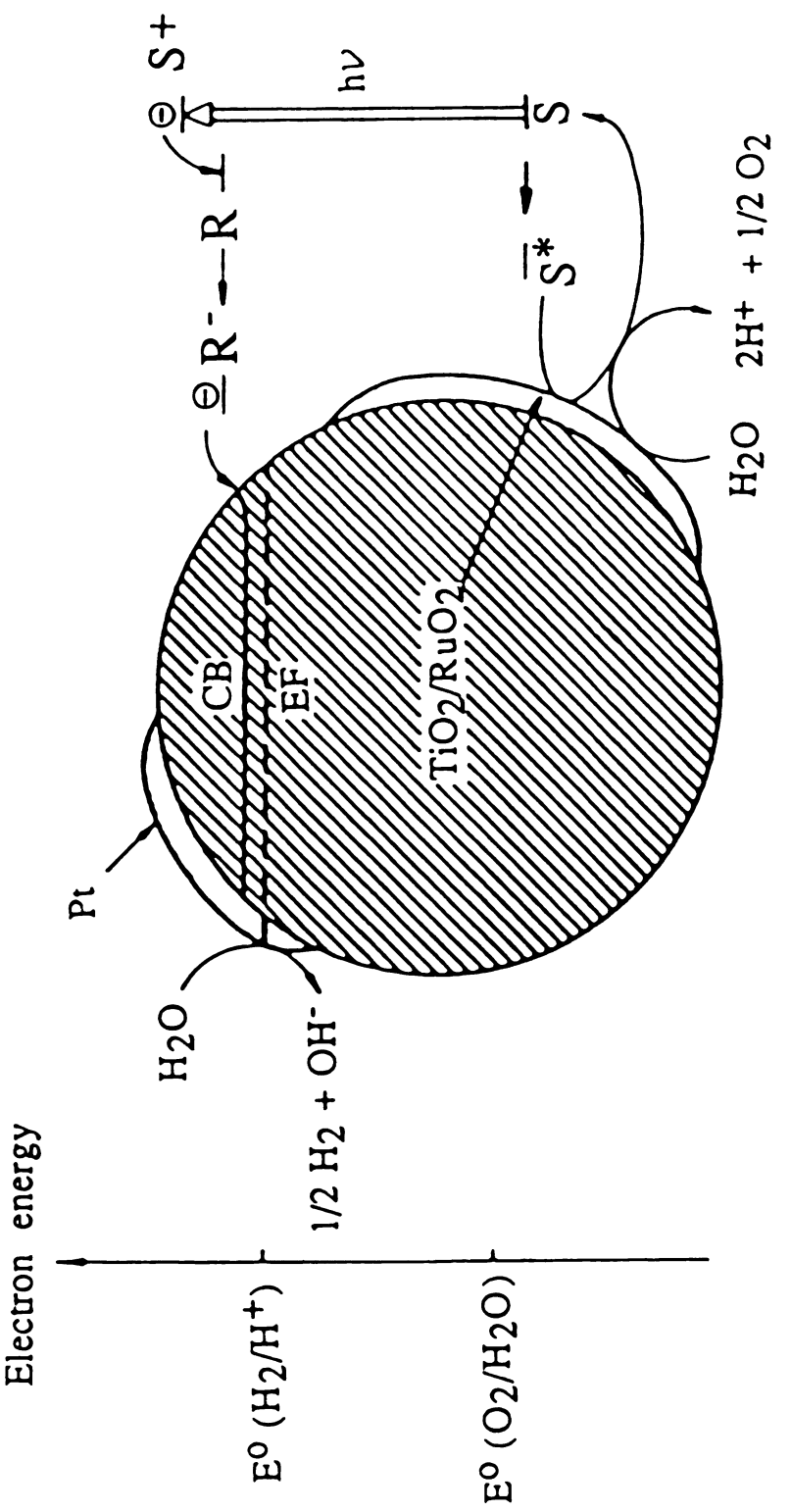
Electron energy
E° (H2/H+)
E° (O2/H2O)
1/2 H2 + OH-
H2O
Pt
CB
EF
TiO2/RuO2
⊖ R- — R
⊖ S+
hν
S
S*
H2O
2H+ + 1/2 O2

Figure 3

by RuO_2. The efficiency of the cycles such as those shown in Figures 2 and 3 are extremely low for several reasons. The reaction yield for H_2O oxidation by RuO_2 is negligibly small. A series of studies by Sutin and coworkers,[20,34] and others[35] have shown that a more efficient system for water oxidation involves cobalt(II) complexes as the water oxidation catalysts. The multistep mechanism which accounts for O_2 production is shown in Scheme II[34b] where the cobalt catalyst and $Ru(bpy)_3^{3+}$ is represented by $[Co^{2+}]$ and [Ru(III)].

$$[Co^{2+}] + 2H_2O \rightleftarrows Co(OH)_2 + 2H^+ \quad (6)$$

$$Co(OH)_2 + [Ru(III)] \rightleftarrows Co(OH)_2^+ + [Ru(II)] \quad (7)$$

$$Co(OH)_2^+ + [Ru(III)] \rightarrow CoO^{2+} + [Ru(II)] + H_2O \quad (8)$$

$$CoO^{2+} + H_2O \rightarrow [Co^{2+}] + H_2O_2 \quad (9)$$

$$CoO^{2+} + [Co^{2+}] \rightarrow CoOCo^{4+} \rightarrow "Co_2O_3"s \quad (10)$$

$$2[Ru(III)] + H_2O_2 \rightarrow 2[Ru(II)] + O_2 + 2H^+ \quad (11)$$

$$4Ru(bpy)_3^{3+} + 2H_2O \rightarrow 4Ru(bpy)_3^{2+} + 4H^+ + O_2 \quad (12)$$

Scheme II

Despite the success of replacing RuO_2 with other catalysts, overall low efficiencies are retained owing to the limited diffusion of reactants, efficient back reaction of primary photoproducts, and difficulties with channelling reactivity selectively along the desired routes in these complicated multifunctional schemes. Even if these

problems are overcome, there remains one major problem confronting these systems: $Ru(bpy)_3^{2+}$ multielectron chemistry is limited to water-splitting and is not applicable to other small molecule (e.g. N_2, CO_2, CO) activation reactions due principally to the lack of suitable catalysts, such as Pt and RuO_2, to couple the single electron transfer steps to the desired multielectron transformation. An alternative approach to the ultimate design of multielectron photochemical schemes is to develop photochemical excited state reaction pathways in which an electronically excited complex can participate directly in multielectron processes. With such systems, the problems inherent with coupling one electron steps to drive overall multielectron processes are circumvented.

A promising approach to photoinduced multielectron reactivity relies on coupling formal oxidation state changes of metal centers into a polynuclear core to drive the multielectron transformation. An issue of paramount importance to this approach is the necessity to maintain the structural integrity of the polynuclear core upon light absorption. For instance, a representative metal-metal bonded polynuclear system is dimanganese decacarbonyl $Mn_2(CO)_{10}$. From molecular orbital theory, the 12 electrons of this d^7-d^7 dimer reside in predominantly metal orbitals of π and δ symmetries. The remaining two electrons populate the metal-metal σ bonding orbital formed from the overlap of the $4d_{z2}$ orbitals. The lowest energy transition in $Mn_2(CO)_{10}$ arises from the promotion of an electron from the σ bonding orbital to σ^* antibonding orbital. Consequently, photoexcitation of these complexes significantly weakens the metal-metal bond, and photofragmentation to give two manganese

pentacarbonyl free radicals is the dominant excited state reaction pathway.[36,37] As is typical of most singly bonded metal-metal systems,[38-41] the photon is consumed for bond breaking and thus the polynuclear complex in its excited state is not preserved for redox chemistry.

This problem of photofragmentation can be avoided by a variety of approaches. The structural integrity of metal-metal cores of dinuclear species can be preserved by bridging the metal-metal core with bidentate ligands. This approach has been most successfully exploited with d^8-d^8 complexes where bridging ligands such as pyrophosphite in $Pt_2(POP)_4^{4-}$ (POP = $(HO_2P)_2O$),[42] pyrazolyl in $Ir_2(\mu\text{-}pz)_2(COD)_2$ (pz = pyrazolyl, COD = cyclooctadiene)[43] and diisocyanoalkanes in $Rh_2((CN)C_nH_{2n}(NC))_4^{44}$ chelate a dinuclear metal center possessing no formal metal-metal bond. Simple molecular orbital arguments suggest that the respective ground and excited state configurations of these binuclear d^8-d^8 complexes are represented as $(d_z2)^2(d_z2^*)^2$ and $(d_z2)^2(d_z2^*)^1(p_z)^1$. Promotion of an electron from the metal-metal antibonding framework to the bonding orbital results in an increased metal-metal interaction in the excited state. Electronic absorption and emission spectra[45-47] and Raman spectroscopy[48-50] of the ground and excited states of these dimers substantiate this prediction.

With the molecular structure preserved in the excited state, a rich photooxidation chemistry of d^8-d^8 complexes has been observed.[51-54] For instance, $Pt_2(POP)_4^{4-}$ photocatalytically converts isopropyl alcohol into acetone and hydrogen.[51] The reaction pathway for this transformation is shown in Figure 4. In this

Figure 4. Reaction cycle for the conversion of isopropanol to acetone and hydrogen by using $Pt_2(POP)_4^{4-}$ as a photocatalyst.

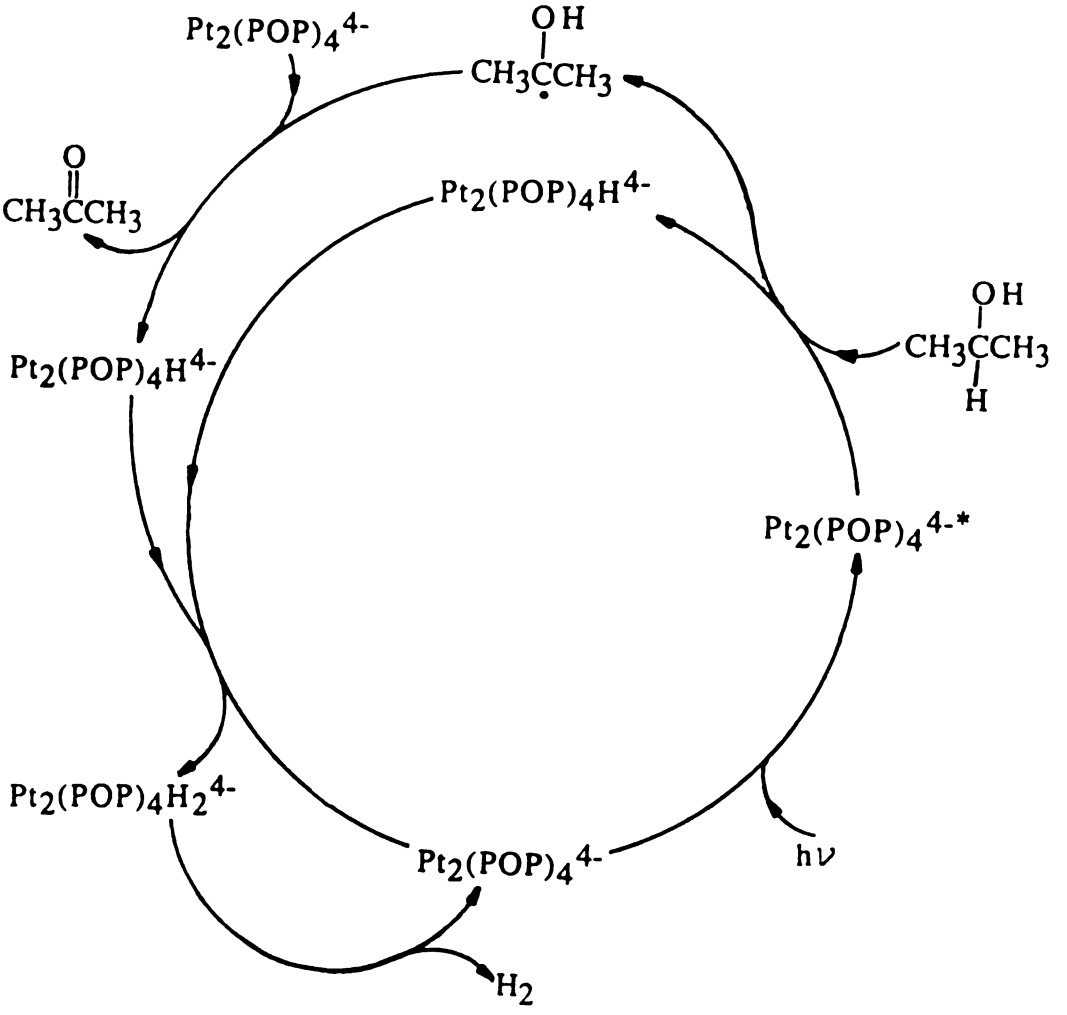
Pt2(POP)4 4-
OH
CH3CCH3
O
CH3CCH3
Pt2(POP)4H4-
OH
CH3CCH3
H
Pt2(POP)4H4-
Pt2(POP)4 4-*
Pt2(POP)4H2 4-
hν
Pt2(POP)4 4-
H2

Figure 4

reaction scheme, electronically excited $Pt_2(POP)_4^{4-}$ abstracts the methine hydrogen of isopropanol to give $Pt_2(POP)_4H^{4-}$ and $(CH_3)_2COH$ radical. Subsequent reaction of this radical with another equivalent of $Pt_2(POP)_4^{4-}$ results in the production of $Pt_2(POP)_4H^{4-}$. The Pt(II)Pt(III) mixed-valent $Pt_2(POP)_4H^{4-}$ intermediate undergoes disproportionation to give $Pt_2(POP)_4^{4-}$ and $Pt_2(POP)_4H_2^{4-}$ which has recently been observed.[51b] Reductive elimination of H_2 from $Pt_2(POP)_4H_2^{4-}$ completes the photocatalytic cycle. The overall two-electron reaction is comprised of a photoinduced one-electron step followed by an ensuing radical reaction. A similar reaction pathway, observed in the reaction of $Ir_2(\mu\text{-}pz)_2(COD)_2$ with 1,2-dichloroethane,[52] is shown in Figure 5. In this scheme, the ensuing thermal reaction of the photoinduced radical is the terminating step of the reduction of 1,2-dichloroethane to ethylene.

Careful examination of the above systems reveal a general characteristic of all photosystems studied to date : a triplet excited state yields photoproducts of triplet spin.[2-5] More generally, excitation of a transition metal complex usually produces a singlet excited state which intersystem crosses to the lowest energy triplet excited state. Relatively small energy gaps between the singlet and corresponding triplet state in conjunction with strong spin orbital coupling results in extremely efficient conversion of the singlet state to the triplet state. The triplet excited state reacts to exclusively yield primary photoproducts arising from electron transfer (s = 1) or atom abstraction (s = 1). This chemistry is summarized in Figure 6. Conversely, multielectron processes such as oxidative-addition, reductive-elimination, and atom transfer inevitably yield singlet

Figure 5. Photoinduced bimolecular reaction of $Ir_2(\mu\text{-}pz)_2(COD)_2$ with 1,2-dichloroethane.

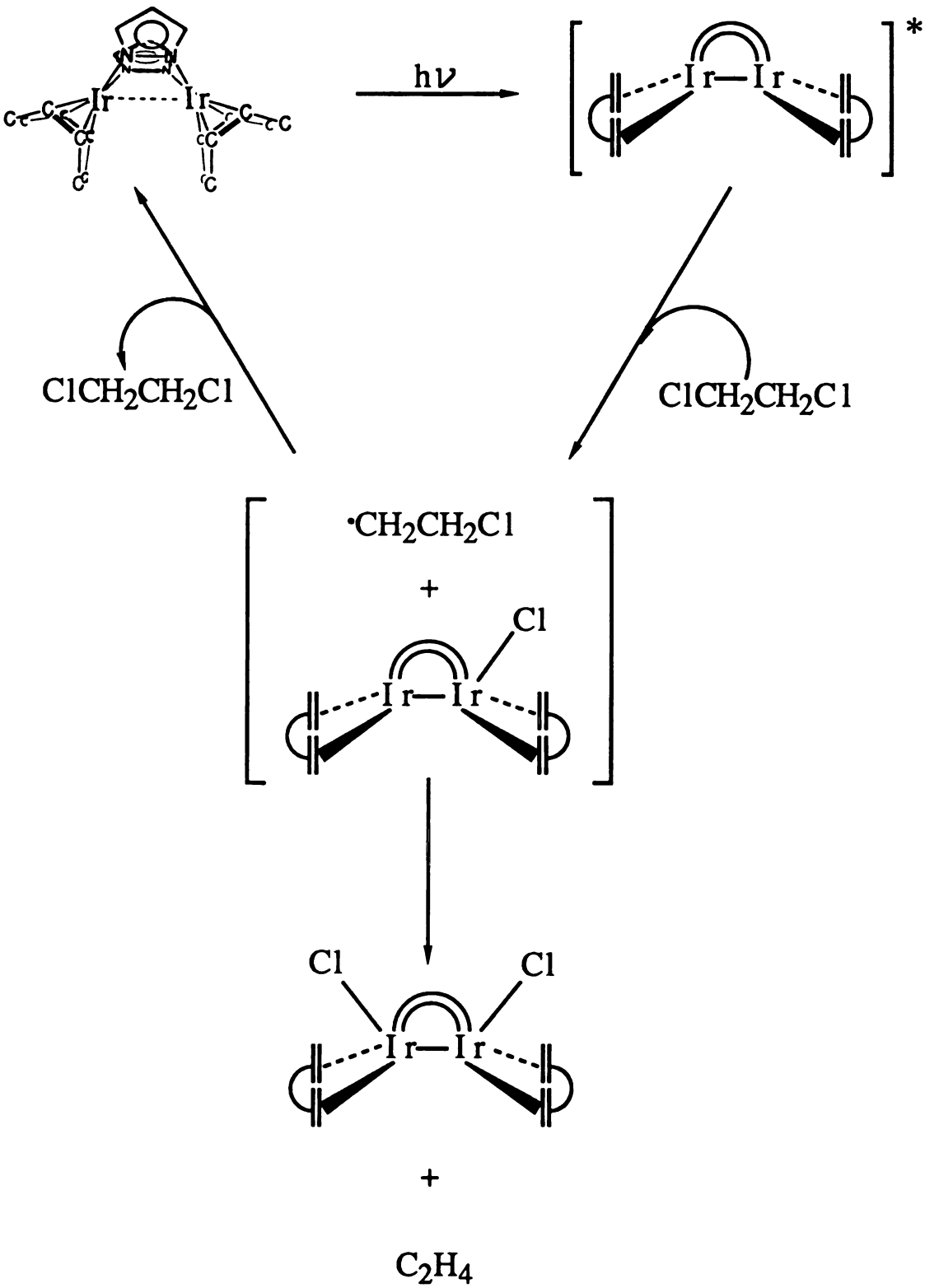

Figure 5

Figure 6. Bimolecular photoreaction pathways from a long-lived triplet excited state of an inorganic complex M. k_r, radiative decay rate; k_{nr}, nonradiative decay rate; and k_{isc}, intersystem crossing rate Bimolecular photoreaction pathways from long-lived triplet excited state of an inorganic complexes M. k_r, radiative decay rate; k_{nr}, non-radiative decay rate; k_{isc}, intersystem crossing rate.

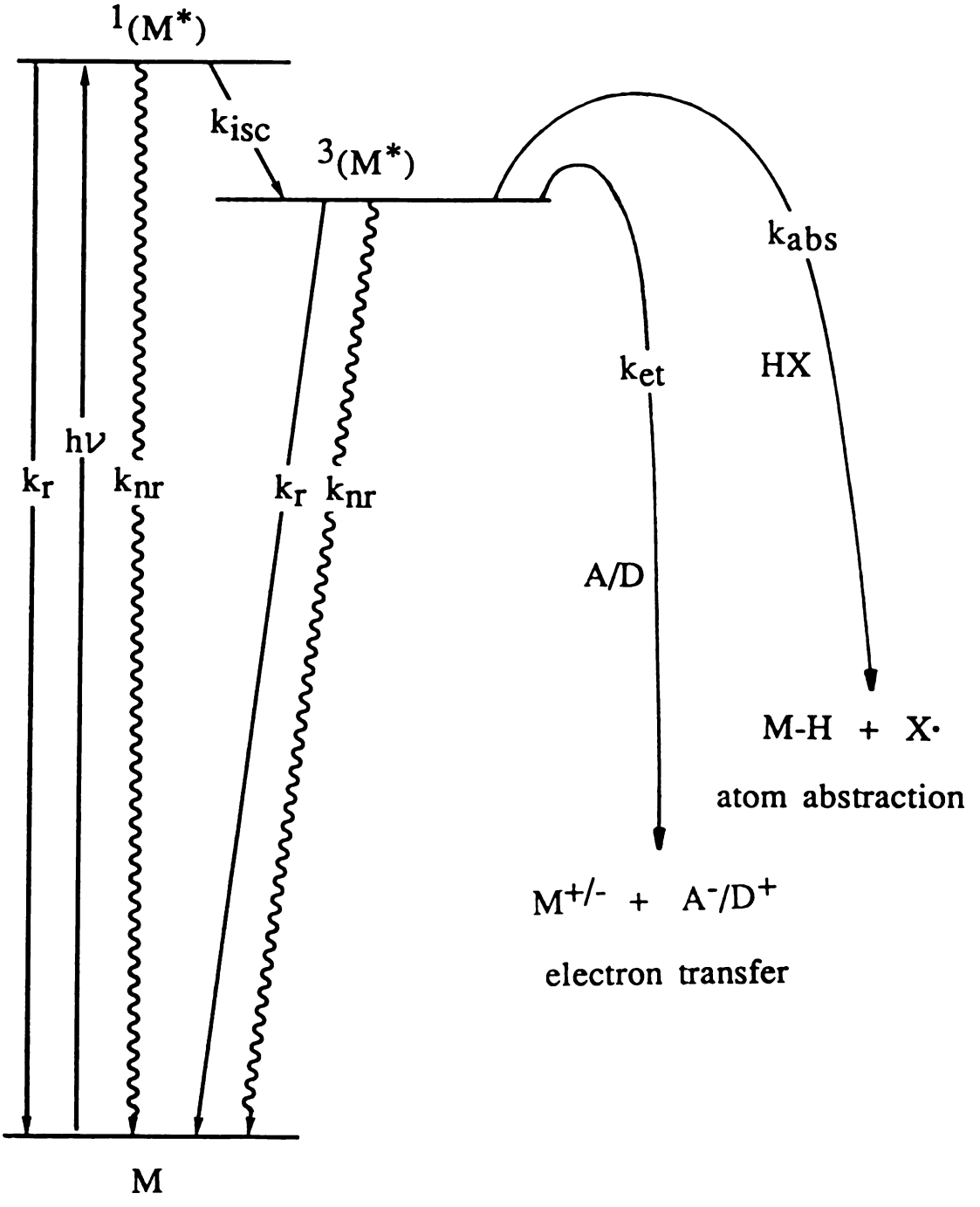
$^1(M^*)$
k_{isc}
$^3(M^*)$
k_{abs}
HX
k_{et}
$h\nu$
k_r
k_{nr}
k_r
k_{nr}
A/D
M-H + X·
atom abstraction
$M^{+/-}$ + A^-/D^+
electron transfer
M

Figure 6

products (Figure 7). Accordingly, spin considerations suggest that successful multielectron photoreagents will derive their reactivity from singlet electronic excited states. The successful development of singlet excited state chemistry, however, will require that intersystem crossing from the singlet state to triplet state be inhibited. In addition a problem of equal significance in the development of singlet excited state chemistry is the short lifetimes of the photoactive state. Unlike triplet states which possess lifetimes from microseconds to milliseconds owing to the spin-forbiddeness of the relaxation process back to ground state, singlet state decay (fluorescence) is usually only a few nanoseconds or even shorter. These intrinsically short lifetimes do not permit the singlet excited state to easily participate in bimolecular reactions. It is undoubtedly these two features of singlet excited states that has inhibited their reactivity. Thus, a critical issue to this thesis is whether inorganic photosystems possessing lowest energy excited states of pure singlet character exist with lifetime long enough to permit bimolecular reactivity.

This question is addressed by beginning with multiply bonded metal-metal ($M^{\underline{n}}M$) dimers. Since their discovery in 1964, numerous $M^{\underline{4}}M$ complexes, comprised primarily of rhenium, chromium, molybdenum and tungsten metal cores with a variegated array of ligating systems, have been discovered primarily due to the efforts of Cotton and coworkers.[55] The prevalence of quadruply bonded metal complexes has stimulated numerous theoretical[56-63] and experimental[64-78] investigations directed toward elucidating their electronic structures.

Figure 7. Proposed bimolecular photoreaction pathways from a long-lived singlet excited state of an inorganic complex M'. The intersystem crossing rate, k_{isc}, is negligible for a large singlet-triplet energy gap.

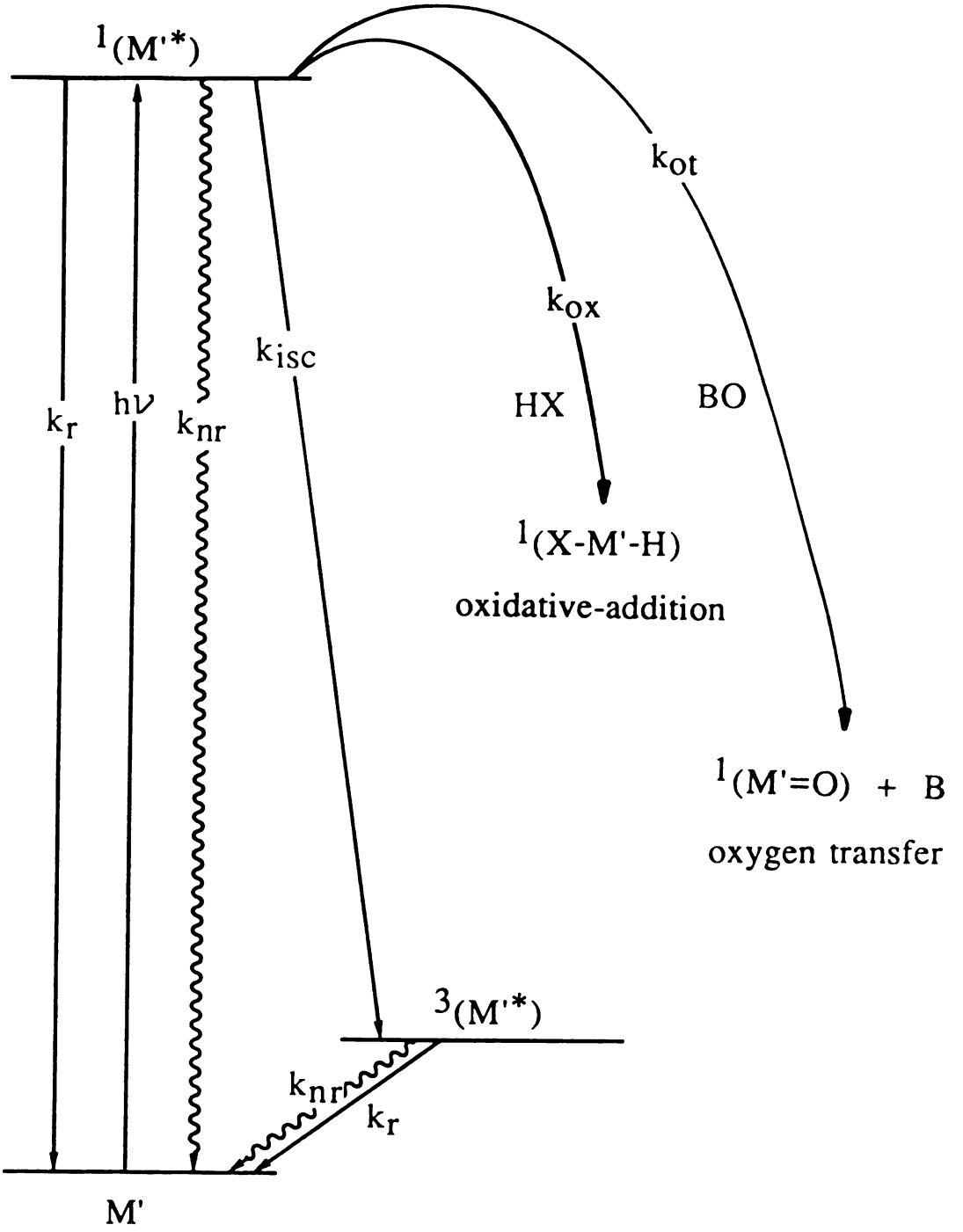
$^1(M'^*)$
k_{ot}
k_{ox}
k_{isc}
$h\nu$
k_r
k_{nr}
HX
BO
$^1(X\text{-}M'\text{-}H)$
oxidative-addition
$^1(M'=O)$ + B
oxygen transfer
$^3(M'^*)$
k_{nr}
k_r
M'

Figure 7

The general molecular orbital diagram depicted in Figure 8[65] has evolved from these studies. The metal-metal bonding in L_4MML_4 quadruply bonded dimers is most easily derived from a MM core ($D_{\infty h}$ symmetry) in which the z axis of a right-handed Cartesian coordinate system is chosen to lie along the metal-metal axis. Linear combinations of the d_{z^2}, (d_{xz}, d_{yz}), and ($d_{x^2-y^2}$, d_{xy}) atomic orbitals on each metal produce bonding and antibonding molecular orbitals of σ, π, and δ symmetries, respectively. The π and δ molecular orbitals are each doubly degenerate in a $D_{\infty h}$ point group. From the nodal theorem and atomic orbital overlap considerations, the molecular orbital energy ordering of the diatomic MM core shown in Figure 8 is obtained. The equidistant positioning of eight ligands in a L_4MML_4 complex perturbs the bonding of the diatomic metal core by lowering the symmetry of the system to D_{4h}, thus, splitting the δ orbital degeneracy. By definition of the coordinate system in Figure 8, the ligands will lie along the x and y axes and their orbitals will overlap with $d_{x^2-y^2}$ as well as s, p_x, p_y (which are not shown in Figure 8) to form its four metal-ligand bonds. The linear combination of the ligand and metal $d_{x^2-y^2}$ orbitals produces $\delta(b_{1g})$ and $\delta^*(b_{2u})$ molecular orbitals which are essentially metal-ligand σ antibonding in character. This antibonding interaction causes the energies of these orbitals to increase dramatically in energy. The energies of the σ, π, and $\delta(d_{xy})$ molecular orbitals, for the most part, are unperturbed as the ligands approach the metal core and the L_4MML_4 molecular orbital diagram for D_{4h} symmetry shown in Figure 8 is obtained. Additionally, the characteristic properties of a diamagnetic ground

Figure 8. Relative energies of the d-derived molecular orbitals in $D_{\infty h}$ M_2 and in a D_{4h} M_2L_8 complex. The ground state of the d^4-d^4 M_2L_8 complex is $^1A_{1g}$ ($\sigma^2\pi^4\delta^2$).

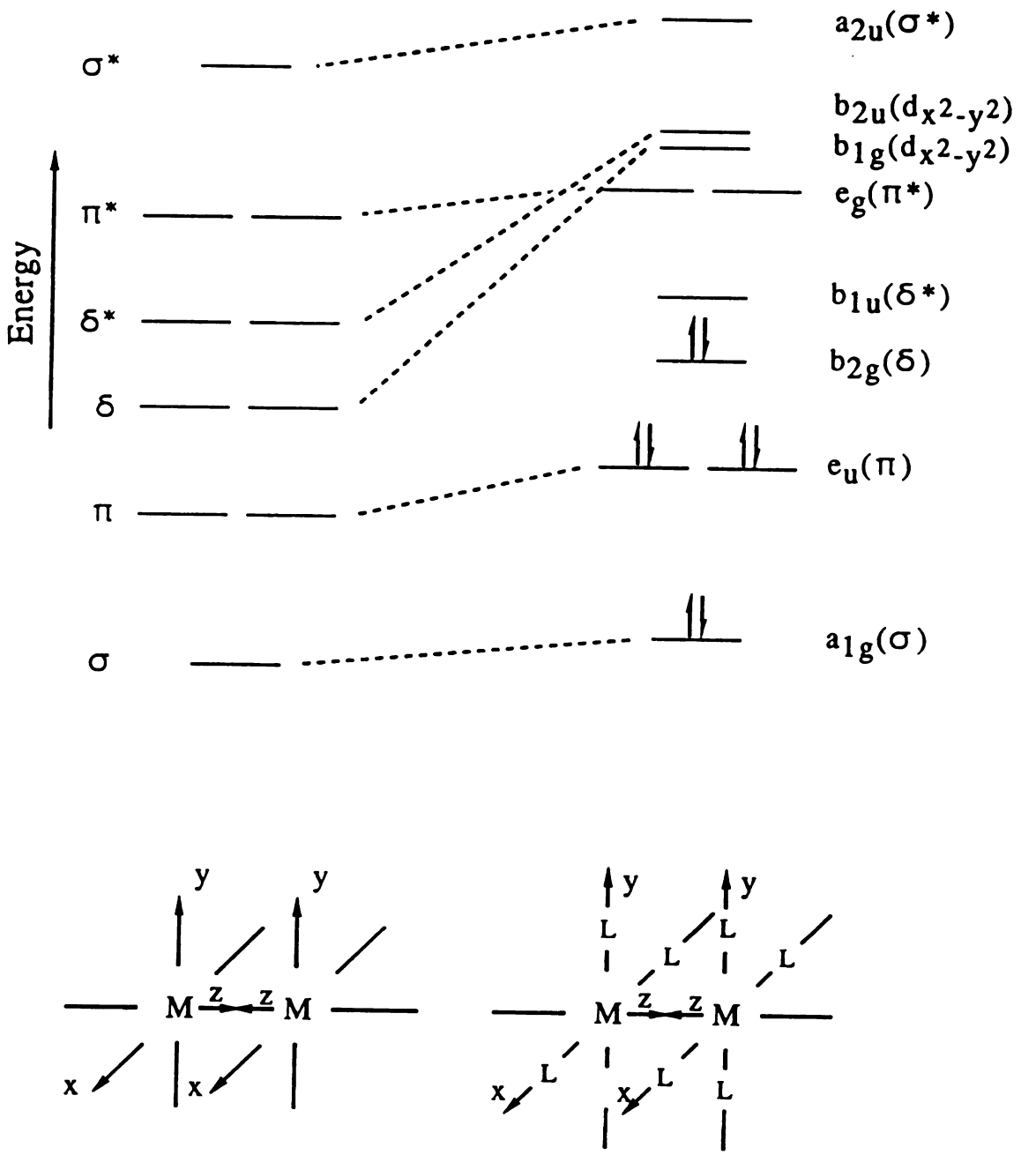
Energy
σ*
π*
δ*
δ
π
σ
a2u(σ*)
b2u(dx2-y2)
b1g(dx2-y2)
eg(π*)
b1u(δ*)
b2g(δ)
eu(π)
a1g(σ)
y
y
M
z
z
M
x
x
L
L
L
L
L
L
L

Figure 8

state, eclipsed ligand geometry (which is necessary for d_{xy} overlap), and exceptionally short metal-metal bond exhibited by quadruply bonded complexes are also explained by this bonding scheme.

According to this simple molecular orbital picture, the lowest energy transition arises from the promotion of an electron from the δ to δ^* molecular orbital. Polarized electronic absorption spectroscopic investigations of various quadruply bonded metal complexes verify that the lowest energy absorption corresponds to the $\delta^2 \rightarrow \delta\delta^*$ transition thereby confirming molecular orbital predictions.[65,68a,69]

Though conceptually quite appealing, the molecular orbital model does not provide an accurate quantitative picture of the electronic structure of quadruply bonded metal dimers, especially in terms of δ bonding. The poor overlap of the d_{xy} orbitals involved in δ bonding suggests that a valence bond description of the electrons in these orbitals would be more appropriate. Such an approach was used in an *ab initio* calculation of the $Re_2Cl_8^{2-}$ electronic structure.[58] Some of the results of which are outlined in Table 1. In the valence bond model, the $^1A_{1g}$ ground state has one electron in each d_{xy} orbital. At slightly higher energy (0.4 eV) is the $^3A_{2u}$ excited state, which still has one electron in each d_{xy} orbital, though now triplet paired. This state correlates with the $^3(\delta\delta^*)$ excited state of the molecular orbital model. Lying much higher in energy are two ionic singlet excited states that arise from antisymmetric ($^1A_{2u}$, 1.8 eV) and symmetric ($^1A_{1g}$, 2.2 eV) combinations of configurations with both d_{xy} electrons on one metal center. These two states correlate with the $^1(\delta\delta^*)$ and $^1(\delta^{*2})$

Table 1. State Orderings in d^4-d^4 Complexes: $[Re_2Cl_8]^{2-}$

E^a/eV	States
2.6	$^3A_{2u}(\pi\pi^*)$
2.6	$^1E_g(\pi\delta^*)$
2.2	$^1A_{1g}(\delta^*\delta^*)$: $^1[(xy_A)(xy_A) + (xy_Bxy_B)]$
1.8	$^1A_{2u}(\delta\delta^*)$: $^1[(xy_A)(xy_A) - (xy_Bxy_B)]$
1.8	$^3E_g(\pi\delta^*)$
0.4	$^3A_{2u}(\delta\delta^*)$: $^3[(xy_A)(xy_B)]$
0.0	$^1A_{1g}(\delta\delta)$: $^1[(xy_A)(xy_B)]$

[a] Reference 58.

molecular orbital configurations, respectively. An important feature of this model is that it predicts a large $^1A_{2u} \rightarrow {}^3A_{2u}$ energy gap and a relatively small separation between the $^1A_{1g}$ ground state and the $^3A_{2u}$ level. This prediction is consistent with energy gaps estimated from magnetic susceptibility measurements of M$\overset{4}{—}$M complexes.[79] Within this manifold of four states, the only spin and dipole allowed transition from the $^1A_{1g}$ ground state is to the $^1A_{2u}$ excited state. This effectively corresponds to a metal-metal charge transfer (MMCT) transition and correlates with $^1(\delta^2) \rightarrow {}^1(\delta\delta^*)$ excitation. On the basis of this valence bond model, the large $^1(\delta\delta^*)$-$^3(\delta\delta^*)$ energy gap should inhibit intersystem crossing and consequently the $\delta\delta^*$ excited state produced upon excitation should be of pure singlet character. This prediction has been verified by several experimental studies. The good 0-0 overlap between the absorption and emission spectra of M$\overset{4}{—}$M dimers at low temperature shows that the long-lived excited states (τ ~ 100 ns)[80-82] of quadruply bonded metal dimers directly correspond to the $^1(\delta\delta^*)$ excited state.[65,81] Moreover, the long lived excited state is not quenched by typical triplet energy transfer acceptor molecules,[83] thereby further verifying the singlet character of the $\delta\delta^*$emissive state

Besides these unique long-lived singlet excited states, the quadruply bonded metal dimers possess many other features that presage their utility as polynuclear multielectron photoreagents. First, the longevity of the $\delta\delta^*$ excited state should permit the electronically excited metal complex to participate in bimolecular reactions. Secondly, M$\overset{4}{—}$M complexes should be capable of maintaining their structural integrity upon irradiation. Theoretical

estimates predict the overall energetic contribution of the δ bond to the metal-metal bond energy to be less than 10%.[58] Irradiation of the $\delta^2 \rightarrow \delta\delta^*$ transition will, therefore, only slightly weaken the metal bond and photoinduced metal-metal bond cleavage reactions will be excluded in these complexes. Third, the multiple metal-metal bond may act as an electron source or sink in multielectron transfer reactions while maintaining a strong metal-metal interaction. Walton and coworkers have prepared a series of L_4MML_4 triply bonded metal complexes with $\sigma^2\pi^4\delta^2\delta^{*2}$ ground state electronic configurations.[84-86] In all cases investigated, these compounds exhibit facile one electron oxidation. The absence of the δ bond in $\sigma^2\pi^4\delta^2\delta^{*2}$ triply bonded complexes does not greatly perturb the L_4MML_4 structural unit as evidenced by the crystal structures of $Re_2Cl_4(PhPMe_2)_4^{n+}$ (n = 0, 1 ,2) complexes which show only slightly shortened Re-Re bond distances (r(Re-Re) of $Re_2Cl_4(PhPMe_2)_4^{n+}$, n = 0, 1, 2 is 2.241(1)Å, 2.218(1)Å and 2.215(2)Å, respectively).[87] The ability of the multiple metal-metal bond to undergo only minor structural reorganization upon changes in δ and δ^* occupancies may greatly facilitate the photoredox chemistry of quadruply bonded metal complexes. Fourth, the metal-metal core is coordinatively unsaturated and substrates may readily add to the redox-active metal center.[88-90] Finally, the lowest energy $\delta^2 \rightarrow \delta\delta^*$ transition falls in the visible spectral region, and low energy photochemistry is therefore possible.

It is rather surprising that the photochemistry of these systems has virtually been ignored in view of the attractive photochemical properties of quadruply bonded metal complexes. Most

photochemical studies to date have been confined to high energy reaction pathways. The $Re_2Cl_8^{2-}$ [91] and $Mo_2Cl_4(PBu_3)_4$ [92] dimers exhibit solvent assisted metal-metal bond cleavage chemistry upon UV irradiation. More generally, however, the metal-metal bond is retained and UV irradiation of $M\overset{4}{-}M$ dimers in acidic solutions results in photooxidation as shown by the following equations,[93-95]

$$Mo_2(SO_4)_4^{4-} + H^+ \xrightarrow{h\nu} Mo_2(SO_4)_4^{3-} + 1/2\ H_2 \quad (13)$$

$$Mo_{2(aq)}^{4+} + 2H^+ \xrightarrow{h\nu} Mo_{2(aq)}(\mu\text{-}OH)_2^{4+} + H_2 \quad (14)$$

$$Mo_2Cl_8^{4-} + H^+ \xrightarrow{h\nu \text{ or } \Delta} Mo_2Cl_8H^{3-} \quad (15a)$$

$$Mo_2Cl_8H^{3-} + H^+ + Cl^- \longrightarrow Mo_2Cl_9^{3-} + H_2 \quad (15b)$$

Photochemistry of $M\overset{4}{-}M$ dimers promoted by visible light has only recently been observed. Dichloromethane or acetonitrile solutions of $Re_2Cl_8^{2-}$ can be photooxiditized (λ_{exc} > 600 nm) to the confacial bioctahedral, $Re_2Cl_9^-$, in the presence of electron acceptors TCNE (tetracyanoethylene) or DDQ (2,3-dichloro-5,6-dicyano-1,4-benzo-quinone) and chloride ion.[96] However, the photochemistry basically entails simple one-electron quenching of the $Re_2Cl_8^{2-}$ excited state to yield $Re_2Cl_9^-$ followed by trapping by chloride ion.

In view of the potentially rich multielectron photochemistry of $M\overset{4}{-}M$ dimers, studies aimed at the systematic development of $^1(\delta\delta^*)$ excited state chemistry were undertaken. A prerequisite for elucidating the photochemistry of $M\overset{4}{-}M$ dimers is a clear

understanding of their excited state dynamics. Accordingly, time-resolved picosecond laser spectroscopic studies of $Mo_2X_4L_4$ and $Mo_2Cl_4(LL)_2$ (where X = Cl, Br, I; L and LL = mono- and bi-dentate phosphine ligand) dimers were performed at Brookhaven National Laboratory. Transient absorption and kinetics results of these studies will presented in Chapter III, along with a discussion of the excited state properties. Chapter IV describes our initial efforts to develop multielectron transformations by quenching reactive hydrides from $M\overset{4}{-}M$ dimers. Investigations of the spectroscopy, electrochemistry and the photoinduced two-electron transfer chemistry of $Mo_2(HPO_4)_4^{n-}$ (n = 2, 3, 4) in acidic solution are presented. An important result of this work was the discovery that protons efficiently quench $^1(\delta\delta^*)$ excited states of $M\overset{4}{-}M$ dimers thereby circumventing multielectron reactivity. Accordingly, Chapter V describes studies focussed on the photochemistry of quadruply bonded Mo_2(II,II) diphenyl phosphate in non-aqueous solutions. The first observations of multielectron chemistry of $M\overset{4}{-}M$ dimers promoted by visible light are presented. Specifically, two-electron photoreductions of organic substrates are effected upon irradiation of nonaqueous solutions containing $Mo_2(O_2P(OC_6H_5)_2)_4$ with wavelengths greater than 500 nm.

CHAPTER II

EXPERIMENTAL

A. Syntheses

1. General Procedures. Synthesis of all complexes were performed by using standard Schlenk-line techniques. All chemicals were reagent grade and were used as received unless otherwise noted. Solvents were rigorously deoxygenated and dried prior to use. For previously prepared compounds, electronic absorption spectroscopy, cyclic voltammetry and NMR (when previously reported) were employed for characterization. The details for characterization of new compounds are presented with the discussion on the preparative method.

2. Syntheses of Dimolybdenum Complexes.

a. $Mo_2(O_2CCH_3)_4$.[97] Molybdenum acetate, the starting compound for most quadruply bonded dimolybdenum species, was prepared by refluxing 10 g of $Mo(CO)_6$ (37.9 mmole) (Aldrich Chemical Co.) in 250 ml of *o*-dichlorobenzene which contained 30 ml of CH_3COOH and 10 ml of $(CH_3CO)_2O$. The solution was refluxed for 5

h. The needle-shaped, yellow crystals which formed with cooling on the sides of the round bottom flask were filtered and washed by Et_2O three times, dried, and stored under vacuum. Molybdenum acetate is fairly air-stable but will decompose if exposed to air longer than one week.

b. $K_4Mo_2Cl_8$.[98] Potassium chloride (6 g, 80 mmole) was added to 200 ml of 12 M HCl(aq) with stirring. The solution immediately changed from yellow to red upon the addition of 5 g of $Mo_2(O_2CCH_3)_4$ (11.7 mmole). After 1 h of stirring, a bright red precipitate was collected, washed with EtOH (0 ^oC) and Et_2O, and then dried under vacuum. Similar to $Mo_2(O_2CCH_3)_4$, $K_4Mo_2Cl_8$ is fairly air-stable.

c. $(NH_4)_5Mo_2Cl_9 \cdot H_2O$.[99] The ammonium salt of $Mo_2Cl_8^{4-}$ was prepared by the same procedures as used for the preparation of $K_4Mo_2Cl_8$, except 4 g of NH_4Cl (76 mmole) was used instead of KCl. A reddish-purple solid precipitated after 1 h of stirring. The solid was collected, washed three times with Et_2O and dried under vacuum.

d. $Cs_3Mo_2Br_8$.[100] A 100 ml 48% HBr(aq) solution containing 1 g of $Mo_2(O_2CCH_3)_4$ (2.3 mmole) was heated to 60 ^oC for 1 h, after which 2.5 g of CsBr in 50 ml of 48% HBr(aq) was added with stirring. The yellow-brown precipitate was collected by suction filtration, washed in succession with EtOH and Et_2O, and dried under vacuum. The solid is air-stable.

e. $Mo_2Cl_4(PMe_3)_4$.[101,81] Dimolybdenum chlorophosphine was prepared by either of two methods: (1) 0.5 g of $(NH_4)_5Mo_2Cl_9 \cdot H_2O$ (0.807 mmole) was added to 50 ml of a premixed MeOH solution which contained 0.32 ml (3.23 mmole) of PMe_3 (Strem chemicals). The final solution was stirred for 3 days, during which the color of the solution slowly changed from red to purple. The purple solid, which formed on the sides of the flask over this period, was collected by suction filtration, washed with 5 ml of H_2O to dissolve unreacted $(NH_4)_5Mo_2Cl_9 \cdot H_2O$, and finally washed three times with 10 ml aliquots of MeOH. The compound was dried and stored under vacuum. (2) The second method employed $Mo_2(O_2CCH_3)_4$ as a starting material. To 40 ml of THF, 0.5 g of $Mo_2(O_2CCH_3)_4$ (1.17 mmole) was dissolved. Under an argon counterflow, 0.59 ml (4.65 mmole) of Me_3SiCl (Aldrich Chemical Co.) and 0.47 ml of PMe_3 (4.74 mmole) were added separately by syringe. The blue solution was refluxed for 10 h. The blue residue collected from removing solvent from the reacted solution was column chromatographed on Florasil by using CH_2Cl_2 as the eluting solvent. The first blue band was collected, and the solvent was removed under vacuum to produce a blue solid. Compound produced by each of these methods exhibit identical properties. Absorption show strong absorption bands at 583 and 325 nm (ϵ = 3110, 3350 M^{-1} cm^{-1}, respectively) and a weak band at 440 nm (ϵ = 200 M^{-1} cm^{-1}). $Mo_2Cl_4(PMe_3)_4$ is air-sensitive and decomposes in 1 h when solid compound is exposed to air. Solutions of the dimer decompose within minutes.

f. $Mo_2Cl_4(PBu_3)_4$.[102] This dimer is most easily prepared by Method 1 of Section A.2.e : 0.5 g of $(NH_4)_5Mo_2Cl_9 \cdot H_2O$ (0.807 mmole) was added to 40 ml of a pre-mixed MeOH solution containing 0.81 ml of PBu_3 (3.25 mmole) (Aldrich Chemical Co.). The purple solution was refluxed for 3 h to yield purple crystals which were collected by suction filtration, and washed with 5 ml of H_2O to remove unreacted $(NH_4)_5Mo_2Cl_9 \cdot H_2O$. The purified solid was subsequently washed with MeOH and Et_2O, dried, and stored under vacuum. $Mo_2Cl_4(PBu_3)_4$ decomposes in air within few minutes. In CH_2Cl_2 solution, $Mo_2Cl_4(PBu_3)_4$ exhibits three strong absorption bands at 588, 330 and 287 nm (ε= 3150, 3820, 3050 $M^{-1}\ cm^{-1}$, respectively), and a weak band at 454 nm (ε = 260 $M^{-1}\ cm^{-1}$).

g. $Mo_2Br_4(PBu_3)_4$.[100] A 30 ml MeOH solution containing 0.5 g of $Cs_3Mo_2Br_8$ (0.407 mmole) and 0.405 ml of PBu_3 (1.63 mmole) was stirred for 3 h. The deep blue crystals, which formed during stirring, were collected, washed with H_2O, EtOH and Et_2O and then dried and stored under vacuum. This air-sensitive complex exhibits two strong absorption bands at 600 and 352 nm and two weak bands at 485 and 460 nm (ε = 3520, 5130, 210, and 162 $M^{-1}\ cm^{-1}$, respectively).

h. $Mo_2I_4(PBu_3)_4$. Procedures analogous to those described for the synthesis of $Mo_2Cl_4(PMe_3)_4$ by Method 2 were employed. A 40 ml THF solution charged with 0.5 g of $Mo_2(O_2CCH_3)_4$ (1.17 mmole), 0.67 ml (4.7 mmole) of Me_3SiI (Aldrich Chemical Co.) and 1.17 ml of PBu_3 (4.7 mmole) was refluxed for 16 h.

The residue, collected by pumping the reacted solution to dryness, was purified with chromatographic procedures identical to those previously described (Section A.2.e). This air-sensitive compound strongly absorbs at 590 nm.

i. **$Mo_2Cl_4(dppm)_2$.**[103] 0.77 g (2.0 mmole) of dppm (dppm = Bis(diphenylphosphino)methane, Aldrich Chemical Co.) was added to 40 ml of MeOH which contained 0.5 g of $(NH_4)_5Mo_2Cl_9 \cdot H_2O$ (0.807 mmole) to yield a blue-green solution. This solution was refluxed for 3 h. The blue crystals, formed during refluxing, were collected by suction filtration, and consecutively washed with H_2O, EtOH and Et_2O. The blue solid is air-stable but in solution, it is air-sensitive, decomposing within an hour after exposure to air. Deoxygenated CH_2Cl_2 solutions of $Mo_2Cl_4(dppm)_2$ exhibit two strong absorption bands at 634 nm (ϵ = 2490 M^{-1} cm^{-1}) and 325 nm (ϵ = 5600 M^{-1} cm^{-1}) and a weak band at 462 nm (ϵ = 900 M^{-1} cm^{-1}).

j. **$Mo_2Cl_4(dmpm)_2$.**[107] 0.5 g of $(NH_4)_5Mo_2Cl_9 \cdot H_2O$ (0.807 mmole) and 0.26 ml (1.63 mmole) of dmpm (dmpm = bis(dimethylphosphino)methane, Strem Chemicals) were reacted in 40 ml of MeOH solution following a procedure analogous to that used for the preparation of $Mo_2Cl_4(dppm)_2$. $Mo_2Cl_4(dmpm)_2$ is an air-sensitive compound, and in CH_2Cl_2 solutions, exhibits two absorption bands at 604 nm (ϵ = 1730 M^{-1} cm^{-1}) and 426 nm (ϵ = 270 M^{-1} cm^{-1}). ^1H NMR: 1.51(s), 3.08(p) (J_{H-P} = 5.1 Hz).

k. $Mo_2Cl_4(dppe)_2$.[103,105] This dimer is prepared by refluxing a 40 ml THF solution charged with 0.5 g of $Mo_2(O_2CCH_3)_4$ (0.17 mmole), 0.59 ml of Me_3SiCl (4.65 mmole) and 0.96 g (2.4 mmole) of dppe (dppe = bis(diphenylphosphino)ethane, Aldrich Chemical Co.) for a minimum of 12 h. The solution changed from deep red to blue within 15 min, and then to mauve after 5 h of refluxing. The mauve precipitate was collected by suction filtration, and washed consecutively with H_2O, EtOH and Et_2O. $Mo_2Cl_4(dppe)_2$ is a very air-stable compound in both solid and solution forms. In CH_2Cl_2 solutions, the compound exhibits four electronic absorption bands at 762, 548, 469, and 345 nm (ε = 1030, 210, 780, and 8050 $M^{-1}\ cm^{-1}$, respectively)

l. $Mo_2Cl_4(dmpe)_2$.[106] This complex is prepared according to the previously described procedure for the synthesis of $Mo_2Cl_4(PMe_3)_4$ by Method 2. A 40 ml THF solution which contained 0.5 g of $Mo_2(O_2CCH_3)_4$ (1.17 mmole), 0.59 ml of Me_3SiCl (4.65 mmole) and 0.4 ml (2.4 mmole) of dmpe (dmpe = bis(dimethylphosphino)ethane, Aldrich Chemical Co.) was refluxed for 8 h. The volume of the final reddish-brown solution was slowly reduced to about 10 ml over 2 h by vacuum distillation. The reddish-brown crystals which formed during solvent evaporation were collected by suction filtration under a heavy argon flow. $Mo_2Cl_4(dmpe)_2$ is an air-sensitive compound which decomposes within an hour in air. The absorption spectrum of this dimer exhibits three weak bands at 803, 565, and 445 nm and a strong absorption at 345 nm (ε = 210, 190, 300, and 3200 $M^{-1}\ cm^{-1}$, respectively).

m. $Mo_2(HPO_4)_4^{4-}$ Anion. The Mo_2(II,II) phosphate complex was synthesized by ligand exchange reactions. Solutions of the dimer were prepared by three methods: (1) $K_4Mo_2Cl_8$ (0.1 g) was added to 10 ml of a 1 M H_3PO_4 solution and stirred under purified argon for 4 h; (2) 0.1 g of $K_4Mo_2(SO_4)_4$[107] was added with stirring to 2 M H_3PO_4 and allowed to react for 2 h; and (3) 1 ml of concentrated H_3PO_4 was added to 10 mM solution of Mo_2^{4+} [108] aquo dimer blanketed with argon. For each of these methods, a pink solution was obtained with a characteristic absorption band at 516 nm. Aqueous solutions of the dimer are extremely sensitive to oxygen decomposing within minutes to dark brown uncharacterized solutions. Even in the absence of oxygen, the quadruply bonded dimer slowly reacts over days to produce blue-gray solutions which exhibit a near-infrared absorption profile diagnostic of $Mo_2(HPO_4)_4^{3-}$ (vide infra). Solutions of the quadruple-bond dimer prepared by each of the three methods are contaminated inevitably with $Mo_2(HPO_4)_4^{3-}$, and accordingly, addition of K_2HPO_4 to any of the above solution yields solid $K_4Mo_2(HPO_4)_4$ contaminated with $K_3Mo_2(HPO_4)_4$. However, addition of zinc amalgam to these solutions smoothly converts $Mo_2(HPO_4)_4^{3-}$ to the quadruply bonded $Mo_2(HPO_4)_4^{4-}$ species, as evidenced by the disappearance of the near-infrared absorption band of $Mo_2(HPO_4)_4^{3-}$. In fact, stirring 2 M H_3PO_4 solutions of $K_3Mo_2(HPO_4)_4$ over zinc amalgam provides a convenient route to the preparation of pure $Mo_2(HPO_4)_4^{4-}$ solutions.

n. $K_3Mo_2(HPO_4)_4$. The potassium salt of $Mo_2(HPO_4)_4^{3-}$ was prepared from solutions of $Mo_2(HPO_4)_4^{4-}$. Addition of Pt foil (1

cm^2) to 25 ml of 1 M H_3PO_4 containing $Mo_2(HPO_4)_4^{4-}$ (0.4 mmole) quantitatively produces $Mo_2(HPO_4)_4^{3-}$ in 2 h. Dropwise addition of a saturated solution of K_2HPO_4 leads to the immediate precipitation of a fine blue-gray powder. The product was filtered under vacuum and washed with three 5 ml portions of 1 M H_3PO_4 at 0 °C. Aliquots for all washings were delivered by cannula. The solid was dried and stored under vacuum. Alternatively, a more facile route to the mixed-valence dimer involved the addition of 0.505 g of $K_4Mo_2Cl_8$ (0.800 mmole) to 15 ml of degassed 1 M H_3PO_4. After the solution was stirred at room temperature for 1 h under argon, 0.108 g of $K_2S_2O_8$ (0.400 mmole) was added to the solution via a sample charger. The red solution quickly turned blue, and a blue-gray powder precipitated from the solution. The solid was collected by using Schlenk-line techniques. Anal. Calcd (Found) for $K_3Mo_2H_4P_4O_{16}$: Mo, 27.68 (27.60). Solids and solutions of the mixed-valence dimer are sensitive to oxygen, but the compound is indefinitely stable under inert atmospheres.

o. $Py_3Mo_2(HPO_4)_4Cl$.[109] A solution of 2.5 ml 2 M H_3PO_4, charged with 0.1 g of $K_4Mo_2Cl_8$ (0.16 mmole), was slowly mixed with 0.3 g of pyridinium chloride (2.62 mmole) dissolved in 2.5 ml 2 M H_3PO_4. The mixture was allowed to stand in air and after 2-3 days, deep purple crystals had formed. A more facile synthesis of Mo_2(III,III) phosphate involved the use of $K_2S_2O_8$ (0.135 g, 0.5 mmole) as an oxidant which was added with stirring to 10 ml of a 1 M H_3PO_4 solution containing 0.316 g of $K_4Mo_2Cl_8$ (0.5 mmole). The solution turned from red to colorless to violet within minutes, and a

violet solid precipitated immediately after the addition of 0.202 g of CsCl (1.2 mmole) in 10 ml of 1 M H_3PO_4. The solid was collected by suction filtration under argon.

p. $Mo_2(O_2P(OC_6H_5)_2)_4$. The Mo_2(II,II) diphenyl phosphate was prepared by a simple ligand substitution reaction. The anion $(C_6H_5O)_2PO_2^-$ was generated by stirring 3.25 g of $(C_6H_5O)_2P(O)OH$ (13 mmole) with 0.702 g of NaOMe (13 mmole) in 60 ml of MeOH. After 10 min, 0.5 g of $(NH_4)_5Mo_2Cl_9 \cdot H_2O$ (0.807 mmole) was added to the above solution which was then heated to reflux for 3 h. A pink precipitate, formed during refluxing, was collected by suction filtration and washed with three 15 ml portions of MeOH. Aliquots for all washings were delivered by cannula. The solid was dried and stored under vacuum. Yield: 76%. Suitable crystals of $Mo_2(O_2P(OC_6H_5)_2)_4 \cdot 2THF$ for X-ray structural determination were obtained by layering a tetrahydrofuran solution of $Mo_2(O_2P(OC_6H_5)_2)_4$ with cyclohexane in a Schlenk tube. Anal. Calcd (Found) for $Mo_2C_{48}H_4O_{16}P_4 \cdot 2C_2H_8O$: Mo; 14.4 (14.87); P, 9.29 (9.17); C, 50.46 (49.93); H, 4.24 (4.15). This newly synthesized dimolybdenum diphenyl phosphate complex is extremely air-sensitive. It decomposes within seconds upon exposure to air. This dimer is not soluble in most organic solvents, but it exhibits fairly good solubilities in halogenated hydrocarbons and THF. A CH_2Cl_2 solution of $Mo_2(O_2P(OC_6H_5)_2)_4$ exhibits a moderate intensity band at 515 nm , which is very similar to $Mo_2(HPO_4)_4^{4-}$ in acidic solution.

q. $Mo_2(O_2P(OC_6H_5)_2)_4BF_4$. The mixed-valent Mo_2(II,III) diphenyl phosphate complex can be prepared by direct oxidation of the Mo_2(II,II) complex. 1.001 g (0.85 mmole) of $Mo_2(O_2P(OC_6H_5)_2)_4$ and 0.099 g (0.85 mmole) of $NOBF_4$ (Aldrich Chemical Co.) were rigorously stirred in 30 ml of CH_2Cl_2. After 45 min the solution changed from pink to green. The volume of solution was reduced to 10 ml by vacuum distillation, whereupon 50 ml of cyclohexane was added. A green precipitate formed immediately. The solid was collected by suction filtration. Anal. Calcd (Found) for $Mo_2C_{48}H_{40}O_{16}P_4BF_4$: C, 45.20 (41.23); H, 3.16 (3.15); P, 9.71 (9.33); F, 5.96 (6.13). Yield 85%. X-ray quality crystals were obtained by layering a dichloromethane solution of $Mo_2(O_2P(OC_6H_5)_2)_4BF_4$ with cyclohexane in a Schlenk tube. The Mo_2(II,III) diphenyl phosphate complex is not as air-sensitive as the corresponding Mo_2(II,II) dimer. Solid exposed to air is stable but not longer than 30 minutes. However, solutions of $Mo_2(O_2P(OC_6H_5)_2)_4$-BF_4 is very air-sensitive; both the solid and solution are thermally unstable, decomposing when heated higher than 80 ^oC.

B. Solvent Purification

1. Solvents Used for Syntheses. Hexane, cyclohexane and diethyl ether were refluxed over Na for no less than 6 h and freshly distilled prior to use. MeOH was also refluxed with Na. The amount of Na added to MeOH was 20% more than the amount required to react with the water contained in a freshly opened bottle (which can be calculated from the water content shown on the label of the bottle).

Benzene, toluene and tetrahydrofuran were refluxed with sodium and small amount of benzophenone to form the blue or purple ketyl radical. Halogenated hydrocarbons such as CH_2Cl_2, $ClCH_2CH_2Cl$, and CH_2Br_2 were refluxed over P_2O_5 for at least 6 h prior to use. Acetonitrile and acetone was purified by refluxing over CaH_2 and anhydrous $CaSO_4$, respectively.

2. High Purity Solvents. All solvents used for electrochemical, spectroscopic and photochemical experiments were purchased from Burdick and Jackson Laboratories (spectroscopic grade). Purified solvents were stored in glass containers which consisted of a 1 liter flask equipped with a Kontes high-vacuum valve. Dichloromethane, 1,2-dichloroethane and isopropanol were degassed by seven freeze-pump-thaw cycles and then vacuum distilled onto activated (heated to 250 ^{o}C under dynamic vacuum (10^{-6} torr) for 12 h) Linde 4 Å molecular sieve contained in the storage flask. Hexane, cyclohexane, and diethyl ether were also degassed by seven freeze-pump-thaw cycles and vacuum distilled onto sodium-potassium alloy. Tetrahydrofuran, benzene, and toluene, again after seven freeze-pump-thaw cycles were distilled into a flask containing sodium-potassium alloy with a small amount of benzophenone. The purple ketyl form of benzophenone formed over a two-day period. Acetonitrile was degassed by seven freeze-pump-thaw cycles and vacuum distilled onto activated Linde 3 Å molecular sieve.

C. Instrumentation and Methods

1. Absorption Spectroscopy. Absorption spectra were recorded with Cary 17D or Cary 2300 spectrophotometers. Extinction coefficients were determined by using high-vacuum cells consisting of a 1-cm quartz cuvette and a 10-ml side arm. These two chambers were separated by two Kontes high-vacuum quick-release teflon stopcocks. For measurements of molar absorptivity coefficients in nonaqueous solution, weighed samples were placed in the cuvette and isolated by the Kontes valve. The appropriate high purity solvent was transfered to the 10-ml side arm by bulb-to-bulb vacuum distillation, and three subsequent freeze-pump-thaw cycles were performed before mixing with the sample. After the absorption spectra was recorded, the solution were pipetted out of the cell and the volume was measured. For measurements in aqueous solutions, known volumes of phosphoric acid were pipetted into the side arm and subject to five freeze-pump-thaw cycles before mixing with weighed samples of solid $K_3Mo_2(HPO_4)_4$ contained in the cuvette cell. For $Mo_2(HPO_4)_4^{4-}$, known concentrations of $Mo_2(HPO_4)_4^{4-}$ were prepared by zinc amalgam reduction of $Mo_2(HPO_4)_4^{3-}$ solutions. Extinction coefficients were calculated from Beer-Lambert plots composed of at least seven points.

2. Steady-State Luminescence Spectroscopy. Emission spectra were recorded on an emission spectrometer constructed at Michigan State University. A detail description of the instrument is described in the doctoral thesis of Mark D. Newsham. Emission

quantum yields, were measured by using $Ru(bpy)_3(ClO_4)_2$ as the quantum yield standard (Φ_e = 0.042 in H_2O at 23 °C). The emission quantum yield was calculated with the following equation,[110]

$$\Phi_x = \Phi_r \times [A_r(\lambda_r)/A_x(\lambda_x)] \times [\eta_x^2/\eta_r^2] \times [D_x / D_r] \qquad (16)$$

where x and r designate the unknown and standard solutions, respectively, η is the average refractive index of the solution, D is the integrated area under the corrected emission spectrum, and $A(\lambda)$ is the absorbance/cm of the solution at the exciting wavelength λ.

3. Time-Resolved Laser Spectroscopy. Picosecond laser spectroscopic experiments were undertaken in Brookhaven National Laboratory. The instrumentation has previously been described.[111]

4. Magnetic Measurements. EPR spectra were recorded by using a Bruker ER 200D X-band spectrometer equipped with an Oxford ESR-9 liquid-helium cryostat. Magnetic fields were measured with a Bruker ER035M gaussmeter, and frequencies were measured with a Hewlett-Packard 5245L frequency counter. Magnetic susceptibility measurements were made with a SHE 800 series variable-temperature SQUID magnetometer.

5. Resonance Raman. Raman spectra were recorded with a Spex 1401 double monochromator and associated Ramalog electronics. A Spectra Physics 165 argon ion laser was the excitation source, and incident powers were 20-40 mW. All spectra were

collected at a 90^{o} scattering geometry from solid samples at room temperature.

6. Electrochemical Measurements. The oxidation-reduction potentials of dimolybdenum complexes were determined by cyclic voltammetry with a Princeton Applied Research (PAR) Model 173 potentiostat, Model 175 programmer, and a Model 179 digital coulometer. The output of the digital coulometer was fed directly into a Houston Instrument Model 2000 X-Y recorder. Cyclic voltammetry measurements of aqueous solutions were performed at room temperature by using a conventional H-cell design and a three-electrode system consisting of a polished glassy carbon working electrode (A = 0.08 cm^2), a Pt wire auxiliary electrode, and a saturated calomel reference electrode. For nonaqueous solutions, a three-electrode system was again used with a standard H-cell configuration. The working electrode was a Pt button, the auxiliary electrode was a Pt gauze, and a Ag wire served as an adequate reference potential. Ferrocene was used as an internal standard. Potentials were related to the SCE reference scale by using a ferrocenium-ferrocene couple of 0.307 V vs. SCE.[112]

7. Photochemistry. Sample irradiations were executed by using a Hanovia 1000-W Hg/Xe high-pressure lamp. The source for ultraviolet light at 254 nm was an Oriel 14W Hg/Ar low-pressure lamp. The beam was collimated and passed through a 10-cm circulating water filter. Photolysis experiments were performed in two-arm evacuable cells equipped with Kontes quick-release teflon

valves. Sample temperatures were thermostated at 15.0 ± 0.5 °C in all photoreactions. The photolysis experimental set-up is shown in Figure 9. Photolyses were accomplished by using Schott color glass high-energy cutoff filters to eliminate the unwanted higher energy light. For quantum yield measurements, excitation wavelengths were isolated by using interference filters with half-band widths of less than 10 nm at the given mercury line (e.g. 254, 313, 367, 405, 436, 546, 577 nm). All interference filters were purchased from Oriel Corporation. Quantum yields were determined with the following expression

$$\Phi_\lambda = [\, n_p/t \,] \;/\; [\, I_o(\lambda)(1-10^{-A\lambda})/t \,] \qquad (17)$$

where n_p is the number of product molecules formed during photolysis, $I_o(\lambda)$ is the intensity of exciting light at wavelength λ, A_λ is the absorbance of reactants at the exciting wavelength λ, and t is the time of irradiation.[113] $I_o(\lambda)$, determined by using the ferrioxalate actinometer,

$$[Fe(C_2O_4)_3]^{3-} \xrightarrow{h\nu} [Fe(C_2O_4)_2]^{2-} + 2CO_2 \qquad (18)$$

follows directly from,

$$I_o(\lambda) = n_{Fe^{2+}} \;/\; [\, (1-10^{-A\lambda}) \times \Phi_\lambda \times t \,] \qquad (19)$$

where A_λ is the absorbance of ferrioxalate at exciting wavelength λ, Φ_λ is the actinometer's quantum yield at λ (listed in Table 2), t is

Figure 9. Experimental apparatus for typical photolysis.

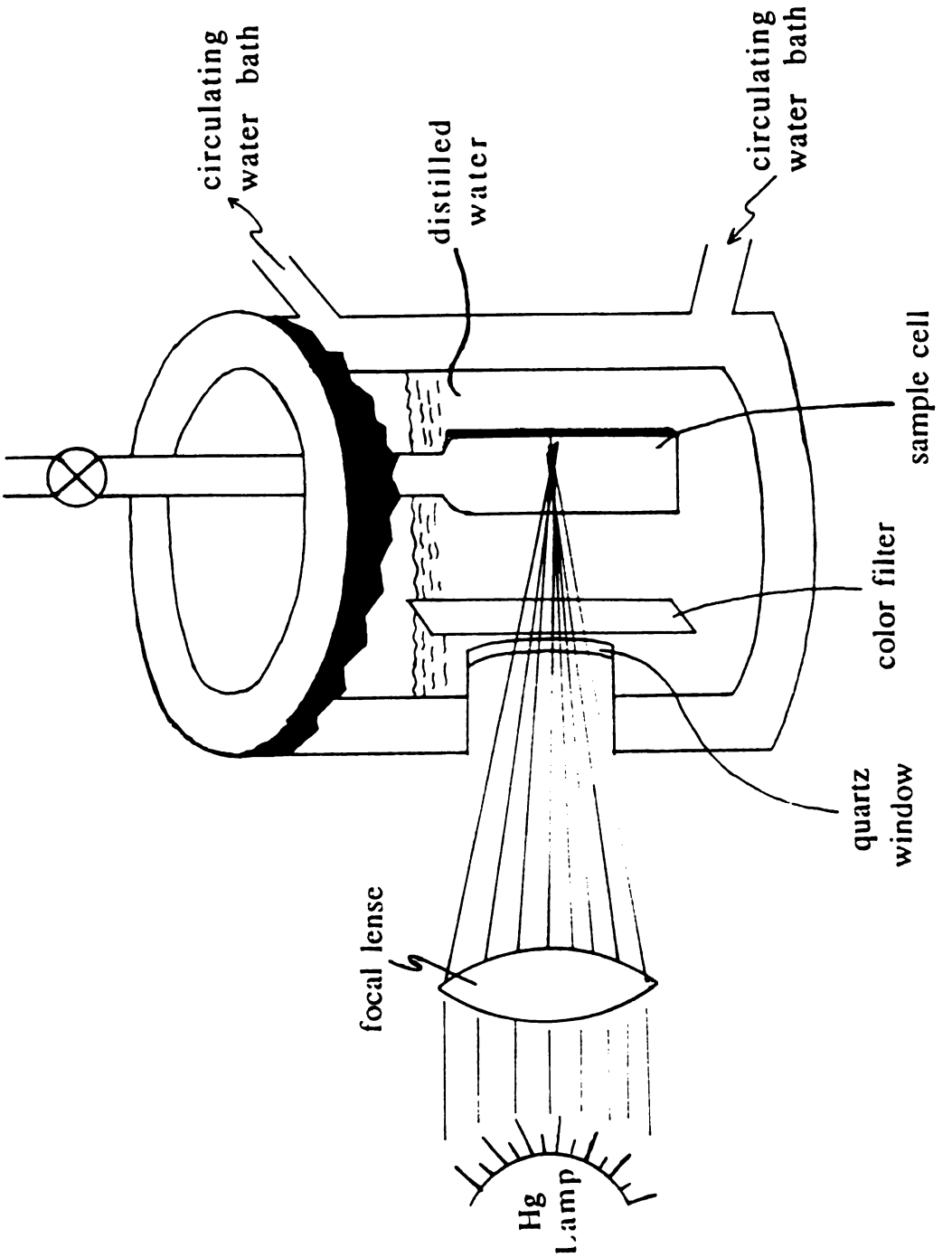
circulating water bath
distilled water
circulating water bath
sample cell
color filter
quartz window
focal lense
Hg Lamp

Figure 9

Table 2. Quantum Yield Data[a] for Ferrioxalate Photoreaction.

λ /nm	$[K_3Fe(C_2O_4)_3]$/M	$\Phi_{Fe}2+$
577	0.15	0.013
546	0.15	0.15
436	0.15	1.01
405	0.006	1.14
367	0.006	1.21
313	0.006	1.24
254	0.006	1.25

[a] Reference 113.

the time for irradiation, and $n_{Fe^{2+}}$ is the number of Fe^{2+} ions formed. Analysis of Fe^{2+} ion is most easily accomplished by complexing the ion with 1,10-phenanthroline. The complexed Fe^{2+} species absorbs strongly at 510 nm ($\epsilon = 1.11\times10^{-4}$ M^{-1} cm^{-1}) in water. $n_{Fe^{2+}}$ is calculated directly from,

$$n_{Fe^{2+}} = [\ 6.023\times10^{20}\times V_1\times V_3\times A_{Fe^{2+}}\ ] / [\ V_2 \times \epsilon_{Fe^{2+}}\ ] \qquad (20)$$

where V_1 is the volume of the actinometer (ml), V_2 is the volume of the aliquot withdrawn for analysis (ml), V_3 is the final volume to which aliquot V_2 is diluted (ml), $A_{Fe^{2+}}$ is the absorbance of ferrous phenanthroline at 510 nm, and $\epsilon_{Fe^{2+}}$ is its molar extinction coefficient.[114] Quantum yields of multiply bonded molybdenum dimers were computed by reexpressing eq. (17) as follows,

$$\Phi_\lambda = [\ \Delta A \times V\times 6.023\times10^{20}\ ] / [\ \epsilon \times I_0\times (1-10^{-A\lambda}) \times t\ ] \qquad (21)$$

where ΔA is the change of absorbance at the monitoring wavelength (1438 nm for $Mo_2(HPO_4)_4^{3-}$ and 516 nm for $Mo_2(O_2P(OC_6H_5)_2)_4$), V is the volume of irradiated solution in ml, ϵ is the molar extinction coefficient of the monitored absorption band (180 and 156 M^{-1} cm^{-1} for $Mo_2(HPO_4)_4^{3-}$ and $Mo_2(O_2P(OC_6H_5)_2)_4$, respectively), A_λ is the absorbance of reactants at excitation wavelength λ, and t is the time employed for photolysis. In quantum yield measurements, the excitation procedures for standard and unknown have to be identical. Therefore, the special photolysis train, shown in

Figure 10, was designed to ensure that the required reproducibility was attained.

8. Gas Analysis. Gas produced from photoreactions was qualitatively identified by gas chromatographic analyses. A Hewlett-Packard 5710A gas chromatograph equipped with a 100/200 carbosieve S-II column and FID detector was employed for GC measurements. Quantitative determination of the gas evolved was made by Toepler pumping the gas above reacted solutions through two traps (liquid-nitrogen traps for hydrogen measurements, and pentane/$N_{2(l)}$ traps for ethylene measurements) into a calibrated volume and manometrically measuring the pressure.

D. Crystal Structure Determinations

1. General Procedures. Crystal structure determinations were performed by Dr. Donald L. Ward of the X-ray Crystal Structure Facility at Michigan State University. Preliminary examination and data collection were performed with Mo Kα radiation (λ = 0.71073Å) on a Nicolet P3F diffractometer. All calculations were performed on a VAX 11/750 computer by using SDP/VAX.[114]

2. $Mo_2(O_2P(OC_6H_5)_2)_4 \cdot 2THF$.

a. Data Collection. A dark purple prismatic crystal of tetrakis(diphenyl phosphate)dimolybdenum, $Mo_2(O_2P(OC_6H_5)_2)_4$, having approximate dimensions of 0.40 x 0.40 x 0.68 mm, was

Figure 10. Experimental apparatus for photoreaction quantum yield measurements.

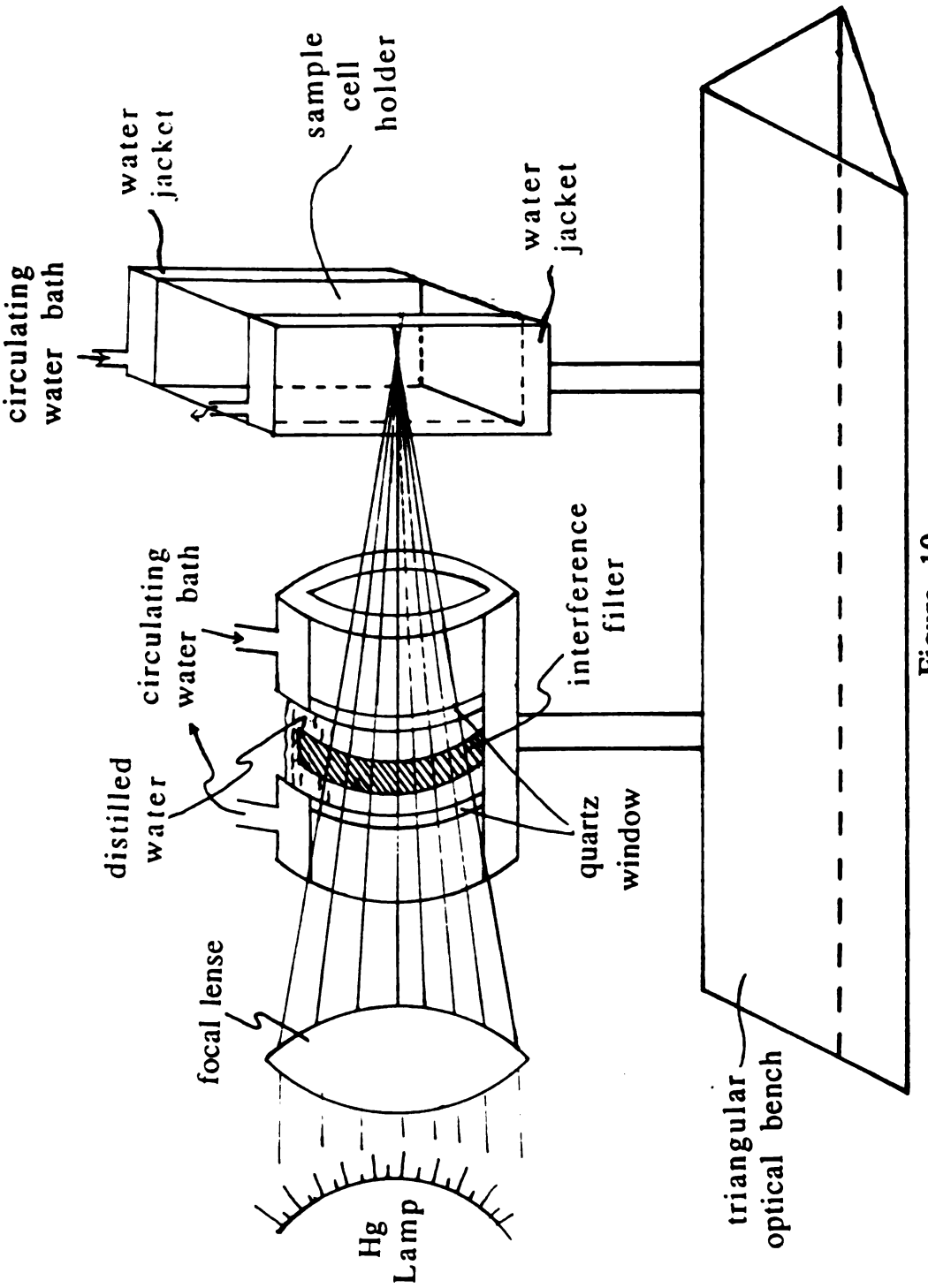
circulating water bath
water jacket
sample cell holder
water jacket
circulating water bath
distilled water
interference filter
quartz window
focal lense
Hg Lamp
triangular optical bench

Figure 10

mounted in a glass capillary with its long axis roughly parallel to the φ axis of the goiniometer.

Cell constants and an orientation matrix for data collection were obtained from least-squares refinement, by using the setting angles of 17 reflections in the range $15 < 2\Theta < 20^{o}$. The monoclinic cell parameters and calculated volume are: a = 13.359(3), b = 29.641(15), c = 14.719(3)Å, $\beta = 93.43(2)^{o}$, V = 5818(6)Å^3. For Z = 4 the calculated density is 1.522 g/cm^3. As a check on crystal quality, omega scans of several intense reflections were measured; the width at half-height was 0.26^{o} with a take-off angle of 6.0^{o}, indicating good crystal quality. From the systematic absences of

$$0k0 \quad k = 2n \tag{22}$$

$$h0l \quad h+l = 2n \tag{23}$$

and from subsequent least-squares refinement, the space group was determined to be $P2_1/n$.

The data were collected at a temperature of 23(1) ^{o}C by using the ω scan technique. The scan rate was 4^{o}/min (in ω). Data were collected to a maximum 2Θ of 45^{o}. The ratio of peak counting time to background counting time was 1:1. The diameter of the incident beam collimator was 1.5 mm and the crystal to detector distance was 19 cm.

b. Data Reduction. A total of 7973 reflections were collected, of which 7597 were unique and not systematically absent. As a check on crystal and electronic stability three representative

reflections were measured every 93 reflections. The slope of the least-squares line through a plot of intensity versus time was -325(6) counts/h which corresponds to a total loss in intensity of 68.5%. A nonlinear decay correction was applied. The correction factors on F ranged from 1.0 to 2.71 with an average value of 1.41.

Lorentz and polarization corrections were applied to the data. The linear absorption coefficient is 5.964 cm^{-1} for Mo Kα radiation. A numerical absorption correction was made. Relative transmission coefficients ranged from 0.801 to 0.863 with an average value of 0.837. A secondary extinction correction was applied.[116] Intensities of equivalent reflections were averaged. The agreement factors for the averaging of the 752 observed and accepted reflections was 2.5% based on intensity and 2.2% based on F_o.

c. Structure Solution and Refinement. The structure was solved by using the direct methods which revealed the positions of the Mo, O, and P atoms. The remaining atoms were located in succeeding difference Fourier syntheses. Hydrogen atoms were included in the refinement but restrained to ride on the atom to which they are bonded. The structure was refined in full-matrix least-squares where the function minimized was $\Sigma w(|F_o| - |F_c|)^2$ and the weight w is defined as 1.0 for all observed reflections.

Scattering factors were taken from Cromer and Waber.[117] Anomalous dispersion effects were included in F_c;[118] the values for $\Delta f'$ and $\Delta f''$ were those of Cromer.[119] Only the 2363 reflections having intensities greater than 3.0 times their standard deviation were used in the refinements. The final cycle of refinement, which

included 351 variable parameters, have not yet converged (largest parameter shift was 2.23 times is esd) with unweighted and weighted agreement factors of,

$$R_1 = \Sigma \ |F_o - F_c| / \Sigma \ F_o = 0.091 \quad (24)$$

$$R_2 = [(\Sigma \ w(|F_o| - |F_c|)^2 / \Sigma \ wF_o^2)]^2 = 0.103 \quad (25)$$

The standard deviation of an observation of unit weight was 10.72. The highest peak in the final difference Fourier had a height of 1.30 e/Å^3 with an estimated error based on σF^{120} of 0.15; the minimum negative peak had a height of -1.03 e/Å^3 with an estimated error based on σF of 0.15.

3. $Mo_2(O_2P(OC_6H_5)_2)_4BF_4$.

a. Data Collection. A dark green prismatic crystal of tetrakis(diphenyl phosphate)dimolybdenum tetrafluoroborate, $Mo_2(O_2P(OC_6H_5)_2)_4BF_4$, having approximate dimensions of 0.40 x 0.40 x 0.8 mm, was mounted in a glass capillary with its long axis roughly parallel to the φ axis of the goiniometer.

Cell constants and an orientation matrix for data collection were obtained from least-squares refinement, by using the setting angles of 20 reflections in the range $20 < 2\Theta < 24^o$. The triclinic cell parameters and calculated volume are: a = 10.917(8), b = 11.793(4), c = 12.430(4)Å, α = 63.45(2) β = 70.38(4), γ = 70.64(5)^o V = 5818(6)Å^3. For Z = 1 the calculated density is 1.608 g/cm^3. As a check on crystal quality, omega scans of several intense reflections were measured; the width at half-height was 0.26^o with a take-off

angle of 6.0°, indicating good crystal quality. From subsequent least-squares refinement, the space group was determined to be $P\bar{1}$.

The data were collected at a temperature of 29.0 °C by using the $\theta/2\theta$ scan technique. The scan rate was 4°/min (in 2θ). Data were collected to a maximum 2θ of 55°. The ratio of peak counting time to background counting time was 1:1. The diameter of the incident beam collimator was 1.5 mm and the crystal to detector distance was 19 cm.

b. Data Reduction. A total of 12192 reflections were collected, of which 6096 were unique and not systematically absent. As a check on crystal and electronic stability three representative reflections were measured every 93 reflections. The slope of the least-squares line through a plot of intensity versus time was -26(5) counts/h which corresponds to a total loss in intensity of 1%. A linear decay correction was applied. The correction factors on F ranged from 1.000 to 1.005 with an average value of 1.002.

Lorentz and polarization corrections were applied to the data. The linear absorption coefficient is 6.625 cm^{-1} for Mo Kα radiation. A numerical absorption correction was made. Relative transmission coefficients ranged from 0.779 to 0.828 with an average value of 0.808. A secondary extinction correction was applied.[116] Intensities of equivalent reflections were averaged. The agreement factors for the averaging of the 12192 observed and accepted reflections was 1.2% based on intensity and 1.0% based on F_o.

c. Structure Solution and Refinement. The structure was solved by using the Patterson heavy-atom method which revealed the positions of the Mo and O atoms. The remaining atoms were located in succeeding difference Fourier syntheses. Hydrogen atoms were refined isotropically. The structure was refined in full-matrix least-squares where the function minimized was $\Sigma w(|F_o| - |F_c|)^2$ and the weight w is defined as 1.0 for all observed reflections.

Scattering factors were taken from Cromer and Waber.[117] Anomalous dispersion effects were included in F_c;[118] the values for $\Delta f'$ and $\Delta f''$ were those of Cromer.[119] Only the 5107 reflections having intensities greater than 3.0 times their standard deviation were used in the refinements. The final cycle of refinement, which included 436 variable parameters, has not yet converged (largest parameter shift was 3.31 times is esd) with unweighted and weighted agreement factors described by equations (24) and (25) with $R_1 = 0.027$ and $R_2 = 0.027$. The standard deviation of an observation of unit weight was 0.654.

CHAPTER III

SPECTROSCOPIC STUDIES OF $Mo_2X_4(PBu_3)_4$ AND $Mo_2Cl_4(LL)_2$ COMPLEXES

A. Background

A prerequisite to the elucidation of the photochemistry of quadruply bonded metal dimers is a clear understanding of their excited state properties. As mentioned in Chapter I, the spectroscopic properties of quadruply bonded dimers have been intensely investigated[64-78] since Cotton and coworkers first identified this class of complexes in 1964. A general conclusion of the absorption studies is that the lowest electronic transition, which typically falls in the visible region, is $\delta^2 \rightarrow \delta\delta^*$.[65] In contrast, the emissive properties of quadruply bonded metal dimer complexes vary significantly and a consistent description of $\delta\delta^*$ luminescence has not yet been achieved.

Promotion of an electron from the δ bonding orbital to the δ^* antibonding orbital results in an excited state with an electronic configuration of $\sigma^2\pi^4\delta\delta^*$ thereby reducing the overall bond order from 4 to 3. Simple group theory shows that the d_{z^2} orbital is totally

symmetric and the linear combinations of d_{xz} and d_{yz} orbitals are also totally symmetric; therefore, for complexes with an electronic configuration of $\sigma^2\pi^4\delta\delta^*$, there is no energy barrier for rotation about the metal-metal bond. Thus, the eclipsed geometry (D_{4h}) of the quadruply bonded complex in the ground state is lowered to D_{4d} or D_4 by torsional rotation of the ML_4 fragments in the $^1(\delta\delta^*)$ excited state.[80] This free rotation provides an effective nonradiative decay pathway from the excited state thereby resulting in low emission quantum yields and short emission lifetimes. The torsional model accounts for the lack of a mirror image between the absorption and emission spectra of many quadruply bonded complexes. Presumably, sterically small ligands of M_2X_8 or $M_2X_4L_4$ complexes permit free rotation about the metal-metal bond. The fact that the apparent origins in low temperature emission spectra for such complexes do not overlap results from distortions along two coordinates (νa_{1g}(M-M) and the torsional mode); this commonly is referred to as a Duschinsky effect.[121] On the other hand, large bulky ligands of quadruply bonded metal dimers such as the phosphines in $Mo_2Cl_4(PMe_3)_4$ and $Mo_2Cl_4(PBu_3)_4$ are interlocked in a D_{2d} geometry and create a large steric barrier to rotation about the metal-metal bond. In these cases, the D_{2d} symmetry is preserved in the $^1(\delta\delta^*)$ excited state and a mirror image of absorption and emission profiles is observed.[80,81]

The above observations imply that the excited state dynamics of quadruply bonded metal dimers are closely related to the molecular structures in the ground and the $^1(\delta\delta^*)$ excited state. Our interest in developing the chemistry of electronically excited

M$\overset{4}{—}$M dimers has prompted us to assess the generality of the $D_{4h} \leftrightarrow D_{4d}$ torsional model, and more generally to define the factors governing the nonradiative processes of M$\overset{4}{—}$M dimers. These studies have become possible with Cotton and coworkers synthesis of a series of complexes with a general formula $Mo_2X_4(LL)_2$, where X is a halide, and LL is a bridging bidentate phosphine ligand.[106,107,122-124] In these complexes, steric restrictions of the LL ligands introduce various angles of internal rotation away from the perfectly eclipsed conformation. The rotation is defined by a torsional angle, χ, shown in Figure 11. The torsional angles of a series of $Mo_2X_4(LL)_2$ complexes as determined by X-ray crystallography are shown in Table 3. When χ is equal to zero, there is no distortion and the molecule is in an eclipsed geometry which maximizes the d_{xy} overlap. The overlap of d_{xy} orbitals decreases with increasing χ, and becomes nonbonding when a completely staggered conformation $\chi = 45^o$ is achieved.[124a]

In this chapter, we report and discuss the absorption, emission, and transient absorption spectroscopic studies of a series of $Mo_2X_4(LL)_2$ complexes possessing various torsional angles. All the lifetime measurements and transient absorption spectra displayed in this chapter were collected at the picosecond laser facility, under the administration and directorship of Dr. Jay Richmond Winkler, at Brookhaven National Laboratory.

Figure 11. (a) D_{2d} structure of quadruply bonded chlorophosphino dimolybdenum $Mo_2X_4L_4$; (b) Newman projection of $Mo_2X_4(LL)_2$ complexes where X = Cl, Br, I; L and LL = mono- and bi-dentate phosphine ligands, respectively.

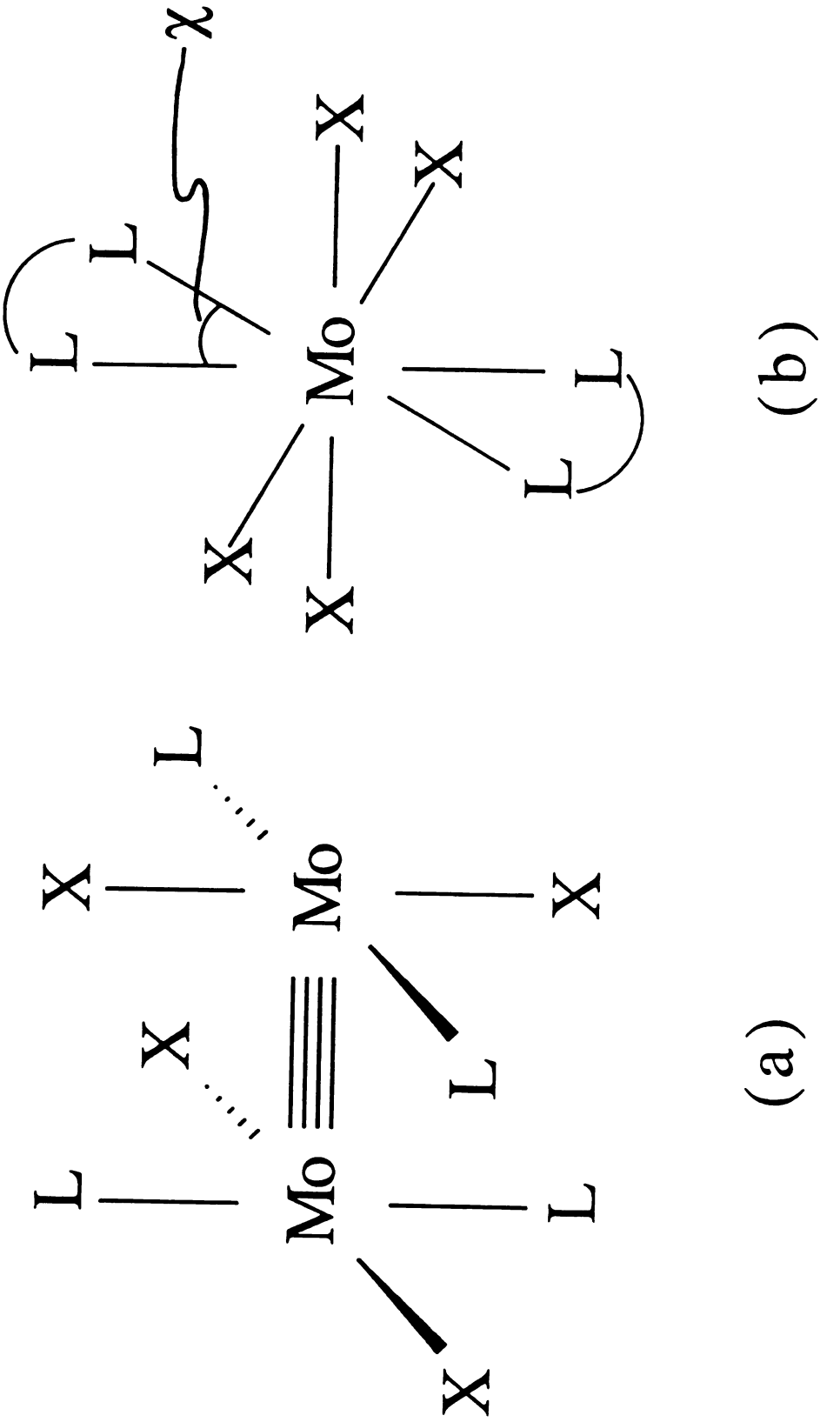

Figure 11

Table 3. Torsional angles of structurally characterized $Mo_2X_4(PBu_3)_4$ and $Mo_2Cl_4(LL)_2$ complexes.

Mo$\overset{4}{-}$Mo complexes	χ/deg	ref.
$Mo_2Cl_4(PBu_3)_4$	0	a
$Mo_2Br_4(PBu_3)_4$	0	a
$Mo_2I_4(PBu_3)_4$	0	a
$Mo_2Cl_4(dppm)_2$	0	122
$Mo_2Cl_4(dmpm)_2$	0	107
$Mo_2Cl_4(dppe)_2$	30.5	123
$Mo_2Cl_4(dmpe)_2$	40	106

[a] X-ray crystal structure determinations of $Mo_2X_4(PBu_3)_4$ complexes, have not been performed. However, the assumed eclipsed geometry for these dimers is reasonable by analogy to the data provided for $Mo_2X_4(PMe_3)_4$ complexes (ref. 78c).

B. Results and Discussion

1. Absorption Spectroscopy. The electronic absorption of $Mo_2X_4(PR_3)_4$ (R = alkyl) complexes has been studied in detail by Gray and Trogler and their coworkers.[68,78,79] Spectra of $Mo_2X_4(PBu_3)_4$ complexes, shown in Figure 12, exhibit a distinct band at ~600 nm possessing an large molar extinction coefficient ($\epsilon \sim 3x10^3\ M^{-1}\ cm^{-1}$) attributable to the $\delta^2 \rightarrow \delta\delta^*$ transition. The shift of this transition to lower energy relative to $Mo_2Cl_8^{4-}$ (515 nm) and "Mo_2O_8" complexes (510-520 nm) may be explained within a simple valence bond framework. As discussed by Trogler *et al.*,[68] good donor ligands (such as phosphine) place significant electron density on the metal centers, thereby expanding the valence shell and increasing the δ overlap. Increased d_{xy} orbital overlap is manifested in the $^1(\delta\delta^*)$ excited state acquiring more covalent character and, as a result, the spin pairing term contribution to the overall transition energy is reduced. Therefore the $^1(\delta\delta^*)$ excited state is shifted to lower energy. The molar extinction coefficients for the $\delta^2 \rightarrow \delta\delta^*$ transition of quadruply bonded metal complexes, in general, are small for a transition which is fully allowed. However, from the work of Mulliken,[125] it is known that the oscillator strength of a one-electron N → V transition is related to the square of the orbital overlap. The relatively low intensity of this transition is therefore a consequence of the small orbital overlap (~0.1) of the d_{xy} orbitals that comprise the δ bond. To this end, the unusually large $^1(\delta\delta^*)$ intensities of the $Mo_2X_4(PR_3)_4$ complexes can be attributed to the enhanced overlap of the δ bond in phosphine ligated

Figure 12. Electronic absorption spectra of $Mo_2X_4(PBu_3)_4$ where X = Cl (——), Br (---), and I (· · ·).

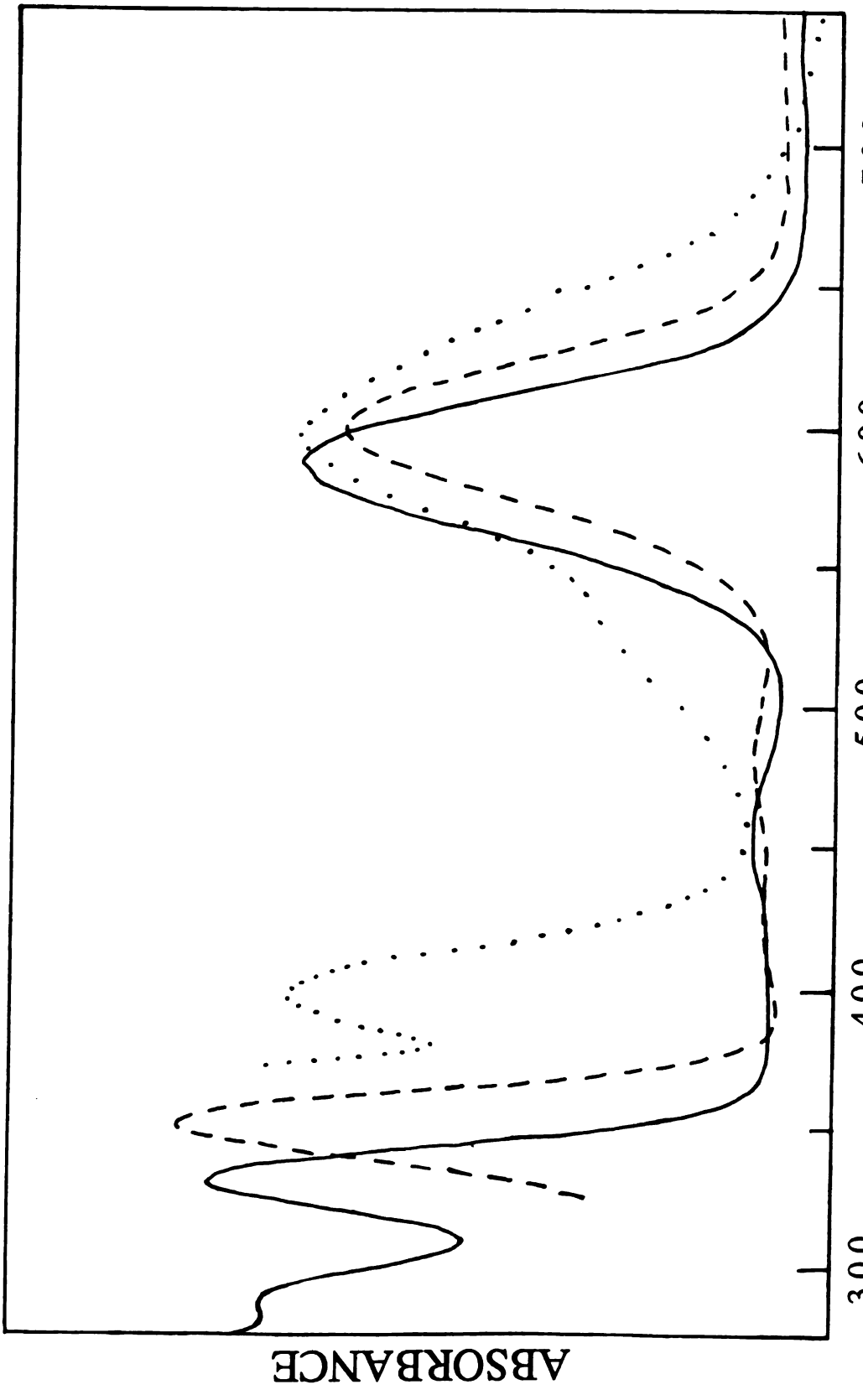

Figure 12

complexes. However as recently pointed out by Hopkins *et al.*,[78] the intensities are much too large to be exclusively accommodated by increased orbital overlap resulting from secondary donor effects by the phosphine ligands. This has led these authors to suggest that the strong $\delta^2 \rightarrow \delta\delta^*$ absorption of $Mo_2X_4(PBu_3)_4$ complexes is due to the stealing of intensity from the lowest energy ligand-to-metal charge transfer (LMCT) transition which occurs at ~330 nm ($\varepsilon \sim 10^4$ M^{-1} cm^{-1}) in the $Mo_2X_4(PBu_3)_4$ complexes.[78d]

The absorption spectra of eclipsed $Mo_2Cl_4(LL)_2$ complexes, $Mo_2Cl_4(dppm)_2$ and $Mo_2Cl_4(dmpm)_2$, are similar to that of $Mo_2Cl_4(PBu_3)_4$. The $\delta^2 \rightarrow \delta\delta^*$ transition and the molar extinction coefficients are 634 nm (ε = 2490 M^{-1} cm^{-1}) and 604 nm (ε = 1730 M^{-1} cm^{-1}) for $Mo_2Cl_4(dppm)_2$ and $Mo_2Cl_4(dmpm)_2$, respectively. In contrast, the staggered $Mo_2Cl_4(LL)_2$ complexes exhibit $^1(\delta^2 \rightarrow \delta\delta^*)$ absorptions of much lower intensity and energy. The $^1(\delta^2 \rightarrow \delta\delta^*)$ transition of $Mo_2Cl_4(dppe)_2$ maximizes at 762 nm (ε = 1030 M^{-1} cm^{-1}) whereas $Mo_2Cl_4(dmpe)_2$ maximizes at 803 nm (ε = 210 M^{-1} cm^{-1}). The lower energy of the $^1(\delta^2 \rightarrow \delta\delta^*)$ transition is due to the decreased d_{xy} orbital overlap and consequently reduced energy splitting of the δ and δ^* levels. The energetic differences between the eclipsed $^1(\delta\delta^*)$ and staggered $^1(\delta\delta^*)$ excited states can readily be attributed to the dependence of the one- and two-electron interactions of the d_{xy} orbital overlaps. It has been shown previously that the δ interaction decreases as the distortion angle increases. A 40^o distortion angle, such as that found in $Mo_2Cl_4(dmpe)_2$, reduces the δ interaction to 0.17 times that found at 0^o.[123] Inasmuch as the δ overlap of the eclipsed molecules are

on the order of S ~ 0.1,[65] the energetic splitting of the one-electron δ and δ^* levels of the $Mo_2Cl_4(dmpe)_2$ is clearly quite small. As shown in Figure 13,[79] the energetic splitting between the covalent $^1(\delta^2)$ ground state and $^3(\delta\delta^*)$ excited state decreases with increasing distortion angle to a nearly degenerate pair (for $\chi = 45^o$). In contrast, the energy of the ionic $^1(\delta\delta^*)$ state is dominated by an electron repulsion term that is roughly invariant over the range of overlaps ($0.01 < S < 0.1$). Thus, even near the zero-overlap limit (40^o torsional angle), $Mo_2Cl_4(dmpe)_2$ exhibits a $^1(\delta^2 \rightarrow \delta\delta^*)$ transition of 12500 cm^{-1} owing to the significant two-electron spin pairing term.

The poor overlap of the d_{xy} orbitals in the torsionally distorted molecules will be manifested in extremely small oscillator strengths. Hence, the question is not why the molar absorption of these complexes is small, but rather by what mechanism do these transitions acquire their intensity. Similar to the $Mo_2X_4(PBu_3)_4$ complexes, intensity stealing from low lying LMCT transitions most reasonably accounts for the high oscillator strengths of the $^1(\delta^2 \rightarrow \delta\delta^*)$ transitions of these staggered $Mo_2Cl_4(LL)_2$ complexes.

2. Emission Spectroscopy. The $Mo_2X_4(PBu_3)_4$ complexes provide the benchmark for the interpretation of the luminescence of quadruply bonded phosphine complexes. Solids and solutions of the $Mo_2X_4(PBu_3)_4$ complexes exhibit intense emission at room and low temperatures. The luminescence spectra mirror the absorption spectra and indeed these complexes were the models for which the torsional model was initially proposed.[80] On the basis of this model, $Mo_2Cl_4(LL)_2$ complexes in which the bidentate phosphine ligands

Figure 13. Energies of the lowest electronic states of $Mo_2Cl_4(PMe_3)_4$ and $Mo_2Cl_4(dmpe)_2$ (ref 79).

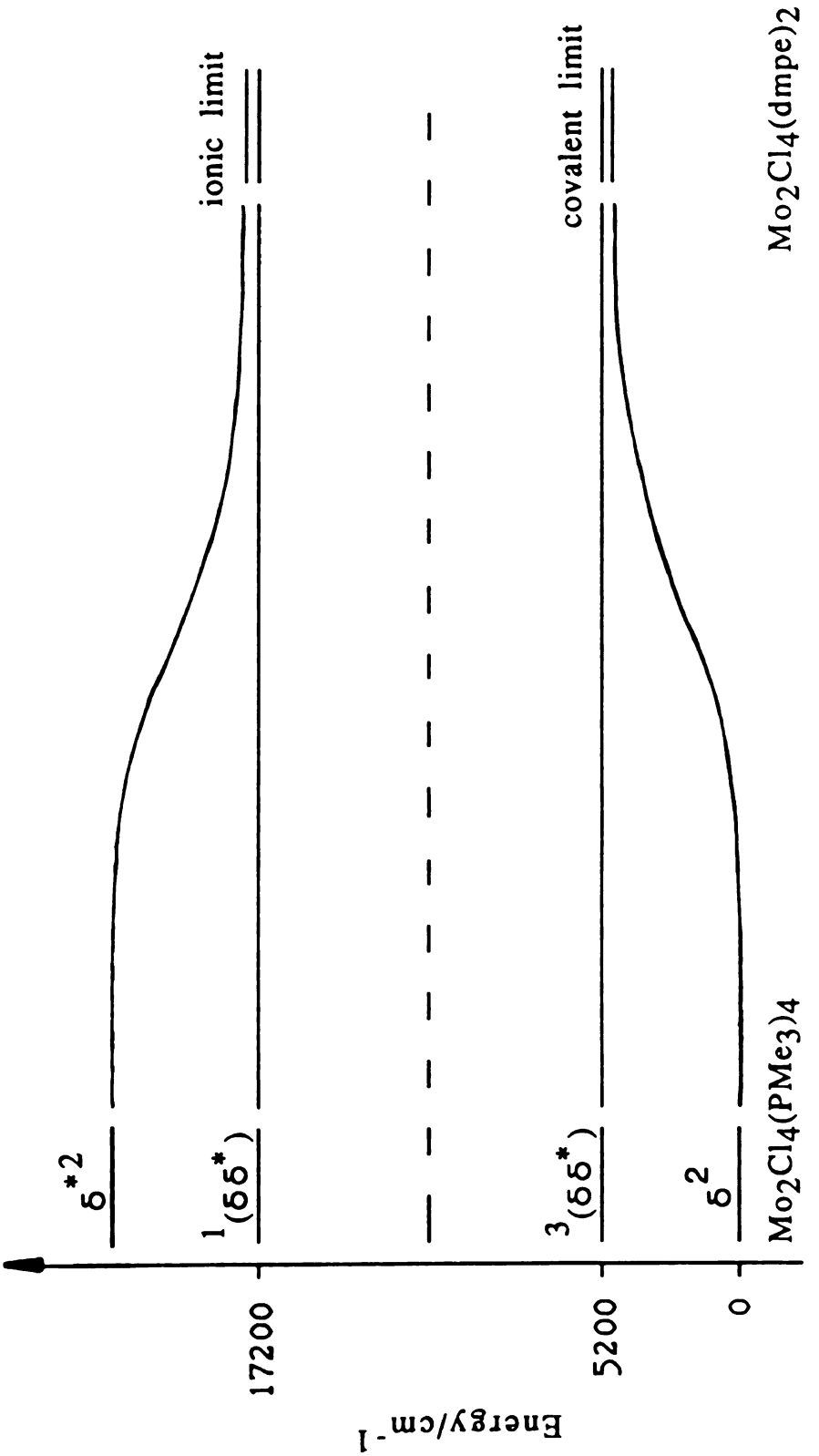
ionic limit
covalent limit
δ*2
1(δδ*)
3(δδ*)
δ2
Mo2Cl4(PMe3)4
Mo2Cl4(dmpe)2
17200
5200
0
Energy/cm-1
L4M-ML4 Tortion Angle

Figure 13

strap the metal-metal bond in an eclipsed conformation would be expected to exhibit strong emission directly from $^1(\delta\delta^*)$ excited state. On the other hand, staggered quadruply bonded $Mo_2Cl_4(LL)_2$ dimers would display weak emissions. But this is not the case. The staggered $Mo_2Cl_4(dppe)_2$ and $Mo_2Cl_4(dmpe)_2$ complexes emit with appreciable intensities in CH_2Cl_2 solution at room temperature whereas $Mo_2Cl_4(dmpm)_2$ emits only weakly, and $Mo_2Cl_4(dppm)_2$ is non-luminescent in CH_2Cl_2 solution at 25 ^oC. The emission spectra of the $Mo_2Cl_4(dppe)_2$, $Mo_2Cl_4(dmpe)_2$, and $Mo_2Cl_4(dmpm)_2$ complexes are show in Figure 14. All four $Mo_2Cl_4(LL)_2$ complexes emit in low temperature glasses (Figure 15). The intensities of the emission parallel that observed at high temperatures. Namely, the staggered complexes luminesce much more intensely than the eclipsed dimers. Typical of binuclear metal-metal emission, the luminescence bands sharpen considerably upon cooling.[126]

Because the complexes do not exhibit vibrational fine structure even at low temperature, the excited state dynamics can not be analyzed by conventional spectroscopic techniques. However, Stokes shifts of the complexes do provide some information. The $^1(\delta^2 \rightarrow \delta\delta^*)$ absorption and emission bands of $Mo_2Cl_4(dppe)_2$ and $Mo_2Cl_4(dmpe)_2$ are shown in Figure 16. It is obvious that both complexes exhibit large Stokes shifts. It should be noted that these Stokes shifts represent a lower limit because the photomultiplier tube of our emission instrument is attenuated significantly for $\lambda >$ 1000 nm. From the valence bond model of quadruply bonded metal dimers, as discussed previously, the δ^2 ground state of $Mo_2Cl_4(dmpe)_2$ and $Mo_2Cl_4(dppe)_2$ is nearly energetically

Figure 14. Emission of $Mo_2Cl_4(LL)_2$ complexes in CH_2Cl_2 solution at room temperature: (a) $Mo_2Cl_4(dmpm)_2$; (b) $Mo_2Cl_4(dppe)_2$; and (c) $Mo_2Cl_4(dmpe)_2$.

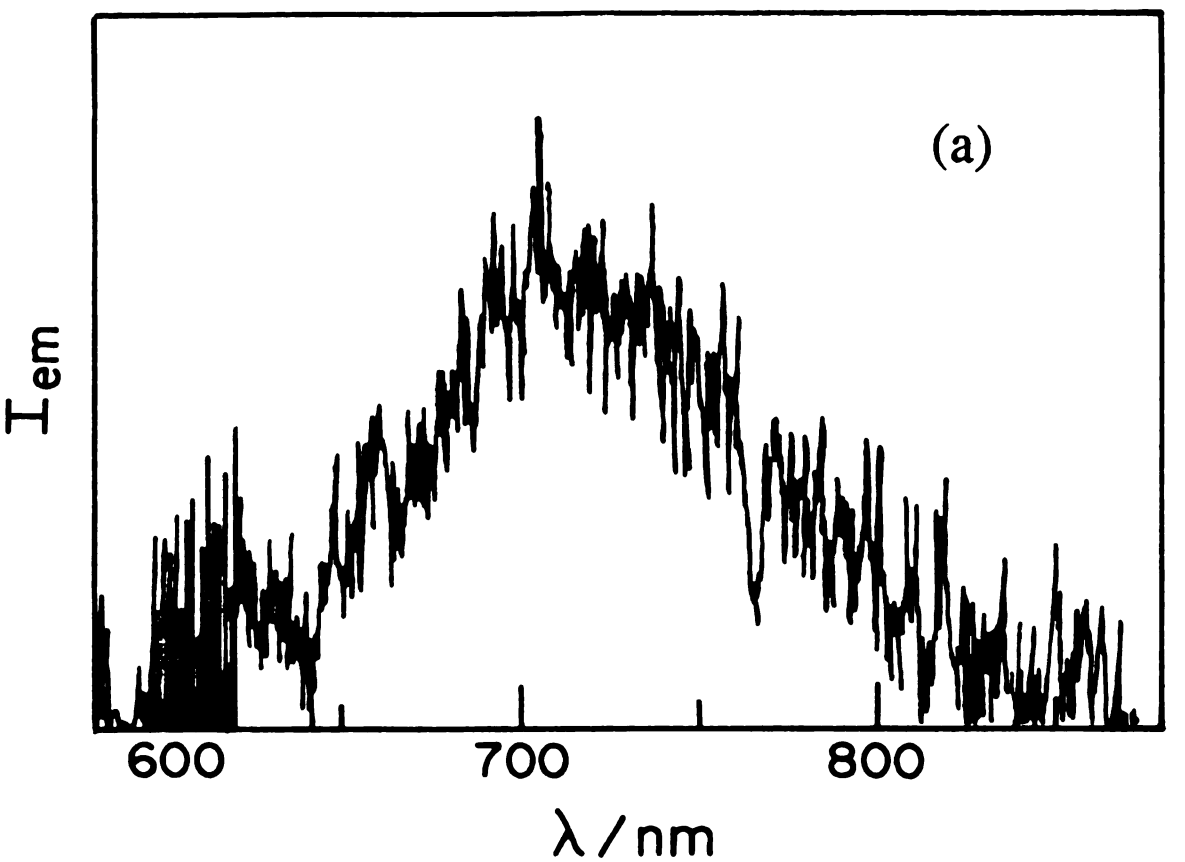

Figure 14

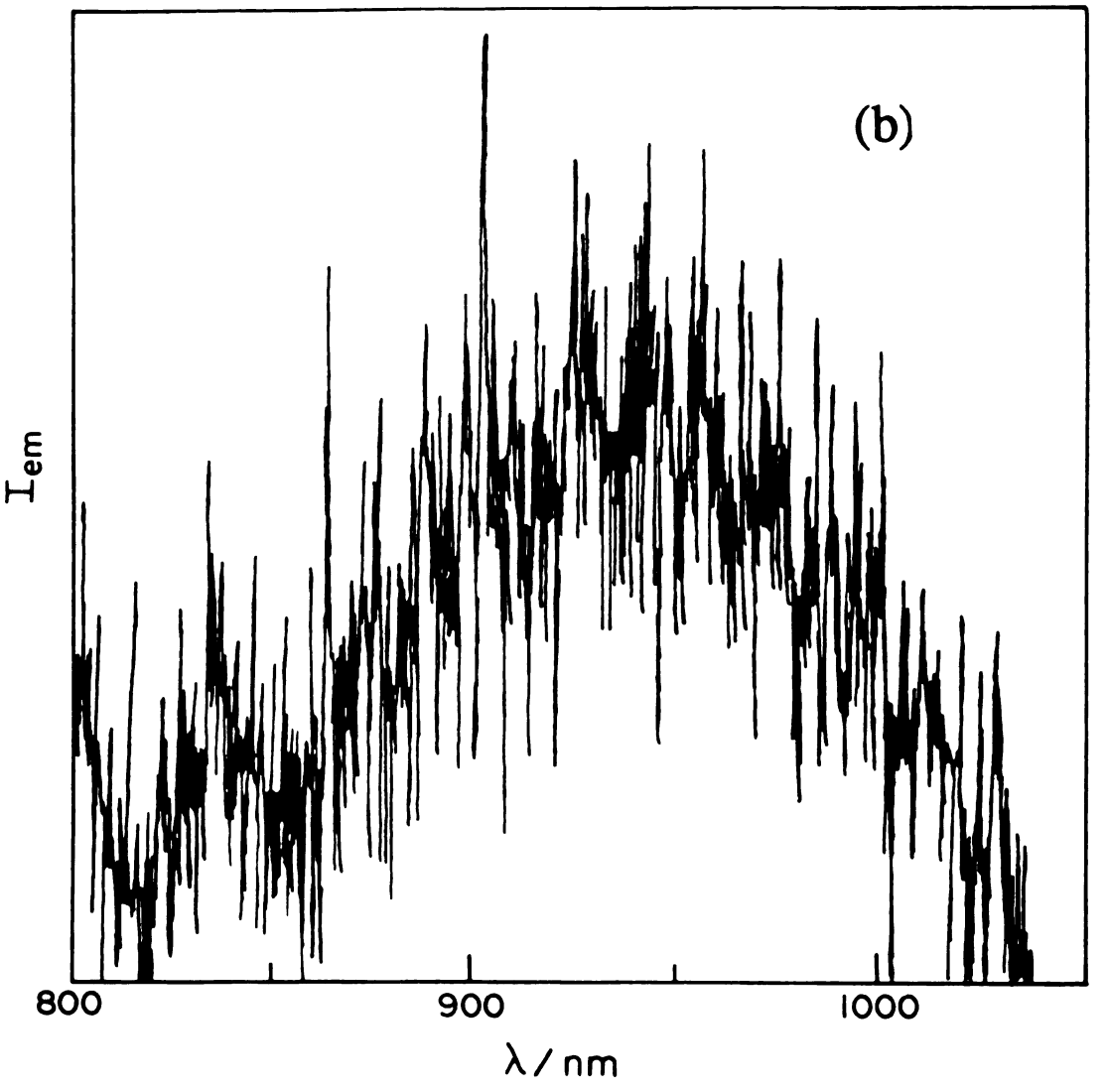

Figure 14

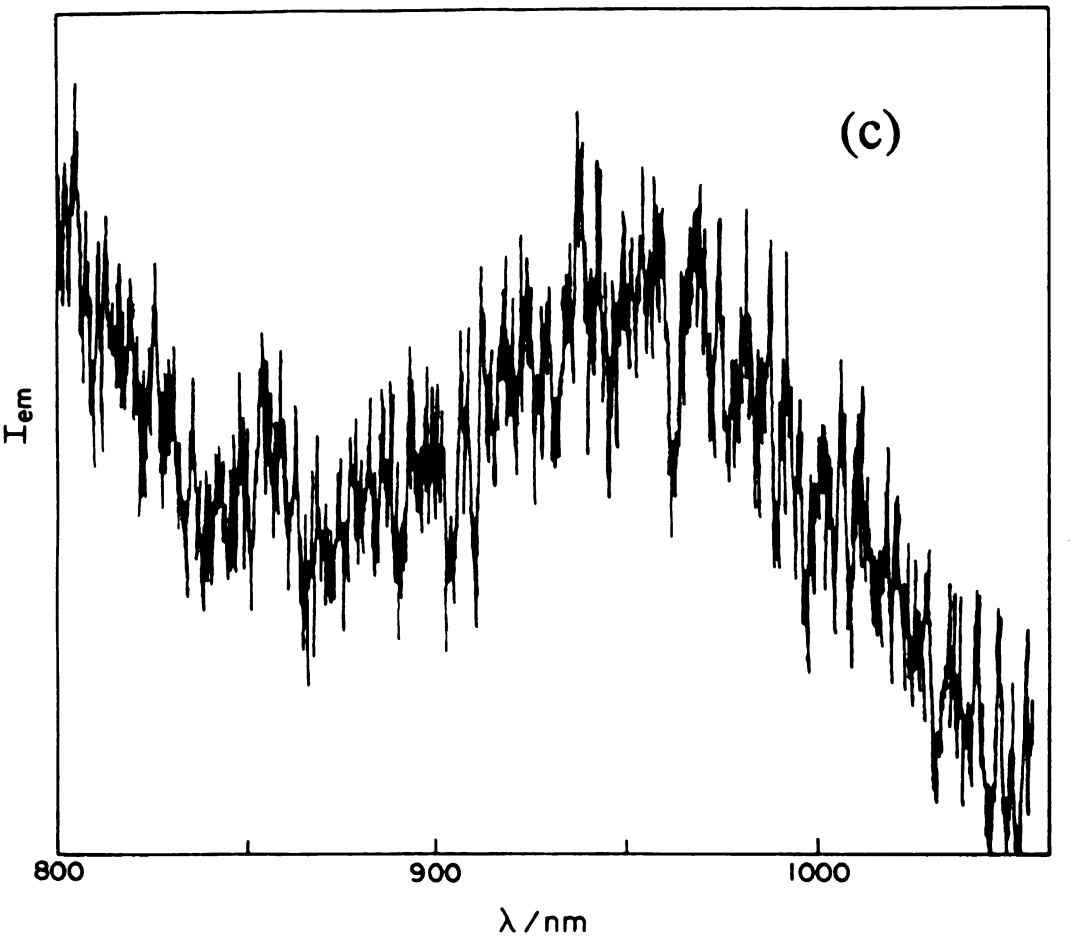

Figure 14

Figure 15. Luminescence of $Mo_2Cl_4(LL)_2$ complexes at 77 K in a CH_2Cl_2/toluene glass: (a) $Mo_2Cl_4(dppm)_2$; (b) $Mo_2Cl_4(dmpm)_2$; (c) $Mo_2Cl_4(dppe)_2$; and (d) $Mo_2Cl_4(dmpe)_2$.

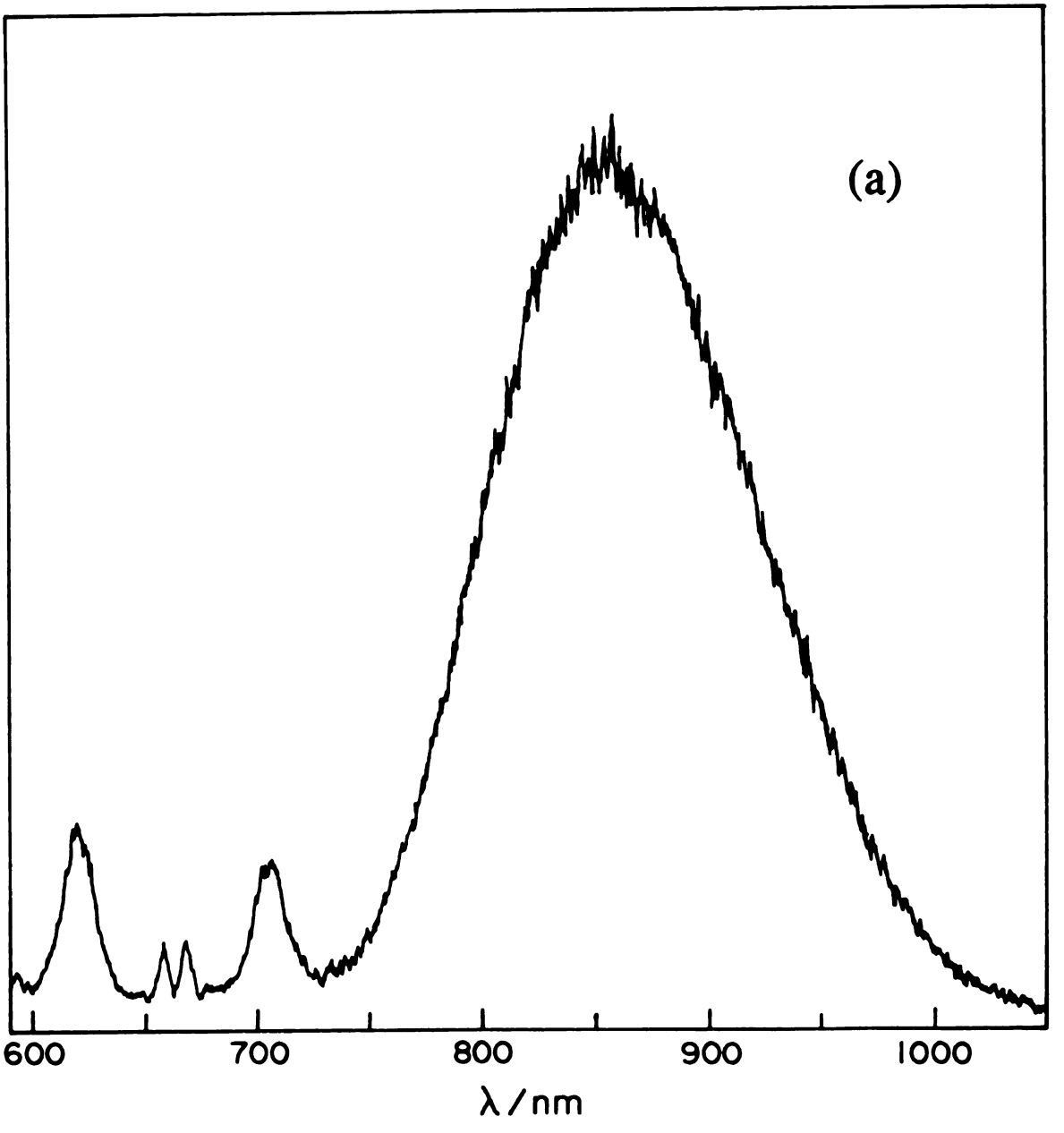

Figure 15

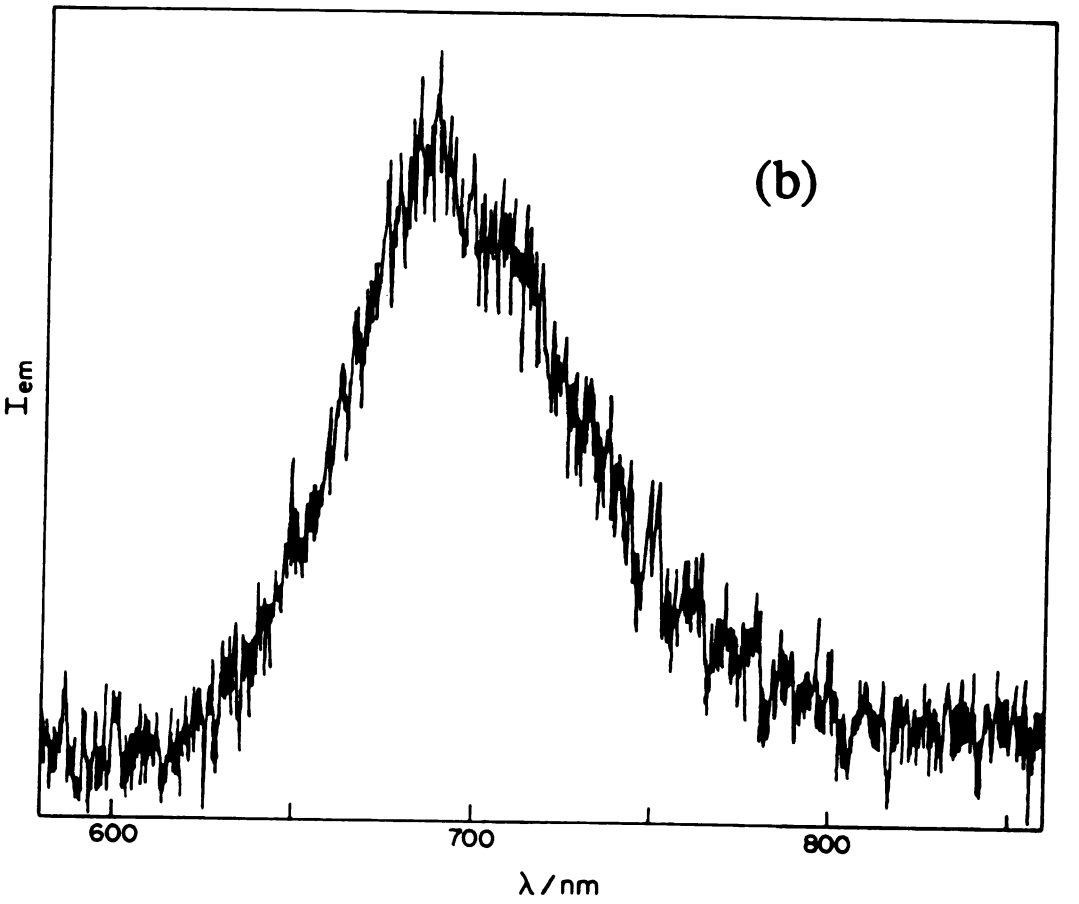

Figure 15

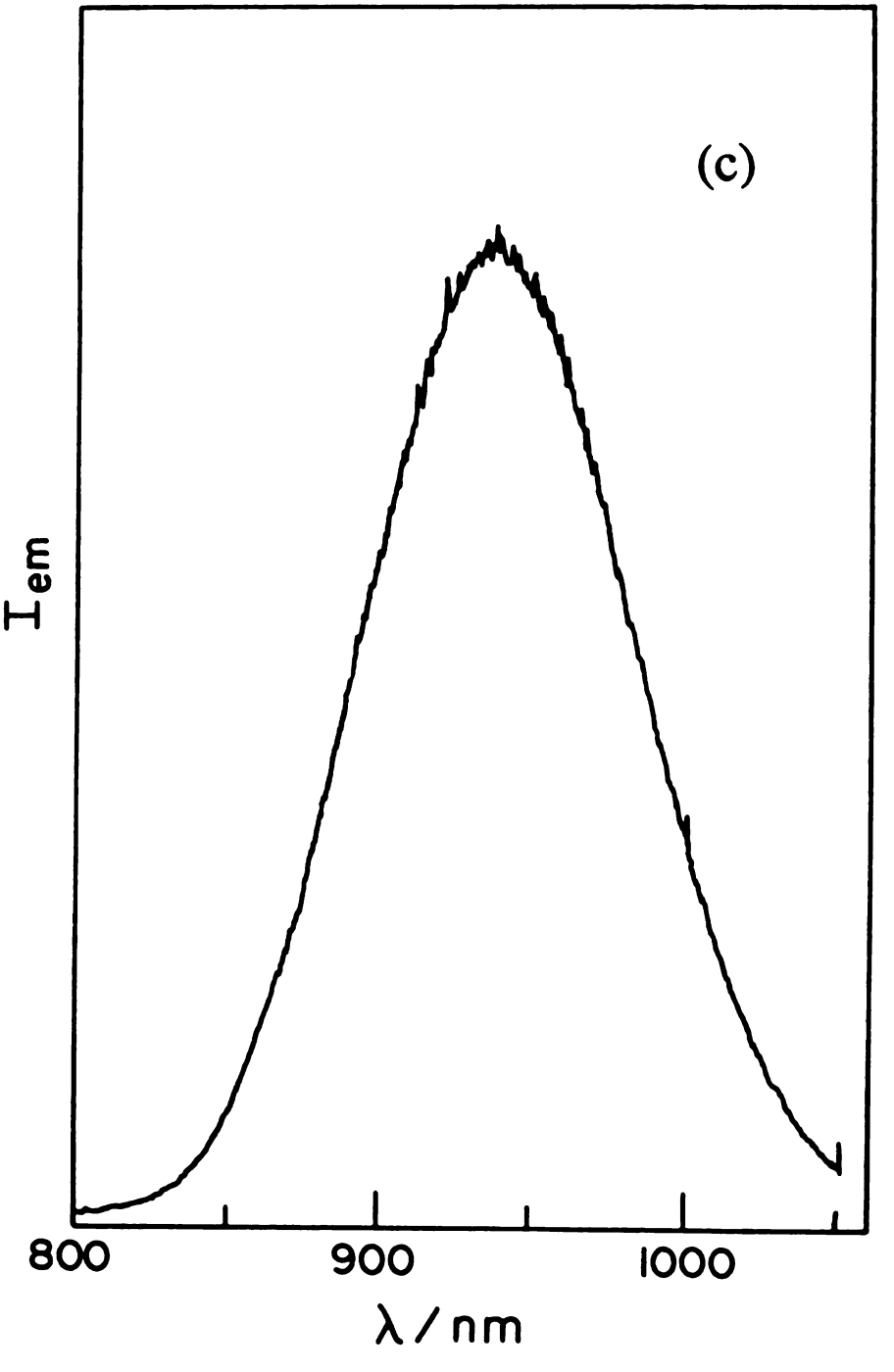

Figure 15

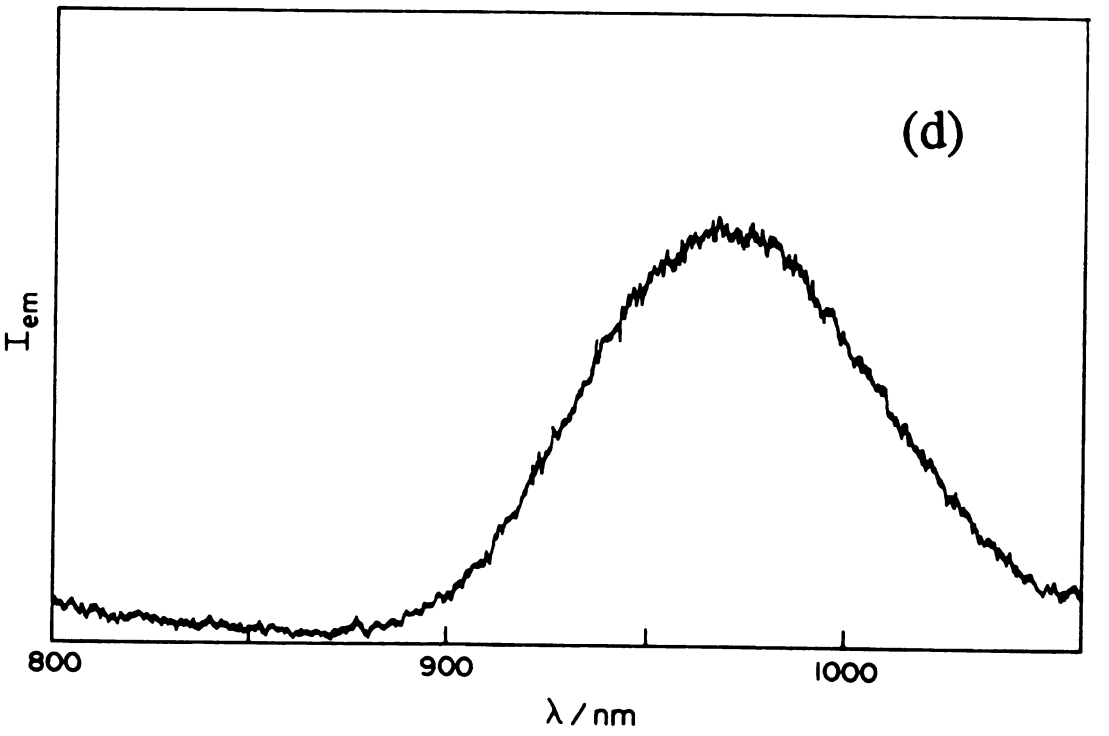

Figure 15

Figure 16. Absorption and emission spectra of $\delta^2 \rightleftarrows \delta\delta^*$ transitions of staggered (a) $Mo_2Cl_4(dppe)_2$ and (b) $Mo_2Cl_4(dmpe)_2$ complexes.

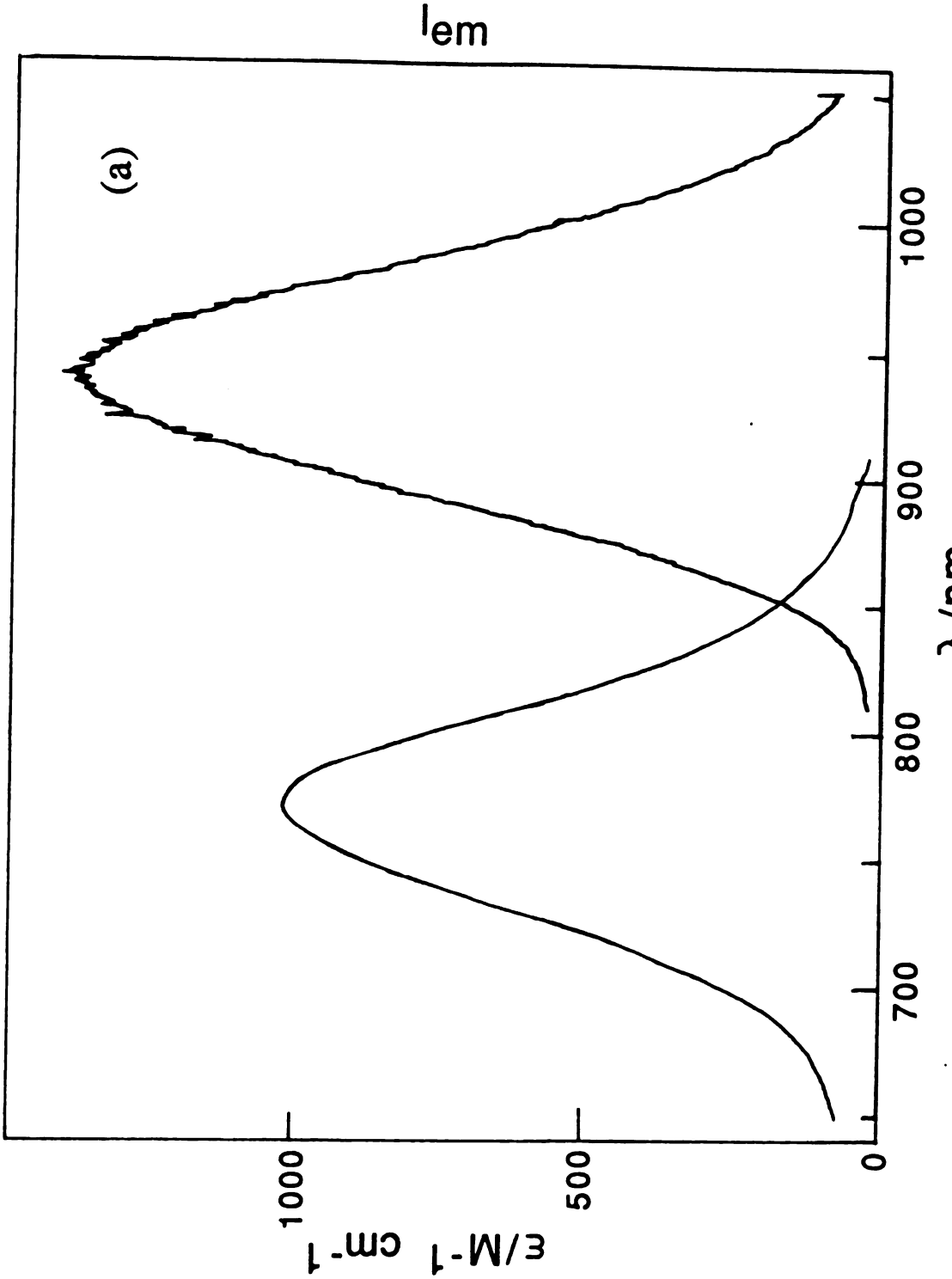

Figure 16

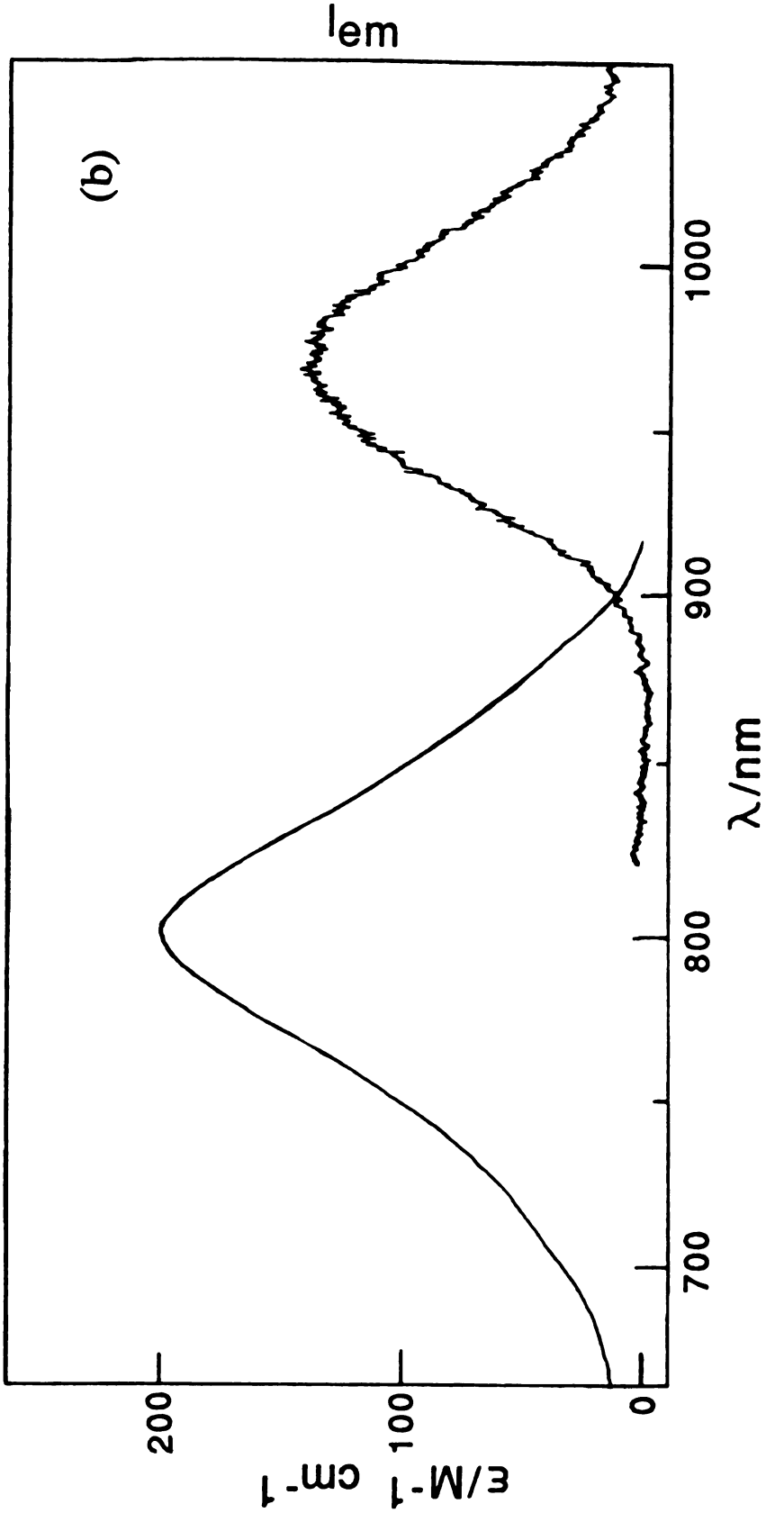

Figure 16

degenerate to the $^3(\delta\delta^*)$ excited state.[79] Therefore, the emission clearly does not originate from $^3(\delta\delta^*)$, and we assign the emission to the $^1(\delta\delta^*)$ excited state. To explain the Stokes shifts of the emission spectra of $Mo_2Cl_4(dmpe)_2$ and $Mo_2Cl_4(dppe)_2$ complexes, we adopt the explanation for the large red-shift from absorption to emission for the $Re_2Cl_8^{2-}$ dimer.[80] Namely, emission is observed from an equilibrium series of complexes possessing torsional angles between a maximized d_{xy} orbital overlap ($\chi = 0^o$) and the configuration with a steric minimum ($\chi = 45^o$). For the $Mo_2Cl_4(dppe)_2$ and $Mo_2Cl_4(dmpe)_2$ complexes the equilibrium geometry is with $\chi = 30.5^o$ and $\chi = 40^o$. Rotation to smaller angles will increase the metal-metal distance owing to steric constraints of the LL backbone. Hence rotation away from the equilibrium torsional angles will result in emission from a spectrum of complexes with metal-metal distances greater than that occurring from simple population of the δ^* antibonding orbital near equilibrium geometry. This will result in luminescence from significantly distorted $Mo_2Cl_4(dppe)_2$ and $Mo_2Cl_4(dmpe)_2$ excited states, and hence large Stokes shifts will be observed.

This explanation is supported by the emission properties of $Mo_2Cl_4(dppe)_2$ dimer in poly(methyl methacrylate) (PMM) films at room temperature. The solution spectrum of the $Mo_2Cl_4(dppe)_2$ complex is frozen by incorporation into the rigid matrix of the PMM film. The emission maximum of $Mo_2Cl_4(dppe)_2$ shifts from 964 nm in CH_2Cl_2 to 936 nm in the PMM film. The decrease in the Stokes shifts upon incorporation into PMM indicates that emission is from a complex geometrically more similar to the ground state structure.

This result is significant because it shows that the distorted $Mo_2Cl_4(LL)_2$ dimers emit directly from staggered $^1(\delta\delta^*)$ excited states.

Emission of $Mo_2Cl_4(dppm)_2$ and $Mo_2Cl_4(dmpm)_2$ complexes exhibit smaller Stokes shifts (Figure 17) than that for complexes with staggered structures. This indicates that emission arises from an excited state complex structurally similar to the ground state. This is not unreasonable because the methylene bridged LL complexes can maintain the geometry of the M$\overset{4}{—}$M complex in the excited state better than that possessing bidentate phosphines with an ethylene backbone. The important point is that the ethylene complexes are distinguished from the methylene complexes by significantly lower emission intensities of the latter (~10^2 less). Of equal significance is that the emission of the eclipsed $Mo_2Cl_4(dppm)_2$ and $Mo_2Cl_4(dmpm)_2$ complexes is 10^4 less than the eclipsed $Mo_2Cl_4(PBu_3)_4$ complexes (Φ_e = 0.013).[80] This discrepancy can not be explained by the simple $D_{4h} \leftrightarrow D_{4d}$ torsional model which predicts nearly equivalent intensities for the two classes of eclipsed complexes.

Some insight into the issue of emission intensities is provided upon closer examination of the molecular and electronic structures of the eclipsed and staggered complexes. The electronic structure of M$\overset{4}{—}$M dimers is significantly affected by the symmetry of the molecule. As shown in Figure 18, the (d_{xz}, d_{yz}) orbitals are no longer energetically degenerate when the symmetry of the chlorophosphine dimolybdenum complexes changes from D_{2d} (e.g. $Mo_2X_4(PBu_3)_4$) to D_{2h} (e.g. $Mo_2Cl_4(dmpm)_2$), whereas the d_{xy} δ-bonding and δ-

Figure 17. Absorption and emission spectra of $\delta^2 \rightleftarrows \delta\delta^*$ transitions of eclipsed (a) $Mo_2Cl_4(dppm)_2$ and (b) $Mo_2Cl_4(dmpm)_2$ complexes.

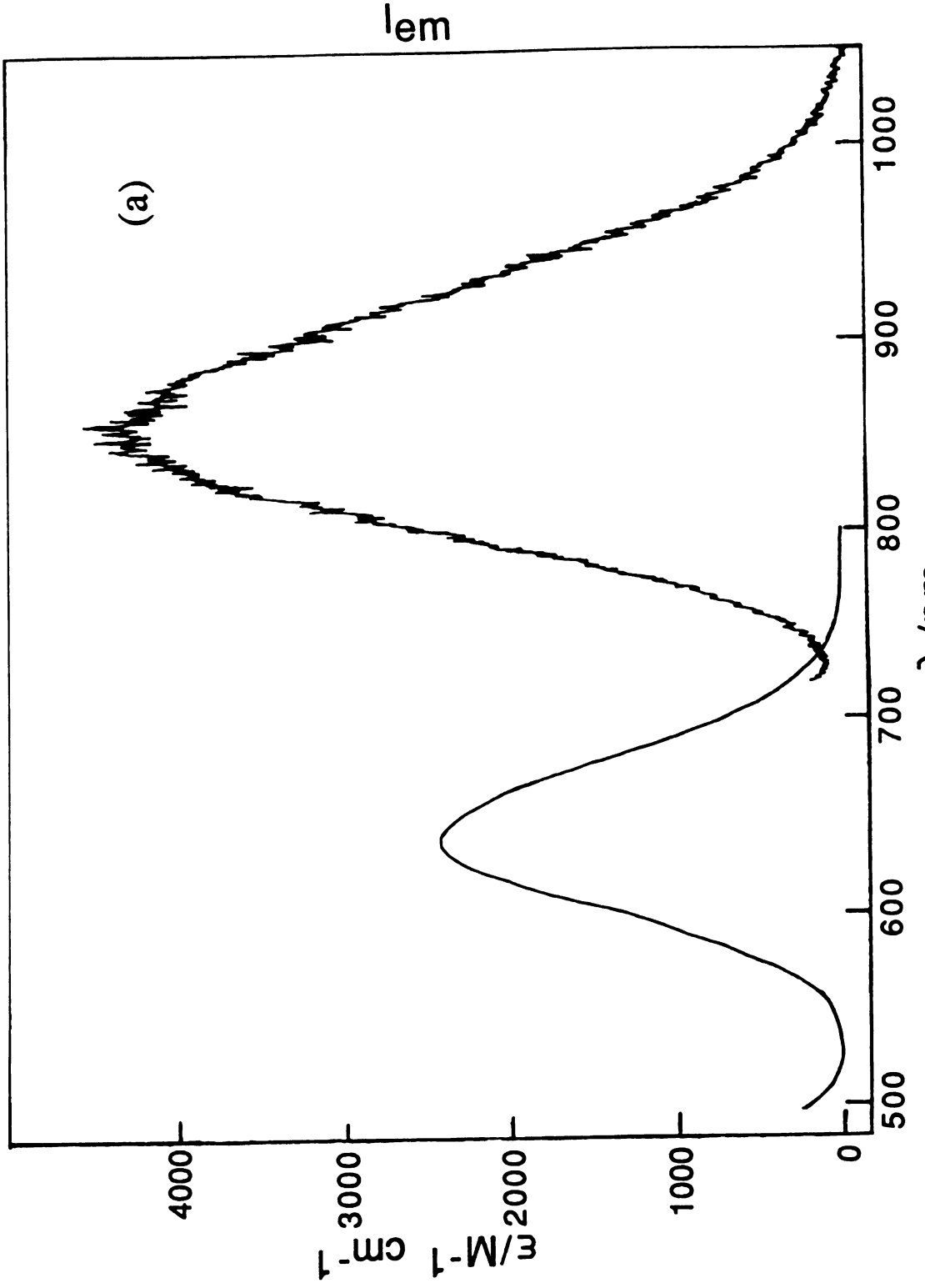
I_{em}
(a)
$\varepsilon/M^{-1}\ cm^{-1}$
4000
3000
2000
1000
0
500
600
700
800
900
1000
λ/nm

Figure 17

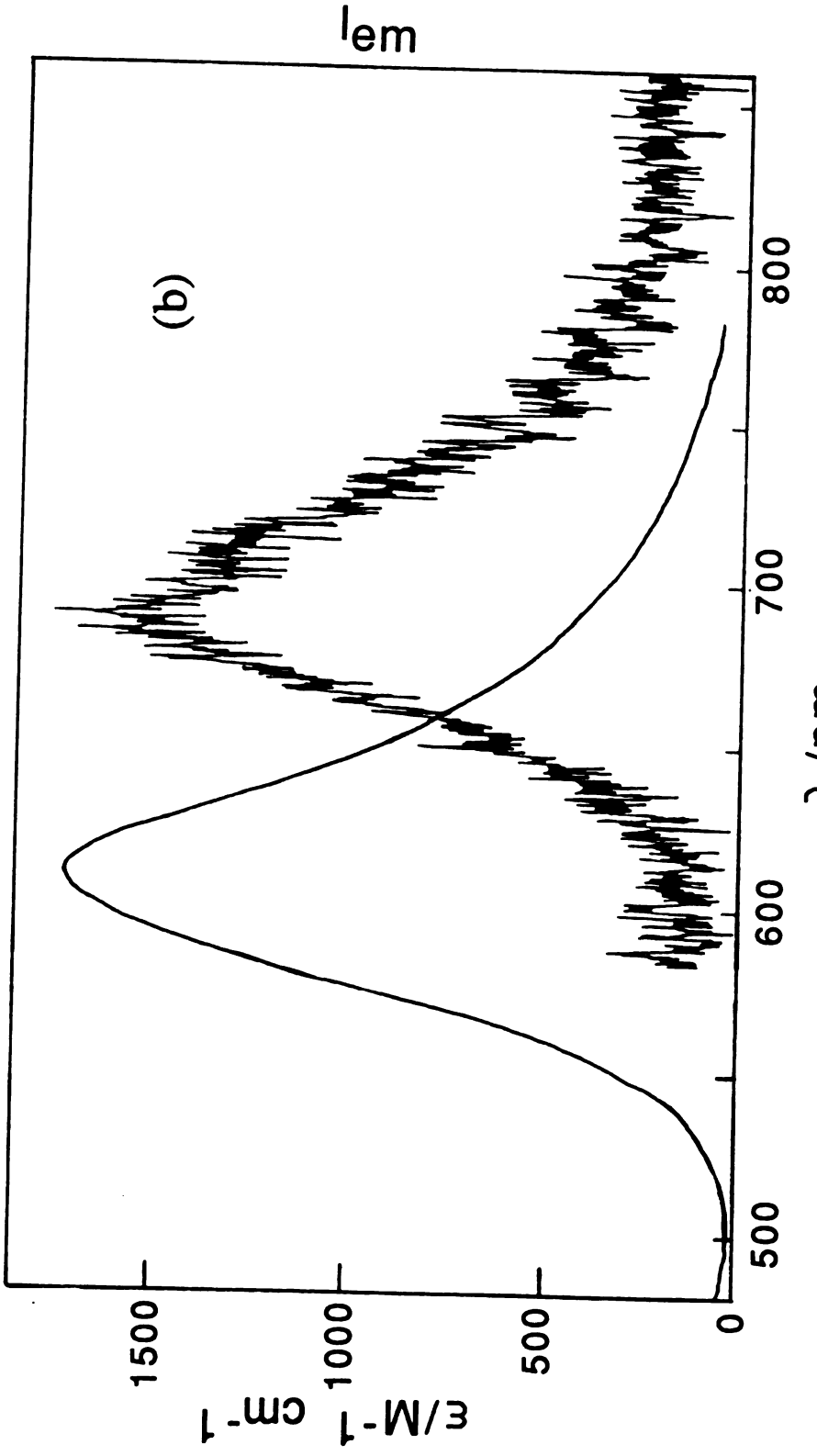

Figure 17

Figure 18. Relative energies of the d-derived molecular orbitals in D_{2d} (i.e. $Mo_2Cl_4(PBu_3)_4$) and D_{2h} (i.e. $Mo_2Cl_4(dppm)_2$) symmetries.

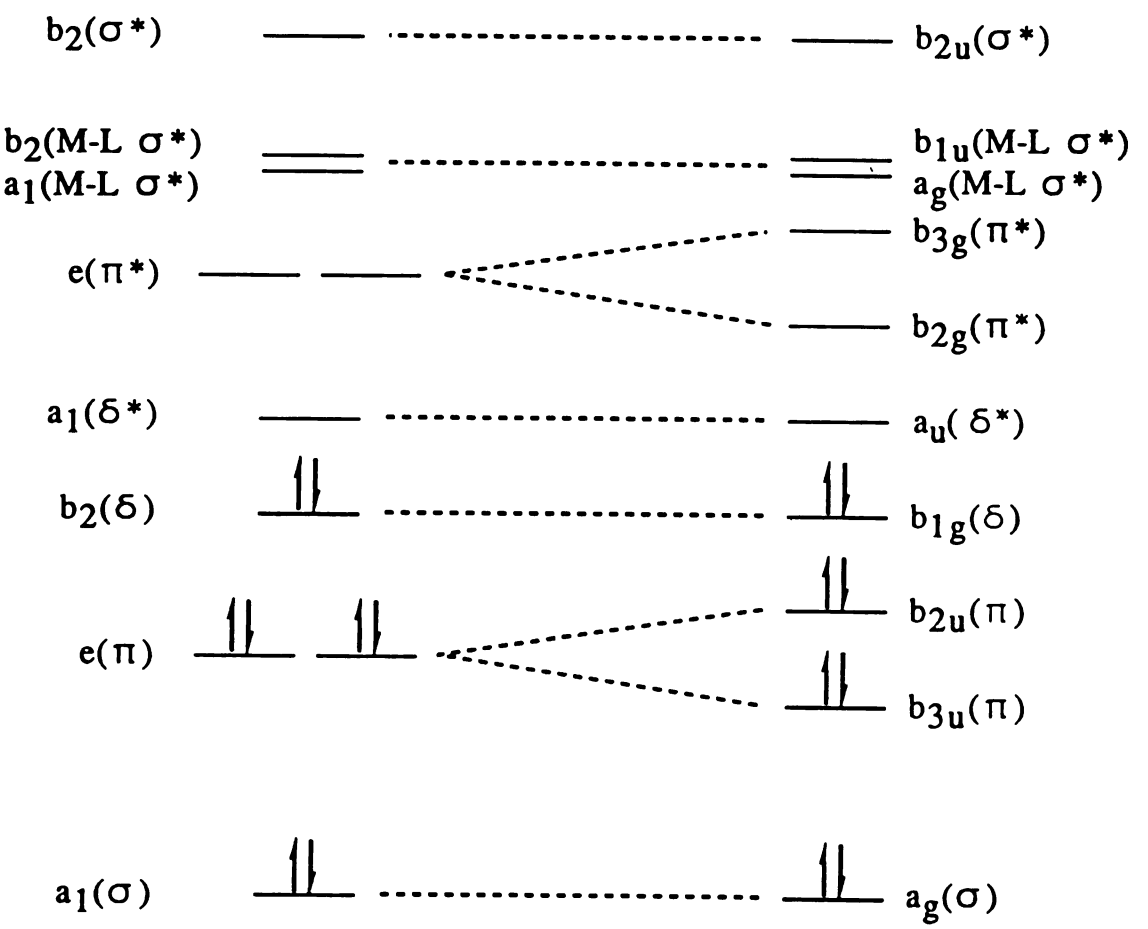

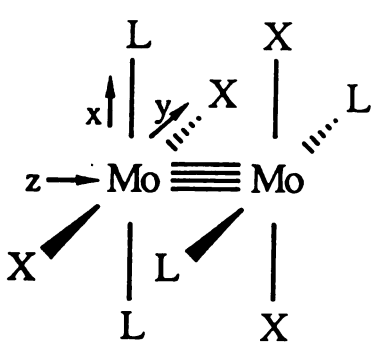

(D_{2d})

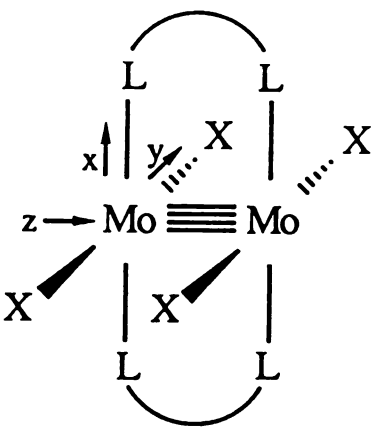

(D_{2h})

Figure 18

antibonding interactions are not greatly perturbed. The energy gaps between π and δ states are smaller for complexes with D_{2h} symmetry and hence contributions (i.e. decreased energy gap) of lower lying states proximate to the excited state will increase the nonradiative decay rate, and hence result in lower emission yields for D_{2h} complexes (i.e. $Mo_2Cl_4(dmpm)_2$). Staggered $Mo_2Cl_4(LL)_2$ complexes possess symmetries between the D_{2d} and D_{2h} structures and therefore, to a first approximation, exhibit higher luminescence intensities than D_{2h} molecules but lower than those of D_{2d} complexes. A more quantitative assignment of the nonradiative processes of these molecules will only be achieved when good theoretical calculations of the energy levels of these $M\overset{4}{—}M$ complexes are in place.

3. Transient Absorption Spectroscopy. Kinetic studies of $Mo_2X_4(PBu_3)_4$ and $Mo_2Cl_4(LL)_2$ complexes were investigated by time-resolved transient absorption spectroscopy. Owing to the relatively weak luminescence intensity of $Mo_2Cl_4(dmpm)_2$ and related complexes, transient species important to nonradiative decay can remain undetected with time-resolved luminescence spectroscopy. This issue is best illustrated by picosecond absorption measurements of $Mo_2Cl_4(PBu_3)_4$. Time-resolved emission spectroscopy identifies a single excited state species with a lifetime of 16 ns.[80] Transient absorption spectroscopy, however, reveals two kinetic decays of lifetimes 9 and 90 ns.[82] The transient species with the 9 ns decay is consistent with the emission lifetime; thus, this species has been assigned to the $^1(\delta\delta^*)$ eclipsed excited state. The

nature of the long-lived 90-ns nonemissive transient species is not yet clear, but three possibilities for the transient are: (1) the low-lying $^3(\delta\delta^*)$ state (~5000 cm^{-1}); (ii) an electronic excited state of $Mo_2Cl_4(PBu_3)_4$ that lies only slightly lower in energy than $^1(\delta\delta^*)$ state but carries very little oscillator strength to the ground state; and (iii) a highly distorted chemical intermediate of $Mo_2Cl_4(PBu_3)_4$. The decay has been attributed to most likely arise from a distorted chemical intermediate.[82]

Because the transient spectroscopy of $Mo_2Cl_4(PBu_3)_4$ is well defined, studies were initiated by recording the spectra of its halide analogues, $Mo_2Br_4(PBu_3)_4$ and $Mo_2I_4(PBu_3)_4$. Figure 19 displays the transient absorption spectra of $Mo_2Cl_4(PBu_3)_4$ (X = Br, I) at 50 ps and 1 ns, respectively, after excitation with a ~25 ps pulse of 532-nm laser light. The spectra, concordant with that of $Mo_2Cl_4(PBu_3)_4$, exhibit a moderately intense absorption maximum at 440 nm, an absorption rising into the near UV, and a bleaching of the $^1(\delta\delta^*)$ transition at ~600 nm. That the moderately intense absorption maxima of $Mo_2Cl_4(PBu_3)_4$, $Mo_2Br_4(PBu_3)_4$, and $Mo_2I_4(PBu_3)_4$ are energetically similar (440, 460, and 440 nm for the chloro, bromo, and iodo, respectively) distinguishes this transition as a metal localized transition or an ligand-to-metal charge transfer (LMCT). Because the energy of the transition is invariant across the halide series, an LMCT involving the phosphine ligands is the preferred assignment.[82] The extinction coefficient of this band is ~2000 M^{-1} cm^{-1}. This value clearly indicates a spin allowed transition but can not distinguish between the LMCT and metal-localized excitations. For the latter, assuming D_{4h} selection rules, five dipole-allowed one-

Figure 19. Transient difference spectra of (a) $Mo_2Br_4(PBu_3)_4$ in CH_2Cl_2 and (b) $Mo_2I_4(PBu_3)_4$ in CH_2Cl_2. The spectra were recorded 50 ps and 1 ns, respectively, after the 532-nm pulse of a Nd:YAG laser (FWHM = 25 ps).

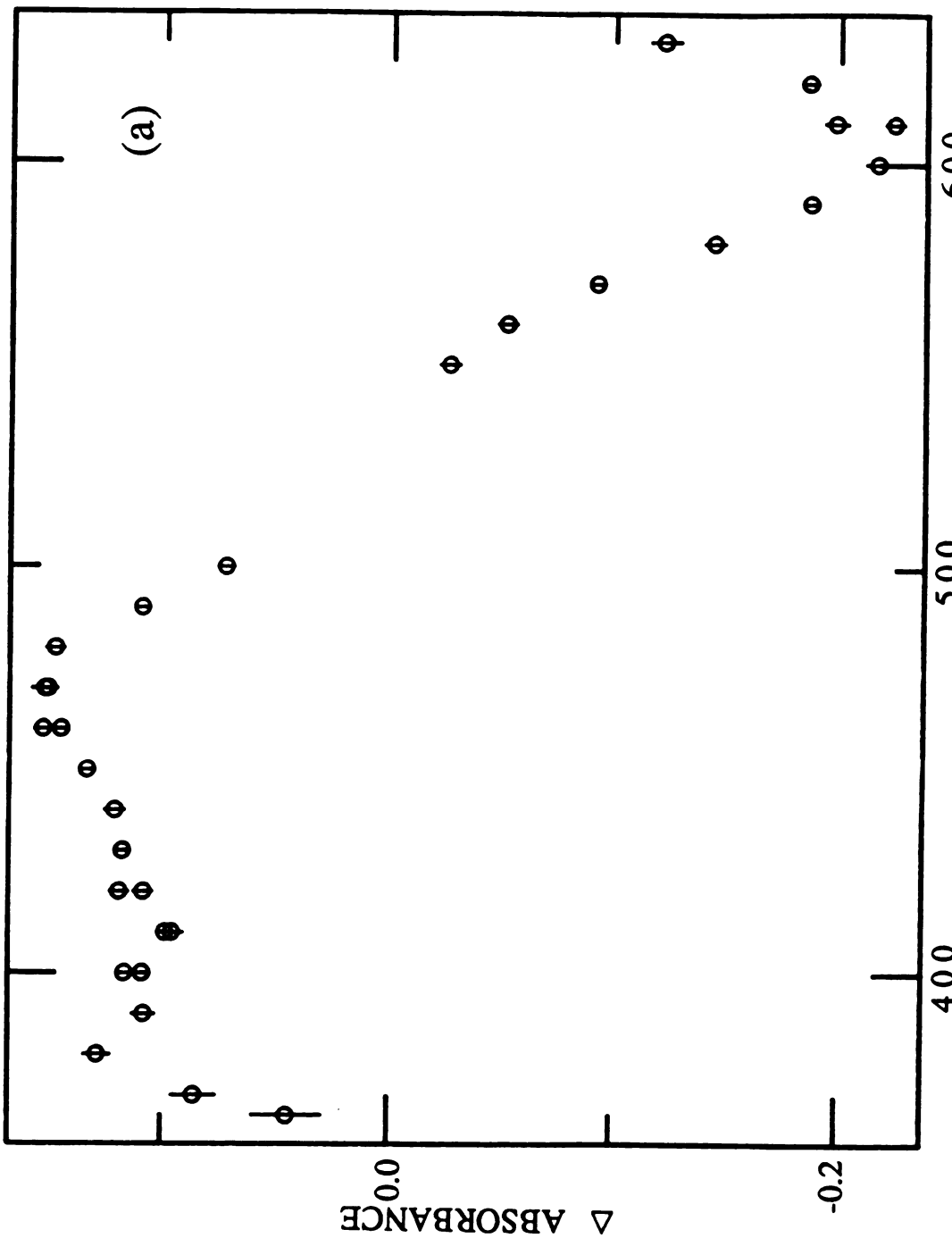

Figure 19

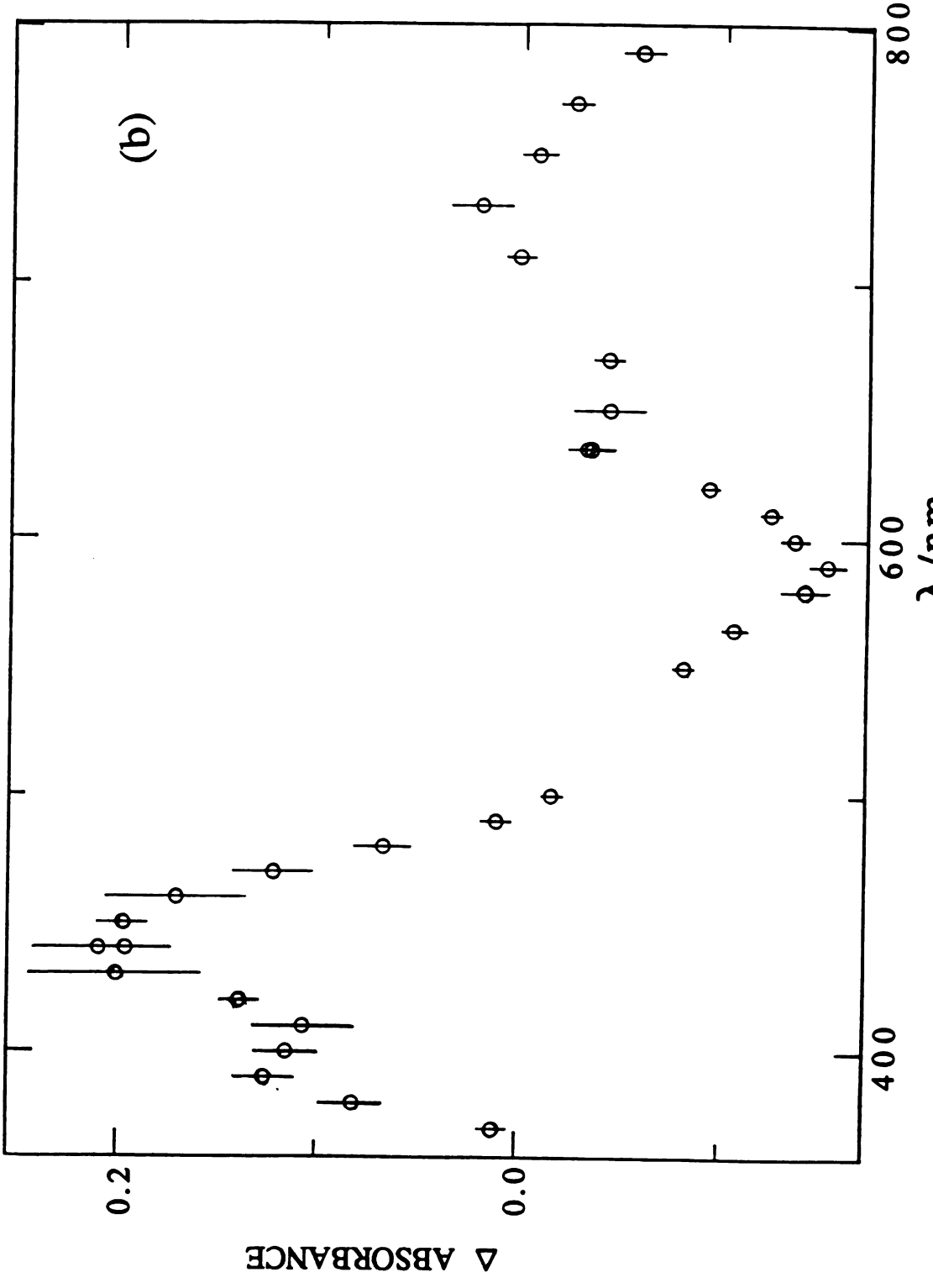

Figure 19

electron metal-localized excitations can arise from a $^1(\delta\delta^*)$ excited state: $\delta \rightarrow \delta^*$; $\pi \rightarrow \pi^*$; $\pi \rightarrow \delta'(d_{x2-y2})$; $\delta^* \rightarrow \pi^*$; and $\pi \rightarrow \delta$. These transitions will produce, respectively, $^1A_{1g}(\delta^{*2})$, $^1A_{1g}(\pi^3\delta\delta^*\pi^*)$, $^1E_g(\pi^3\delta\delta^*\delta')$, $^1E_g(\delta\pi^*)$, and $^1E_g(\pi\delta^*)$ states. The level arising from the 440 nm absorption must lie ~39000 cm^{-1} above the ground state, and calculations suggest that[58] of the five metal localized transitions, the $\delta^* \rightarrow \pi^*$ excitation is the most plausible assignment for this feature. However, the data of $Mo_2X_4(PBu_3)_4$ series do not provide an unequivocal assignment to either $\delta^* \rightarrow \pi^*$ or LMCT.

The kinetics of $Mo_2Cl_4(PBu_3)_4$ excited state decay can readily be ascertained from these transient absorption spectra. For the chloro, bromo, and iodo complexes, the ~440 nm absorption and $^1(\delta\delta^*)$ bleaching signals decay biexponentially. The shorter lifetime component in each case is nearly identical to the measured luminescence lifetimes (τ = 9, 2, 6 ns for chloro, bromo, and iodo $Mo_2X_4(PBu_3)_4$ complexes, respectively). Because the luminescence spectrum of each complex is a mirror image of the $^1(\delta^2 \rightarrow \delta\delta^*)$ transition, the short-lived transient is assign to the eclipsed $^1(\delta\delta^*)$ excited state. The longer lived species (τ = 90, 34, 108 ns for chloro, bromo, and iodo $Mo_2X_4(PBu_3)_4$ complexes, respectively) is due to one of the three possibilities mentioned previously. In an effort to provide further insight into the nature of this longer lived non-luminescent intermediate, the transient absorption spectra of $Mo_2Cl_4(LL)_2$ complexes were investigated

The transient absorption spectra of the $Mo_2Cl_4(LL)_2$ complexes is similar to that of the $Mo_2Cl_4(PBu_3)_4$ dimer. Spectra, collected 25-100 ps after the excitation pulse (shown in Figure 20), exhibit a

Figure 20. Transient difference spectra of the following $Mo_2Cl_4(LL)_2$ complexes: (a) $Mo_2Cl_4(dppm)_2$, recorded 75 ps after a 355-nm laser excitation pulse; (b) $Mo_2Cl_4(dmpm)_2$, recorded 25 ps after a 532-nm laser excitation pulse; (c) $Mo_2Cl_4(dppe)_2$, recorded 100 ps after a 532-nm laser excitation pulse; and (d) $Mo_2Cl_4(dmpe)_2$, recorded 100 ps after a 355-nm laser excitation pulse.

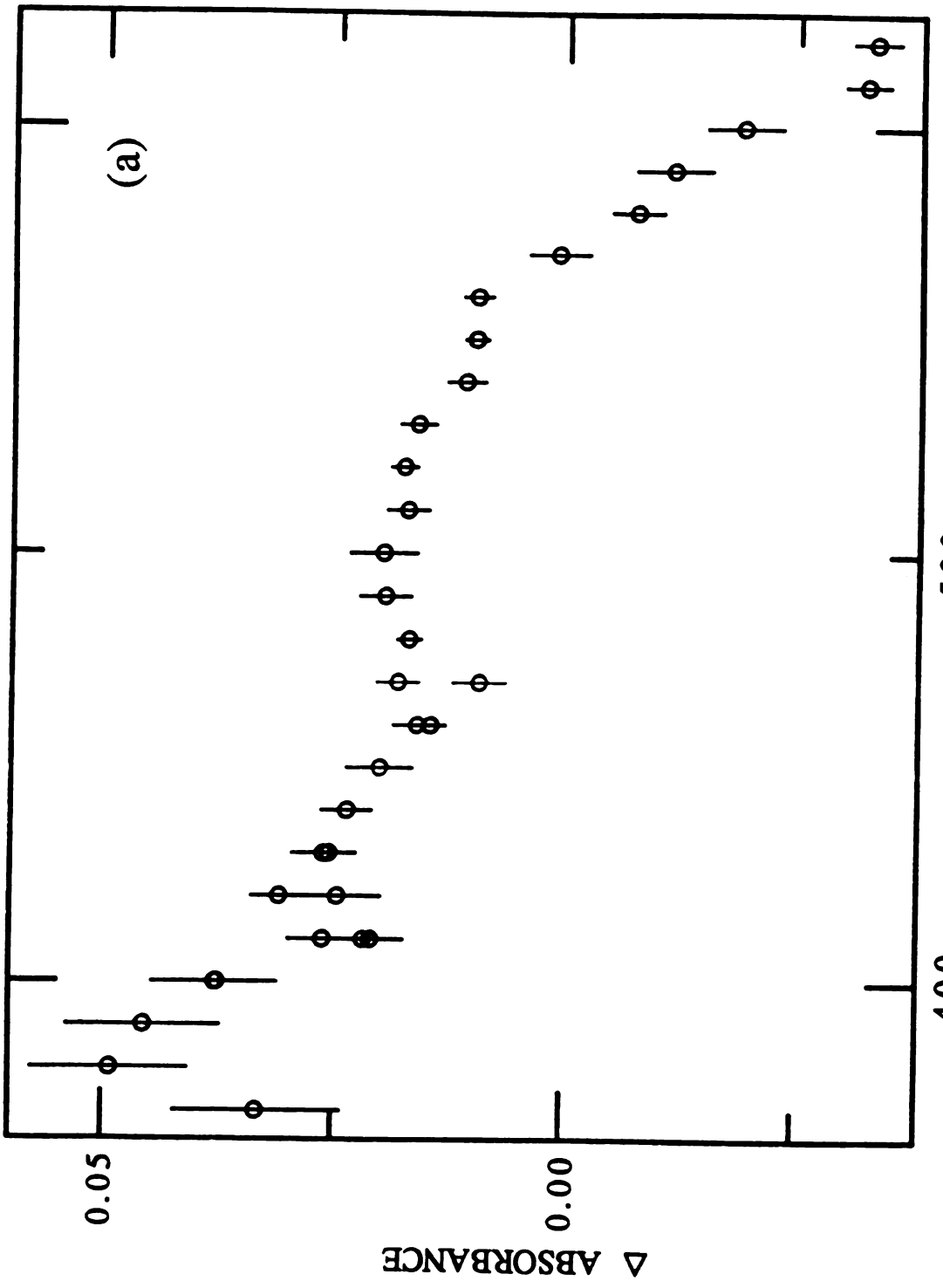

Figure 20

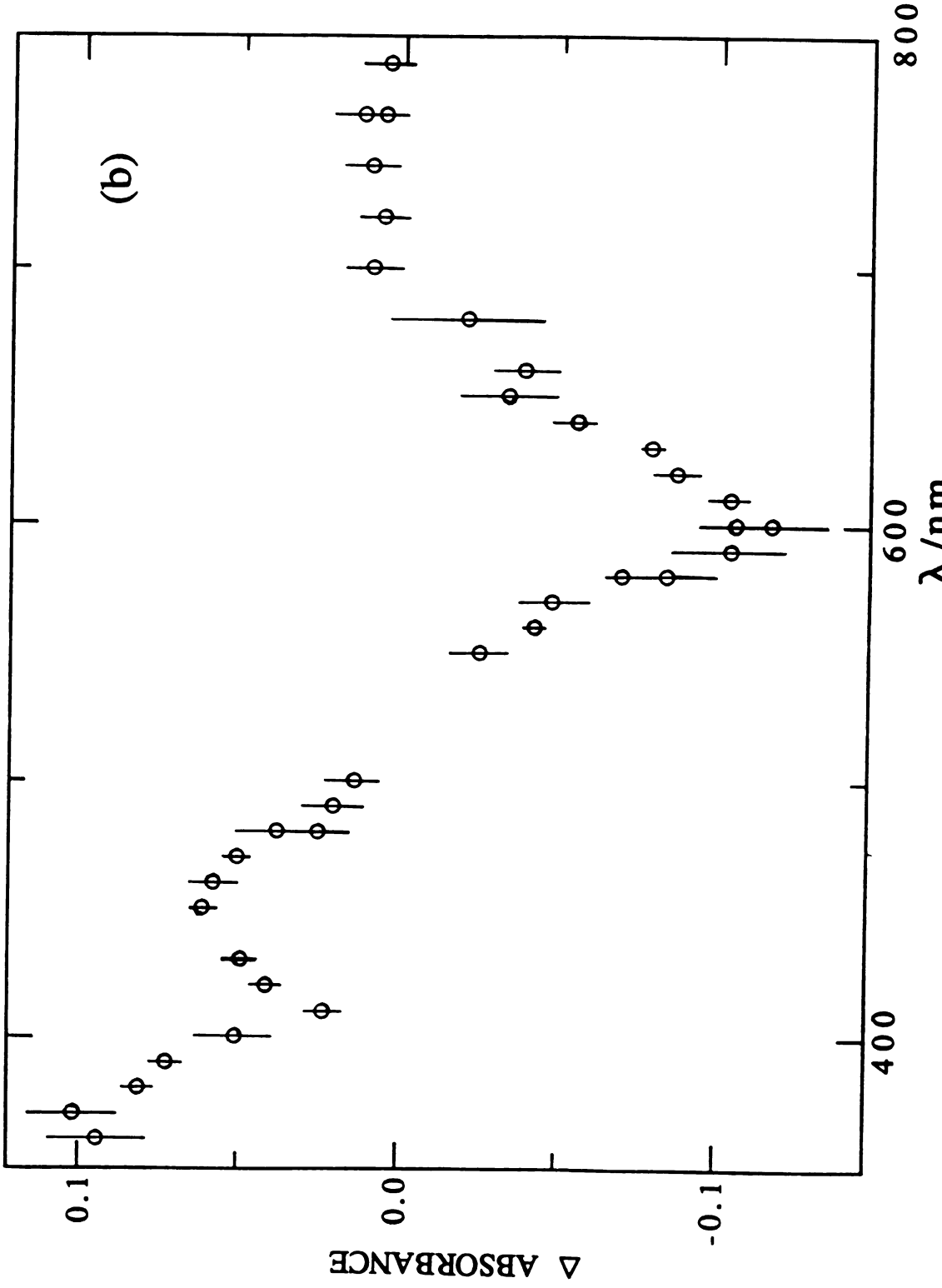

Figure 20

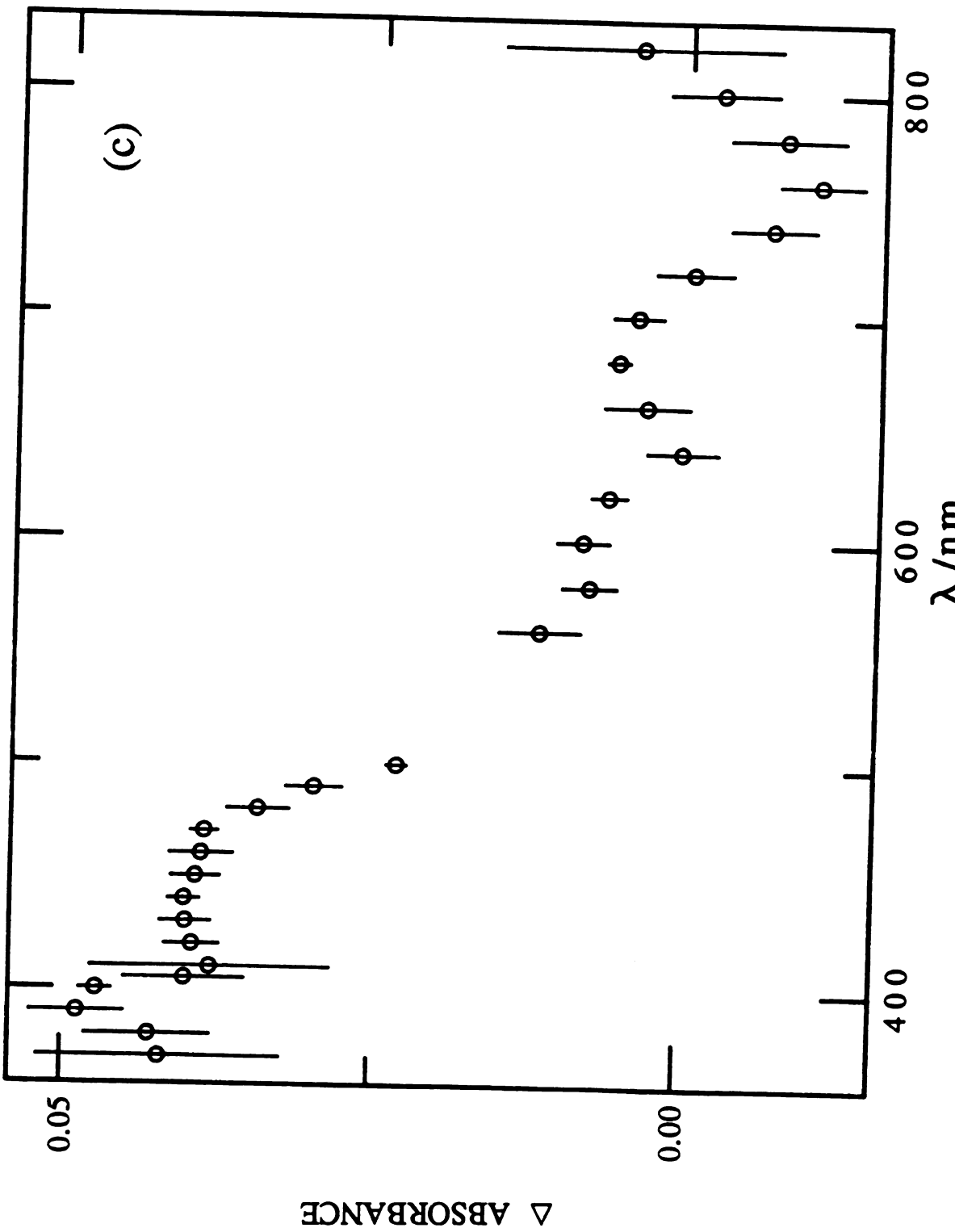

Figure 20

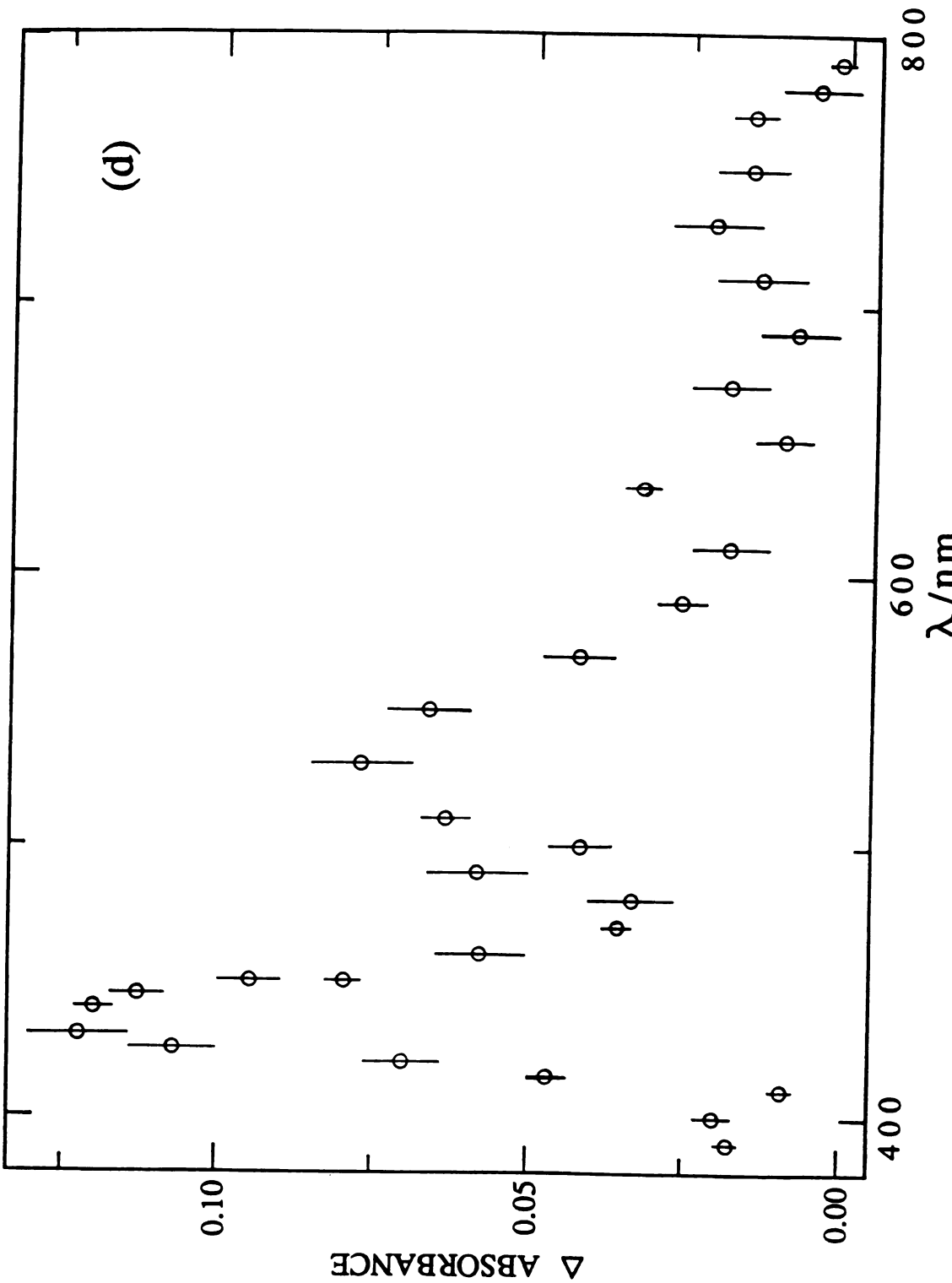

Figure 20

prominent bleaching signal corresponding to the $^1(\delta\delta^*)$ transition. It should be noted that the bleaching of $Mo_2Cl_4(dmpe)_2$ lies well into the red and is weak owing to low response of the photomultiplier tube. However the leading edge of the bleaching signal is clearly distinguishable in Figure 20(d). The spectra of the four complexes are dominated by pronounced absorption in the 430-450 nm; the spectra of $Mo_2Cl_4(dmpe)_2$ displays an additional absorption at 525 nm. The extinction coefficient of the ~440 nm bands of Mo_2Cl_4-$(dppm)_2$, $Mo_2Cl_4(dmpm)_2$, and $Mo_2Cl_4(dppe)_2$ are 1000-3000 M^{-1} cm^{-1}. On this basis, the intensity of the 525 nm band of $Mo_2Cl_4(dmpe)_2$ identifies it as the corresponding transition, and thus the 435-nm absorption of the $Mo_2Cl_4(dmpe)_2$ complex is unique. This is further suggested by the fact that the band halfwidth of the 435 nm is much smaller than that of the other observed absorptions in $Mo_2Cl_4(LL)_2$ complexes. The obvious question becomes what transition is responsible for the respective 430, 450, 470, and 525 nm absorptions of the $Mo_2Cl_4(dppm)_2$, $Mo_2Cl_4(dmpm)_2$, $Mo_2Cl_4(dppe)_2$, and $Mo_2Cl_4(dmpe)_2$ complexes. The energy and intensities of these absorptions suggest them to be analogous to those observed in the spectra of the $Mo_2X_4(PBu_3)_4$ complexes. We have previously suggested that the ~440-nm absorption for the electronically excited $Mo_2X_4(PBu_3)_4$ complexes is attributed to either a $\delta^* \rightarrow \pi^*$ transition or a charge-transfer transition involving the phosphine ligands. Consideration of the electronic structure of $M\overset{4}{-}M$ complexes imply that the red-shift in the absorption along the series $Mo_2Cl_4(dppm)_2$, $Mo_2Cl_4(dmpm)_2$, $Mo_2Cl_4(dppe)_2$, and $Mo_2Cl_4(dmpe)_2$ is inconsistent with a $\delta^* \rightarrow \pi^*$ transition. The π and

π^* orbitals of the $M\overset{4}{-}M$ complexes are cylindrically symmetric about the metal-metal axis and hence the energy of these orbitals is invariant to rotation about the metal-metal bond. The δ-δ^* splitting however will decrease dramatically with rotation owing to stabilization of the δ^* orbital and destabilization of the δ orbital with a decreasing δ interaction. To this end, the $\delta^* \rightarrow \pi^*$ transition should blue-shift with increasing χ. On the other hand, charge transfer transitions to the δ^* orbital will red-shift as χ increases. Therefore, the most likely assignment of the transition leading to transient absorption in $Mo_2Cl_4(LL)_2$ and $Mo_2Cl_4(PBu_3)_4$ complexes is not metal-localized but ligand(phosphine)-to-metal(δ^*)-charge-transfer. The assignment of the 435-nm band in the spectrum of $Mo_2Cl_4(dmpe)_2$ has not been elucidated at this time.

Although the transient absorption spectra of the four $Mo_2Cl_4(LL)_2$ complexes suggest that the complexes are similar, analysis of the lifetime decay of the transient show that the diphenylphosphine complexes (i.e. $Mo_2Cl_4(dppm)_2$ and Mo_2Cl_4-$(dppe)_2$) are distinctly different from their dimethylphosphine counterparts (i.e. $Mo_2Cl_4(dmpm)_2$ and $Mo_2Cl_4(dmpe)_2$). Figure 21 presents the decay kinetics of the transient species of the Mo_2Cl_4-$(dmpm)_2$ and $Mo_2Cl_4(dmpe)_2$ complexes. In both cases the transients decay by monoexponential kinetics with lifetimes of 43 and 960 ps for the $Mo_2Cl_4(dmpm)_2$ and $Mo_2Cl_4(dmpe)_2$, respectively. The decay kinetics of $Mo_2Cl_4(dmpm)_2$ were obtained from the $^1(\delta\delta^*)$ bleaching signal and thus the 43 ps represents the $^1(\delta\delta^*)$ lifetime of the excited state. Because the bleaching signal of the $Mo_2Cl_4(dmpe)_2$ complex is not easily observed, the direct

Figure 21. Transient kinetics for dimethylphosphine complexes: (a) $Mo_2Cl_4(dmpm)_2$ recorded at 600 nm (excitation by 2^{nd} harmonic of a Nd:YAG, FWHM = 25 ps) (b) $Mo_2Cl_4(dmpe)_2$, recorded at 450 nm (excitation by 3^{rd} harmonic of a Nd:YAG, FWHM = 25 ps).

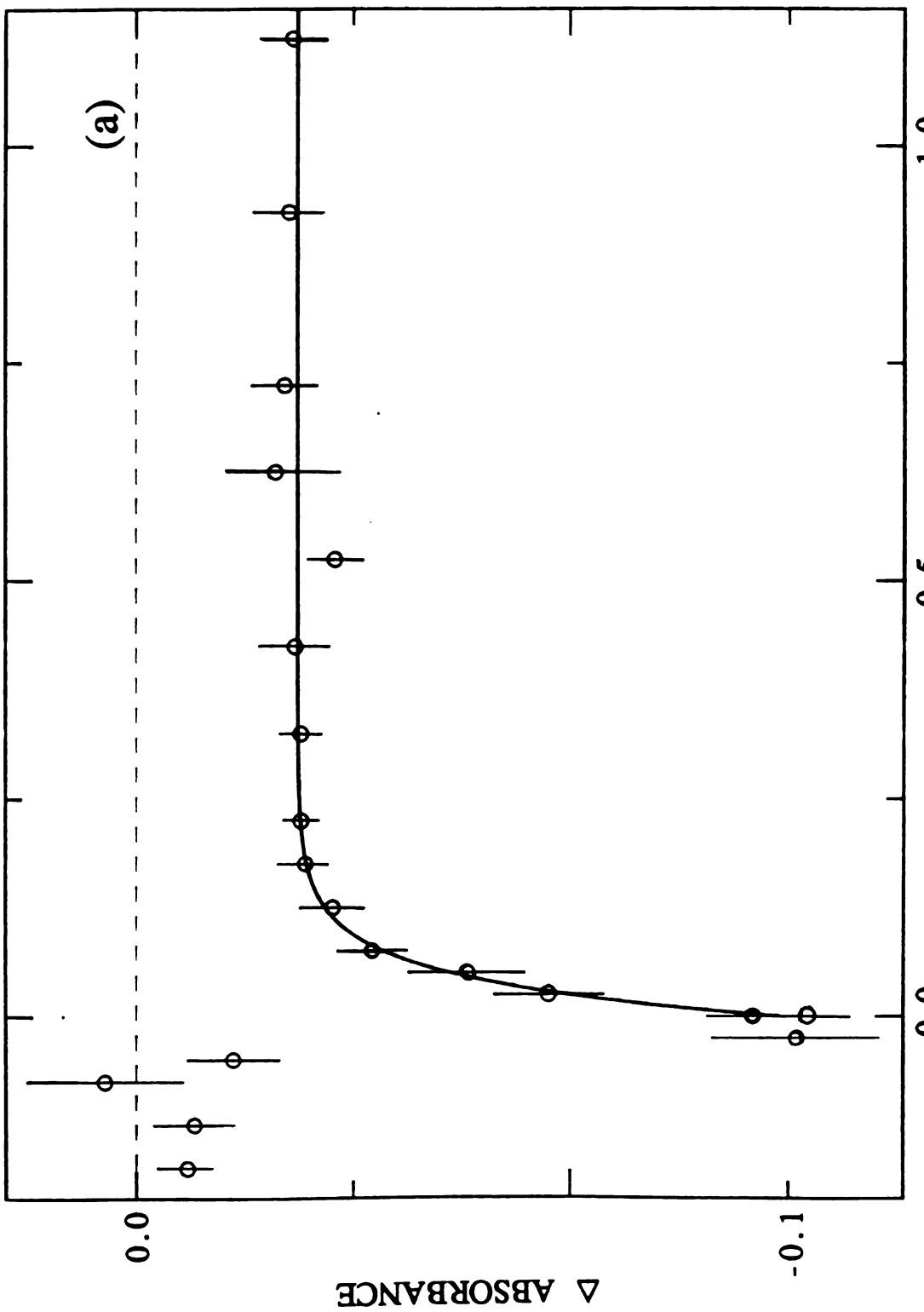

Figure 21

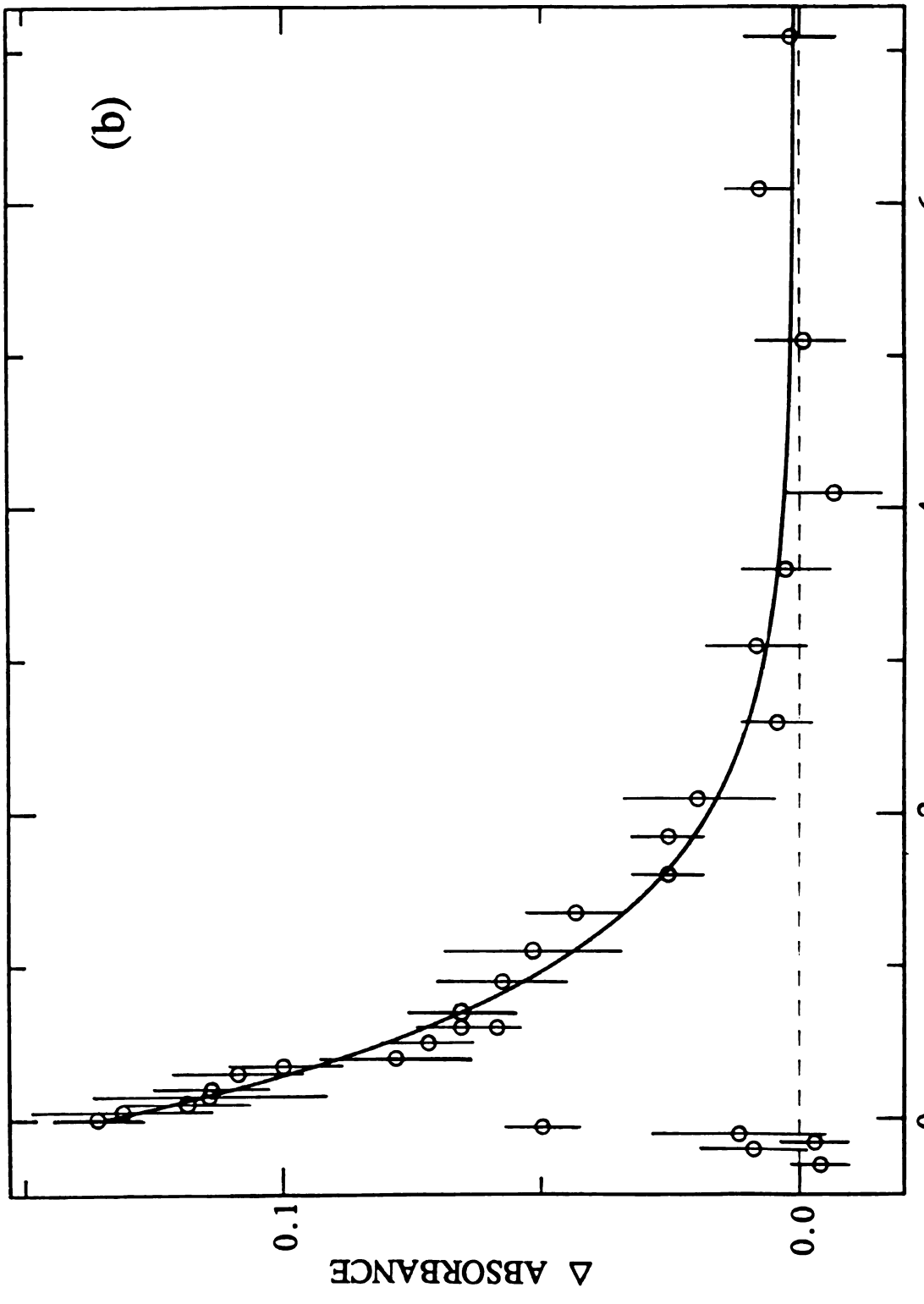

Figure 21

analysis of $^1(\delta\delta^*)$ is not feasible. However, it is reasonable that the prompt decay of the transient absorption is also the lifetime of the $^1(\delta\delta^*)$ excited state. These excited state properties of the bidentate methylphosphine complexes are parallel to those of the monoexponential $^1(\delta\delta^*)$ decay of the unbridged methylphosphine dimer, $Mo_2Cl_4(PMe_3)_4$. Analogously, the phenyl substituted bridged phosphine complexes, $Mo_2Cl_4(dppm)_2$ and $Mo_2Cl_4(dppe)_2$, exhibit decay kinetics similar to unbridged phosphine complexes possessing bulky substituents. The transient absorption at 400 nm and $^1(\delta\delta^*)$ bleaching at 620 nm decay by the same kinetics indicating that the transient spectrum arises from a single species (exemplary decays for $Mo_2Cl_4(dppm)_2$ are shown in Figure 22). These data are fit extremely well with two decay lifetimes of 130 ps and 2.1 ns for $Mo_2Cl_4(dppm)_2$. As shown in Figure 23, a similar biexponential decay process was observed from the $^1(\delta\delta^*)$ excited state of $Mo_2Cl_4(dppe)_2$ (lifetimes of 410 ps and 2.4 ns). By analogy to $Mo_2Cl_4(PBu_3)_4$, the shorter lifetime is assigned to $^1(\delta\delta^*)$ excited state and the longer lifetime corresponds to a non-luminescent transient intermediate. Although the data does not allow unequivocal assignment of the long-lived intermediate, it is interesting that the lifetime decay kinetics of $Mo_2X_4(PR_3)_4$ and $Mo_2Cl_4(LL)_2$ are related to the cone angle and basicity of the phosphine ligands. For $Mo_2X_4(PMe_3)_4$ and the bidentate analogues $Mo_2Cl_4(dmpm)_2$ and $Mo_2Cl_4(dmpe)_2$, the coordinated phosphines possess the smallest cone angle (PMe_3= 118°, dmpe= 107°) and strongest Lewis basicity.[127] These complexes decay directly from the $^1(\delta\delta^*)$ and their excited state dynamics are not mediated by any

Figure 22. Transient kinetics for $Mo_2Cl_4(dppm)_2$ in CH_2Cl_2 solution. The decay kinetics were recorded at (a) 400 nm and (b) 620 nm (excitation by 3^{rd} harmonic of a Nd:YAG, FWHM = 25 ps).

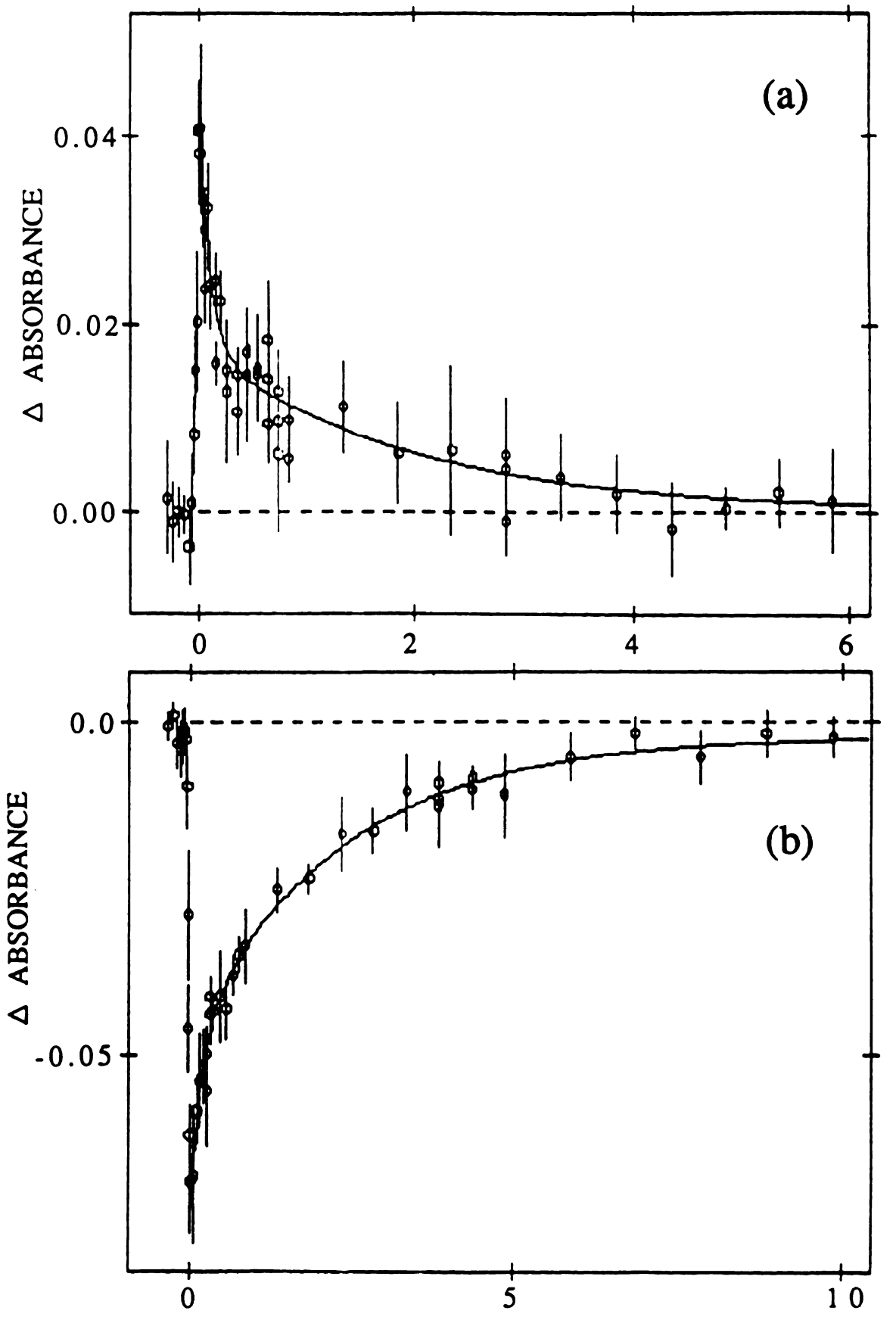

Figure 22

Figure 23. Transient kinetics of $Mo_2Cl_4(dppe)_2$ in CH_2Cl_2 solution. The decay kinetics were recorded at 420 nm (excitation by 2^{nd} harmonic of a Nd:YAG, FWHM = 25 ps).

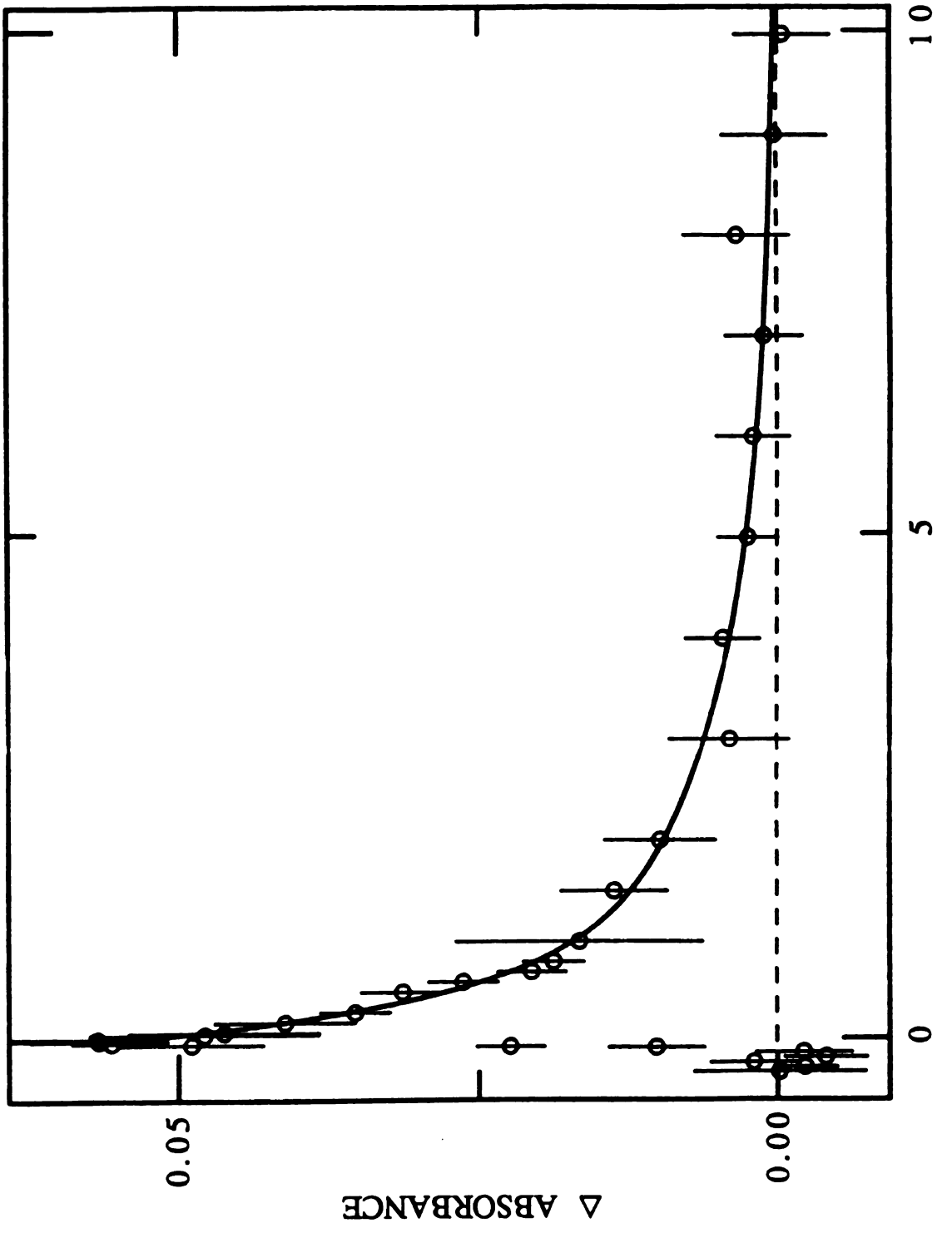

Figure 23

other intermediates. Conversely, $Mo_2Cl_4(PBu_3)_4$, $Mo_2Cl_4(dppm)_2$, and $Mo_2Cl_4(dppe)_2$ possess phosphines with much larger cone angles (PBu_3 = 132°, dppm = 121°, dppe = 125°).[127] The fast bimodel decays and lower quantum yields of these species are consistent with the formation of a chemical intermediate correlated with the cone angle of the phosphine. In this regard, numerous studies have shown that the dissociation of phosphines from metal centers is related intimately to the phosphine's cone angle.[127,128] An obvious explanation of the bimodel decay kinetics is that a chemical intermediate is formed by dissociation of phosphine from the metal core in the $^1(\delta\delta^*)$ excited state followed by recombination of the phosphine with the coordinatively unsaturated intermediate. The observed lifetimes for the chemical intermediate are well above the diffusion controlled limit for a bimolecular process. Thus if dissociation does occur, then it must do so within the solvent cage. This model also explains the similarity between the lifetimes of the chemical intermediate derived from bridged and unbridged complexes. For the latter, although the rate for recombination of the phosphine on the metal core should be much larger owing to a chelate effect, this effect will be attenuated for processes occurring within a solvent cage.

In summary, subtle factors appear to be governing the excited state dynamics of $M\overset{4}{-}M$ complexes. Excited state lifetimes and emission quantum yields are not explained fully by a simple torsional model. Eclipsed $Mo_2Cl_4(LL)_2$ (D_{2h}) complexes are weakly luminescent while torsionally distorted $Mo_2Cl_4(LL)_2$ (D_2) complexes possess much higher emission quantum yields. Rather, the excited

state dynamics are dictated by the symmetry of the M$\overset{4}{—}$M complex. The trend of decreasing quantum yields along the series of eclipsed $Mo_2X_4(PMe_3)_4$ (D_{2d}) > staggered $Mo_2Cl_4(LL)_2$ (D_2) > eclipsed $Mo_2Cl_4(LL)_2$ (D_{2h}) suggests that it is the presence of states proximate to the $^1(\delta\delta^*)$ singlet that are important to nonradiative decay and not the torsional angle about the metal-metal bond.

A single excited state following excitation is observed for halophosphine M$\overset{4}{—}$M complexes when the substituents on the phosphines are sterically small. However, with increasing steric bulk, the presence of two transient intermediates are observed, one of which is attributable to the $^1(\delta\delta^*)$ excited state and the other to a long-lived chemical intermediate. Although a definitive assignment of this intermediate is not possible, the data are consistent with formation of a coordinatively unsaturated transient produced by simple excited state dissociation of phosphine within a solvent cage.

CHAPTER IV

PHOTOCHEMISTRY OF NOVEL DIMOLYBDENUM PHOSPHATE COMPLEXES IN ACIDIC SOLUTION

A. Background

Conversion of a $M\overset{n}{-}M$ dimer with a metal-metal bond order of 4 to a species of bond order of 3 conceptually represents the simplest multielectron transformation available to a $M\overset{n}{-}M$ system. The overall reaction constitutes a two-electron oxidation of the metal-metal core. Multielectron studies were initiated by exploring the oxidation photochemistry of $M\overset{4}{-}M$ dimers in acidic solution with the goal of promoting the following reaction sequence

$$M\overset{4}{-}M \xrightarrow{h\nu} M\overset{4}{-}M^{*} \quad (26)$$

$$M\overset{4}{-}M^{*} + HB \longrightarrow M\overset{3}{-}M(H) + B^{-} \quad (27)$$

$$M\overset{3}{-}M(H) + HB \longrightarrow M\overset{3}{-}M^{2+} + H_2 + B^{-} \quad (28)$$

Scheme III

In this scheme, electronically excited $M^{\underline{4}}M$ reacts with HB in a two-electron oxidation step to produce a hydride intermediate and Brønsted base B^-. Trapping the hydride with another equivalent of HB gives oxidized dimer $M^{\underline{3}}M$ and hydrogen. It should be noted that the hydride production reaction is fundamentally important to excited state multielectron chemistry because it represents one of the simplest multielectron reaction pathways available to the excited quadruply bonded dimer. Practically, the reaction is important because metal hydrides are crucial intermediates in small molecule activation schemes such as those for water splitting chemistry. The hydrogen donor is not limited to a Brønsted acid but in principle can involve any small molecule reactant. Thus, the reaction chemistry described in Scheme III is significant in regard to our efforts in designing new excited state reactivity patterns.

Examination of Scheme III reveals that hydrogen production relies on a quadruple bond ⇔ triple bond conversion. Although, conceptually quite appealing, photoreaction to triply bonded species is an exceptional reaction pathway and the excited state reaction chemistry of $M^{\underline{4}}M$ dimers has been limited primarily to single-electron photoreactions. For instance, the photochemistry of $Mo_2(SO_4)_4^{4-}$ is exemplary of typical $M^{\underline{4}}M$ species: under relatively strong oxidizing conditions ($\lambda_{exc} > 254$ nm), irradiation of $Mo_2(SO_4)_4^{4-}$ in H_2SO_4 is confined to the production of the one electron product $Mo_2(SO_4)_4^{3-}$.[93] Presumably, the chemical instability of the triply bonded sulfate dimer precludes multielectron photochemistry. Accordingly, we set out to synthetically design $M^{\underline{n}}M$ complexes which could undergo triple/quadruple

photoconversions. In this context, the discovery of the triply bonded phosphate complex $Mo_2(HPO_4)_4^{2-}$ [109] stimulated our interest because the Mo_2 phosphate system could possibly provide insight into the mechanism of multielectron photoredox chemistry of $M\overset{n}{-}M$ dimers in acidic solution with the successful preparation of quadruply bonded molybdenum phosphate dimer. The existence of the quadruply bonded Mo_2(II,II) sulfate complex suggested that the Mo_2(II,II) phosphate could be prepared in view of the electronic and structural similarities of HPO_4^{2-} and SO_4^{2-}. This chapter describes the spectroscopy and electrochemistry of $Mo_2(HPO_4)_4^{4-}$ and $Mo_2(HPO_4)_4^{3-}$ dimers as well as the photoinduced two-electron oxidation of $Mo_2(HPO_4)_4^{4-}$ in acidic solution.

B. Results and Discussion

1. Magnetic and Spectroscopic Characterization of $Mo_2(HPO_4)_4^{n-}$ (n = 2, 3, 4) Species. A central result to emerge from exhaustive spectroscopic studies of multiply bonded metal-metal dimers is a consistent description of the electronic structure of these complexes in terms of a σ, π, and δ molecular orbital framework.[55a,65] One consequence of this model is the prediction that dimers of bond orders 4 ($\sigma^2\pi^4\delta^2$) and 3 ($\sigma^2\pi^4$) will possess a diamagnetic ground state whereas the mixed-valence dimer of bond order 3.5 ($\sigma^2\pi^4\delta^1$) will be paramagnetic. Investigation of the magnetic properties of $Mo_2(HPO_4)_4^{3-}$ and $Mo_2(HPO_4)_4^{4-}$ were of interest because these studies in connection with a previous susceptibility measurement on the pyridinium salt of $Mo_2(HPO_4)_4^{2-}$

which was shown to be diamagnetic,[129] would provide magnetic data on the first homologous M—M series possessing a $\sigma^2\pi^4\delta^n$ (n = 0, 1, 2) ground state configuration. The predicted paramagnetic behavior of $Mo_2(HPO_4)_4^{3-}$ is confirmed by magnetic susceptibility measurements of solids from 5 to 300 K at a field of 5500 G. Correction for the diamagnetic contribution to magnetic moment was provided by the room temperature magnetic susceptibility of the pyridinium salt of $Mo_2(HPO_4)_4^{2-}$. The susceptibility data is shown in Table 4. The temperature dependence of the magnetic susceptibility follows Curie law behavior (Figure 24) and the magnetic moment of $K_3Mo_2(HPO_4)_4$ is 1.58 BM. In accordance with susceptibility results, EPR spectra of the pyridinium salt of frozen solution of $K_3Mo_2(HPO_4)_4$ at 5 K (Figure 25) show a paramagnetic species in an axial environment, $g_\perp$ = 1.894, $g_\parallel$ = 1.886. As described in detailed studies of the EPR spectra of $Mo_2(SO_4)_4^{3-}$,[130] and other M—M dimers,[131] the EPR signal is consistent with a species in which the unpaired electron is coupled between two equivalent molybdenum nuclei.

Reduction of $Mo_2(HPO_4)_4^{3-}$ by one electron will yield a quadruply bonded complex which should exhibit rigorous diamagnetism. Unfortunately, the accurate determination of the magnetic susceptibility of $Mo_2(HPO_4)_4^{4-}$ is precluded by our inability to cleanly isolate salts of the quadruple bond complex from the mixed-valence dimer. Indeed, EPR spectra of solid samples of $K_4Mo_2(HPO_4)_4$ at 5 K show signals identical to that of $K_3Mo_2(HPO_4)_4$. That the intensity of the signal varies with sample preparation indicates that the observed paramagnetism arises from

Table 4. Magnetic Susceptibility of $K_3Mo_2(HPO_4)_4$.

T/ K	χ_M[a]/emu mol^{-1}	$1/\chi_M$/emu^{-1}mol
5	0.066219	15.1014
6	0.053052	18.8494
8	0.038362	26.0675
10	0.030215	33.0961
12	0.024878	40.1962
14	0.021185	47.2032
15	0.019661	50.8621
16	0.018452	54.1947
18	0.016427	60.8754
20	0.014713	67.9671
22	0.013333	75.0188
25	0.011682	85.6018
27	0.010850	92.1149
30	0.009801	102.0346
35	0.008420	118.7719
40	0.007454	134,1562
45	0.006638	150.6478
50	0.006053	165.2073
55	0.005517	181.2744
60	0.005124	195.1715
65	0.004741	210.9260
70	0.004455	224.4669
75	0.004171	239.7794
80	0.003725	268.4924
85	0.003725	295.6743
90	0.003561	280.8279
95	0.003382	295.6743
100	0.003241	308.5087
110	0.003004	332.8562
120	0.002763	361.9910
129	0.002595	385.4307
140	0.002545	393.0045

Table 4 (cont'd.).

148	0.002321	430.9230
163	0.002301	434.5937
166	0.002071	482.8352
184	0.002086	479.2715
191	0.001923	520.0479
205	0.001913	522.6572
221	0.001723	580.4167
223	0.001754	570.0604
254	0.001565	638.8144
255	0.001612	620.3859
279	0.001436	696.5729
281	0.001470	679.7634
310	0.001415	706.5141

[a] Data were corrected from the diamagnetic contribution by using the magnetic susceptibility of $Py_3Mo_2(HPO_4)_4Cl$ at room temperature (χ_M = -100x10^{-6} emu mol^{-1}).[129]

Figure 24. Temperature dependence of the corrected magnetic susceptibility of $K_3Mo_2(HPO_4)_4$.

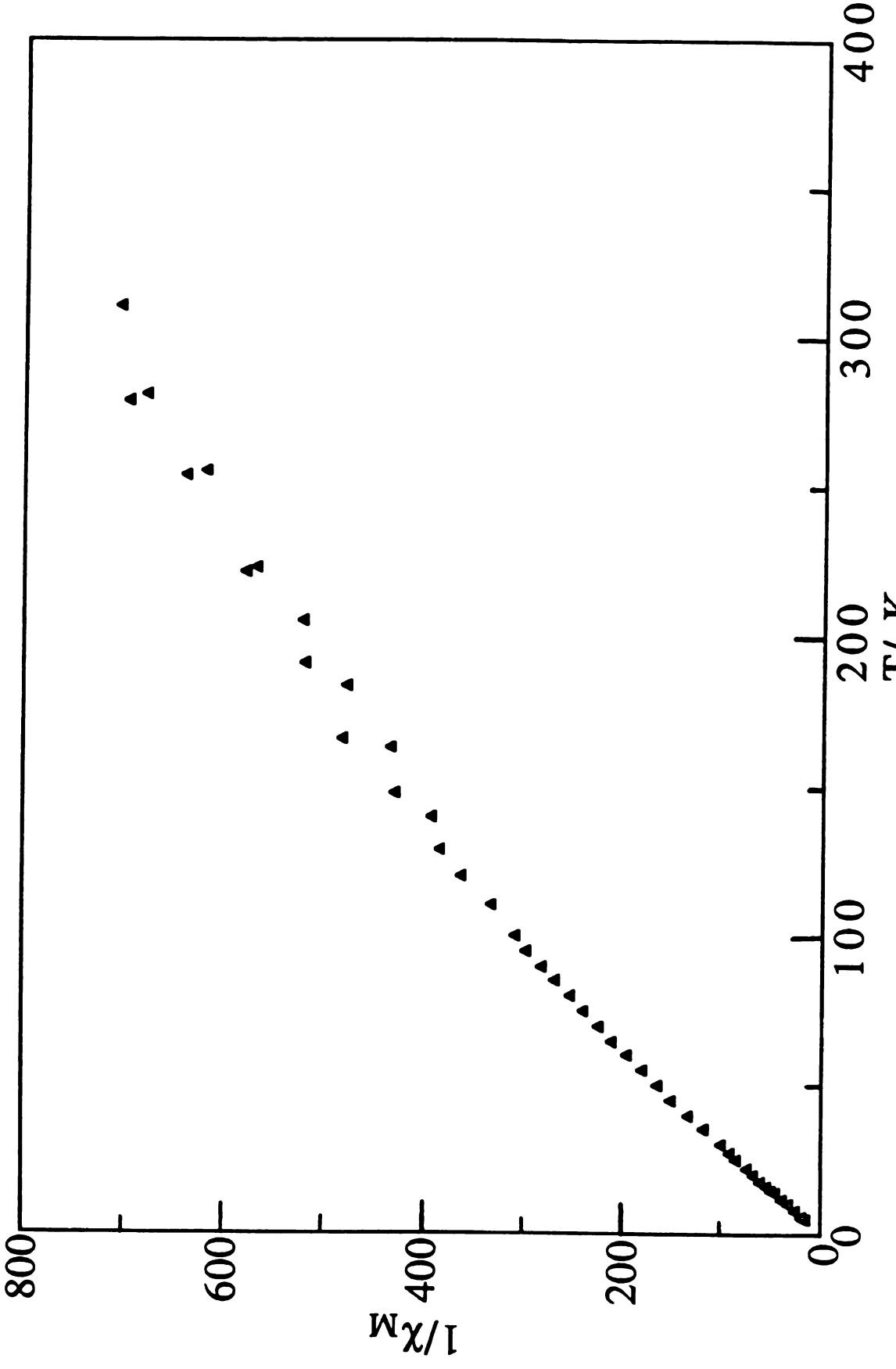

Figure 24

Figure 25. X-band (9.460 GHz) EPR spectrum of a frozen solution of $K_3Mo_2(HPO_4)_4$ in 7.5 M H_3PO_4 at 5 K.

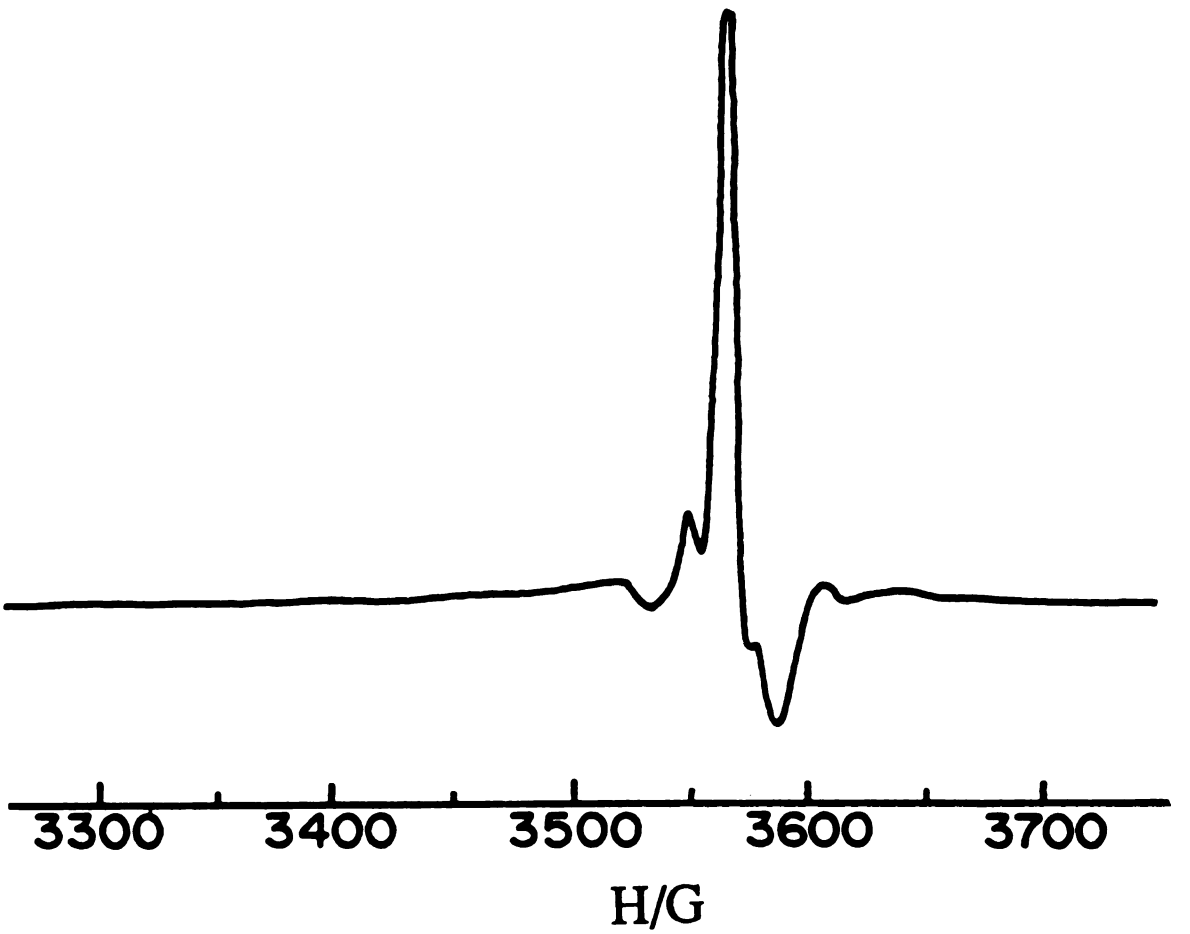

Figure 25

$Mo_2(HPO_4)_4^{3-}$ impurities and no evidence for a distinct EPR signal attributable to $Mo_2(HPO_4)_4^{4-}$ can be discerned. Thus, to the best of our knowledge, the magnetic properties of Mo_2 phosphate series are accommodated by the electronic structure model of M—M (D_{4h}) dimers.

Solids and solutions of $Mo_2(HPO_4)_4^{4-}$ are pink in color. Figure 26 displays the electronic absorption spectrum of the dimer in 2 M H_3PO_4. The lowest energy absorption band (λ_{max} = 516 nm, ϵ = 196 $M^{-1}\,cm^{-1}$) is comparable in energy and intensity to that of $Mo_2(SO_4)_4^{4-}$ and by analogy is assigned to the $\delta^2 \rightarrow \delta\delta^*$ transition. As expected for a dipole allowed transition, the band sharpens upon cooling solutions to 77 K, but the integrated intensity of the band remains constant; the absorption profile remains vibrationally featureless at low temperature. In addition to the $\delta^2 \rightarrow \delta\delta^*$ transition, visible and ultraviolet absorption systems in $Mo_2(HPO_4)_4^{4-}$ have direct analogues in $Mo_2(SO_4)_4^{4-}$ spectra. The absorption (λ = 408 nm, ϵ = 27 $M^{-1}\,cm^{-1}$) immediately to higher energy of the $\delta^2 \rightarrow \delta\delta^*$ transition is especially noteworthy; a similar positioned band in $Mo_2(SO_4)_4^{4-}$ has tentatively been assigned to the $\pi \rightarrow \delta^*$ transition.[129]

The electronic absorption spectrum of $Mo_2(HPO_4)_4^{3-}$ (Figure 27) is dominated by a prominent absorption profile in the near-infrared (λ_{max} = 1438 nm; ϵ = 180 $M^{-1}\,cm^{-1}$) and two weak visible bands at 595 nm (ϵ = 10 $M^{-1}\,cm^{-1}$) and 420 nm (ϵ = 8 $M^{-1}\,cm^{-1}$). Similar to the quadruply bonded dimers, the spectra of Mo_2(II,III) sulfate and phosphate are nearly identical. The results of previous spectroscopic studies of $Mo_2(SO_4)_4^{3-}$ are consistent with the

Figure 26. Electronic absorption spectrum of $Mo_2(HPO_4)_4^{4-}$ ion in 2 M H_3PO_4 at room temperature.

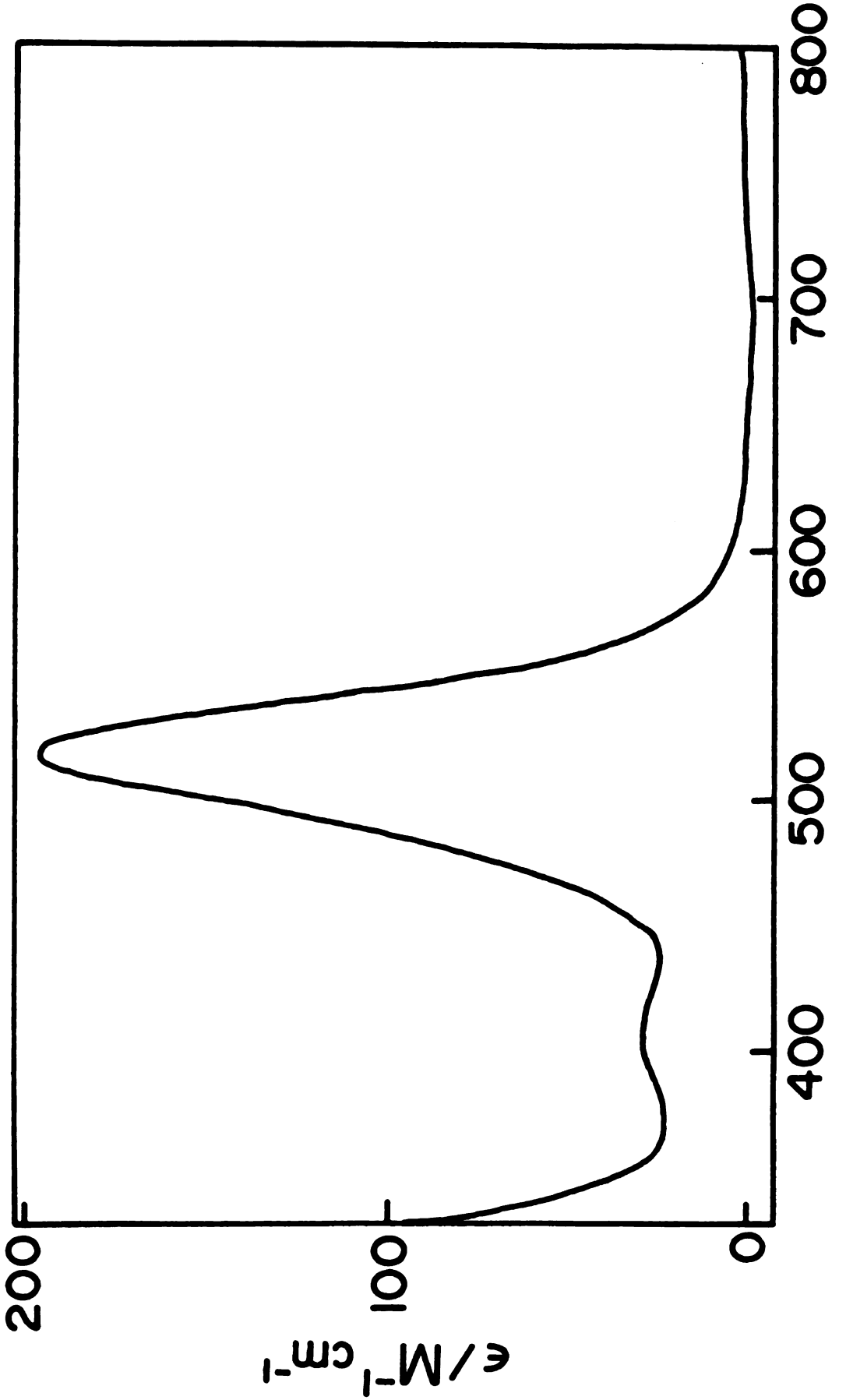

Figure 26

Figure 27. Electronic absorption spectrum of $K_3Mo_2(HPO_4)_4$ in 2 M H_3PO_4 at 25 ^oC.

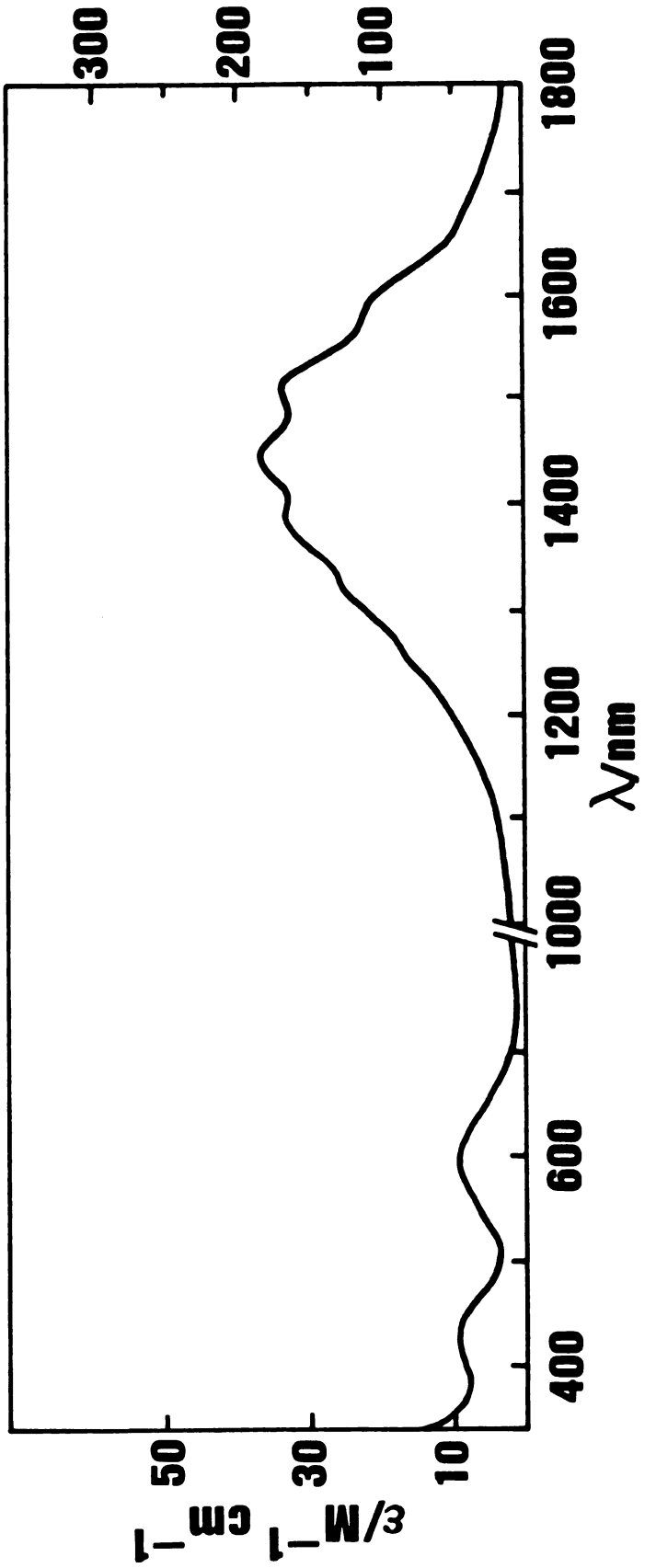
300
200
100
1800
1600
1400
1200
1000
600
400
λ/nm
50
30
10
ε/M⁻¹ cm⁻¹

Figure 27

assignment of the near-infrared absorption band to the $\delta \rightarrow \delta^*$ ($^2B_{1u} \leftarrow {}^2B_{2g}$) transition.[93,132] This significant red shift of the $\delta \rightarrow \delta^*$ transition of mixed-valence Mo_2 dimers is explained by the absence of two-electron term contributions to the transition energy for $\sigma^2\pi^4\delta^1$ configured ground state species. Similar to $Mo_2(SO_4)_4^{3-}$ ion, the $\delta \rightarrow \delta^*$ absorption band of $Mo_2(HPO_4)_4^{3-}$ exhibits a vibrational progression in solution at room temperature. As shown in Figure 28, the vibrational peaks sharpen considerably upon cooling the phosphoric acid solution to 77 K. The 334 cm^{-1} spacing is consistent with a progression in the symmetric metal-metal stretching vibration.

With regard to the visible absorption profile of $Mo_2(HPO_4)_4^{3-}$, the analogous absorption bands at 417 and 595 nm in $Mo_2(SO_4)_4^{3-}$ have been assigned by Hopkins *et al.* to the $\pi \rightarrow \delta^*$ and $\pi \rightarrow \delta$ transitions, respectively.[129] These assignments, which resulted from a comparative analysis of Mo_2(II,II) and Mo_2(II,III) sulfate and Mo_2(III,III) phosphate spectra, are predicated on the assumption that bridging SO_4^{2-} and HPO_4^{2-} ligands will perturb the electronic structure of a Mo_2 core in a similar fashion. In this context, the absorption spectra of the homologous Mo_2 phosphate series reported herein confirm this contention and accordingly support the $\pi \rightarrow \delta$ and $\pi \rightarrow \delta^*$ assignments for the visible absorption bands of $Mo_2(HPO_4)_4^{3-}$ and $Mo_2(SO_4)_4^{3-}$.

Raman spectra of solid samples of $Mo_2(HPO_4)_4^{n-}$ (n = 2, 3, 4) at room temperature were recorded with 4880 Å excitation light. The excitation frequency falls within the contour of the metal localized absorption profiles and significant enhancement of Raman peaks

Figure 28. Near-infrared absorption band of $K_3Mo_2(HPO_4)_4$ in a frozen phosphoric acid solution at 77 K.

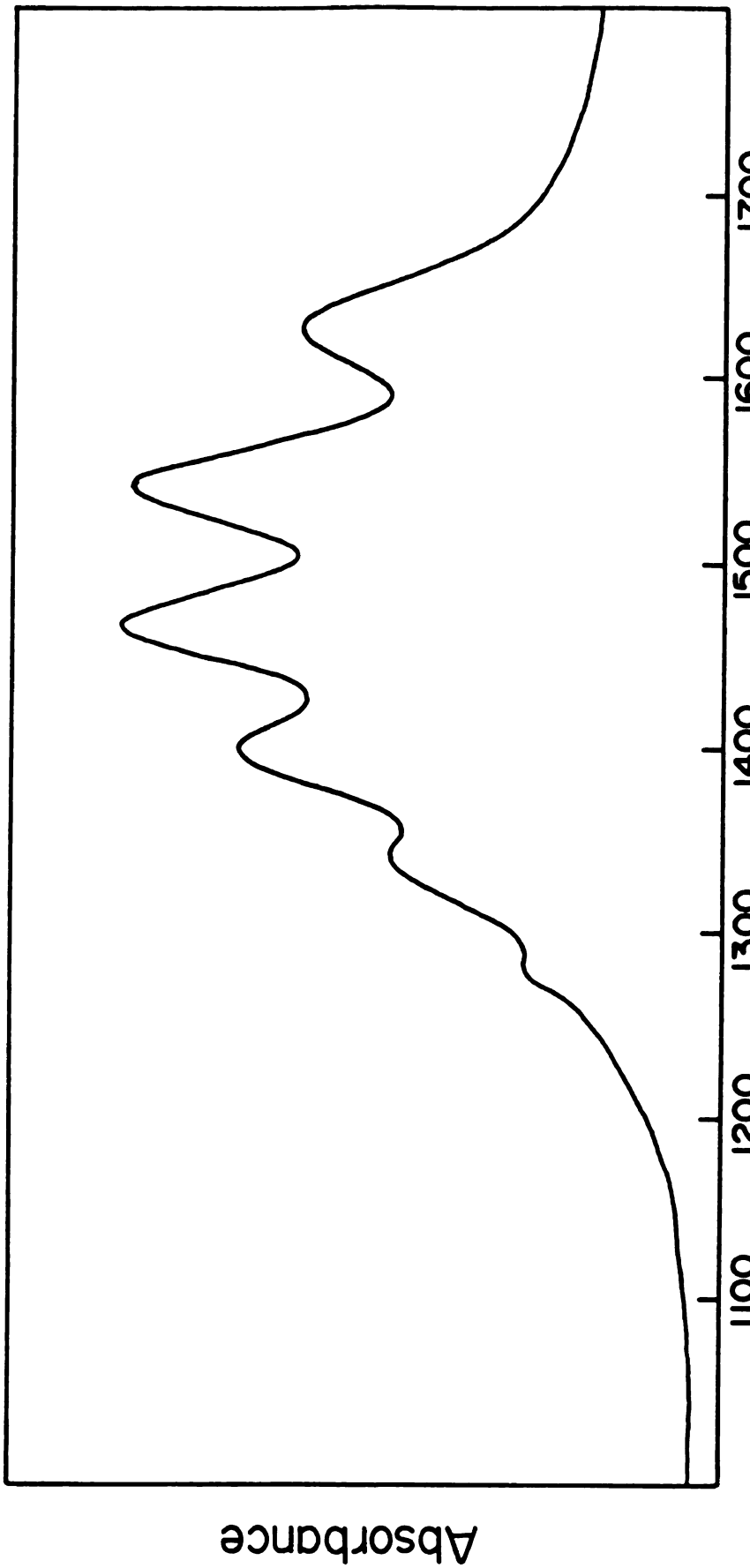

Figure 28

associated with metal-metal vibrations can be expected.[133] Prominent bands are observed at 345, 352, and 356 cm^{-1} in Raman spectra of Mo_2(II,II), Mo_2(II,III), and Mo_2(III,III) phosphate, respectively; this latter frequency is in excellent agreement with a previous study of $Mo_2(HPO_4)_4^{2-}$ in which a band at 358 cm^{-1} was attributed to νa_{1g}(Mo-Mo).[129] Assignment of the observed bands in the Mo_2 phosphate series to νa_{1g}(Mo-Mo) is consistent with their frequencies which will fall squarely within the 350-400 cm^{-1} range which characterizes metal-metal vibrations in $M\overset{n}{-}M$ dimers and is also supported by the presence of energetically similar peaks in Mo_2 sulfate dimers.[134] Given the νa_{1g}(Mo-Mo) assignment, a striking result of $Mo_2(HPO_4)_4^{n-}$ (n = 2, 3, 4) Raman spectra is the observed increase in metal-metal stretching frequency with decreasing bond order. Precedent for this puzzling trend has heretofore existed as an anomaly in the Raman spectra of Mo_2(II,II) (νa_{1g}(Mo-Mo) = 371 cm^{-1}) and Mo_2(II,III) (νa_{1g}(Mo-Mo) = 373, 386 cm^{-1}) sulfate. An explanation for this apparent inconsistency is the ability of the bridging ligand to modulate the metal-metal frequency,[135] although, the origin of this effect has not clearly been established. Nevertheless, the Raman results of the phosphate and sulfate series clearly demonstrate the ability of bridging ligands to vitiate predictions using simple bond order arguments.

2. Oxidation-Reduction Chemistry. The cyclic voltammogram of $Mo_2(HPO_4)_4^{2-}$ in 1 M H_3PO_4, shown in Figure 29, exhibits two oxidation processes. Reversible electrochemical behavior is suggested by linear plots of the cathodic and anodic currents vs.

Figure 29. Cyclic voltammogram of a 2.5 mM solution of the pyridinium salt of $Mo_2(HPO_4)_4^{4-}$ in 2 M H_3PO_4. The scan rate was 2 mV s^{-1}.

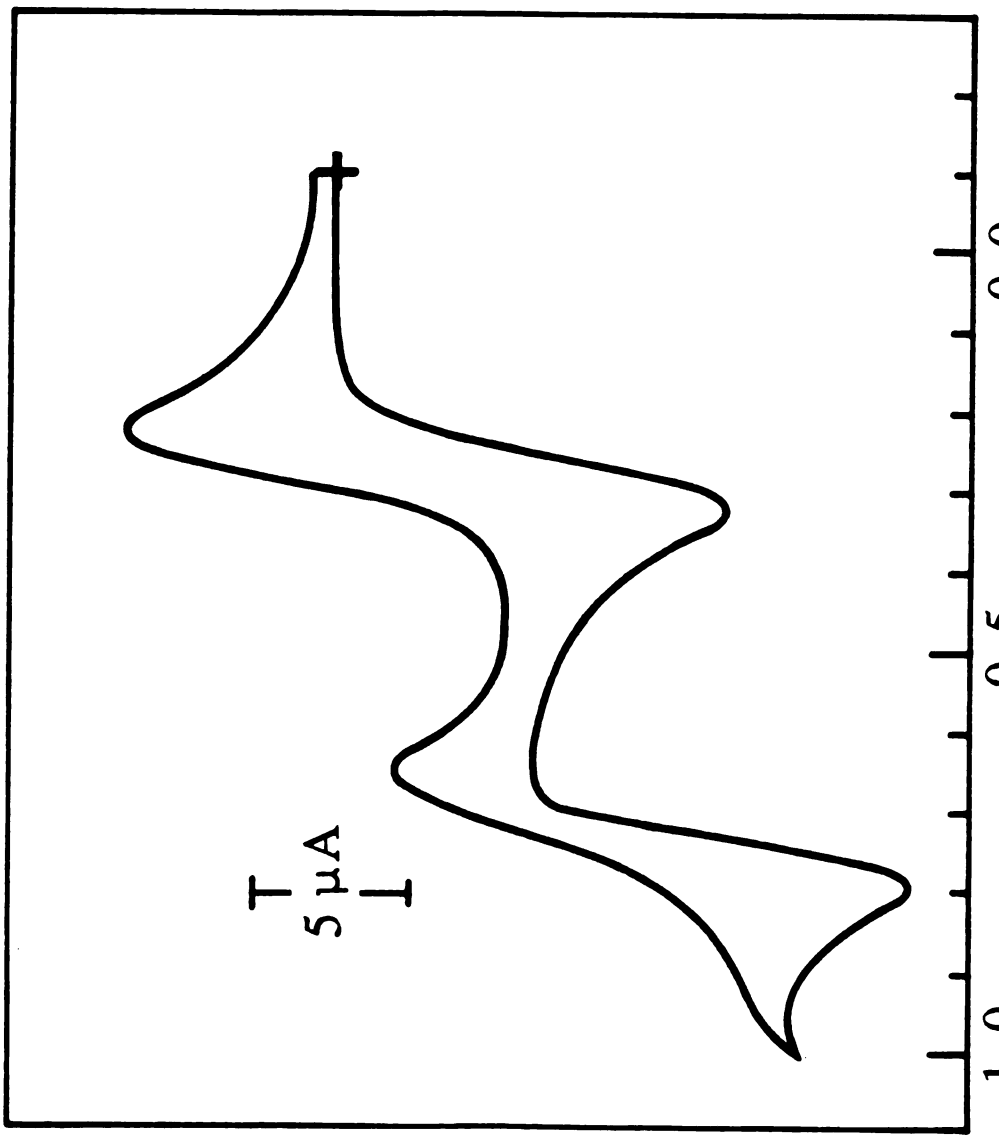

Figure 29

$\nu^{1/2}$ (scan rate, ν: 5-100 mV sec^{-1}), and values of 0.98 ± 0.04 for ratios of the anodic and cathodic peaks currents.[112] The identities of these two electrode processes are revealed by electrochemical experiments on solutions of the quadruply bonded and mixed-valent phosphate dimers. Cyclic voltammograms identical to the one displayed in Figure 29 are observed upon scanning th electrode potential from the appropriate resting potentials of solutions of Mo_2(II,II) and Mo_2 (II,III) phosphates. These results lead us to assign the waves at -0.25 V and -0.67 V vs. SCE to the $Mo_2(HPO_4)_4^{2-/3-}$ and $Mo_2(HPO_4)_4^{3-/4-}$ couples, respectively. The syntheses of Mo_2 phosphate dimers and their reaction chemistry are easily understood in the context of the above electrochemcial results. Our observation that solids of $Mo_2(HPO_4)_4^{4-}$ precipitated from acidic solutions are inevitably contaminated with $Mo_2(HPO_4)_4^{3-}$ is consistent with the negative potential of the $Mo_2(HPO_4)_4^{3-/4-}$ couple with respect to the standard hydrogen electrode. Indeed $Mo_2(HPO_4)_4^{4-}$ in 2 M H_3PO_4 solution slowly converts to $Mo_2(HPO_4)_4^{3-}$ as evidenced by the disappearance of the $^1(\delta^2 \rightarrow \delta\delta^*)$ absorption band at 516 nm and the concomitant growth of the $^2(\delta \rightarrow \delta^*)$ absorption of Mo_2-$(HPO_4)_4^{3-}$. Closer analysis of the reaction reveals the quantitative conversion of quadruple bond dimer to mixed-valence species ($\tau_{1/2}$ = 27.5 h) and chromatographic analysis identifies hydrogen as a reaction product. Toepler pumping the gas above completely reacted solutions reveals that 0.39 moles of H_2/mole of $Mo_2(HPO_4)_4^{4-}$ is evolved thereby establishing the overall reaction stoichiometry as

$$Mo_2(HPO_4)_4^{4-} + H^+ \rightarrow Mo_2(HPO_4)_4^{3-} + 1/2\ H_2 \qquad (29)$$

Reduction of protons to hydrogen radicals is a highly energetic process [$E(H^+/H) = 2.6$ V vs. NHE],[136] and hence, direct reaction of the quadruple bond dimer with H^+ to $Mo_2(HPO_4)_4^{2-}$ produce the mixed-valence dimer is not thermodynamically feasible. We propose that $Mo_2(HPO_4)_4^{4-}$ reacts in acidic solution to $Mo_2(HPO_4)_4^{2-}$ which then reacts in a comproportionation reaction to produce mixed-valence dimer according to the following,

$$Mo_2(HPO_4)_4^{4-} + 2\ H^+ \rightarrow Mo_2(HPO_4)_4^{2-} + H_2 \qquad (30)$$

$$Mo_2(HPO_4)_4^{4-} + Mo_2(HPO_4)_4^{2-} \rightarrow 2\ Mo_2(HPO_4)_4^{3-} \qquad (31)$$

Consistent with reactions (30) and (31) is our observation that addition of a phosphoric acid solution of $Mo_2(HPO_4)_4^{2-}$ to one of $Mo_2(HPO_4)_4^{4-}$ leads to the immediate and quantitative production of Mo_2-$(HPO_4)_4^{3-}$. In view of previous studies of $M\overset{n}{-}M$ dimers which have demonstrated large rate constants for electron exchange reactions involving δ orbitals,[83] the facility of reaction (27) is not surprising since the comproportionation simply involves the transfer of an electron between the δ orbitals of the Mo_2 phosphato dimers. We therefore believe that the slow thermal conversion of $Mo_2(HPO_4)_4^{4-}$ to $Mo_2(HPO_4)_4^{3-}$ in phosphoric acid solutions, in the context of the above scheme, is a consequence of large kinetic barriers associated with reaction (30).

3. Photochemistry. In striking contrast to the slow thermal chemistry, reaction of $Mo_2(HPO_4)_4^{4-}$ in acidic solution is markedly accelerated by ultraviolet irradiation. Spectral changes for the room temperature irradiation ($\lambda > 335$ nm) of $Mo_2(HPO_4)_4^{4-}$ in 2 M D_3PO_4 are shown in Figure 30. An initial decrease in the intensity of the $\delta^2 \rightarrow \delta\delta^*$ absorption band of $Mo_2(HPO_4)_4^{4-}$ is accompanied by an increase in the $\delta \rightarrow \delta^*$ absorption of $Mo_2(HPO_4)_4^{3-}$. Ensuing reaction of the mixed-valence dimer is revealed by the disappearance of the near-infrared $\delta \rightarrow \delta^*$ absorption. A series of weak changes in the visible region is observed with continued irradiation and the photolysis reaction terminates with an absorption profile distinguished by a strong absorption band at 385 nm and a weaker band at 685 nm. The absence of an isobestic point during the photolysis reaction, and the growth and decay of the characteristic near-infrared band of $Mo_2(HPO_4)_4^{3-}$ are consistent with a multistep photooxidation pathway with subsequent reaction of the Mo_2 primary photoproduct.

Further analysis of the $Mo_2(HPO_4)_4^{4-}$ photoreaction was pursued with investigations of the photochemistry of Mo_2(II,III) and Mo_2(III,III) phosphate dimers. Irradiation ($\lambda > 335$ nm) of $Mo_2(HPO_4)_4^{3-}$ in 2M D_3PO_4 produces the spectral changes illustrated in Figure 31. The intensity of the near-infrared band of $Mo_2(HPO_4)_4^{3-}$ monotonically decreases and bands at 420 and 540 nm appear during the initial stages of irradiation. With continued irradiation, the 540-nm band disappears and absorptions grow in at 385 and 690 nm. This latter spectrum is identical to the terminating spectrum of $Mo_2(HPO_4)_4^{4-}$ photolysis. The quantum yield for the

Figure 30. Electronic absorption spectral changes during irradiation ($\lambda > 335$ nm) of $Mo_2(HPO_4)_4^{4-}$ in 2 M D_3PO_4. Due to spectral congestion in the visibile spectral region, the 45-min trace is not illustrated between 350 and 800 nm. The absorbance sensitivity in the visible spectral region is twice that of the infrared spectral region.

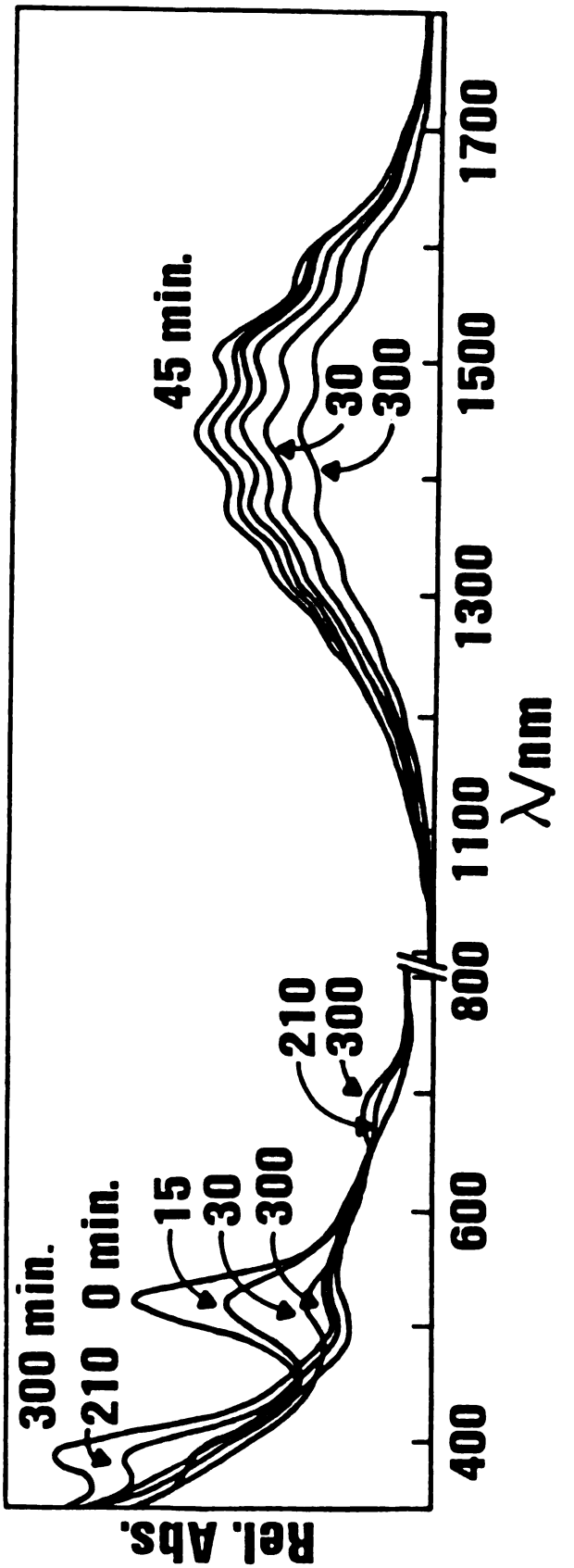
Rel. Abs.
400
600
800
1100
1300
1500
1700
λ/nm
300 min.
210
0 min.
15
30
300
210
300
45 min.
30
300

Figure 30

Figure 31. Absorption changes resulting from irradiating (λ > 335 nm) 2 M D_3PO_4 solutions of $Mo_2(HPO_4)_4^{3-}$. The visible absorbance scale is 5 times greater than the near-infrared absorbance scale.

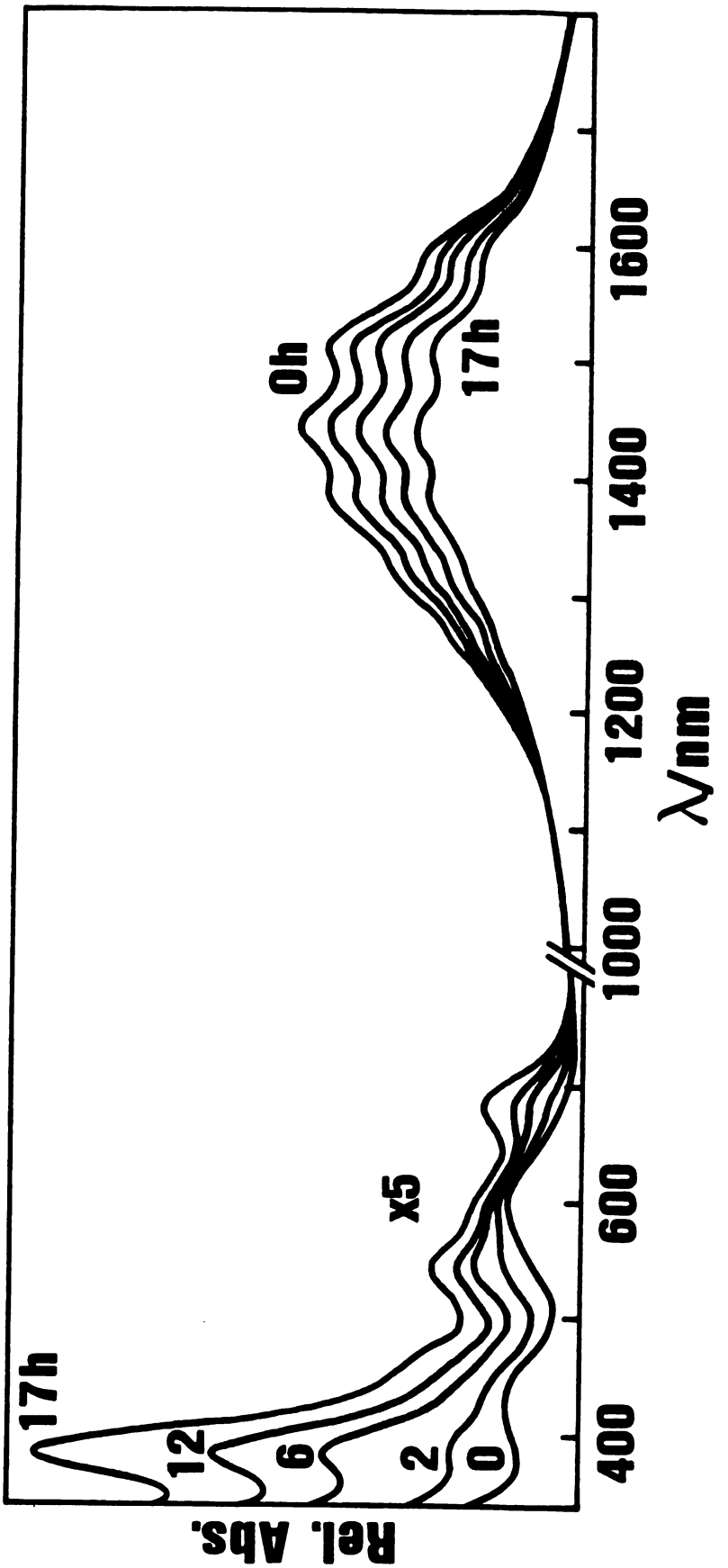

Figure 31

disappearance of $Mo_2(HPO_4)_4^{3-}$ is 0.046 (λ_{exc} = 313 nm) whereas no reaction is observed for solutions of the mixed-valence dimer stored in the dark at room temperature.

The appearance of the 540-nm band during the early stages of $Mo_2(HPO_4)_4^{3-}$ photolysis is consistent with the formation of $Mo_2(HPO_4)_4^{2-}$ as a primary photoproduct. Support for this contention is provided by the photochemistry of $Mo_2(HPO_4)_4^{2-}$. Figure 32 displays the absorption changes accompanying irradiation (λ > 335 nm) of 2 M D_3PO_4 solutions of $Mo_2(HPO_4)_4^{2-}$. Smooth conversion of $Mo_2(HPO_4)_4^{2-}$ to the photoproduct, characterized by the 385- and 685-nm absorptions, is observed and in contrast to Mo_2(II,II) and Mo_2(II,III) photochemistry, isobestic points at 500 and 608 nm attest to a stoichiometric photoreaction. While the identity of this ubiquitous photoproduct has not yet been revealed, a clue to its identity is provided by comparison to the absorption spectra of other dimolybdenum oxo and hydroxo cores.[137-146] Table 5 displays absorption maxima and molar absorptivity coefficients of polynuclear molybdenum complexes. Examination of these data reveals that the absorption spectrum of the primary photoproduct of $Mo_2(HPO_4)_4^{2-}$ photolysis ($\lambda_{max}(\epsilon)$: 385 nm (1800 M^{-1} cm^{-1}); 690 nm (350 M^{-1} cm^{-1})) closely matches that of the Mo_2(III,III)-μ-dihydroxo complex.[131] These results suggest that irradiation of $Mo_2(HPO_4)_4^{2-}$ triple bond dimer promotes ligand substitution of the phosphate to yield the μ-hydroxo species. The slight wavelength discrepencies between the primary photoproduct and the $Mo_2(III,III)(\mu\text{-}OH)_2(aq)$ complex may be due to the differences of the ancillary ligands (H_2O vs. HPO_4^{2-}) on the $Mo_2(\mu$-

Figure 32. Electronic absorption spectral changes during irradiation ($\lambda > 335$ nm) of $Mo_2(HPO_4)_4^{2-}$ in 2 M D_3PO_4. No absorption bands appear in the near-infrared spectral region during the photolysis reaction.

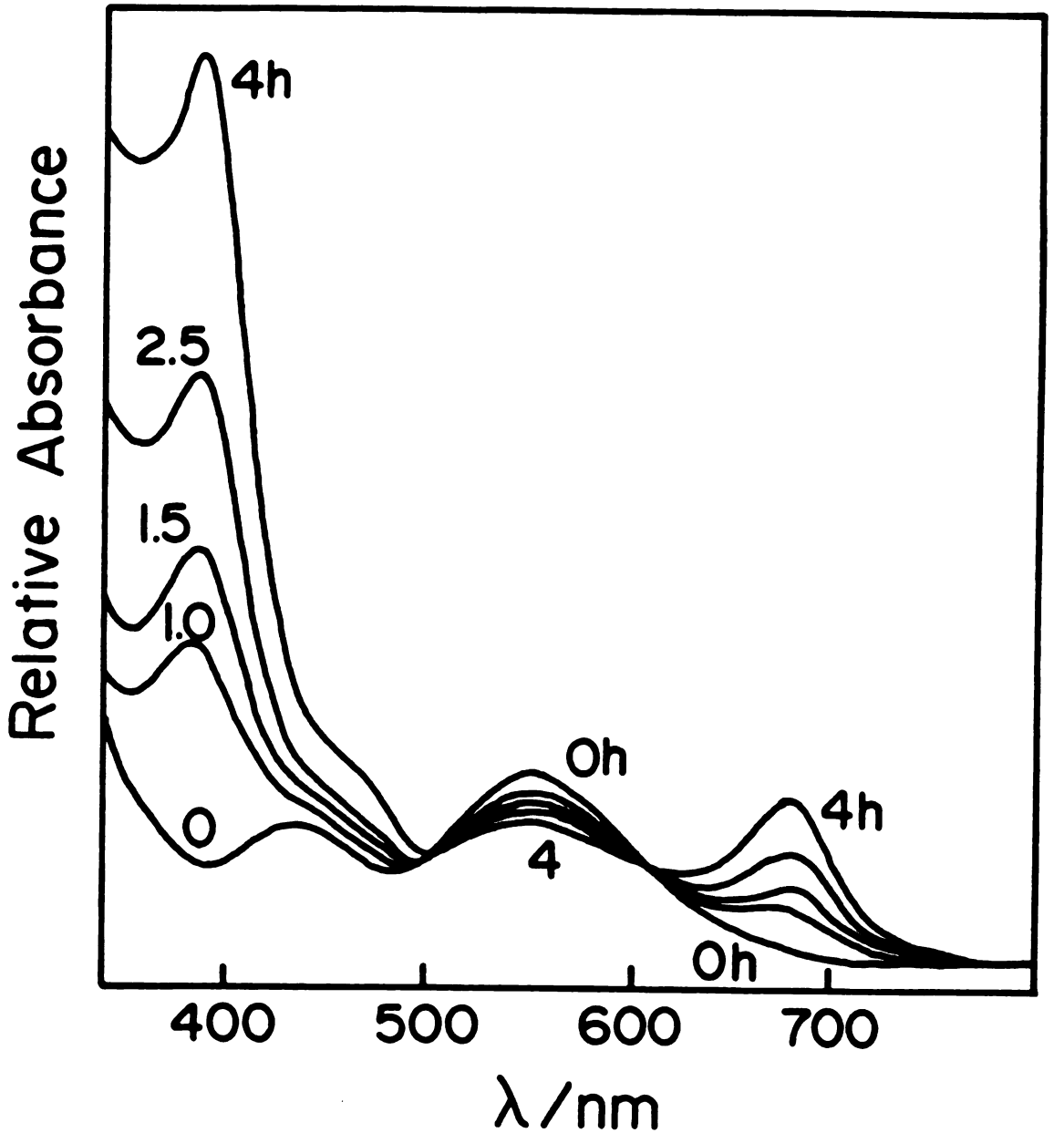

Figure 32

Table 5. Electronic Absorption Maxima of Dimolybdenum Ions in Aqueous Solution.

Formula	oxidation state	A/nm[a]	ref.
$Mo_2(aq)^{4+}$	II,II	503(337), 370(40)	108
$Mo_2(SO_4)_4^{4-}$		515(250), 405(30)	107
$Mo_2(HPO_4)_4^{4-}$		516(196), 405(30)	b
$Mo_2(SO_4)_4^{3-}$	II,III	595(10), 415(8)	130
$Mo_2(HPO_4)_4^{3-}$		595(10), 415(8)	b
$Mo(H_2O)_6^{3+}$	III	380(16), 308(28)	137
$MoCl_6^{3-}$		525(32), 420(45)	138
$Mo_2(\mu\text{-}OH)_2(H_2O)_n^{4+}$	III,III	624(110), 572(96), 360(910)	139
$Mo_2(HPO_4)_4^{2-}$		548(107), 428(63)	109
$Mo_3O(\mu\text{-}OH)_3(H_2O)_n^{4+}$	III,III,III	825(135), 635(240), 420(300)	140

Table 5 (cont'd.).

$Mo_3O(\mu\text{-}OH)_3(H_2O)_n^{5+}$	III,III,IV	1050(95), 495(115), 398(230)	140
$Mo_3(OAc)_6(EtO)_2(aq)^{2+}$		550(260), 480(250), 390(320)	141
$Mo_3O_2(OAc)_6(H_2O)_3^{2+}$	IV,IV,IV	509(450), 428(460)	142
$Mo_3O_4(C_2O_4)_6(H_2O)^{2-}$		518(310), 390(650)	143
$Mo_3O_4(H_2O)_9^{4+}$		505(63), 303(265)	144
$Mo_2O_4(H_2O)_6^{2+}$	V,V	384(103), 290(3162)	145

[a] Molar extinction coeffients are in parenthesis. [b] This work.

$OH)_2^{4+}$ core. This hypothesis can be tested by investigating the substitution chemistry of $Mo_2(\mu\text{-}OH)_2(aq)^{4+}$ in phosphate containing solutions. Interestingly continued ultraviolet photolysis of the proposed $Mo_2(\mu\text{-}OH)_2^{4+}$ phosphate photoproduct yields a species with the absorption spectrum shown in Figure 33. Detection of hydrogen above reacted solutions by gas chromatography suggests that the $Mo_2(\mu\text{-}OH)_2^{4+}$ core is photooxidized. This observation is confirmed by the fact that addition of $K_2S_2O_8$ to phosphoric acid solutions of $Mo_2Cl_8^{4-}$ yields a product with an absorption spectrum identical to the one shown in Figure 33. These results are consistent with photooxidation $Mo_2(\mu\text{-}OH)_2^{4+}$ phosphate produce a high valent Mo_2 oxo or hydroxo core (e.g. $Mo_2O_4^{2+}$).

The above photochemical results of $Mo_2(HPO_4)_4^{n-}$ (n = 2, 3, 4,) dimers substantiate a sequential oxidation pathway. The relatively complicated series of spectral changes induced by irradiation of $Mo_2(HPO_4)_4^{4-}$ solutions are explained by a reaction scheme in which the final photoproduct (λ_{max} = 385 and 685 nm) is generated directly from $Mo_2(HPO_4)_4^{2-}$, which in turn is a primary photoproduct of $Mo_2(HPO_4)_4^{3-}$ which is the primary photoproduct of $Mo_2(HPO_4)_4^{4-}$. Gas chromatography reveals a concomitant production of hydrogen with each of these discrete dimer photo-processes. A reaction sequence accommodating these observations is shown by equation (32). As previously noted, ensuing $Mo_2(HPO_4)_4^{2-}$ photo-oxidation leads to the generation of a presently undetermined higher valent molybdenum species and hydrogen. Thus the overall photochemical reaction corresponds to a multielectron process which involves the exchange of at least two electrons.

Figure 33. Terminating electronic absorption spectrum of photolyzed ($\lambda > 335$ nm) phosphoric acid solutions of $Mo_2(HPO_4)_4^{n-}$ (n = 2, 3, 4).

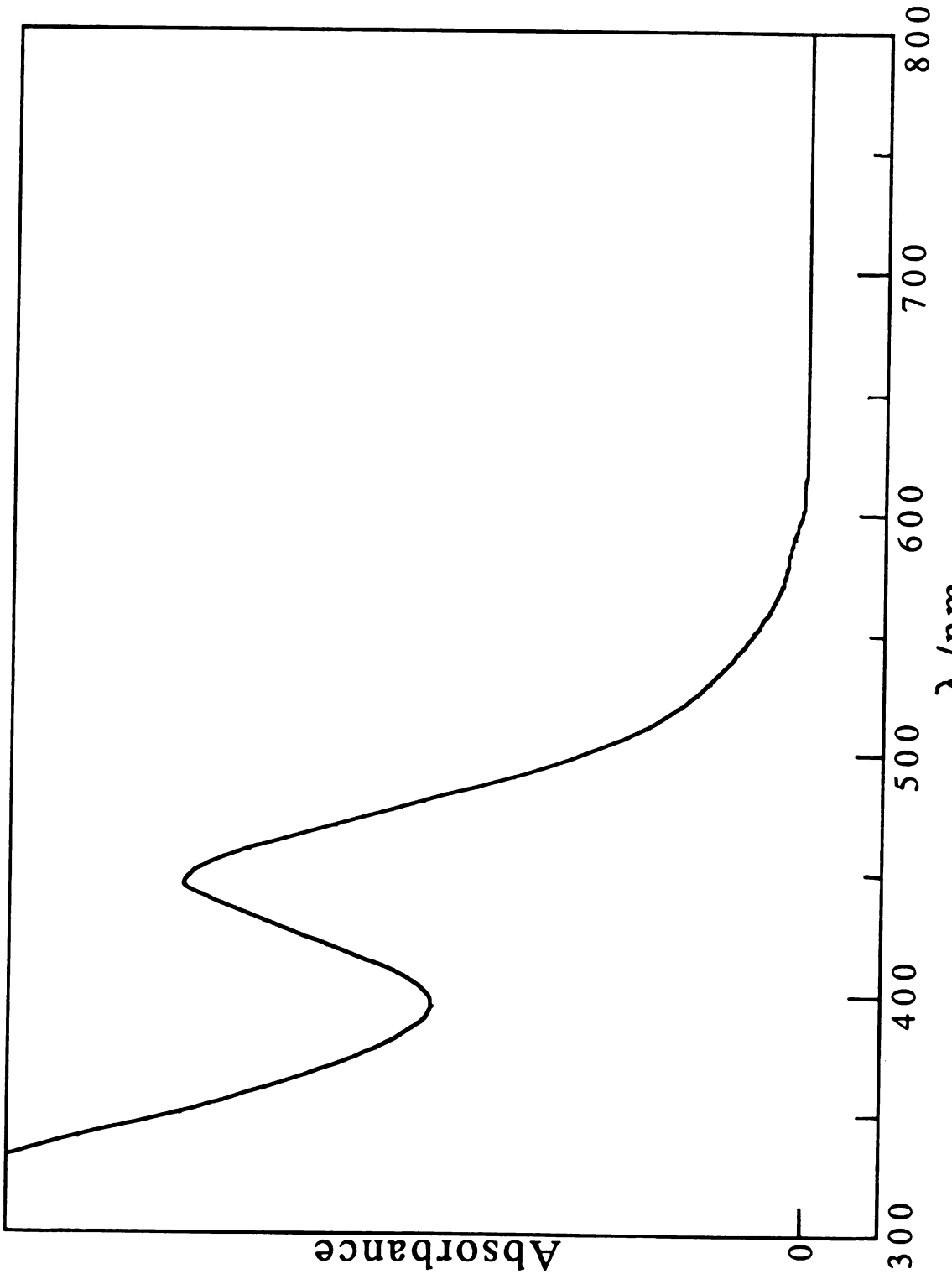

Figure 33

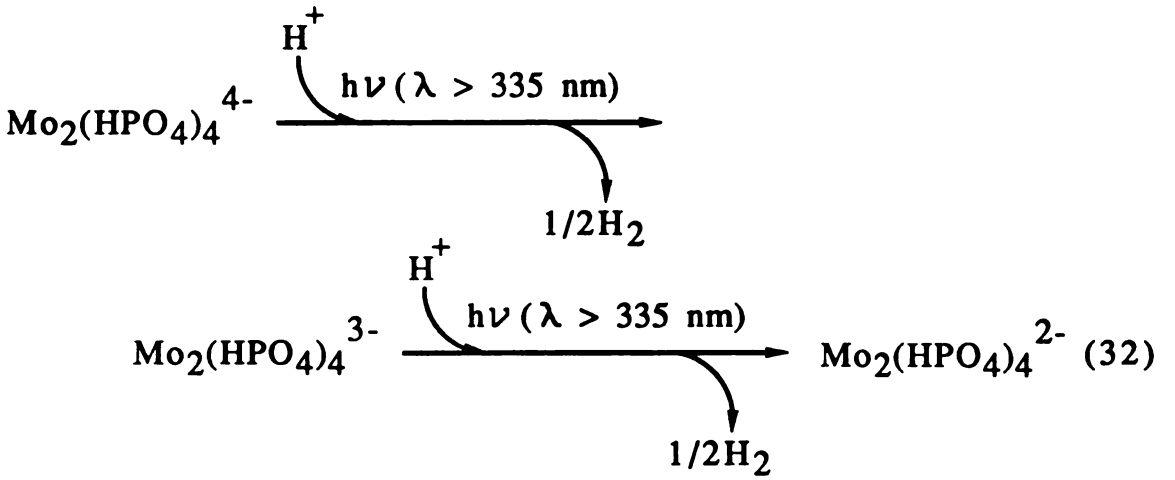

(32)

In an effort to ascertain the nature of the intermediates leading to hydrogen production, we photolyzed solutions of $Mo_2(HPO_4)_4^{4-}$ and $Mo_2(HPO_4)_4^{3-}$ under atmospheres of N_2O, which is an effective trap of highly energetic radical intermediates. Ultraviolet irradiation (λ_{exc} > 335 nm) of $Mo_2(HPO_4)_4^{4-}$ and $Mo_2(HPO_4)_4^{3-}$ in N_2O saturated 2 M H_3PO_4 solutions yields the one-electron photo-oxidized Mo_2 phosphato complex and N_2. These results are consistent with the generation of H atoms as primary photoproduct of Mo_2 phosphato dimers because nitrogen, which is generated at the expense of hydrogen formation, is a product expected from a reaction of hydrated hydrogen atoms with N_2O.[147] Annihilation of two hydrogen atoms or subsequent oxidation of the starting complex by a hydrogen atom to yield H^- followed by a facile proton trapping reaction will result in hydrogen production.

Insight into the nature of the photoactive state of the Mo_2 phosphate systems is provided by the wavelength dependence of $Mo_2(HPO_4)_4^{n-}$ (n = 2, 3, 4) photoprocesses. The photochemistry of each of the Mo_2 phosphate system is inhibited as the irradiation

wavelength is increased. Illustrative of this reactivity trend is the photooxidation reaction $Mo_2(HPO_4)_4^{3-}$ which proceeds promptly with ultraviolet irradiation but is suppressed upon shifting the excitation wavelength into the visible spectral region; Figure 34 summarizes the wavelength dependence of the reaction quantum yield. No photoreaction can be detected when $Mo_2(HPO_4)_4^{3-}$ solutions are irradiated at wavelengths longer than 475 nm. Between 300 and 400 nm, the quantum yield increases monotonically with decreasing irradiation wavelengths. And for wavelengths less than 300 nm, the quantum yield asymptotically approaches a limiting value of 0.05. Similarly, facile conversion of $Mo_2(HPO_4)_4^{4-}$ is observed for excitation wavelengths less than 367 nm, whereas solutions of $Mo_2(HPO_4)_4^{4-}$ do not photoreact with irradiations into the $^1(\delta^2 \rightarrow \delta\delta^*)$ absorption band. These results imply that the photoreactivity of the Mo_2 phosphato dimers is not associated with the lowest energy metal localized transition of the Mo_2 core but rather with high energy excited states that lie in the ultraviolet spectral region.

In an effort to identify these high energy photoactive excited states, the ultraviolet absorption spectra of the Mo_2 phosphato complexes in 2 M H_3PO_4 was recorded. As illustrated in Figure 35, a prominent absorption band dominates the ultraviolet spectral region of the three phosphato dimers (λ_{max}, $Mo_2(HPO_4)_4^{4-}$ = 206 nm; λ_{max}, $Mo_2(HPO_4)_4^{3-}$ = 210 nm; λ_{max}, $Mo_2(HPO_4)_4^{2-}$ = 220 nm). The relative insensitivity of the band maximum to the oxidation state of the Mo_2 core suggests that the transition is metal localized. Theoretical calculations predict that the allowed $\pi \rightarrow \pi^*$ transition of

Figure 34. Action spectrum of the photolysis reaction: $Mo_2(HPO_4)_4^{3-} + H^+ \rightarrow Mo_2(HPO_4)_4^{2-} + 1/2\ H_2$. Quantum yields were measured by monitoring the $\delta \rightarrow \delta^*$ absorption band of $Mo_2(HPO_4)_4^{3-}$.

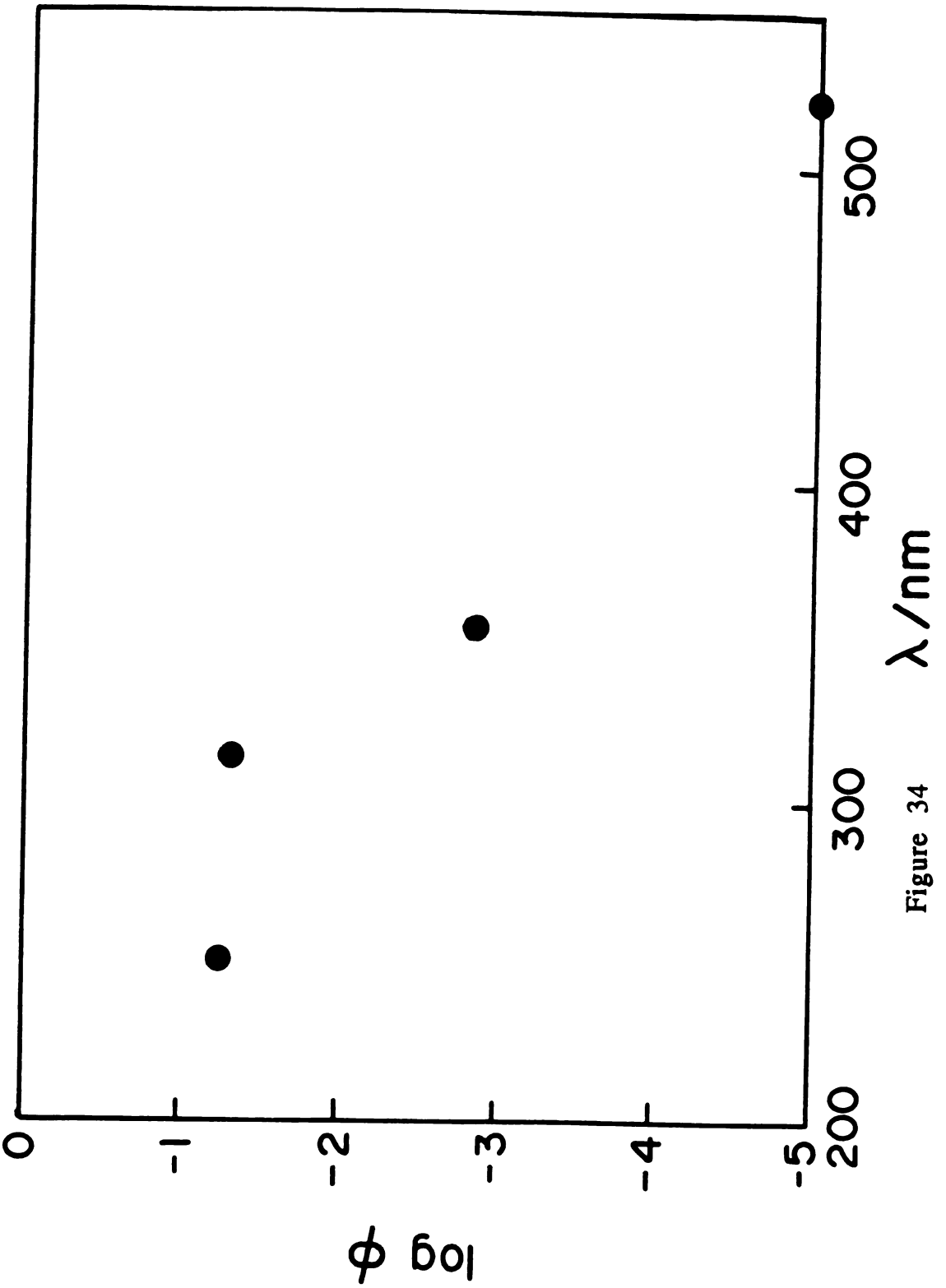

Figure 34

Figure 35. Ultraviolet absorption bands of $Mo_2(HPO_4)_4^{4-}$ (---), $Mo_2(HPO_4)_4^{3-}$ (—), and $Mo_2(HPO_4)_4^{2-}$ (· · ·) in 2 M H_3PO_4 at 25 °C.

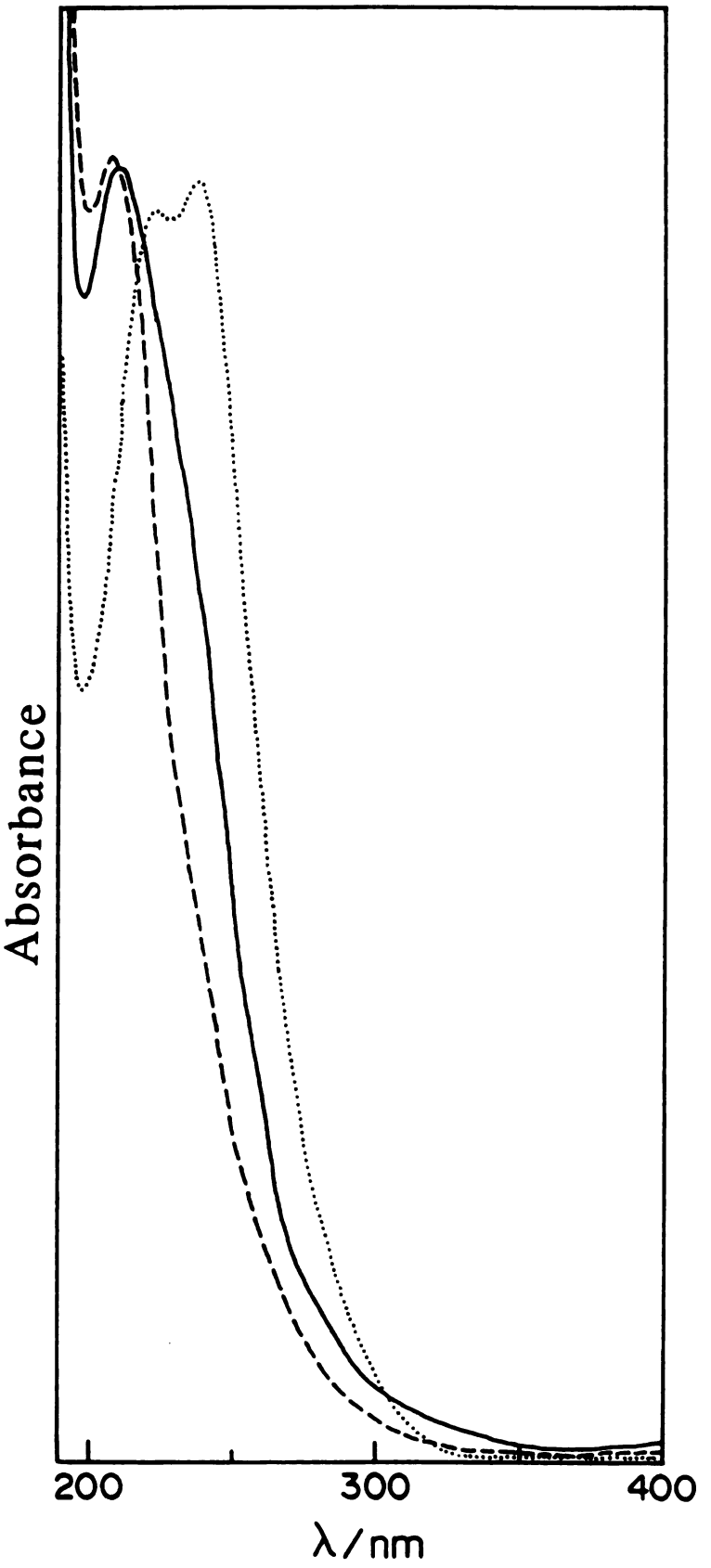

Figure 35

M$\overset{4}{-}$M dimers should be observed in ultraviolet energy region,[148] and polarized absorption spectroscopic studies[149] support this contention. Accordingly, we assign the 206 nm absorption of $Mo_2(HPO_4)_4^{4-}$ to the $\pi \rightarrow \pi^*$ transition. The modest red-shift of the band across the Mo_2(II,II), Mo_2(II,III), and Mo_2(III,III) series is consistent with a concomitant decrease in the metal-metal interaction. An additional absorption band is observed at 237 nm of Mo_2(III,III) phosphate. That this absorption is not present at lower energies in the spectra of Mo_2(II,III) and Mo_2(II,II) phosphato dimers precludes its assignment to a transition corresponding to oxidation of the metal core, such as charge-transfer-to-solvent (CTTS), because absorption bands attributable to transitions of this type would exhibit a marked red-shift with reduction of the metal core. Conversely, the absence of this band in Mo_2(II,II) and Mo_2(II,III) phosphate spectra is presumably due to its blue-shift into the hard-ultraviolet thereby suggesting that the transition exhibits significant LMCT character. Thus, although the $\pi\,\pi^*$ and LMCT excited states of the Mo_2(II,III) dimer are potentially photoreactive, our inability to detect charge transfer excited states in the 200-250 nm region for the Mo_2(II,II) and Mo_2(II,III) phosphato complexes implies that the photoreactivity of these species is derived exclusively from $\pi \rightarrow \pi^*$ excitation. From molecular orbital point of view, this assignment is consistent with the observed chemistry because the metal centered π^* antibonding orbital exhibits significant electron density away from the metal-metal core along the z direction. Thus promotion of one electron from π bonding to π^* antibonding orbitals increases the probability of electron transfer

from the metal core to substrates occupying the open axial coordination sites. It is at these axial coordination sites which protons are most likely to reside.

The smooth conversion of Mo_2(II,II) phosphate to Mo_2(III,III) phosphate dimer with the concomitant production of hydrogen clearly demonstrates the capacity of the $M^{\underline{n}}M$ core to engender multielectron photochemical transformations by coupling the oxidation-reduction chemistry of the two metal centers along a controlled reaction pathway. It is evident from the reduction potentials of the Mo_2 phosphato complexes that the overall reaction is thermodynamically favored and hence the stabilities of the $Mo_2(HPO_4)_4^{4-}$ and $Mo_2(HPO_4)_4^{3-}$ ions in H_3PO_4 must necessarily arise form large kinetic barriers associated with oxidation of the Mo_2 cores. Our results demonstrate that these barriers are easily surmounted along photochemical reaction pathways. The $\pi \rightarrow \pi^*$ assignment of the photoreactive state of Mo_2 phosphato complexes conforms with the general reactivity pattern which has developed for $M^{\underline{n}}M$ dimers in acidic solution. Namely, low-energy metal-localized excited states are not responsible for the photooxidation chemistry of $M^{\underline{n}}M$ dimers in protic environments. We believe that the proposed photochemical mechanism is not specific to Mo_2 phosphato complexes but may be extended to accommodate the photochemistry of other Mo_2O_8 complexes in acidic solution.[94] For instance, the electronic absorption spectra of $Mo_2(SO_4)_4^{3-}$ and $Mo_2(SO_4)_4^{4-}$ are completely analogous to the spectra of the corresponding Mo_2 phosphato complexes in that an intense absorption band whose energy is independent of the oxidation state

of the Mo_2 core (λ_{max} = 239 and 235 nm of $Mo_2(SO_4)_4^{3-}$ and $Mo_2(SO_4)_4^{4-}$, respectively) dominates the ultraviolet region. These data support assignment of the band to a $\pi \rightarrow \pi^*$ transition, and it is reasonable to propose that the photoreactivity of the $Mo_2(SO_4)_4^{4-}$ system, similar to the phosphato series, originates from $\pi \rightarrow \pi^*$ excitation. The two-electron photochemistry of the Mo_2 phosphate system, as opposed to the one-electron transformations of the sulfate system, reflects the increased susceptibility of the Mo_2 core toward oxidation when ligated by phosphate. This difference between the oxidation-reduction properties of Mo_2 phosphato and sulfato complexes may derive from the fact that the ligands of the former complex possess a dissociable proton. In this connection, phosphoric acid and its ions exhibit enhanced proton ionization upon coordination to a metal; and ionization is enhanced further when the ions chelate a metal center.[150,151] In view of the relatively high charge of the Mo_2 core and the bridging coordination geometry of phosphate, significantly reduced interactions of a proton with the oxygens of PO_4^{3-} may be expected. Weak or complete dissociation of a proton from one or more of the HPO_4^{2-} ligands will increase the overall negative charge of the complex and facilitate oxidation of the Mo_2 core. If this model is correct then the reported electrochemistry and photochemistry should exhibit a large pH dependence. Unfortunately, the insolubility and instability of Mo_2 phosphate dimers in H_3PO_4 solution at concentrations less than 2 M precludes pH dependence studies. The ability of the phosphate ion to significantly shift the oxidation potential of metal cores to more

positive values may be responsible for the unique photooxidation chemistry of the dimolybdenum phosphate system in acidic solution.

CHAPTER V

PHOTOCHEMISTRY OF A NOVEL DIMOLYBDENUM DIPHENYL PHOSPHATE IN NONAQUEOUS SOLUTION

A. Background

The multielectron photochemistry of quadruply bonded $Mo_2(HPO_4)_4^{4-}$ is derived clearly from sequential one-electron oxidation steps. The desired two-electron oxidative-addition pathway described in Scheme III is not observed. However, the photochemistry of the $Mo_2(HPO_4)_4^{n-}$ system is similar to other $M\overset{4}{-}M$ systems in acidic solution and establishes a general reactivity pattern: $M\overset{n}{-}M$ dimers do not exhibit appreciable lifetimes in acidic solution and consequently photoreactivity is confined to high energy, pseudo unimolecular one-electron processes. For the specific case of the $Mo_2(HPO_4)_4^{4-}$ system, the $\delta\delta^*$ excited state is short lived and the photoreactivity is derived from the one-electron reduction of H^+ by the highly energetic $\pi\pi^*$ state (Figure 36). The issue of paramount importance to multielectron reactivity is by what mechanism the $\delta\delta^*$ excited state is deactivated in acidic solution.

Figure 36. Photoreaction pathway of "Mo_2O_8" complexes in acidic solutions, where "Mo_2O_8" corresponds to $Mo_2(aq)_x^{4+}$, $Mo_2(SO_4)_4^{4-}$, and $Mo_2(HPO_4)_4^{4-}$.

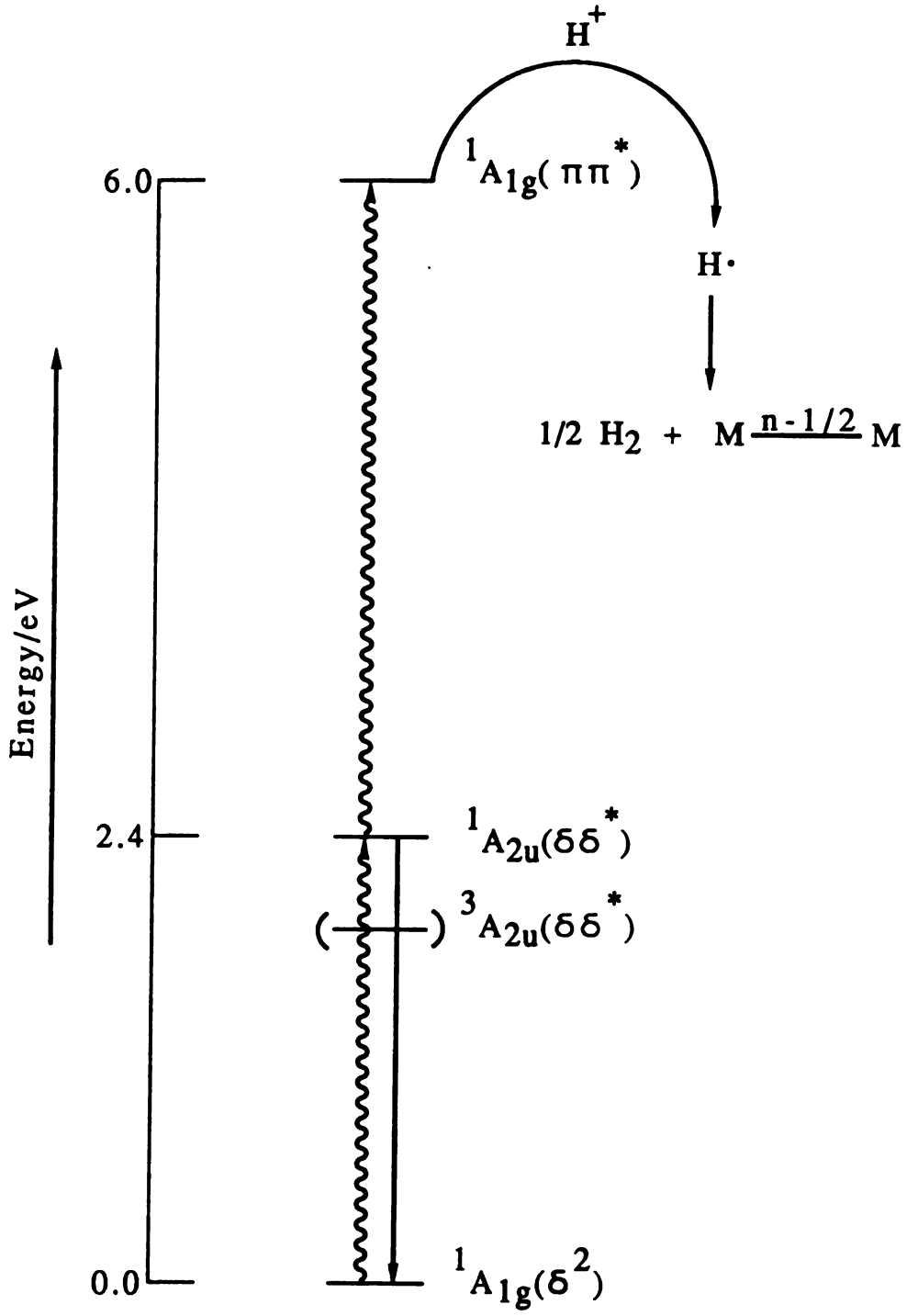

Figure 36

X-ray crystallography has identified stable hydride  products from the reaction of protons with the quadruple bond core.[152] In these complexes, the metal in the M-M core has been formally oxidized by one electron with subsequent two-electron reduction of H^+ to H^-. Alternatively, a resonant structure for an 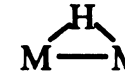 core is one where the core is simply protonated,

(a) (b) (33)

We believe that for most $M\overset{4}{-}M$ systems the major contributing structure is (b). Indeed, we have shown the $\delta\delta^*$ excited states are efficiently quenched by protons and a quenching mechanism consistent with the above discussion is shown in Figure 37. In this scheme protons quench the $\delta\delta^*$ excited state to give a "hydride-like" intermediate which expels the proton from the metal core to yield ground state $M\overset{4}{-}M$ dimer and H^+. Therefore, the photon energy is wasted in the proton quenching process and reactivity derived from the $\delta\delta^*$ excited state is circumvented.

These results suggest to us that if $\delta\delta^*$ multielectron photochemistry is to be observed, the proton quenching of $\delta\delta^*$ excited state and the energy consuming back proton transfer step must be inhibited. Owing to our knowledge of Mo_2 phosphate systems coupled with the demonstrated photoredox chemistry of

Figure 37. Proton quenching of $M\overset{4}{-}M$ excited states.

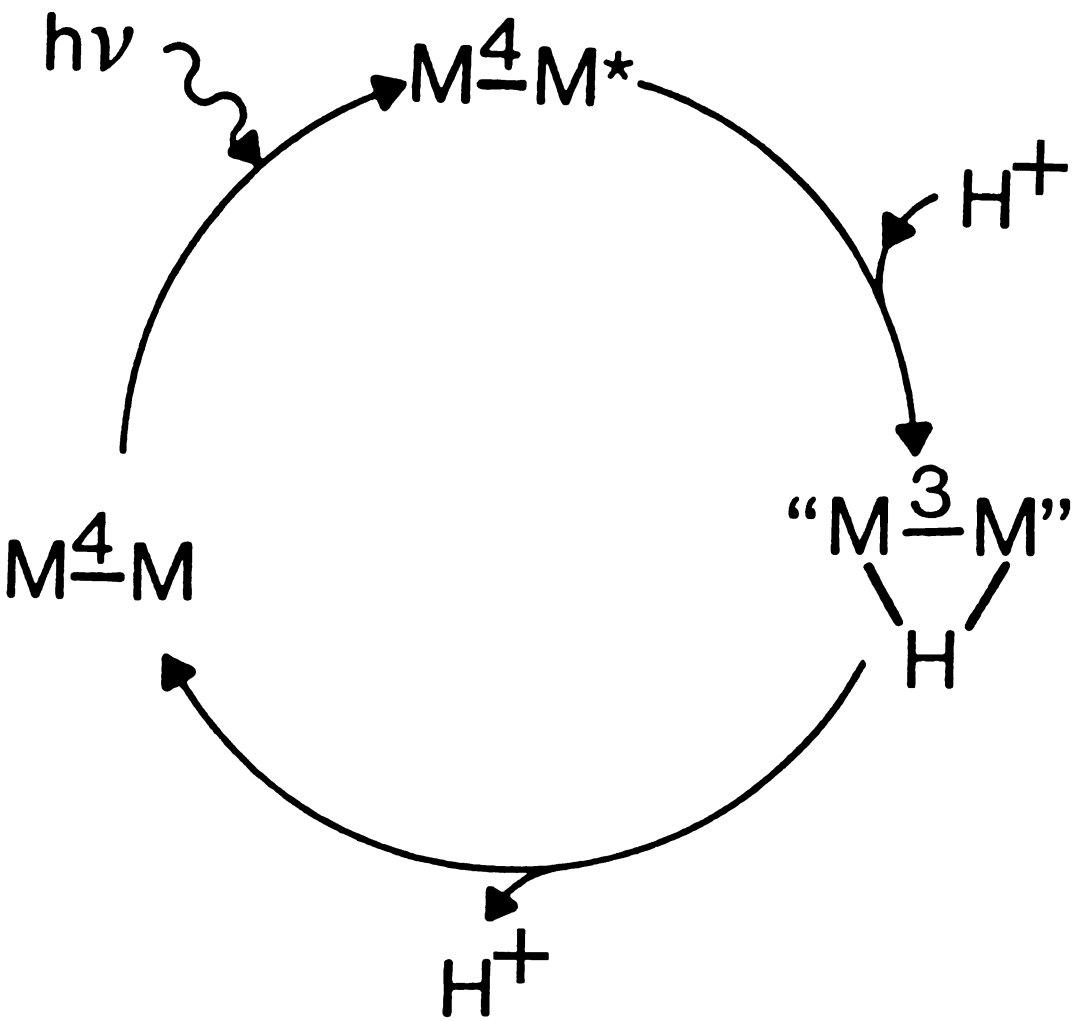

Figure 37

$Mo_2(HPO_4)_4^{4-}$, we initiated studies on the synthesis of Mo_2 phosphates which could be introduced into aprotic environments. To this end, we have prepared the quadruply bonded tetrakis(diphenyl phosphate)dimolybdenum $Mo_2(O_2P(OC_6H_5)_2)_4$ complex which exhibits good solubility in nonaqueous solvents.

The compound reacts with oxidants such as $NOBF_4$ to yield the one-electron oxidized mixed-valence species $Mo_2(O_2P(OC_6H_5)_2)_4BF_4$. Both the quadruple-bond and mixed-valence species have been characterized by X-ray crystallography, electronic spectroscopic, and electrochemical methods. In contrast to the high energy photochemistry of $Mo_2(HPO_4)_4^{4-}$ in acidic solution, the photochemistry of $Mo_2(O_2P(OC_6H_5)_2)_4$ in halogenated hydrocarbon solvent is promoted by visible irradiation. The chemistry and photochemistry of this new complex is presented in this chapter.

B. Results and Discussion

1. Structures of $Mo_2(O_2P(OC_6H_5)_2)_4\cdot 2THF$ and $Mo_2(O_2P(OC_6H_5)_2)_4BF_4$. The molecular structures of $Mo_2(O_2P(OC_6H_5)_2)_4\cdot 2THF$ and $Mo_2(O_2P(OC_6H_5)_2)_4BF_4$ are typical structures of multiply bonded dimolybdenum complexes.[55] Molecules of the quadruply bonded dimer occupy general positions of the space group $P2_1/n$ whereas the mixed-valent species is situated on inversion sites of the $P\bar{1}$ space group. Crystallographic data for the two complexes are listed in Table 6. Molecular structures of the two dimers and atom numbering schemes are

Table 6. Crystallographic Data of $Mo_2(O_2P(OC_6H_5)_2)_4 \cdot 2THF$ and $Mo_2(O_2P(OC_6H_5)_2)_4BF_4$

	$Mo_2(O_2P(OC_6H_5)_2)_4 \cdot 2THF$	$Mo_2(O_2P(OC_6H_5)_2)_4BF_4$
space group	$P2_1/n$	$P\bar{1}$
cryst syst	monoclinic	triclinic
a, Å	13.359(3)	10.917(8)
b, Å	29.641(15)	11.793(4)
c, Å	14.719(3)	12.430(4)
α, deg		63.45(2)
β, deg	93.43	70.38(4)
γ, deg		70.64(5)
V, Å^3	5818(6)	1316.8(12)
d, g/gm	1.522	1.608
Z	4	1
radiation	Mo Kα	Mo Kα
abs coeff(μ(Mo Kα)), cm^{-1}	5.964	6.625
2θ limits, deg	45	55
no. of reflens collcd	7973	12192
no. of unique reflens	7597	6096
no. of unique reflens used with $F_o > 3\sigma$	2363	5107
R(F)	.091	.027
$R_w(F)$	.103	.027
GOF	10.7	.654

illustrated in Figures 38 and 39. The positional parameters for heavy atoms (e.g. Mo, P, and O) are listed in Tables 7 and 8 for $Mo_2(O_2P(OC_6H_5)_2)_4 \cdot 2THF$ and $Mo_2(O_2P(OC_6H_5)_2)_4BF_4$, respectively. Tables 9 and 10 list selected bond distances; and the selected bond angles are listed in Tables 11 and 12 for quadruply-bonded and mixed-valent species, respectively.

Even though the molecular structures of both compounds appear similar, closer examination reveals some significant differences between the two molecules. The most noticeable difference is the Mo-Mo bond distance which increases from 2.154 Å in $Mo_2(O_2P(OC_6H_5)_2)_4 \cdot 2THF$ to 2.191 Å in $Mo_2(O_2P(OC_6H_5)_2)_4BF_4$. This increase of 0.04 Å resulting from the oxidation of the dimer by one electron is comparable to that observed for the Mo_2 sulfates which exhibit a lengthening of the Mo-Mo bond by 0.05 Å upon oxidation (2.111 Å and 2.164 Å for quadruple bond and mixed-valence complexes, respectively)[130]. One-electron oxidation of the quadruple bond reduces the formal δ bond order from 1 to 1/2. Besides a decreased bond order, the increased formal charge on each metal (from +2 to +2.5) causes a constriction of the valence orbitals of the metal atoms and corresponding decreased orbital overlap.

Because of the longer metal-metal bond distance in the mixed-valent species, there is less steric strain of phosphate ligands bridging the one-electron oxidized metal core. The five membered $Mo_2(O_2P)$ ring possesses trans O-Mo-O angles close to 180^o in the mixed-valent species as compared to the more strained angles in the quadruple-bond compound (e.g. 171^o and 167^o respectively). This is manifested in the mixed-valent species to possess a higher

Figure 38. Structure and labeling scheme for the quadruply bonded complex $Mo_2(O_2P(OC_6H_5)_2)_4 \cdot 2THF$. Atoms are represented by their 50% probability ellipsoids. Due to structural congestion, the two tetrahydrofuran molecule are not illustrated.

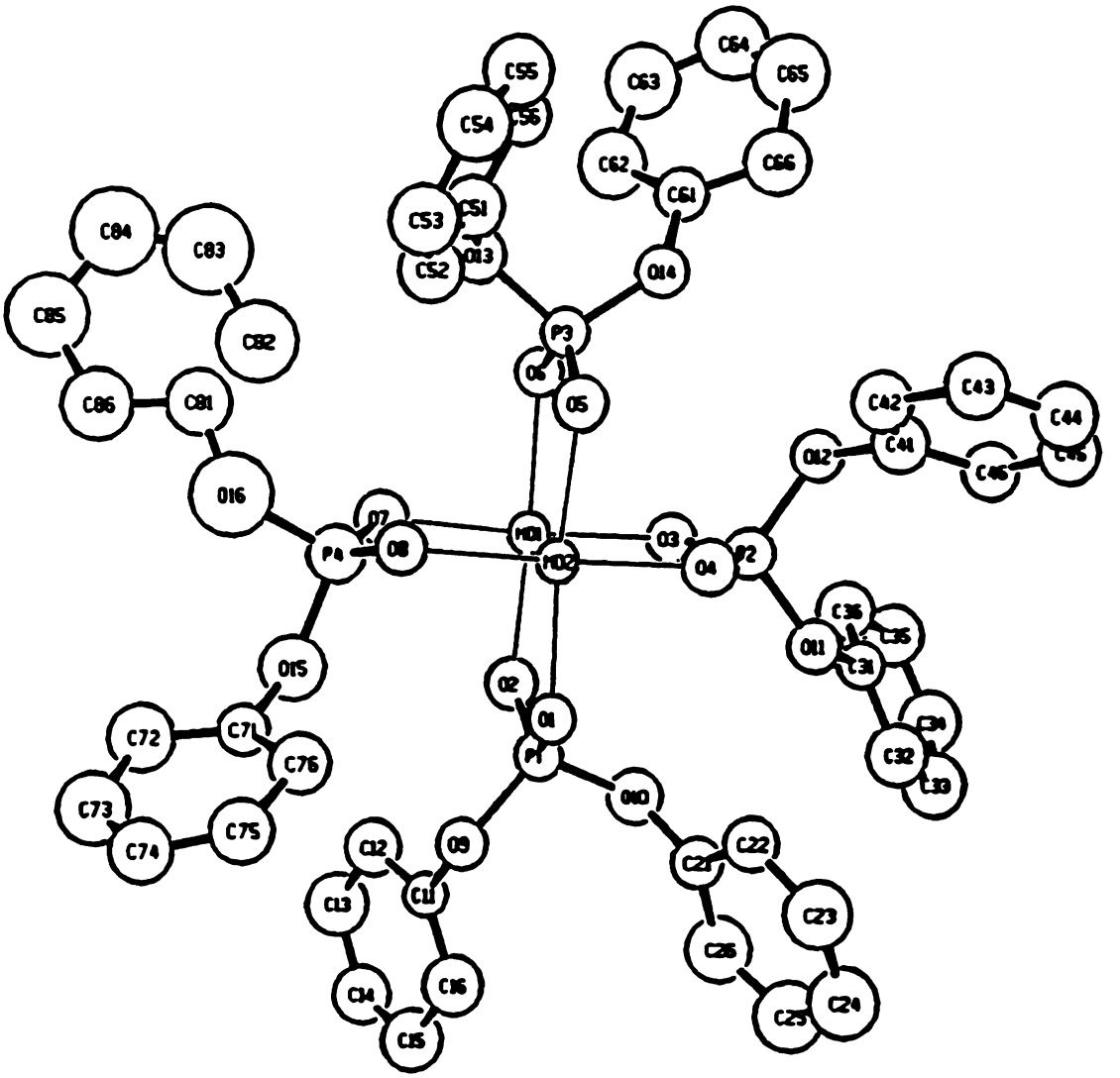
C64
C65
C63
C55
C54
C56
C66
C62
C61
C53
C51
C52
O13
O14
C84
C83
C85
C82
P3
O6
O5
C86
C81
C42
C43
C44
C41
C45
C46
O12
O16
O7
P4
O8
M01
M02
O3
O4
P2
C36
C35
O11
C31
O15
O2
O1
C72
C71
C76
P1
C32
C33
C73
C75
C74
O10
O9
C12
C22
C21
C13
C11
C23
C26
C14
C16
C25
C24
C15

Figure 38

Figure 39. Structure and labeling scheme for the mixed-valence complex $Mo_2(O_2P(OC_6H_5)_2)_4BF_4$. Atoms are represented by their 40% probability ellipsoids.

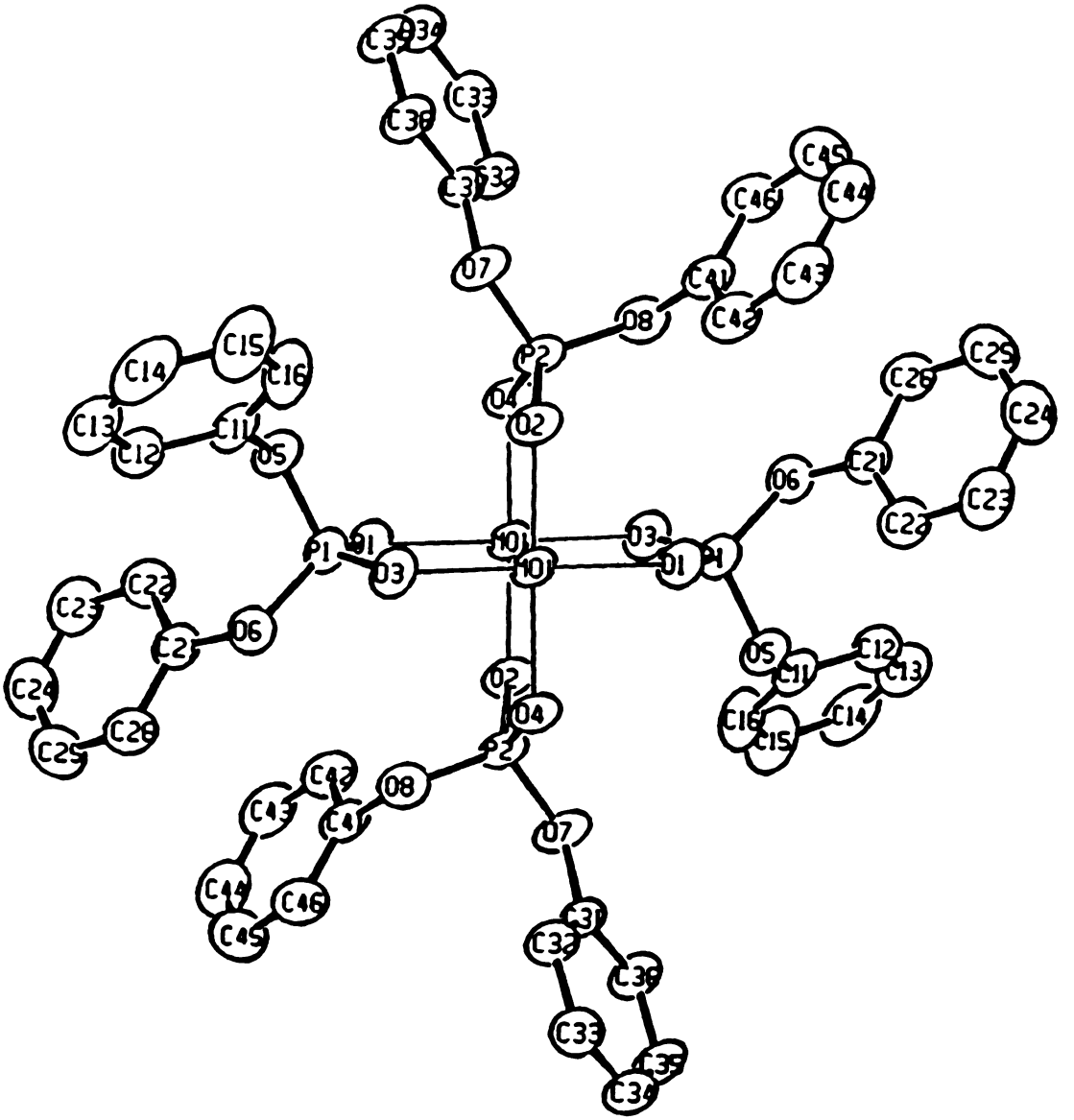
C34
C33
C38
C32
C45
C46
C44
O7
C41
C43
O8
C42
P2
C15
C16
C14
O4
C26
C25
C13
C11
O2
C24
C12
O5
C21
O6
C23
C22
O1
O3
P1
O1
O3
P1
C22
C23
O6
C2
C24
C28
C25
O5
C11
C12
C13
O2
C16
C15
C14
O4
P2
C42
O8
C43
C41
O7
C44
C46
C45
C31
C32
C38
C33
C35
C34

Figure 39

Table 7. Selected Atomic Positional Coordinates of $Mo_2(O_2P(OC_6H_5)_2)_4 \cdot 2THF$

atom	x	y	z
Mo(1)	0.82506	0.11940	0.26235
Mo(2)	0.66364	0.11702	0.25292
P(1)	0.74433	0.10992	0.45245
P(2)	0.73685	0.21593	0.28329
P(3)	0.74340	0.13519	0.06147
P(4)	0.75817	0.02147	0.24665
O(1)	0.64447	0.10769	0.39247
O(2)	0.83149	0.10697	0.40465
O(3)	0.83597	0.19041	0.28522
O(4)	0.64912	0.18690	0.27072
O(5)	0.65419	0.13151	0.10958
O(6)	0.84402	0.13110	0.11602
O(7)	0.84850	0.05124	0.23834
O(8)	0.66053	0.04395	0.23834
O(9)	0.73567	0.06964	0.52455
O(10)	0.75655	0.15712	0.50616
O(11)	0.72432	0.24283	0.37444
O(12)	0.74407	0.25134	0.20039
O(13)	0.74688	0.09620	-0.01629
O(14)	0.73748	0.18258	0.01391
O(15)	0.76189	-0.00184	0.34847
O(16)	0.75853	-0.02398	0.18216

Table 8. Selected Atomic Positional Coordinates of $Mo_2(O_2P(OC_6H_5)_2)_4BF_4$

atom	x	y	z
Mo(1)	0.00738	-0.09327	-0.00349
P(1)	0.25799	0.01683	-0.16557
P(2)	0.13565	-0.13277	0.19945
O(1)	0.19858	-0.10096	-0.11524
O(2)	0.08782	-0.20395	0.15108
O(3)	-0.17874	-0.11616	0.10870
O(4)	-0.07255	-0.01050	-0.15827
O(5)	0.26835	0.07531	-0.30863
O(6)	0.40088	-0.01817	-0.14397
O(7)	0.10424	-0.20480	0.34273
O(8)	0.28892	-0.14036	0.15318

Table 9. Selected Bond Distances of $Mo_2(O_2P(OC_6H_5)_2)_4 \cdot 2THF$

Bond	Distances/Å	Bond	Distances/Å
Mo(1) -Mo(2)	2.154		
Mo(1) -O(2)	2.123	Mo(2) -O(1)	2.103
-O(3)	2.135	-O(4)	2.098
-O(6)	2.211	-O(5)	2.149
-O(7)	2.078	-O(8)	2.205
P(1) -O(1)	1.556	P(2) -O(3)	1.524
-O(2)	1.399	-O(4)	1.457
-O(9)	1.606	-O(12)	1.617
P(3) -O(5)	1.426	P(4) -O(7)	1.506
-O(6)	1.529	-O(8)	1.482
-O(13)	1.629	-O(15)	1.648
-O(14)	1.569	-O(16)	1.648

Table 10. Selected Bond Distances for $Mo_2(O_2P(OC_6H_5)_2)_4BF_4$

Bond	Distances / Å
Mo(1) -Mo(1)	2.191
Mo(1) -O(1)	2.082
-O(2)	2.073
-O(3)	2.067
-O(4)	2.074
P(1) -O(1)	1.513
-O(3)	1.509
-O(5)	1.572
-O(6)	1.559
P(2) -O(2)	1.514
-O(4)	1.515
-O(7)	1.563
-O(8)	1.562

Table 11. Selected Bond Angles of $Mo_2(O_2P(OC_6H_5)_2)_4 \cdot 2THF$

Bond Angle	Angles/°	Bond Angle	Angles/°
Mo(1)-Mo(2) -O(1)	97.0	Mo(2)-Mo(1) -O(2)	92.2
-O(4)	93.4	-O(3)	95.8
-O(5)	93.2	-O(6)	96.6
-O(8)	93.0	-O(7)	96.8
O(2)-Mo(1) -O(3)	91.0	O(1)-Mo(2) -O(4)	89.9
-O(6)	171.1	-O(5)	168.9
-O(7)	90.1	-O(8)	92.9
O(3)-Mo(1) -O(6)	89.3	O(4)-Mo(2) -O(5)	85.7
-O(7)	167.3	-O(8)	172.9
O(6)-Mo(1) -O(7)	87.7	O(5)-Mo(2) -O(8)	90.8
O(1)-P(1) -O(2)	115.0		
-O(9)	104.5	O(2)-P(1) -O(9)	112.4
-O(10)	111.9	-O(10)	103.8
O(3)-P(2) -O(4)	113.6		
-O(11)	111.8	O(4)-P(2) -O(11)	106.3
-O(12)	104.2	-O(12)	111.8
O(5)-P(3) -O(6)	117.9		
-O(13)	110.8	O(6)-P(3) -O(13)	104.6
-O(14)	105.6	-O(14)	108.9
O(7)-P(4) -O(8)	114.7		
-O(15)	109.8	O(8)-P(4) -O(15)	111.3
-O(16)	113.7	-O(16)	106.0
Mo(1) -O(2)-P(1)	120.0	Mo(1) -O(1)-P(1)	113.5
-O(3)-P(2)	115.8	-O(4)-P(2)	121.3
-O(6)-P(3)	112.1	-O(5)-P(3)	120.1
-O(7)-P(4)	115.2	-O(8)-P(4)	113.3

Table 12. Selected Bond Angles of $Mo_2(O_2P(OC_6H_5)_2)_4BF_4$

Bond Angle	Angles/°
Mo(1)-Mo(1) -O(1)	94.6
-O(2)	94.8
-O(3)	94.9
-O(4)	94.5
O(1)-Mo(1) -O(2)	89.7
-O(3)	170.5
-O(4)	90.1
O(2)-Mo(1) -O(3)	88.6
-O(4)	170.8
O(3)-Mo(1) -O(4)	90.1
Mo(1) -O(1)-P(1)	117.6
-O(2)-P(2)	116.9
-O(3)-P(1)	118.2
-O(4)-P(2)	117.2

symmetry structure, which includes a center of inversion, despite identical virtual symmetries (D_{4h}) for both complexes.

2. Oxidation-Reduction Chemistry. The cyclic voltammogram of $Mo_2(O_2P(OC_6H_5)_2)_4$ in CH_2Cl_2 is shown in Figure 40a. Two reversible oxidation processes are observed upon anodically scanning solutions containing the quadruple bond complex. Reversible electrochemical behavior is indicated by linear plots of the cathodic and anodic currents vs. $\nu^{1/2}$ (scan rate, ν: 20-200 mV sec^{-1}), and values of 0.99 ± 0.02 for ratios of the anodic and cathodic peak currents.[112] Figure 40b illustrates the cyclic voltammogram of the mixed-valence species $Mo_2(O_2P(OC_6H_5)_2)_4BF_4$. The two complexes exhibit identical $E_{1/2}$ values (+0.067 and +0.997 V vs. SCE), with the quadruple bond having two reversible oxidations, whereas the mixed-valence complex possesses one reversible oxidation and one reversible reduction. These results clearly show that the wave at 0.067 V vs. SCE corresponds to the $Mo_2(O_2P(OC_6H_5)_2)_4^{0/+}$ couple. Owing to the reversibility of the wave at 0.997 V vs. SCE at all scan rates, we assign this wave to the $Mo_2(O_2P(OC_6H_5)_2)_4^{+/2+}$ couple.

Table 13 collects the reduction potentials of the "Mo_2O_8" complexes $Mo_2(SO_4)_4^{4-}$,[130] $Mo_2(HPO_4)_4^{4-}$, and $Mo_2(O_2P(OC_6H_5)_2)_4$. Inspection of these data obviously reveal that the ligands perturb the redox properties of the metal core in a different manner. Not surprisingly, proton association with the ligands of the Mo_2 sulfato and diphenyl phosphate complexes is unlikely and the Mo_2(II,III)/Mo_2(II,II) reduction potentials are similar. It is

Figure 40. Cyclic voltammograms of (a) $Mo_2(O_2P(OC_6H_5)_2)_4$ and (b) $Mo_2(O_2P(OC_6H_5)_2)_4BF_4$ in CH_2Cl_2 solution at 23 ^oC. NBu_4PF_6 was used as the supporting electrolyte, scan rate = 20 mV s^{-1}.

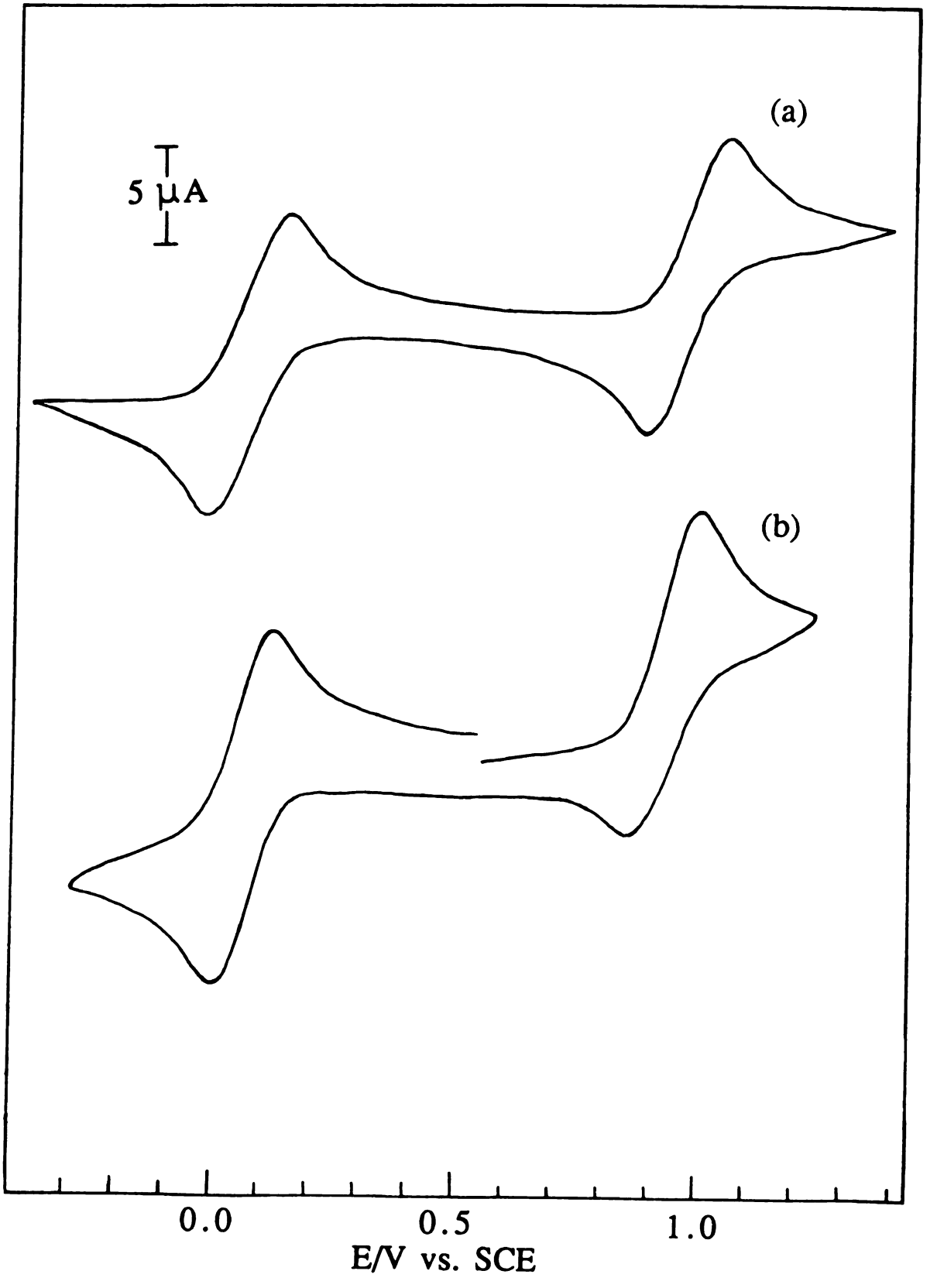

Figure 40

Table 13. The Formal Reduction Potentials of the Mo_2(II,III)/(II,II) and Mo_2(III,III)/(II,III) Couples of Mo_2 Sulfato, Phosphato, and Diphenyl Phosphate Complexes

Complexes	$E_{1/2}$/V vs. SCE Mo_2(II,III)/(II,II)	$E_{1/2}$/V vs. SCE Mo_2(III,III)/(II,III)
Sulfato	+0.25	a
Phosphato	-0.67	-0.24
Diphenyl phosphate	+0.06	+1.00

[a] Not available.

noteworthy that the $Mo_2(III,III)/Mo_2(II,III)$ couple for the sulfato complex lies in the background of solvent (in this case H_2O) and heretofore has not been determined. On the basis of the energy separation between the $Mo_2(II,III)/Mo_2(II,II)$ and $Mo_2(III,III)/Mo_2(II,III)$ couples of the diphenyl phosphate complex, we predict the latter couple of the sulfato complex to lie at 1.19 V vs. SCE. As originally inferred in Chapter IV, the very negative potentials of $Mo_2(HPO_4)_4^{4-}$ oxidation processes is attributed to the dissociation of a proton from one or more of the HPO_4^{2-} ligands. The electronic and structural similarities of the HPO_4^{2-} and $O_2P(OR)^-$ ligands are virtually identical and hence the only logical explanation for the ~1.0 V shift to negative potentials for $Mo_2(HPO_4)_4^{4-}$ is that the negative charge of the $Mo_2(HPO_4)_4^{4-}$ is increased by proton dissociation, thereby facilitating oxidation of the Mo_2 core.

Similar to the $Mo_2(HPO_4)_4^{4-}$ system, it is easy to understand the syntheses of the molybdenum diphenyl phosphates and their reactions on the basis of the oxidation-reduction potentials. Although oxidation of the quadruple bond complex by $NOBF_4$ proceeds smoothly to the pure mixed-valence compound $Mo_2(O_2P(OC_6H_5)_2)_4BF_4$, oxidation to $Mo_2(O_2P(OC_6H_5)_2)_4^{2+}$ by using $NOBF_4$ can not be achieved. From the redox potentials, it is understandable that the NO^+/NO couple (estimated to be ~0.85 to 1.0 V vs. SCE in nonaqueous solution)[153] is insufficient to bring about the second oxidation. Even stronger oxidants, such as magic green (tris(4-bromophenyl)aminium hexachloroantimonate ($E_{1/2}$= 1.04 V vs. SCE) or dichloroiodobenzene (estimated 0.9 to 1.2 V vs. SCE) with just enough potential to generate the dication $Mo_2(O_2P(OC_6H_5)_2)_4^{2+}$,

yield only the mixed-valence $Mo_2(O_2P(OC_6H_5)_2)_4^+$ product. This may be a result of significant kinetic barriers for generating the dication. Unfortunately, solutions of the $Mo_2(O_2P(OC_6H_5)_2)_4BF_4$ dimer decompose upon heating, and hence the oxidations must be run at or below room temperature. An alternate method to the synthesis of the dication species is by using bulk-electrolysis. The dication complex can be generated in solution at electrodes whose potentials are as high as 1.7 V vs. SCE. Unfortunately, this dication species failed to recrystallize. Although small concentrations of impurities (mostly higher-valent molybdenum complexes) from the bulk-electrolysis obscure the visible absorption region (from our experience on the Mo_2 phosphate system, we believe that the dication should exhibit weak absorption in visible region), the absence of near-infrared absorption suggests that the dication $Mo_2(O_2P(OC_6H_5)_2)_4^{2+}$ species is generated in solution and that electrochemical preparation of this triply bonded species is plausible.

3. Magnetic and Spectroscopic Characterization of $Mo_2(O_2P(OC_6H_5)_2)_4$ and $Mo_2(O_2P(OC_6H_5)_2)_4BF_4$. Typical of $M\overset{4}{-}M$ complexes, Mo_2(II,II) diphenyl phosphate has a $\sigma^2\pi^4\delta^2$ ground state electronic configuration and will possess a diamagnetic ground state. Oxidation by one electron to yield the paramagnetic mixed-valence complex whose EPR spectrum recorded on frozen solutions at 5 K is shown in Figure 41. An axial doublet signal with $g_\perp = 1.909$ and $g_\parallel = 1.863$ is observed at low temperatures and is consistent with a species in which the unpaired electron is coupled between two equivalent molybdenum nuclei.

Figure 41. X-band (9.434 GHz) EPR spectrum of a frozen solution of $Mo_2(O_2P(OC_6H_5)_2)_4BF_4$ in CH_2Cl_2 solution at 17 K.

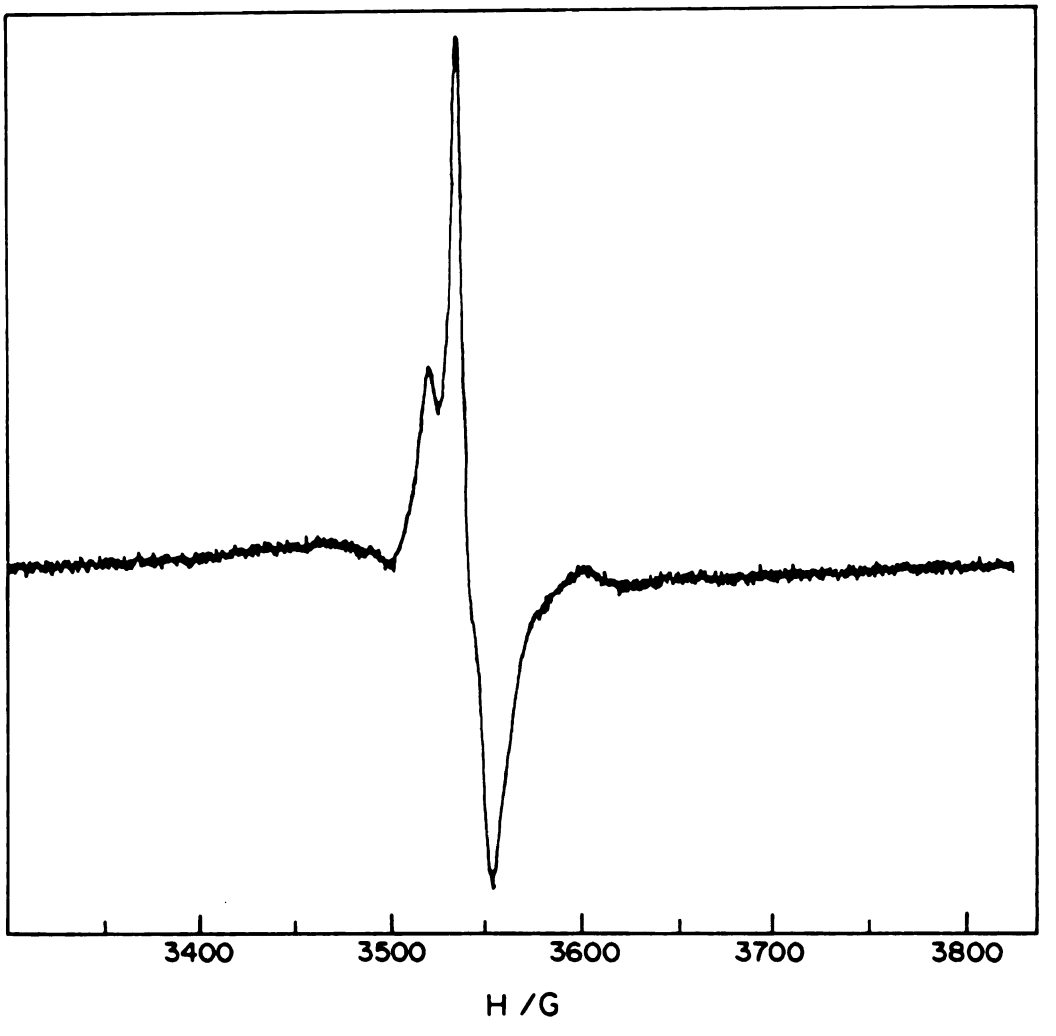

Figure 41

The absorption profiles of the Mo_2 diphenyl phosphates in the visible and near infrared are directly analogous to the phosphates. Figure 42 illustrates the electron absorption spectrum of the $Mo_2(O_2P(OC_6H_5)_2)_4$ complex in CH_2Cl_2 solution. The lowest energy absorption band (λ_{max} = 515 nm, ϵ = 156 M^{-1} cm^{-1}) is comparable in energy and intensity to that of $Mo_2(HPO_4)_4^{4-}$. The next higher energy absorption band at 404 nm (ϵ = 38 M^{-1} cm^{-1}) is assigned to the $\pi \rightarrow \delta^*$ transition.[129] The electronic absorption spectrum of $Mo_2(O_2P(OC_6H_5)_2)_4BF_4$, shown in Figure 43, is dominated by a prominent absorption profile in the near-infrared (λ_{max} = 1469 nm (ϵ=142 M^{-1} cm^{-1})) and a weak visible band at 600 nm (ϵ= 27 M^{-1} cm^{-1}). From the previous spectroscopic studies on $Mo_2(SO_4)_4^{3-}$, we are able to assign the near-infrared absorption band to the $\delta \rightarrow \delta^*$ ($^2B_{1u} \leftarrow {}^2B_{2g}$) transition.[93,132] As with the Mo_2 phosphates, the large red-shift of the $\delta \rightarrow \delta^*$ transition in mixed-valence Mo_2 dimer is explained by the absence of two electron spin pairing term contributions of the $\sigma^2\pi^4\delta^1$ configured ground state species. Similar to $Mo_2(SO_4)_4^{3-}$ and $Mo_2(HPO_4)_4^{3-}$ ions, the $\delta \rightarrow \delta^*$ absorption band of $Mo_2(O_2P(OC_6H_5)_2)_4BF_4$ exhibits a vibrational progression in solution at room temperature. The 308 cm^{-1} energy spacing is consistent with the symmetric metal-metal stretching vibration. The lower energy of the progression as compared with the $Mo_2(SO_4)_4^{3-}$ and $Mo_2(HPO_4)_4^{3-}$ (352 and 334 cm^{-1}, respectively) is probably due to the longer M-M bond distance of this mixed-valent Mo_2 diphenyl phosphate. The 600-nm band in $Mo_2(O_2P(OC_6H_5)_2)_4BF_4$ is a direct analogue to the lower energy absorption in Mo_2(II,III) sulfato and phosphato complexes and is by analogy,

Figure 42. Electronic absorption and emission spectra of $Mo_2(O_2P(OC_6H_5)_2)_4$ in CH_2Cl_2 solution at 25 ^oC.

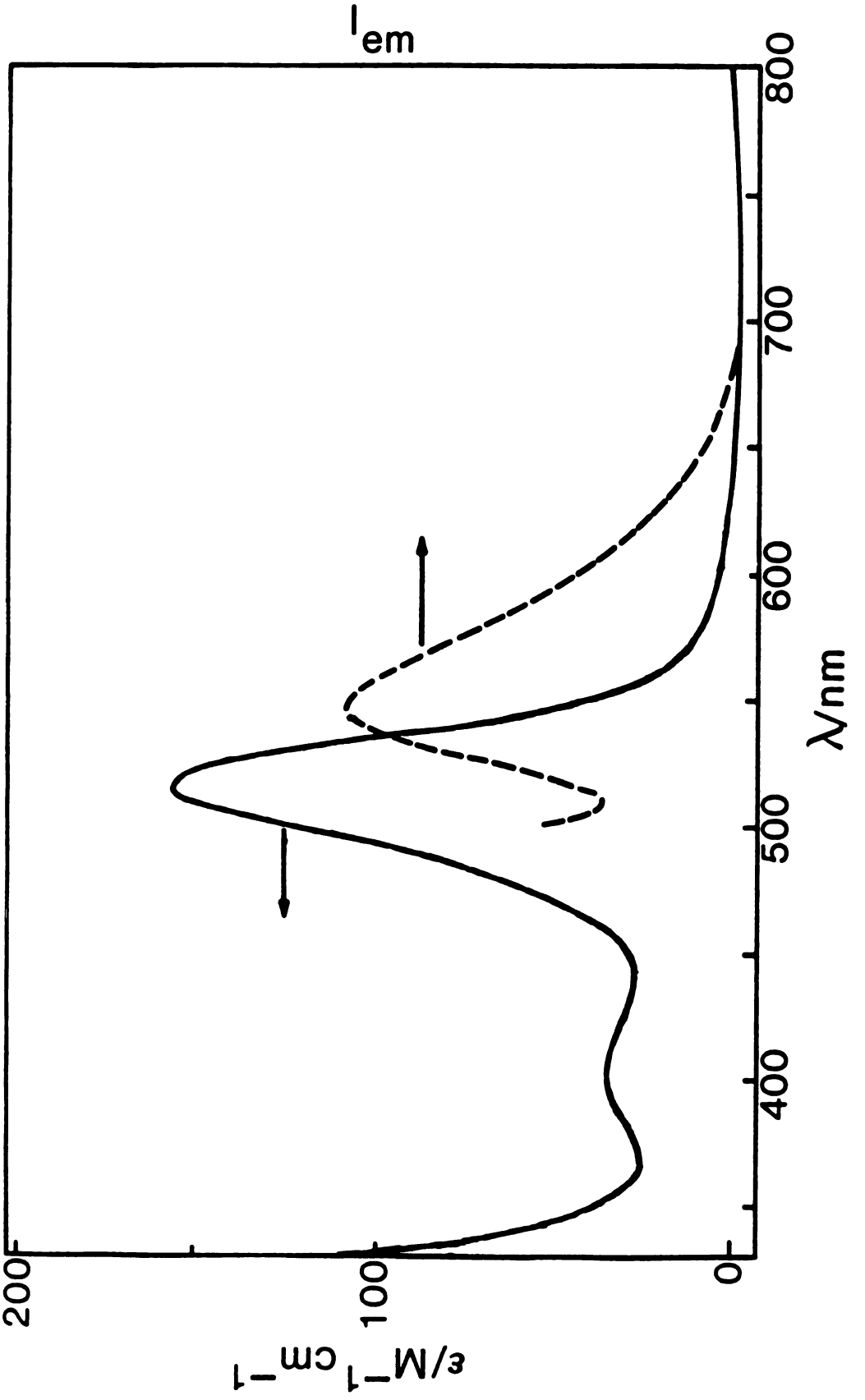

Figure 42

Figure 43. Electronic absorption spectrum of $Mo_2(O_2P(OC_6H_5)_2)_4BF_4$ in CH_2Cl_2 solution at 25 ^oC.

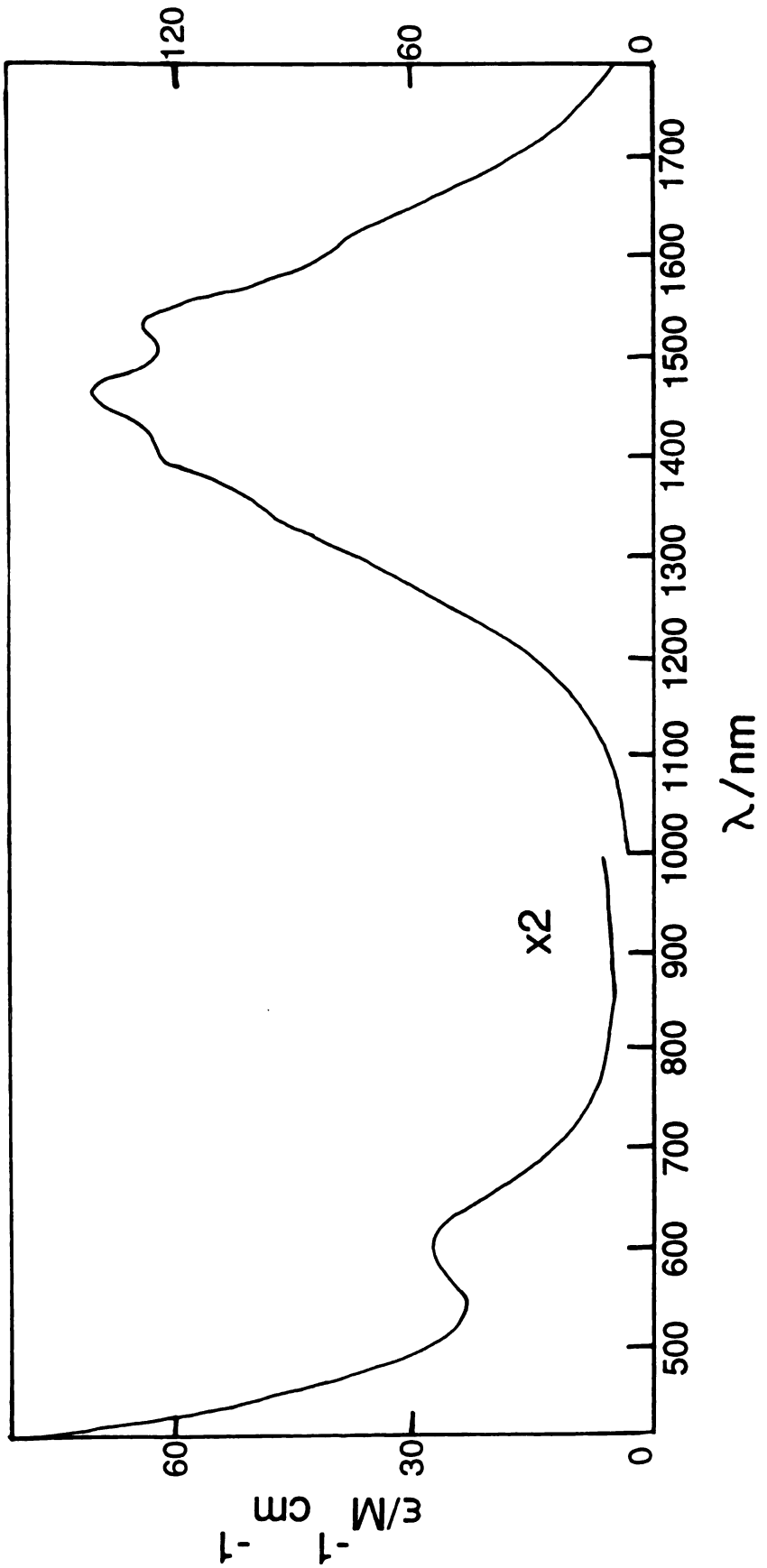
120
60
0
500
600
700
800
900
1000
1100
1200
1300
1400
1500
1600
1700
λ/nm
x2
60
30
0
ε/M cm
-1 -1

Figure 43

assigned to the $\pi \rightarrow \delta$ transition. The lack of higher energy absorptions in the visible spectral region could be explained by the strong ultraviolet absorption from the $\pi \rightarrow \pi^*$ transition of the aromatic ring of the ligands (λ_{max} = 260 nm) which tails into the visible and presumably shields the weak absorption of the other metal-localized transitions.

In spite of the similarities of the absorption properties of $Mo_2(O_2P(OC_6H_5)_2)_4$ to $Mo_2(HPO_4)_4^{4-}$, there is one major spectroscopic difference between these two compounds. The new Mo_2(II,II) diphenyl phosphate species emits in nonaqueous solution as shown in Figure 42. This observation supports our original hypothesis that Mo_2O_8 quadruple-bond dimers do not emit in aqueous solution because of proton quenching of the $\delta\delta^*$ state. Because the emission quantum yield for this complex is quite low, the lifetime of the excited state was measured by transient absorption spectroscopy. The transient absorption band at 460 nm decays exponentially after the 532-nm laser excitation pulse (FWHM = 25 ps). By using a monoexponential fitting method, the decay lifetime is 68 ns (Figure 44). This excited state lifetime is long enough to permit bimolecular reactivity.

4. Photochemistry. In striking contrast to the high energy photoreactions of $Mo_2(HPO_4)_4^{n-}$ in acidic solution, $Mo_2(O_2P(OC_6H_5)_2)_4$ reacts with halogenated hydrocarbon solvents upon low energy irradiation. This low energy photoreaction directly originates from the long-lived $^1(\delta\delta^*)$ excited state. Spectral changes for the photoreaction of $Mo_2(O_2P(OC_6H_5)_2)_4$ in 1,2-dichloroethane

Figure 44. Transient absorption kinetics of $Mo_2(O_2P(OC_6H_5)_2)_4$ in THF solution. The decay kinetics were recorded at 460 nm and excitation was with a 532 nm Nd:YAG laser pulse (FWHM = 25 ps).

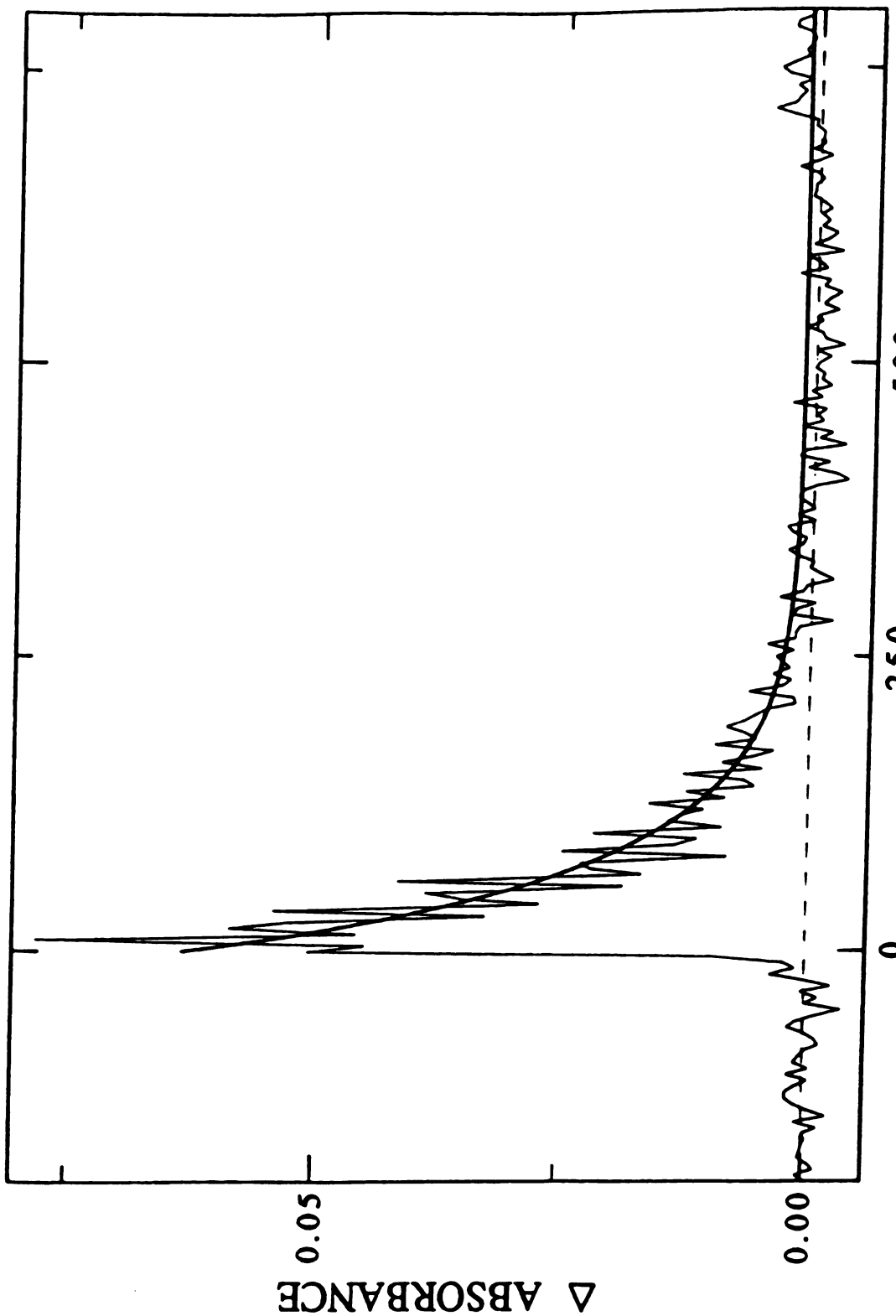

Figure 44

upon irradiation into $\delta^2 \rightarrow \delta\delta^*$ absorption (λ_{exc} = 530 nm) are shown in Figure 45. An initial decrease in the intensity of the $\delta^2 \rightarrow \delta\delta^*$ absorption band is accompanied by a concomitant increase in the near-infrared region. It is noteworthy that the near-infrared absorption arising from the photoreaction of $Mo_2(O_2P(OC_6H_5)_2)_4$ in $ClCH_2CH_2Cl$ is not identical to the absorption of $Mo_2(O_2P(OC_6H_5)_2)_4{}^+BF_4{}^-$. The band maximum of the photolyzed product is red-shifted (1470 nm for $Mo_2(O_2P(OC_6H_5)_2)_4{}^+BF_4{}^-$ and 1501 nm for photoproduct) and more intense. Because Cl^- is the most possible anion generated in dichloroethane solution, the oxidized photoproduct is very likely to have chloride in the axial coordination position. This assumption has been verified by Fast Atom Bombardment Mass Spectroscopy (FABMS). The highest molecular weight cluster found in photolyzed $ClCH_2CH_2Cl$ solutions of $Mo_2(O_2P(OC_6H_5)_2)_4$ displays a parent ion peak at 1225 amu (Figure 46) which is consistent with the molecular weight of $Mo_2(O_2P(OC_6H_5)_2)_4Cl$ (mol wt = 1223.33). We attribute the red-shifted and increased absorption intensity of the $\delta \rightarrow \delta^*$ transition of the photolyzed product to coordination of chloride in the axial coordination site. This hypothesis is confirmed with the independent synthesis of the $Mo_2(O_2P(OC_6H_5)_2)_4Cl$. The absorption spectrum of CH_2Cl_2 solutions of $Mo_2(O_2P(OC_6H_5)_2)_4$ recorded after addition of 0.5 equivalents of the oxidant $C_6H_5ICl_2$ exhibits a strong absorption band at 1494 nm ($\varepsilon \sim 362\ M^{-1}\ cm^{-1}$) as shown in Figure 47. The intensity and energy of this band closely match that of the final near-infrared photolysis spectrum (λ_{max} = 1501 nm, $\varepsilon \sim 391\ M^{-1}\ cm^{-1}$). The photochemically and chemically produced spectra also

Figure 45. Electronic absorption spectral changes during irradiation (λ_{exc} > 530 nm) of $Mo_2(O_2P(OC_6H_5)_2)_4$ in $ClCH_2CH_2Cl$ solution at 25 ^oC. The visible absorbance scale is 2 times greater than the near-infrared absorbance scale.

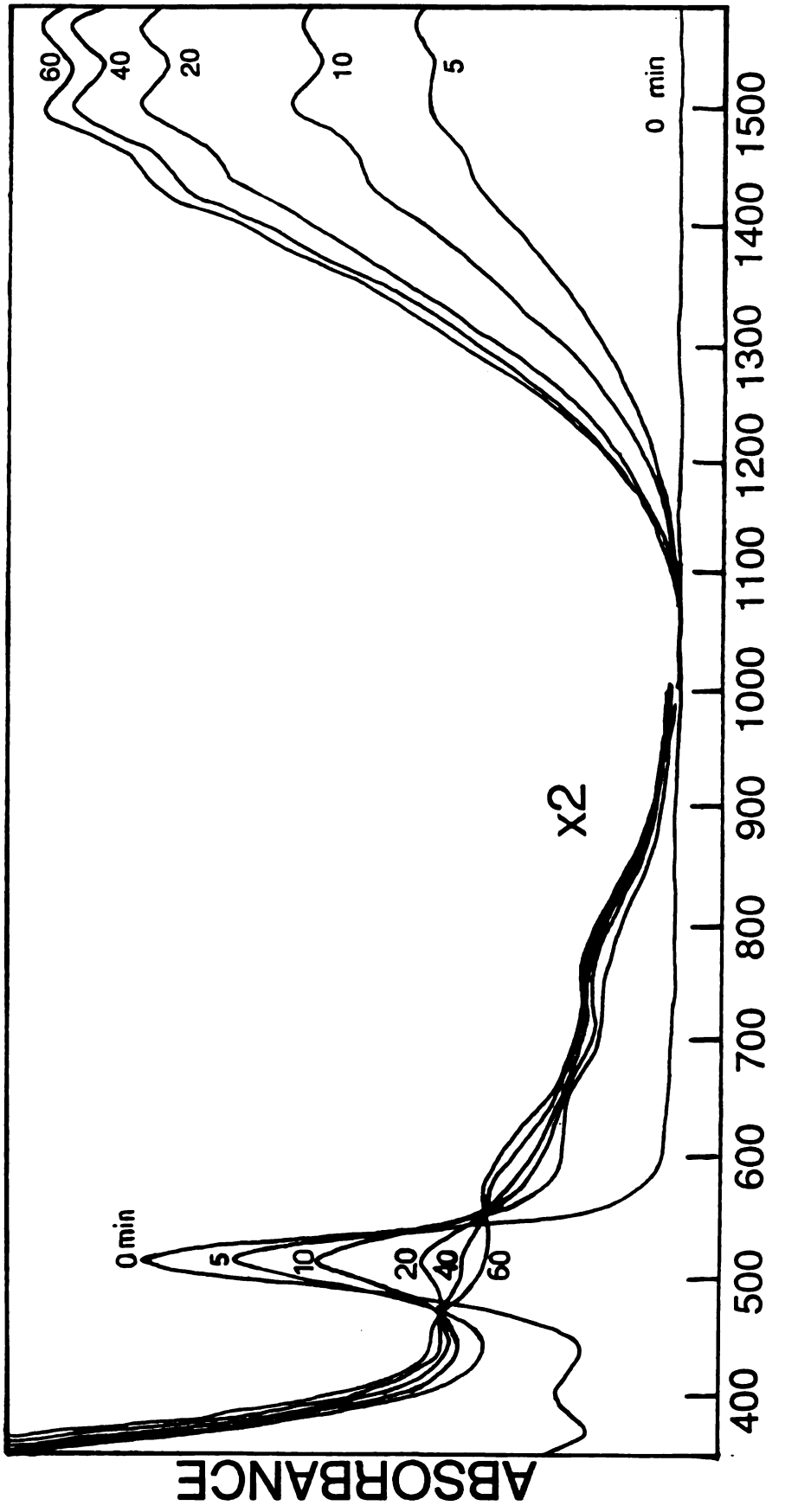
ABSORBANCE
400
500
600
700
800
900
1000
1100
1200
1300
1400
1500
λ/nm
x2
0 min
5
10
20
40
60
60
40
20
10
5
0 min

Figure 45

Figure 46. FABMS spectrum of a photolyzed $ClCH_2CH_2Cl$ solution of $Mo_2(O_2P(OC_6H_5)_2)_4$.

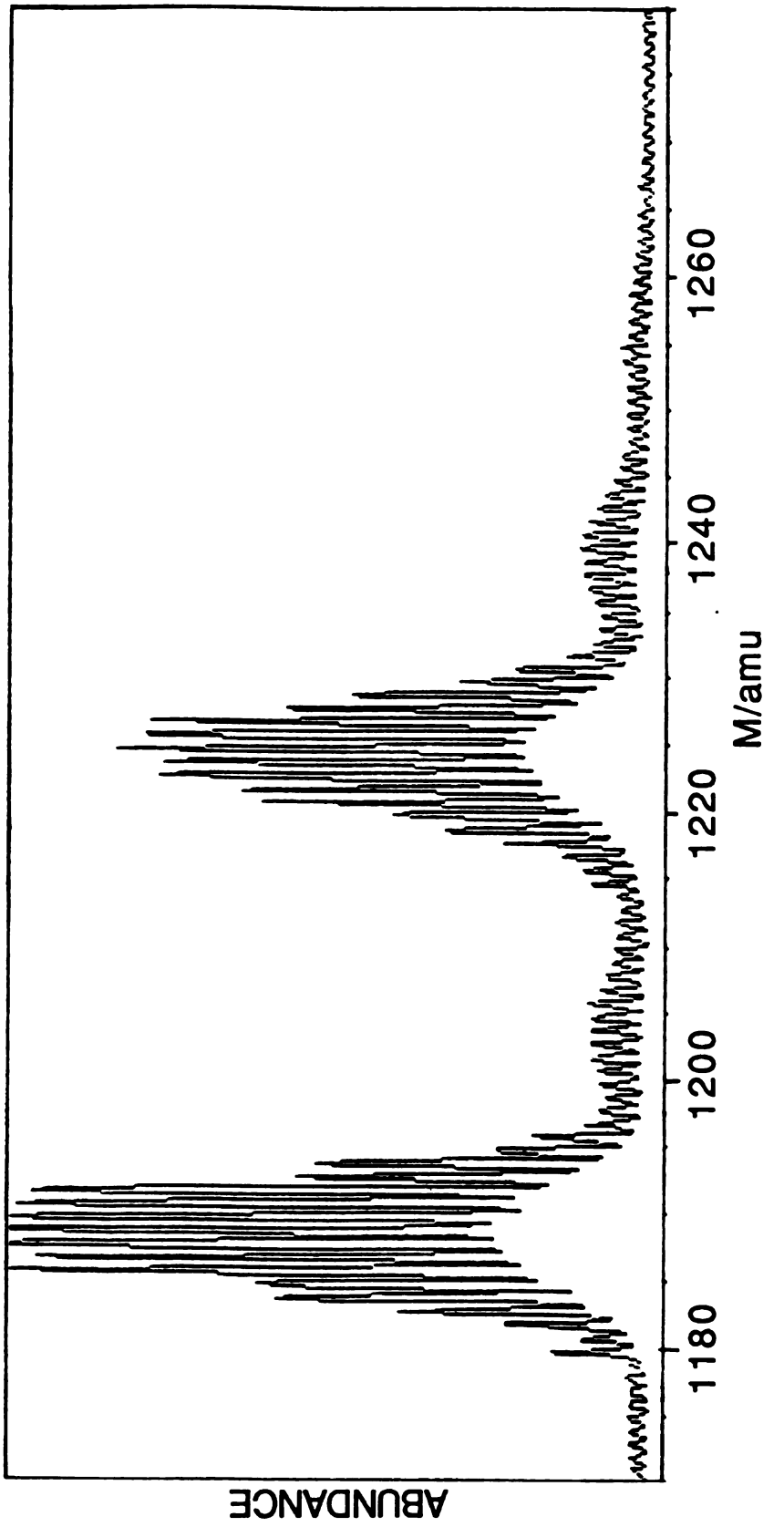

Figure 46

Figure 47. Electronic absorption spectrum of the product of the reaction between $Mo_2(O_2P(OC_6H_5)_2)_4$ and 0.5 equivalent of $C_6H_5ICl_2$ in CH_2Cl_2 solution at room temperature.

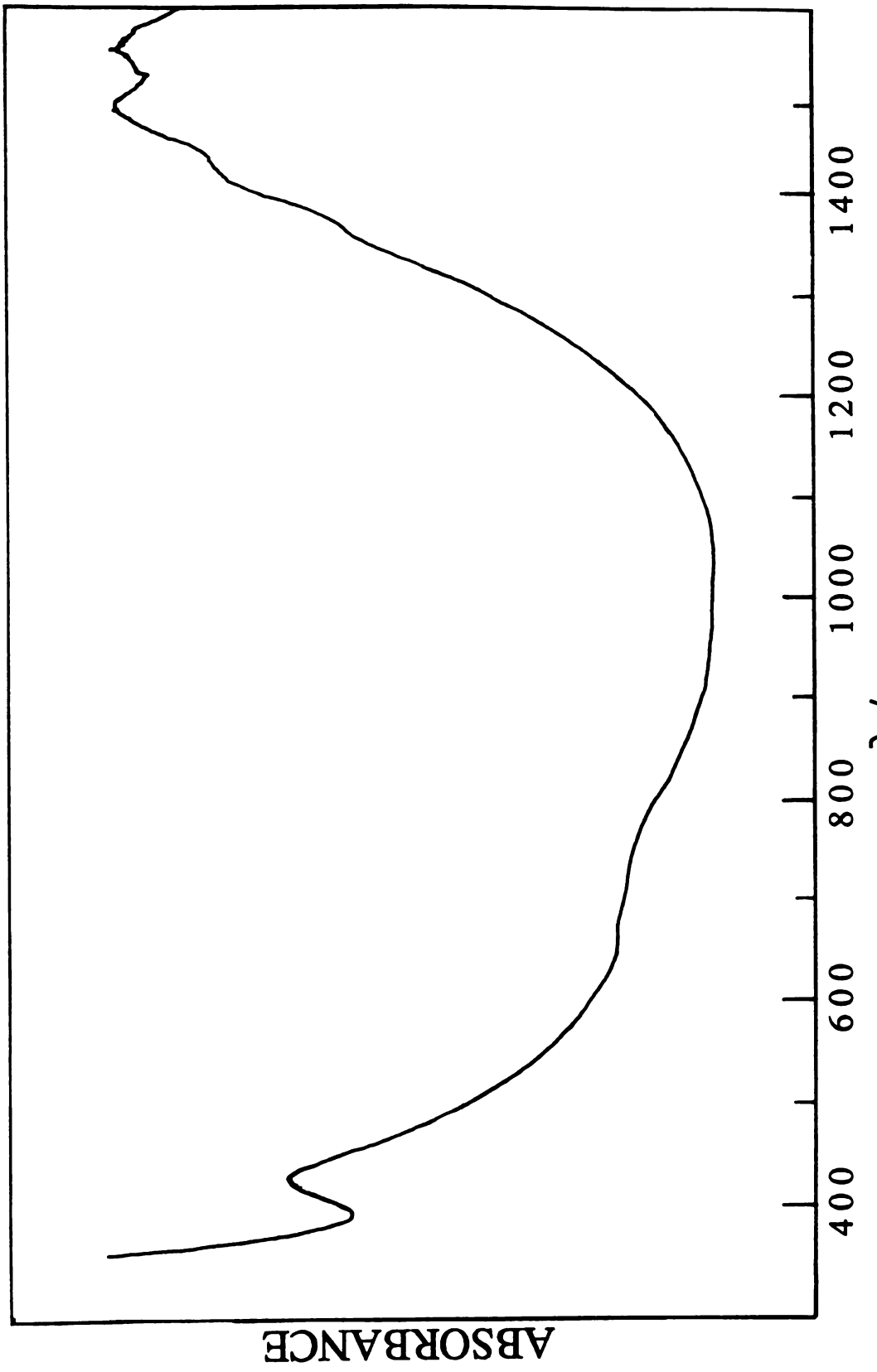

Figure 47

are in close agreement in the visible except that the 450-nm band is much more pronounced in the latter. Additionally, the 605-nm band present in the spectrum of photolyzed solutions is not as pronounced for solutions containing chemically oxidized product. Interestingly the $Mo_2(O_2P\text{-}(OC_6H_5)_2)_4BF_4$ species does exhibit a band at 605 nm and more intense absorption to the ultraviolet. These results suggest that photolyzed solutions consist of a mixture of $Mo_2(O_2P(OC_6H_5)_2)_4Cl$ and $Mo_2(O_2P(OC_6H_5)_2)_4^+$ owing to the establishment of an equilibrium between coordinated chloride and free mixed-valence species,

$$Mo_2(O_2P(OC_6H_5)_2)_4Cl \rightleftarrows Mo_2(O_2P(OC_6H_5)_2)_4^+ + Cl^- \qquad (34)$$

Since the absorption of $Mo_2(O_2P(OC_6H_5)_2)_4Cl$ is much stronger than $Mo_2(O_2P(OC_6H_5)_2)_4BF_4$ in the near infrared region, the final spectrum of photolyzed solutions in the near infrared region will be dominated by the appearance of $Mo_2(O_2P(OC_6H_5)_2)_4Cl$ with minor blue-shifts of the band maximum. Additionally, the visible absorption features of photolyzed solutions match those obtained from the sum of the absorption of $Mo_2(O_2P(OC_6H_5)_2)_4Cl$ and $Mo_2(O_2P(OC_6H_5)_2)_4^+BF_4^-$.

The FABMS data in conjunction with chemical oxidation results suggest that the initial photoreaction step is

$$Mo_2(O_2P(OC_6H_5)_2)_4 + ClCH_2CH_2Cl \xrightarrow{h\nu} \cdot CH_2CH_2Cl + [\, Mo_2(O_2P(OC_6H_5)_2)_4^+ \rightleftarrows Mo_2(O_2P(OC_6H_5)_2)_4Cl \,] \qquad (35)$$

The photogenerated chloroethane radical is a very reactive species, and thermal reaction with unreacted quadruple bond species is thermodynamically favorable, to yield the chloro-substituted product and ethylene,

$$\cdot CH_2CH_2Cl + Mo_2(O_2P(OC_6H_5)_2)_4 \rightarrow Mo_2(O_2P(OC_6H_5)_2)_4Cl + CH_2CH_2 \quad (36)$$

As discussed above, the equilibrium described by reaction (34) is quickly established. Consistent with this proposed mechanism is our measurement of ethylene above reacted solutions. Gas chromatographic analysis reveals ethylene as the only detectable organic product, and manometric measurements determine 0.51 ± 0.03 equivalents is produced. The slightly higher measurement of ethylene (according to reaction (35) and (36) only 0.50 equivalents of ethylene should be produced) is indicative of the secondary reaction,

$$\cdot CH_2CH_2Cl + Mo_2(O_2P(OC_6H_5)_2)_4Cl \rightarrow Mo_2(O_2P(OC_6H_5)_2)_4Cl_2 + CH_2CH_2 \quad (37)$$

which should become important as the concentration of $Mo_2(O_2P(OC_6H_5)_2)_4$ is depleted. Our observation of the loss of the initial isosbestic point at long photolysis times in Figure 45 is consistent with reaction (37) becoming a significant pathway as the quadruple bond photoreacts.

The $Mo_2(O_2P(OC_6H_5)_2)_4$ dimer also reacts with other halogenated reactants. The spectral changes of $Mo_2(O_2P(OC_6H_5)_2)_4$ in CH_2Cl_2 during visible excitation (λ_{exc} > 530 nm) are shown in Figure 48. An absorption profile exhibiting a moderately intense band at 542 nm and a strong band at 420 nm combined with absorption in near infrared spectral region at 1494 nm. Although the final spectrum in the near infrared is very similar to the one-electron oxidized species with Cl^-, the visible spectrum clearly differs from that obtained for $ClCH_2CH_2Cl$ photochemistry. These observations suggest the following photoreaction scheme,

$$Mo_2(O_2P(OC_6H_5)_2)_4 + CH_2Cl_2 \xrightarrow{h\nu} Mo_2(O_2P(OC_6H_5)_2)_4Cl + \cdot CH_2Cl \quad (38)$$

$$\cdot CH_2Cl + \cdot CH_2Cl \rightarrow ClCH_2CH_2Cl \quad (39)$$

The generated 1,2-dichloroethane can then photoreact with quadruply bonded species as described by reactions (35) and (36). However that the visible absorption spectrum is not consistent with exclusive production of $Mo_2(O_2P(OC_6H_5)_2)_4Cl$ or $Mo_2(O_2P(OC_6H_5)_2)_4^+$ clearly identifies a more complicated photochemical scheme. The chloromethane radical is extremely reactive and it is reasonable to assume that the following reactions are competitive with dimerization,

$$\cdot CH_2Cl + Mo_2(O_2P(OC_6H_5)_2)_4 \rightarrow Mo_2(O_2P(OC_6H_5)_2)_4CH_2Cl \quad (40)$$

$$\cdot CH_2Cl + Mo_2(O_2P(OC_6H_5)_2)_4Cl \rightarrow CH_2ClMo_2(O_2P(OC_6H_5)_2)_4Cl \quad (41)$$

Figure 48. Electronic absorption spectral changes during irradiation (λ_{exc} > 530 nm) of $Mo_2(O_2P(OC_6H_5)_2)_4$ in CH_2Cl_2 solution at 25 °C.

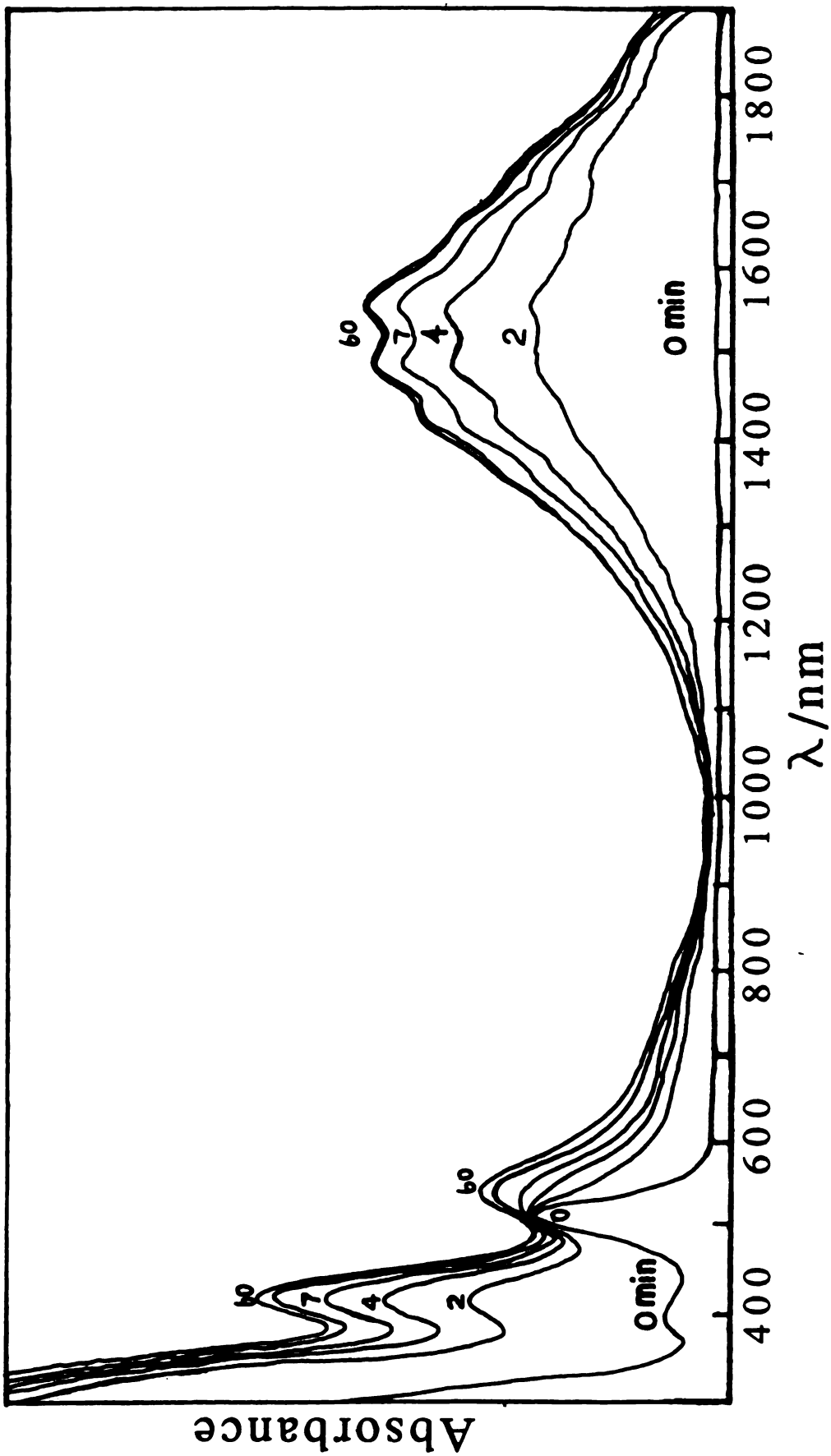
Absorbance
400
600
800
1000
1200
1400
1600
1800
λ/nm
0min
2
4
7
60
0min
2
4
7
60

Figure 48

The Mo_2(III,III) organometallic products would definitely exhibit intense absorptions in the visible spectral region. However, the inorganic products of CH_2Cl_2 photolysis have not yet been isolated and thus it is impossible to unequivocally identify the photoreaction pathway from the data available at this time.

CHAPTER VI

FINAL REMARKS

The studies described herein demonstrate that $M\overset{4}{-}M$ complexes are good multielectron photoreagents. The redox activity of the individual metal centers of the binuclear metal core can be coupled to drive overall multielectron photoprocesses. This principle is demonstrated by the photochemistry of $Mo_2(HPO_4)_4^{n-}$ (n = 2, 3, 4) complexes in acidic solution in which the sequential one-electron chemistry of the metal centers provides the two-electron reduction of protons to hydrogen. An important discovery from these studies is that the $^1(\delta\delta^*)$ excited state is efficiently quenched by proton transfer. Therefore, in acidic solution, the $^1(\delta\delta^*)$ excited state is not preserved for bimolecular reaction. Our approach to circumvent this quenching process by employing synthetic strategies to design $M\overset{4}{-}M$ complexes with similar structures but readily soluble in nonaqueous solutions was a successful one. The newly synthesized $Mo_2(O_2P(OC_6H_5)_2)_4$ complex luminesces from the $^1(\delta\delta^*)$ excited state in nonaqueous solutions at room temperature with an appreciably long lifetime of 68 ns. This long-lived singlet excited state dominates the photoreactivity of this molecule and in contrast

to $Mo_2(HPO_4)_4^{4-}$, $Mo_2(O_2P(OC_6H_5)_2)_4$ exhibits low energy two-electron photochemistry. This system is significant because it represents the first example of a multielectron process originating from the $^1(\delta\delta^*)$ excited state.

Although the Mo_2(II,II) diphenyl phosphate photochemistry constitutes a two-electron process driven by a single electron, the reaction is not a concerted multielectron process of the $^1(\delta\delta^*)$ excited state. Molecular models of $Mo_2(O_2P(OC_6H_5)_2)_4$ reveal that the metal-metal core, important for multielectron reactivity is shielded by the diphenyl phosphate ligands. These results suggest that $Mo_2(O_2P(OC_6H_5)_2)_4$ photochemistry is confined to attack by substrate at the axial coordination sites of the metal-metal core. Quantum yield data support this analysis. The photoreaction quantum yield of $Mo_2(O_2P(OC_6H_5)_2)_4$ with 1,2-dichloroethane decreases dramatically with increasing ligating ability of solvent. These data are displayed in Table 14. The quantum yield decreases from 0.040 to 0.001 by changing the solvent from 1,2-dichloroethane to acetonitrile. Computer generated molecular models of the $Mo_2(O_2P(OC_6H_5)_2)_4 \cdot 2THF$ crystal structure shows that the two THF molecules occupying the axial sites insulate the metal-metal core from substrate. Consequently solvent coordination is reflected in the reduction of the photoreaction quantum yield. Therefore, substrates directly attack only one metal instead of the binuclear metal-metal core. Hence the advantages of using $M\overset{4}{-}M$ complexes are attenuated by axial attack and one-electron photoredox chemistry is observed.

This analysis suggests that $M\overset{4}{-}M$ multielectron photochemistry will only be observed for substrates which can approach

Table 14. Quantum Yield Data for Photoreaction of $Mo_2(O_2P(OC_6H_5)_2)_4$ and $ClCH_2CH_2Cl$ in Various Nonaqueous Solutions

Solvent	$[ClCH_2CH_2Cl]/M$	Φ^a
$ClCH_2CH_2Cl$	13(neat)	0.040
C_6H_6	9	0.031
THF	9	0.014
CH_3CN	9	0.001

[a] Measured by using ferrioxalate actinometer. λ_{exc} = 546 nm.

the metal core in an equatorial position. Thus the steric congestion of the equatorial planes of the $M\overset{4}{-}M$ dimers must be reduced. The best structures would have two bridging ligands to prevent the free rotation of the $^1(\delta\delta^*)$ excited state and four small monodentate ligands to minimize steric crowding. The bridging ligands could be in either trans or cis positions.

In summary, quadruply bonded $M\overset{4}{-}M$ dimers are promising multielectron photoreagents. The photochemistry described herein represents the first examples of multielectron $^1(\delta\delta^*)$ excited state chemistry. The singlet character of the $^1(\delta\delta^*)$ excited state appears to be important in promoting multielectron reactivity but energy wasting quenching reactions, such as proton quenching, must be precluded. Additionally, attack by substrate in the equatorial plane of the metal-metal core appears to be a crucial feature for concerted multielectron reactivity. If these conditions are met, photochemical studies of $M\overset{n}{-}M$ dimers should continue to open new avenues of excited state chemistry.

REFERENCES

1. Adamson, A. W.; Sporer, A. H. *J. Am. Chem. Soc.* **1958**, *80*, 3865.

2. (a) Sutin, N.; Creutz, C. *Adv. Chem. Ser.* **1978**. *No. 168*, 1.(b) Sutin, N.; Creutz, C. *Pure Appl. Chem.* **1980**, *52*, 2717.

3. Balzani,V.; Scandola, F. In. *Photochemital Conversion and Storage of Solar Energy*, Connolly, J. S. Ed.; Academic: New York, 1981, Chapter 4.

4. Julliard, M.; Chanon, M. *Chem. Rev.* **1983**, *83*, 425.

5. Kavarnos, G. J.; Turro, N. J. *Chem. Rev.* **1986**, *86*, 401.

6. (a) Marcus, R. A. *J. Chem. Phys.* **1956**, *24*, 966. (b) Marcus, R. A. *Ann. Rev. Phys. Chem.* **1964**, *15*, 155.

7. (a) Meyer, T. J. *Acc. Chem. Res.* **1978**, *11*, 94. (b) Meyer, T. J. *Prog. Inorg. Chem.* **1983**, *30*, 389.

8. Sutin, N. *Prog. Inorg. Chem.* **1983**, *30*, 441.

9. Sutin, N.; Creutz, C. *J. Chem. Educ.* **1983**, *60*, 809.

10. Marcus, R. A.; Sutin, N. *Biochim. Biophys. Acta*, **1985**, *811*, 265.

11. Brunschwig, B. S.; Sutin, N. *Comments Inorg. Chem.* **1987**, *6*, 209.

12. Isied, S. S. *Prog. Inorg. Chem.* **1984**, *32*, 443.

13. (a) Mayo, S. L.; Eills, W. R.; Coutchley, R. J.; Gray, B. H. *Science.* **1986**, *233*, 948. (b) Axup, A. W.; Albin, M.; Mayo, S. L.; Coutchley, R. J.; Gray, B. H. *J. Am. Chem. Soc.* **1988**, *110*, 435.

14. Elias, H.; Chou, M. H.; Winkler, J. R. *J. Am. Chem. Soc.* **1988**, *110*, 429.

15. (a) McLendon, G.; Guarr, T.; McGuire, M.; Mimolo, K.; Strauch, S.; Tayler, K. *Coord. Chem. Rev.* **1985**, *64*, 113. (b) McLendon, G.; Guarr, T. *Coord. Chem. Rev.* **1985**, *68*, 1. (c) Mclendon, G. *Acc. Chem. Res.* **1988**, *21*, 160.

16. Stein, G. *Israel J. Chem.* **1975**, *14*, 213.

17. Balzani, V.; Bolletta, F.; Gandolfi, M. T.; Maestri, M. *Top. Curr. Chem.* **1978**, *75*, 1.

18. (a) Maverick, A. W.; Gray, H. B. *Pure Appl. Chem.* **1980**, *52*, 2339. (b) Maverick, A. W.; Gray, H. B. *Science*, **1981**, *214*, 1201.

19. Crentz, C.; Sutin, N. *Natl. Acad. Sci. U.S.A.* **1975**, *72*, 2858.

20. Sutin, N. *J. Photochem.* **1979**, *10*, 19.

21. Whitten, D. G. *Acc. Chem. Res.* **1980**, *13*, 83.

22. (a) Bock, C. R.; Meyer, T. J.; Whitten, D. G. *J. Am. Chem. Soc.* **1974**, *96*, 4710. (b) Young, R. C.; Meyer, T. J.; Whitten, D. G. *J. Am. Chem. Soc.* **1975**, *97*, 4781.

23. Lin, C. T.; Bottcher, W.; Chou, M.; Creutz, C.; Sutin, N. *J. Am. Chem. Soc.* **1976**, *98*, 6536.

24. (a) Kiwi, J.; Gratzel, M. *Angew. Chem. Int. Ed. Engl.* **1978**, *17*, 860. (b) Kiwi, J.; Gratzel, M. *Angew. Chem. Int. Ed. Engl.* **1979**, *18*, 624. (c) Gratzel, M. *Acc. Chem. Res.* **1981**, *14*, 376.

25. Kiwi, J. *J. Chem. Soc., Faraday Trans. II*, **1982**, *78*, 339.

26. Sprintschnik, G.; Sprintschnik, H. W.; Kirsch, P. P.; Whitten, D. G. *J. Am. Chem. Soc.* **1976**, *98*, 2337.

27. (a) Lehn, J. M.; Sauvage, J. P. *Nouv. J. Chim.* **1977**, *1*, 449. (b) Lehn, J. M. In *Photochemical Conversion Storage of Solar Energy*, Connolly, J. S. Ed.; Academic Press: New York, 1981, Chapter 6.

28. Zameraev, K. I.; Parmon, V. N. In *Energy Resources Through Photochemistry and Catalysis*, Gratzel, M. Ed.; Academic Press: New York, 1983, Chapter 5.

29. (a) Duonghong, D.; Borgarello, E.; Gratzel, M. *J. Am. Chem. Soc.* **1981**, *103*, 4685. (b) Borgarello, E.; Kiwi, J.; Pelizzetti, E.; Visca, M.; Gratzel, M. *J. Am. Chem. Soc.* **1981**, *103*, 6324.

30. Gratzel, M.; Kalyanasundaram, K.; Kiwi, J. *Struct Bonding*, **1982**, *49*, 37.

31. Mclendon, G. In *Energy Resources Through Photochemistry and Catalysis*, Gratzel, M. Ed.; Academic Press: New York, 1983, Chapter 4.

32. Kalyanasundaram, K. In *Energy Resources Through Potochemistry and Catalysis*, Gratzel, M. Ed.; Academic Press: New York, 1983, Chapter 7.

33. Kalyanasundaram, K.; Gratzel, M.; Pelizzetti, E. *Coord. Chem. Rev.* **1986**, *69*, 57.

34. (a) Brunschwig, B. S.; Chou, M. H.; Creutz, C.; Ghosh, P. K. Sutin, N. *J. Am. Chem. Soc.* **1983**, *105*, 4832. (b) Ghosh, P. K. Brunschwig, B. S.; Chou, M. H.; Creutz, C.; Sutin, N. *J. Am. Chem. Soc.* **1984**, *106*, 4772. (c) Liu, D. K. ;Brunschwig, B. S.; Creutz, C.; Sutin, N. *J. Am. Chem. Soc.* **1986**, *108*, 1749.

35. Shafirovich, V. Ya.; Khannanov, N. K.; Strelets, V. V. *Nouv. J. Chim.* **1980**, *4* , 81.

36. (a) Wrighton, M. S.; Ginley, D. S. *J. Am. Chem. Soc.* **1975**, *97*, 2065. (b) Wrighton, M. S. *Top. Curr. Chem.* **1976**, *65*, 37.

37. Fox, A. J.; Poe, A.; Ruminski, R. *J. Am. Chem. Soc.* **1982**, *104*, 7327.

38. Kobayashi, T.; Yasufuku, K.; Iwai, J.; Yesaka, H.; Noda, M.; Ohtani, H. *Coord. Chem. Rev.* **1985**, *64* ,1.

39. Meyer, T. J.; Caspar, J. V. *Chem. Rev.* **1985**, *85*, 187.

40. Geoffroy, G. L.; Wrighton, M. S. *Oragnometallic Chemistry*; Academic Press: New York, 1979.

41. Wrighton, M. S.; Graff, J. L.; Luong, J. C.; Reichel, C. L.; Robbins, J. L. *ACS, Symposium Ser.* **1980**, *No. 155*, 85.

42. (a) Sperline, R.; Dickson, M. K.; Roundhill, D. M. *J. Chem. Soc., Chem. Commun.* **1977**, 62. (b) Filomena dos Remediopinto, M.A.; Sadler, P. J.; Neidle, S.; Sanderson, M. R.; Subbiah, A.; Kuroda, R. J. *J. Chem. Soc., Chem. Commun.* **1980**, 13. (c) Alexander, K. A.; Bryan, S.A.; Dickson, M. K.; Hedden, D.; Roundhill, D. M. *Inorg. Synth.* **1986**, *24*, 211.

43. (a) Coleman, A. W.; Eadie, D. T.; Stobart, S. R.; Zaworotko, M. J.; Atwood, J. L. *J. Am. Chem. Soc.* **1982**, *104*, 922. (b) Beveridge, K. A.; Bushnell, G. W.; Stobart, S. R.; Atwood, J. L.; Zaworotko, M. J. *Organometallics* **1983**, *2*, 1447.

44. (a) Mann, K. R.; Gordon, J. G., II; Gray, H. B. *J. Am. Chem. Soc.* **1975**, *97*, 3553. (b) Lewis, N. S.; Mann, K. R.; Gordon, J. G., II; Gray, H. B. *J. Am. Chem. Soc.* **1976**, *98*, 7461.

45. Che, C-M.; Butler, L. G.; Gray, H. B. *J. Am. Chem. Soc.* **1981**, *103*, 7796.

46. (a) Rice, S. F.; Gray, H. B. *J. Am. Chem. Soc.* **1983**, *105*, 4571. (b) Rice, S. F.; Gray, H. B. *J. Am. Chem. Soc.* **1981**, *103*, 1593. (c) Rice, S. F.; Milder, S. J.; Gray, H. B.; Goldbeck, R. A.; Kliger, D. A. *Coord. Chem. Rev.* **1982**, *43*, 349.

47. Marshall, J. L.; Stobart, S. R.; Gray, H. B. *J. Am. Chem. Soc.* **1984**, *106*, 3027.

48. Stein, P.; Dickson, M. K.; Roundhill, D. M. *J. Am. Chem. Soc.* **1983**, *105*, 3489.

49. Che, C-M.; Butler, L. G.; Gray, H. B.; Crooks, R. M.; Woodruff, W. H. *J. Am. Chem. Soc.* **1983**, *105*, 5492.

50. Dallinger, R. F.; Miskowski, V. M.; Gray, H. B.; Woodruff, W. H. *J. Am. Chem. Soc.* **1981**, *103*, 1595.

51. (a) Roundhill, D. M. *J. Am. Chem. Soc.* **1985**, *107*, 4354. (b) Roundhill, D. M.; Atherton, S. J.; Shen, Z-P. *J. Am. Chem. Soc.* **1987**, *109*, 6076.

52. Caspar, J. V.; Gray, H. B. *J. Am. Chem. Soc.* **1984**, *106*, 3029.

53. (a) Mann, K. R.; Lewis, N. S.; Miskowski, V. M.; Erwin, D. K.; Hammond, G. S.; Gray, H. B. *J. Am. Chem. Soc.* **1977**, *99*, 5525. (b) Miskowski, V. M.; Sigal, I. S.; Mann, K. R.; Gray, H. B.; Milder, S. J.; Hammond, G. S.; Ryason, P. R. *J. Am. Chem. Soc.* **1979**, *101*, 4383. (c) Sigal, I. S.; Gray, H. B. *J. Am. Chem. Soc.* **1981**, *103*, 2220.

54. (a) Gray, H. B.; Mann, K. R.; Lewis, N. S.; Thich, J. A.; Richman, R. M. *Adv. Chem. Ser.* **1978**, *No. 168*, 44. (b) Mann, K. R.; Gray, H. B. *Adv. Chem. Ser.* **1979**, *No. 173*, 225. (c) Gray, H. B.; Miskowski, V. M.; Milder, S. J.; Smith, T. P.; Maverick, A. W.; Buhr, J. D.; Gladfelter, W. L.; Sigal, I. S.; Mann, K. R. *Fundamental Research in Homogeneous Catalysis*; Tsutsui, M., Ed.; Plenum: New York, 1979; Vol. 3.

55. (a) Cotton, F. A.; Walton, R. A. *Multiple Bonds Between Metal Atoms;* Wiley-Interscience: New York, 1982 and reference therein. (b) Cotton, F. A.; Walton, R. A. *Structure and Bonding*, **1985**, *62*, 1 and references therein.

56. Mortola, A. P.; Moskowitz, J. W.; Rosch, N.; Cowman, C. D.; Gray, H. B. *Chem. Phys. Lett.* **1975**, *32*, 283.

57. Norman, J. G.; Kolari, H. J. *J. Am. Chem. Soc.* **1975**, *97*, 33.

58. Hay, P. J. *J. Am. Chem. Soc.* **1982**, *104*, 7007.

59. Mathisen, K. B.; Wahlgren, U.; Pettersson, L. G. M. *Chem. Phys. Lett.* **1984**, *104*, 336.

60. Stromberg, A.; Pettersson, L. G. M.; Wahlgren, U. *Chem. Phys. Lett.* **1985**, *118*, 389.

61. Hall, M. B. *Polyhedron*, **1987**, *6*, 679.

62. Ziegler, T.; Tschinke, V.; Becke, A. *Polyhedron*, **1987**, *6*, 685.

63. Bursten, B. E.; Clark, D. L. *Polyhedron*, **1987**, *6*, 695.

64. (a) Cowman, C. D.; Gray, H. B.; *J. Am. Chem. Soc.* **1973**, *95*, 8177. (b) Cowman, C. D.; Trogler, W. C.; Gray, H. B. *Isr. J. Chem.* **1977**, *15*, 308. (d) Miskowski, V. M.; Goldbeck, R. A.; Kliger, D. S.; Gray, H. B. *Inorg. Chem.* **1979**, *18*, 86.

65. Trogler, W. C.; Gray, H. B. *Acc. Chem. Res.* **1978**, *11*, 232.

66. (a) Cotton. F. A.; Martin, D. S.; Fanwick, P. E.; Peters, T. J.; Webb, T. R. *J. Am. Chem. Soc.* **1976**, *98*, 4681. (b) Fanwick, P. E.; Martin, D. S.; Cotton. F. A.; Webb, T. R. *Inorg. Chem.* **1977**, *16*, 2103. (c) Trogler, W. C.; Cowman, C. D.; Gray, H. B.; Cotton. F. A. *J. Am. Chem. Soc.* **1977**, *99*, 2993.

67. Rice, S. F.; Wilson, R. B.; Solomon, E. I. *Inorg. Chem.* **1980**, *19*, 3425.

68. (a) Manning, M. C.; Trogler, W. C. *Inorg. Chem.* **1982**, *21*, 2797-2800. (b) Manning, M. C.; Trogler, W. C. *J. Am. Chem. Soc.* **1983**, *105*, 5311.

69. Martin, D. S.; Newman, R.A.; Fanwick, P. E. *Inorg. Chem.* **1982**, *21*, 3400.

70. Fraser, I. F.; Peacock, R. D. *Chem. Phys. Lett.* **1983**, *98*, 620.

71. Clark, R. J. H.; Stead, M. J. *Inorg. Chem.* **1983**, *22*, 1214.

72. Lichtenberger, D. L.; Blevins, C. H. *J. Am. Chem. Soc.* **1984**, *106*. 1636.

73. Robbins, G. A.; Martin, D. S. *Inorg. Chem.* **1984**, *23*, 2086.

74. (a) Martin, D. S.; Huang, H.-W.; Newman, R. A. *Inorg. Chem.* **1984**, *23*, 699-701. (b) Huang, H.-W.; Martin, D. S. *Inorg. Chem.* **1985**, *24*, 96.

75. (a) Fanwick, P. E. *Inorg. Chem.* **1985**, *24*, 258-263. (b) Fanwick, P. E.; Bursten, B. E.; Kaufmann, G. B. *Inorg. Chem.* **1985**, *24*, 1165.

76. Dallinger, R. F. *J. Am. Chem. Soc.* **1985**, *107*, 7202.

77. (a) Morris, D. E.; Sattelberger, A. P.; Woodruff, W. H. *J. Am. Chem. Soc.* **1986**, *108*. 8270.

78. (a) Zietlow, T. C.; Hopkins, M. D.; Gray, H. B. *J. Solid State Chem.* **1985**, *57*, 112. (b) Hopkins, M. D.; Gray, H. B.; Miskowski, V. M. *Polyhedron*, **1987**, *6*, 705. (c) Hopkins, M. D.; Schaefer, W. P.; Bronikowski, M. J.; Woodruff, W. H.; Miskowski, V. M.; Dallinger, R. F.; Gray, H. B. *J. Am. Chem. Soc.* **1987**, *109*, 408. (d) Hopkins, M. D.; Miskowski, V. M.; Gray, H. B. *J. Am. Chem. Soc.* **1988**, *110*, 1787.

79. Hopkins, M. D.; Zietlow, T. C.; Miskowski, V. M.; Gray, H. B. *J. Am. Chem. Soc.* **1985**, *107*, 510.

80. Miskowsi, V. M.; Goldbeck, R. A.; Kliger, D. S.; Gray, H. B. *Inorg. Chem.* **1979**, *18*, 86.

81. Hopkins, M. D.; Gray, H. B. *J. Am. Chem. Soc.* **1984**, *106*, 2468.

82. Winkler, J. R.; Nocera, D. G.; Netzel, T. L. *J. Am. Chem. Soc.* **1986**, *108*, 4451.

83. Nocera, D. G.; Gray, H. B. *J. Am. Chem. Soc.* **1981**, *103*, 7349.

84. (a) Zietlow, T. C.; Klendworth, D. D.; Nimry, T.; Salmon, D. J.; Walton, R. A. *Inorg. Chem.* **1981**, *20*, 947. (b) Tetrick, S. M.; Coombe, V. T.; Heath, G. A.; Stephenson, T. A.; Walton, R. A. *Inorg. Chem.* **1984**, *23*, 4567. (c) Dunbar, K. R.; Walton, R. A. *Inorg. Chem.* **1985**, *24*, 5.

85. Walton, R. A. *Isr. J. Chem.* **1985**, *25*, 196.

86. (a) Conner, K. A.; Gennett, T.; Weaver, M. J.; Walton, R. A. *J. Electroanal. Chem.* **1985**, *196*, 69. (b) Root, D. R.; Blevins, C. H.; Lichtenberger, D. L.; Sattelberger, A. P.; Walton, R. A. *J. Am. Chem. Soc.* **1986**, *108*, 953. (c) Anderson, L. B.; Bakir, M.; Walton, R. A. *Polyhedron*, **1987**, *6*, 1483.

87. Cotton, F. A.; Dunbar, K. R.; Falvello, L. R.; Tomas, M.; Walton, R. A. *J. Am. Chem. Soc.* **1983**, *105*, 4950.

88. Cotton, F. A.; Powell, G. L. *J. Am. Chem. Soc.* **1984**, *106*. 3371.

89. (a) Cotton, F. A.; Daniels, L. M.; Dunbar, K. R.; Falvello, L. R.; Tetrick, S. M.; Walton, R. A. *J. Am. Chem. Soc.* **1985**, *107*. 3524. (b) Cotton, F. A.; Dunbar, K. R.; Price, A. C.; Schwolzer, W.; Walton, R. A. *J. Am. Chem. Soc.* **1986**, *108*. 4843.

90. (a) Bucknor, S.; Cotton, F. A.; Falvello, L. R.; Reid, A. H., Jr.; Schmulbach, C. D. *Inorg. Chem.* **1987**, *26*, 2954. (b) Canich, J. M.; Cotton, F. A.; Dunbar, K. R.; Falvello, L. R. *Inorg. Chem.* **1988**, *27*, 804.

91. Geoffroy, G. L; Gray, H. B.; Hammond, G. S. *J. Am. Chem. Soc.* **1974**, *96*, 5565.

92. Trogler, W. C.; Gray, H. B. *Nouv. J. Chim.* **1977**, *1*, 475.

93. Erwin, D. K.; Geoffroy, G. L; Gray, H. B.; Hammond, G. S.; Solomon, E. I.; Trogler, W. L.; Zagars, A. A. *J. Am. Chem. Soc.* **1977**, *99* , 3620.

94. Trogler, W. L.; Erwin, D. K.; Geoffroy, G. L; Gray, H. B.; *J. Am. Chem. Soc.* **1978**, *100* , 1160.

95. (a) Cotton, F. A.; Kalbacher, B. J. *Inorg. Chem.* **1976**, *15*, 522. (b) Bino, A.; Cotton, F. A. *J. Am. Chem. Soc.* **1979**, *101*, 4150.

96. Nocera, D. G.; Gray, H. B. *Inorg. Chem.* **1984**, *23*, 3686.

97. (a) Stephenson, T. A.; Bannister, E.; Wilkinson, G. *J. Chem. Soc.* **1964**, 4150. (b) Lawton, D.; Mason, R. *J. Am. Chem. Soc.* **1965**, *87*, 921.

98. (a) Brencic, J. V.; Cotton, F. A. *Inorg. Chem.* **1969**, *8*, 7. (b) Brencic, J. V.; Cotton, F. A. *Inorg. Chem.* **1970**, *9*, 351.

99. Brencic, J. V.; Cotton, F. A. *Inorg. Chem.* **1970**, *9*, 346.

100. San Filippo, J. Jr.; Sniadoch, H. J.; Grayson, R. L. *Inorg. Chem.* **1974**, *13*, 2121.

101. Cotton, F. A.; Extine, M. W.; Felthouse, T. R.; Kolthammer, W. S.; Lay, D. G. *J. Am. Chem. Soc.* **1981**, *103*, 4040.

102. San Filippo, J., Jr. *Inorg. Chem.* **1972**, *11*, 3140.

103. Best, S. A.; Smith, T. J.; Walton, R. A. *Inorg. Chem.* **1978**, *17*, 99.

104. Cotton, F. A.; Falvello, L. R.; Harwood, W. S.; Powell, G. L.; Walton, R. A. *Inorg. Chem.* **1986**, *25*, 3949.

105. Agaskar, P. A.; Cotton, F. A *Inorg. Chem.* **1984**, *23*, 3383.

106. Cotton, F. A.; Powell, G. L. *Inorg. Chem.* **1983**, *22*, 1507.

107. Taube, H.; Bowen, A. R. *Inorg. Chem.* **1974**, *13*, 2245.

108. Bowen, A. R.; Taube, H. *J. Am. Chem. Soc.* **1971**, *193*, 3287.

109. (a) Bino, A.; Cotton, F. A. *Inorg. Chem.* **1979**, *18*, 3562. (b) Bino, A.; Cotton, F. A. *Angew. Chem. Int. Ed. Engl.* **1979**, *18*, 462. (c) Bino, A.; Cotton, F. A. *Inorg. Chem.* **1981**, *20*, 623.

110. Demas, N. J.; Crosby, G. A. *J. Phys. Chem.* **1971**, *75*, 991.

111. Winkler, J. R.; Netzel, T. L.; Creutz, C.; Sutin, N, *J. Am. Chem. Soc.* **1987**, *109*, 2381.

112. Bard, A. J.; Faulkner, L. R. *Electrochemical Methods. Fundamental and Applicationsl*; Wiley-Interscience: New York, 1980.

113. Gordon, A. J.; Ford, R. A. *The Chemist's Companions A Handbook of Practical Data, Techniques, and References*; Wiley-Interscience: New York, 1972.

114. Calvert, J. G.; Pitts, J. N. *Photochemistry*; Wiley-Interscience: New York, 1966.

115. Frenz, B. A. *"The Enraf-Nonius CAD 4 SDP - A Real - time System for Concurent X-Ray Data Collection an Crystal Structure Determination,"* in Computing in Crystallography, Schenk, H.; Olthof-Hazelkamp, R.; canKonigsveld, H.; Bassi, G. C. Eds; Delft University Press: Delft, Holland, 1978.

116. Zachariasen, W. H.; *Acta Crystallogr.*, **1963**, *16*, 1139.

117. Cromer, D. T.; Waber, J. T. *"International Tables for X-Ray Crystallography"*, Vol. IV, The Kynoch Press, Birmingham, England, 1974, Table 2.2B.

118. Ibers, J. A.; Hamilton, W. C. *Acta Crystallogr.*, **1964**, *17*, 781.

119. Cromer, D. T. *"International Tables for X-Ray Crystallography,"* Vol. IV, The Kynoch Press, Birmingham, England, 1974, Table 2.3.1.

120. Cruickshank, D. W. J. *Acta Crystallogr.*, **1949**, *2*, 154.

121. Duschinky, F. *Acta Phys. Chim.* URSS, **1937**, *7*, 55.

122. Abbott, E. H.; Bose, K. S.; Cotton, F. A.; Hall, W. T.; Sekutowski, J. C. *Inorg. Chem.* **1978**, *17*, 3240.

123. Cotton, F. A.; Fanwick, P. E.; Fitch, J. W.; Glicksman, H. D.; Walton, R. A. *J. Am. Chem. Soc.* **1979**, *101*, 1752.

124. (a) Campbell, F. L., III; Cotton, F. A.; Powell, G. L. *Inorg. Chem.* **1985**, *24*, 177. (b) Campbell, F. L., III; Cotton, F. A.; Powell, G. L. *Inorg. Chem.* **1985**, *24*, 4384.

125. Mulliken, R. S. *J. Chem. Phys.* **1939**, *7*, 20.

126. Stiegman, A. E.; Miskowski, V. M. *J. Am. Chem. Soc.* **1988**, *110*, 4053.

127. Tolman, C. A. *Chem. Rev.* **1977**, *77*, 313.

128. Tolman, C. A.; Seidel, W.C.; Gosser, L. W. *J. Am. Chem. Soc.* **1974**, *96*, 53.

129. Hopkins, M. D.; Miskowski, V. M.; Gray, H. B. *J. Am. Chem. Soc.* **1986**, *108*. 959.

130. Cotton, F. A.; Frenz, B. A.; Pedersen, E.; Webb, T. R. *Inorg. Chem.* **1975**, *14*, 391.

131. (a) Cotton, F. A.; Pedersen, E.; Webb, T. R. *Inorg. Chem.* **1975**, *14*, 388. (b) Cotton, F. A.; Pedersen, E. *J. Am. Chem. Soc.* **1975**, *97*. 303.

132. Fanwick, P. E.; Martin, D. S.; Webb, T. R.; Robbins, G. A.; Newman, R. A. *Inorg. Chem.* **1978**, *17*, 2723.

133. (a) Clark, R. J. H.; Franks, M. L. *J. Am. Chem. Soc.* **1975**, *97*. 2691. (b) Clark, R. J. H.; Stead, M. J. *Inorg. Chem.* **1983**, *22*, 1214.

134. (a) Angell, C. L.; Cotton, F. A.; Frenz, B. A.; Webb, T. R. *J. Am. Chem. Soc., Chem. Commun.* **1973**, 399. (b) Reference 13, Chapter 8.

135. Loewenschuss, A.; Shamir, J.; Ardon, M. *Inorg. Chem.* **1976**, *15*, 238.

136. Baxendale, J. H. *Rad. Res. Suppl.* **1964**, *4*, 139.

137. Bowen, A. R.; Taube, H. *J. Am. Chem. Soc.* **1971**, *93*, 3287.

138. Sasaki, Y.; Skyes, A. G. *Am. Chem. Soc., Chem. Commun.* **1973**, 767.

139. Ardon, M.; Pernick, A. *Inorg. Chem.* **1974**, *13*, 2275.

140. Richens, D. T.; Skyes, A. g. *Inorg. Chem.* **1982**, *21*, 418.

141. Bino, A.; Ardon, M.; Maro, I.; Maftory, M.; Dori, Z. *J. Am. Chem. Soc.* **1976**, *98*, 7093.

142. Cotton, F. A.; Dori, Z.; Marler, D. O.; Schwotzer, W. *Inorg. Chem.* **1984**, *23*, 4033.

143. Bino, A.; Cotton, F. A.; Dori, Z. *J. Am. Chem. Soc.* **1978**, *100*, 5252.

144. Murmann, R. K.; Shelton, M. E. *J. Am. Chem. Soc.* **1980**, 102, 3984.

145. (a) Ardon, M.; Pernick, A. *Inorg. Chem.* **1973**, *12*, 1484. (b) Sasaki, Y.; Skyes, A. G. *Am. Chem. Soc., Dalton Trans.* **1974**, 1968

146. Richens, D. T.; Skyes, A. G. *Comments Inorg. Chem.* **1981**, *1*, 141.

147. Anbar, M. *Adv. Chem. Ser.* **1965**, *No. 50*, 55.

148. (a) Norman, J. G., Jr.; Kolari, H. J. *J. Am. Chem. Soc., Chem. Commun.* **1974**, 303. (b) Norman, J. G., Jr.; Kolari, H. J. *J. Am. Chem. Soc.* **1975**, *97*. 33. (c) Mathisen, K. B.; Wahlgren, U.; Pettersson, L. G. M.; Wahlgren, U. *Chem. Phys. Lett.* **1984**, *104*, 336. (d) Stromberg, A.; Pettersson, L. G. M.; Wahlgren, U. *Chem. Phys. Lett.* **1985**, *118*, 389.

149. Mortola, A. P.; Moskowitz, J. W.; Rosch, N.; Cowman, C. D.; Gray, H. B. *Chem. Phys. Lett.* **1975**, *32*, 283.

150. Schmidt, W.; Taube, H. *Inorg. Chem.* **1963**, *2*, 698.

151. Ilan, Y. *Inorg. Chem.* **1985**, *24*, 4223.

152. (a) Bennett, M. J.; Brencic, J. V.; Cotton, F. A. *Inorg. Chem.* **1969**, *8*, 1060. (b) Cotton, F. A.; Kalbacher, B. J. *Inorg. Chem.* **1976**, *15*, 522. (c) Bino, A.; Cotton, F. A. *Angew. Chem. Int. Ed. Engl.* **1979**, *18*, 332.

153. Mocella, M. T.; Okamoto, M. S.; Barefield, E. K. *Synth. React. Inorg. Met.-Org. Chem,* **1974**, *4*, 69.